

Evaluation of minimal factor H therapy administered to kidneys during *ex vivo* normothermic perfusion as a treatment to reduce ischaemia reperfusion injury.

# **Chloe Connelly**

Thesis submitted in partial fulfilment of the requirements for the degree of Doctor of Philosophy

**Translational and Clinical Research Institute** 

**Newcastle University** 

October 2024

#### **Abstract**

**Introduction:** Kidney availability for transplantation is limited, necessitating the use of marginal organs which are more susceptible to ischaemia reperfusion injury (IRI). A key driver of IRI is the complement system, particularly the alternative pathway (AP), of which a key regulator is factor H (FH). Homodimeric mini-factor H (HDM-FH) is an FH based construct with improved AP regulation compared to full length FH. *Ex vivo* normothermic perfusion (EVNP) can be used to administer therapeutics directly to organs to assess their efficacy.

**Methods:** HDM-FH was produced in transfected mammalian cells and validated *in vitro*. Kidneys were retrieved from 6-week-old, 60 kg white landrace pigs. Initially, stepwise changes were made to an established EVNP model, N=1, then initial warm ischaemic times (WIT) and static cold ischaemic times (CIT) were standardised and extended, N=3. Following this, 5 mg HDM-FH was administered to one kidney of a pair via an EVNP circuit, N=8. Kidneys were perfused for 6 hours with whole autologous blood. Kidney function, complement activation and downstream ischaemic injury were measured to assess the efficacy of HDM-FH.

**Results:** 25 minutes initial WIT and 16 hours CIT significantly increased C3 deposition (p=0.0104). HDM-FH bound within glomeruli of kidneys, particularly on the endothelium and basement membrane, and correlated with C3 deposition prior to perfusion (p=0.0482). HDM-FH administration led to reduced deposition of Bb (p=0.0096) and C1q (p=0.0051), reduced urinary C5a (p=0.0022) reduced tissue apoptosis (p=0.0011) and reduced infiltration of neutrophils (p=0.0146) macrophages (p=0.0209) and T-cells (p=0.0404) at the end of perfusion, although it did not affect kidney function.

**Conclusions:** Extended WIT and CIT of porcine kidneys can induce complement activation and ischaemic injury, which HDM-FH can reduce when administered during EVNP. HDM-FH has the potential therefore to improve graft survival in transplanted kidneys, particularly in kidneys from marginal donors.

# **Acknowledgements**

This project would not have been possible without my supervisory team or the MRC who provided funding for this project. I would like to thank Professor Kevin Marchbank whose door is always open to us, providing a huge amount of knowledge, support, and whisky and haggis each year on Burns night, and for being possibly the easiest to reach supervisor anyone has ever had. I would like to thank Professor Neil Sheerin for always valuing his staff, showing faith in me by suggesting that I undertake this PhD while working as a technician and supporting my development throughout. A few sentences could never do justice for my thanks for Dr Beth Gibson, who has guided me physically, emotionally, technically and professionally throughout this entire project. Thank you for being there for the many 3 am starts and slightly less frequent late nights, this would not have been possible without you.

I would like to thank my dear friends Mr Balaji Mahendran and Mr Sam Tingle for (very) rapidly learning to retrieve and bench pig kidneys for this project, for spending many unsociable hours helping out at the farm and perfusion lab, and being constant sources of both support and entertainment. I very am grateful to Mark Brett and Emma Malcom for facilitating this work, helping everything to run so smoothly at Cockle Park despite some less-than-ideal conditions. I would further like to thank Lucy Bates and Ms Emily Thompson for first welcoming me to the world of kidneys and imparting their perfusion wisdom onto me. On a technical level, the MSB and CEUS analysis in this project would not have been possible without Sam Tingle and George Kourounis, whose IT skills far surpass mine. The mammoth task of drug production would have not been possible without the design input and lab hours from Dr Beth Gibson and Harriet Denton.

I am thankful to Professors Claire Harris and John Dark for fitting me into their very busy work schedule/retirement for my annual progress reviews in which they always provided invaluable advice and feedback.

I was very fortunate to supervise two excellent students during my PhD, Madison Cooper and Min Wu, who contributed to some of the data collection and analysis in this thesis. I have also been fortunate to work within the amazingly supportive complement and transplant groups, and would like to thank in particular, Professor Simi Ali, Dr Jenny Gilmour, Dr Chong Yun Pang, Dr Emily Glover, Marnie Brown, Laura Sture, Dr Kate Smith-Jackson and anyone else who I have ever badgered for help.

Lastly, I would like to thank my support network outside of the lab. Thank you James for keeping me, the cats, and my car alive throughout this and for cheering me on every step of the way. Most importantly, I could not have reached this point at all without my parents Julie and Mick who have supported my academic career from the start and always believed in me. I hope to do them and the rest of my family proud as the first ever Doctor Connelly.

Work carried out by others that contributed to this thesis are outlined below:

Retrieval and benching of porcine kidneys: Balaji Mahendran, Samuel Tingle

EVNP experiments: Beth Gibson, Balaji Mahendran, Samuel Tingle

Production of Porcine HDM-FH: Beth Gibson

Production of Human HDM-FH: Beth Gibson, Harriet Denton

Analysis of CEUS data: Samuel Tingle

Processing of MSB data, Georgios Kourounis

# **Table of contents**

CHAPTER 1.	Introduction	1
1.1 Kidr	ney transplantation – current practice, challenges and utilisation	1
1.1.1	Kidney transplantation – current practice, challenges and utilisation	1
1.1.2	Living donation, donation after brain death and donation after circulatory death	3
1.1.3	The use of marginal organs	4
1.1.4	The effect of transplant parameters on outcomes	5
1.2 Isch	aemia reperfusion injury and the immune response to transplantation	6
1.2.1	Mechanisms and consequences of ischaemia reperfusion injury	6
1.2.1.1	Cell-death	7
1.2.1.2	Endothelial dysfunction	9
1.2.2	The innate immune response to ischaemia reperfusion injury	10
1.2.3	The adaptive immune response to ischaemia reperfusion injury	10
1.3 The	Complement System	12
1.3.1	The classical pathway	13
1.3.2	The lectin pathway	14
1.3.3	The alternative pathway	15
1.3.4	The terminal pathway	16
1.3.5	Complement receptors	17
1.3.6	Complement regulators	19
1.3.7	Complement therapeutics	20
1.4 Con	nplement in ischaemia reperfusion injury	23
1.4.1	Complement activation exacerbates ischaemia reperfusion injury	23
1.4.2	Clinical evidence of the involvement of complement in ischaemia reperfusion injury	y 25
1.4.3	Animal models investigating complement and ischaemia reperfusion injury	26
1.4.4	Complement therapeutics for ischaemia reperfusion	27
1.5 Fact	or H	31
1.5.1	Factor H structure and function	31
1.5.2	Factor H related proteins	32
1.5.3	Factor H in disease	33
1.5.4	Mini factor H	34
1.5.5	Homodimeric minimal-factor H	35
1.6 Mad	chine perfusion of kidneys	37
1.6.1	Hypothermic machine perfusion	37
1.6.2	Ex vivo normothermic perfusion	37
1.6.3	Therapies administered during ex vivo normothermic perfusion	38

1.7	Hypothesis.		42
1.8	Aims and ob	jectives	43
СНАРТЕ	R 2. Mate	erials and Methods	45
2.1	Ethics		45
2.2	Normothern	nic machine perfusion of porcine kidneys	45
2.2	1 Retriev	al of porcine kidneys.	45
2.2	2 Normo	thermic machine perfusion	46
2.2	3 Collecti	on and processing of samples	49
2.2	4 Perfusa	ite blood gas analysis	50
2.2	5 Function	nal parameters	51
2.3	Histology an	d immunofluorescent staining	52
2.3	1 Haema	toxylin and Eosin staining	53
2.3	2 Periodi	c acid-Schiff staining	53
2.3	3 Martius	s Scarlet Blue staining	53
2	.3.3.1 Qu	uantification of erythrocytes in Martius scarlet blue stained sections	54
2.3	4 Immun	ofluorescent staining of FFPE sections	55
2	.3.4.1 Inc	direct immunostaining	55
2	.3.4.2 Td	T-mediated dUTP Nick-End Labelling	58
2.3	5 Immun	ofluorescent staining of cryosections	59
2	.3.5.1 Inc	direct immunostaining	59
2.3	6 Quanti	fication of immunofluorescent staining	62
2.4	Protein anal	ysis	64
2.4	1 Enzyme	e-linked Immunosorbent Assays	64
2.5	Classical had	emolytic assays	67
CHAPTE	R 3. Porc	ne <i>Ex Vivo</i> Normothermic Perfusion Model Set Pp	70
3.1	Introduction	l	70
3.2	Specific met	hods	73
3.2	1 Initial c	hanges to an established porcine EVNP model	73
3.2	2 Extensi	on and standardisation of warm and cold ischaemic times	75
3.2	3 Compa	rison of EVNP with and without a kidney	75
3.3	Results		76
3.3	1 Stepwis	se changes to perfusion set up	76
3	.3.1.1 Ph	ysiological parameters and kidney function	77
3	.3.1.2 Co	mplement activation	79
3.3	2 Extensi	on of cold ischaemic times	81
3	.3.2.1 Re	nal physiology	81
3	.3.2.2 Ce	Ilular metabolism and function	84

	3.3.2.3	Histology	86
	3.3.2.4	Immunofluorescence	88
	3.3.2.5	Perfusate and urine composition	94
3	.3.3	Blood only perfusion experiment showing complement activity in EVNP system	າ 97
3.4	Disc	ussion	99
CHAPT	ΓER 4.	Production and In Vitro Testing of Homodimeric Mini-Factor H	107
4.1	Intro	oduction	107
4.2	Met	hods	112
4	.2.1	HDM-FH production in mammalian cells	112
	4.2.1.1	Cell maintenance and subculture	112
	4.2.1.2	Cell counting	112
	4.2.1.3	Cryopreservation	113
	4.2.1.4	Chinese Hamster Ovary Cell transfection	113
	4.2.1.5	Monoclonal selection and expansion	116
	4.2.1.6	Cell expansion in roller bottles	116
4	.2.2	Protein purification and concentration	117
	4.2.2.1	Generation of an OX-24 protein G column	117
	4.2.2.2 and bu	Affinity purification, metal ion affinity chromatography purification, conce	
	4.2.2.3	Triton X-114 assisted endotoxin removal	118
4	.2.3	Surface plasmon resonance	118
	4.2.3.1	Extraction of porcine and human C3 and conversion of C3 to C3b	119
	4.2.3.2	Immobilisation of porcine and human C3b onto a Sensor Chip CM5	119
	4.2.3.3	Affinity analysis of HDM-FH to porcine and human C3b	120
4	.2.4	Administration of human HDM-FH to porcine kidneys	120
4	.2.5	Testing HDM-FH using classical haemolytic assay	121
4.3	Resi	ults	122
4	.3.1	Size and purity of construct	122
4	.3.2	HDM-FH binding to porcine tissue at 4°C	123
4	.3.3	Classical Haemolytic assay assessing HDM-FH in human and porcine serum	126
4	.3.4	Binding profile of HDM-FH to porcine and human C3b	126
4.4	Disc	ussion	128
CHAP	ΓER 5.	Administration of Homodimeric Mini – Factor H to Porcine Kidneys	134
5.1	Intro	oduction	134
5.2	Spe	cific Methods	135
5	.2.1	Administration of HDM-FH to kidneys	135
5	.2.2	Ultrasound imaging	135

	5.2.2.1	Contrast enhanced ultrasound imaging of porcine kidneys	135
	5.2.2.2	Analysis of CEUS images	136
5	.2.3	Colocalisation of HFM-FH with glomerular structures	138
5	.2.4	Western blot	139
	5.2.4.1	Bicinchoninic Acid Protein Assay	139
	5.2.4.2	Sample preparation and separation by SDS-PAGE	139
	5.2.4.3	Protein transfer	139
	5.2.4.4	Protein normalisation	139
	5.2.4.5	Immunoblotting and visualisation	140
5.3	Resu	ılts	141
5	.3.1	HDM-FH binding	141
	5.3.1.1	HDM-FH in kidneys throughout perfusion	141
	5.3.1.2	Colocalisation of HDM-FH with glomerular structures	143
5	.3.2	Physiological parameters and kidney function	145
	5.3.2.1	Renal physiology	145
	5.3.2.2	Electrolyte concentration	148
	5.3.2.3	Cellular metabolism	148
	5.3.2.4	Renal function	150
	5.3.2.5	Contrast enhanced ultrasound	150
	5.3.2.6	Neutrophil gelatinase-associated lipocalin	152
5	.3.3	Complement regulation	153
	5.3.3.1	C3 and C3 activation products	153
	5.3.3.2	C5a	157
	5.3.3.3	Factor B	157
	5.3.3.4	C1q	159
	5.3.3.5	Haemolytic activity of perfusate	161
5	.3.4	Inflammatory cytokines and chemokines	163
5	.3.5	Fibrinogen and microthrombi	164
	5.3.5.1	Fibrinogen	165
	5.3.5.2	Erythrocytes	166
5	.3.6	Glycocalyx shedding	168
	5.3.6.1	Hyaluronan	168
5	.3.7	Cell death	169
	5.3.7.1	Apoptosis	169
5	.3.8	Immune cell infiltration	171
	5.3.8.1	CD3ε-UNLB	171
	5.3.8.2	CD163	172

5	5.3.8.3	Neutrophil elastase	174
5.4	Discus	ssion	176
CHAPTE	R 6.	Project Conclusion, Summary, Limitations and Future Directions	184
6.1	Projec	t summary and discussion	184
6.2	Concl	usions	190
6.3	Study	limitations	191
6.4	Future	e directions	192
CHAPTE	R 7.	Publications and Conferences	196
7.1	Public	ations	196
7.2	Confe	rences	197
CHAPTE	R 8.	References	199

# Table of figures

Figure 1.1 CKD stages according to kidney disease improving global outcomes classification	on. 2
Figure 1.2 Diagram of ischaemic periods during organ retrieval and transplantation	4
Figure 1.3 Schematic summary of the mechanisms of ischaemia reperfusion injury	7
Figure 1.4 The pathways and morphological processes of apoptosis	8
Figure 1.5 The classical pathway of complement activation	13
Figure 1.6 The lectin pathway of complement activation	14
Figure 1.7 The alternative pathway of complement activation	15
Figure 1.8 The formation of the membrane attack complex	16
Figure 1.9 The role of the complement system in ischaemia reperfusion injury	24
Figure 1.10 The binding sites of factor H	32
Figure 1.11 The structure of HDM-FH	35
Figure 2.1 Diagram of EVNP circuit	47
Figure 2.2 Diagram of experimental timeline with sampling schedule	50
Figure 2.3 LABKIT mask identifying erythrocytes	55
Figure 2.4 Schematic showing lysis of sensitised sheep red blood cells following the addit	ion
of serum	67
Figure 3.1 Flow chart to determine EVNP conditions in the first stage of model optimisati	ons.
	74
Figure 3.2 Flow chart showing successful porcine EVNP optimisation	76
Figure 3.3 Physiological parameters throughout EVNP.	
Figure 3.4 Plasma creatinine throughout EVNP.	79
Figure 3.5 C3 deposition in glomeruli pre-perfusion and at 360 minutes of perfusion	80
Figure 3.6 C3a levels in perfusate throughout perfusion	80
Figure 3.7 Renal resistance in kidneys with 2-hour and 16-hour cold ischaemic times	
throughout perfusion	82
Figure 3.8 Renal blood flow in kidneys with 2-hour and 16-hour cold ischaemic times	
throughout perfusion	
Figure 3.9 Urine output in kidneys with 2-hour and 16-hour cold ischaemic times through	
perfusion	83
Figure 3.10 Electrolyte levels in kidneys with 2-hour and 16-hour cold ischaemic times	
throughout perfusion	
Figure 3.11 Creatinine clearance from perfusate over the first three hours of perfusion	
Figure 3.12 Periodic acid-Schiff-stained kidney section from 2-hour CIT kidneys and 16-hour	
CIT kidneys taken at 5 minutes and 360 minutes of perfusion	
Figure 3.13 Haematoxylin & eosin-stained kidney section taken at 360 minutes of perfusi	
showing an influx of immune cells	
Figure 3.14 Fibrinogen within kidney glomeruli	89
Figure 3.15 Glomerular deposition of fibrinogen pre-perfusion and at 360 minutes of	
perfusionperfusion	
Figure 3.16 Apoptotic cells in kidney tissue.	91
Figure 3.17 Percentage of apoptotic cells in kidney sections pre-perfusion and at 360	
minutes of perfusion	
Figure 3.18 C3 deposition in kidney glomeruli.	93

Figure 3.19 Glomerular deposition of C3 pre-perfusion and at 360 minutes of perfusion	94
Figure 3.20 C3a levels in perfusate from 5 minutes to 360 minutes of perfusion	95
Figure 3.21 Hyaluronan levels in perfusate pre-perfusion and at 360 minutes of perfusion	. 95
Figure 3.22 IL-6 levels in urine at 30 and 360 minutes of perfusion	96
Figure 3.23 IL-8 levels in urine at 30 and 360 minutes of perfusion	96
Figure 3.24 Complement consumption in an EVNP circuit with and without a kidney	
throughout perfusion	97
Figure 3.25 C3a levels in an EVNP circuit with and without a kidney throughout perfusion.	98
Figure 4.1 Vector map for human HDM-FH	114
Figure 4.2 Vector map for porcine HDM-FH	115
Figure 4.3 Sensorgram of amine coupling of porcine and human C3b on a CM5 Sensor Chi	р
surface	
Figure 4.4 Porcine and human FH	122
Figure 4.5 Chromatogram of human HDM-FH elution from an OX-24 column	123
Figure 4.6 Cold perfusion of control kidneys with methylene blue	124
Figure 4.7 Immunofluorescent images showing OX-24 binding within kidney tissue followi	ing
cold flush with HDM-FH	125
Figure 4.8 Glomerular area positive for OX-24 following cold perfusion with HDM-FH	125
Figure 4.9 Control of complement in porcine and human serum by HDM-FH	126
Figure 4.10 Steady state affinity of human FH/HDM-FH to porcine/human C3b on a CM5	
chip	127
Figure 4.11 The FH SCRs 1-4/C3b complex.	130
Figure 4.12 The crystal structure of SCRs 18-20.	132
Figure 5.1 Imaging plane for ultrasound imaging	136
Figure 5.2 Representative contrast enhanced ultrasound loop with regions of interest	
selected	
Figure 5.3 Example intensity time plots from CEUS	138
Figure 5.4 Immunofluorescent images showing OX-24 binding within tissue of kidneys	
treated with HDM-FH from 30 minutes to 360 minutes of perfusion	
Figure 5.5 Glomerular area positive for OX-24 from 30 minutes to 360 minutes of perfusion	
within tissue of kidneys treated with HDM-FH	142
Figure 5.6 OX-24 binding at 360 minutes of perfusion correlated with C3 deposition pre-	
perfusion in tissue of kidneys treated with HDM-FH	143
Figure 5.7 Immunofluorescent images depicting HDM-FH colocalisation with glomerular	
structures within tissue of a kidney treated with HDM-FH at 360 minutes of perfusion	
Figure 5.8 Signal overlap of HDM-FH with glomerular structure markers within tissue of a	
kidney treated with HDM-FH at 360 minutes of perfusion	145
Figure 5.9 Physiological parameters of kidneys treated with HDM-FH and control kidneys	
from 5 minutes to 360 minutes of perfusion	147
Figure 5.10 Electrolyte concentration in perfusate of kidneys treated with HDM-FH and	
control kidneys from 5 minutes to 360 minutes of perfusion	
Figure 5.11 Cellular metabolism of kidneys treated with HDM-FH and control kidneys from	
minutes to 360 minutes of perfusion.	149
Figure 5.12 Clearance of creatinine from perfusate of kidneys treated with HDM-FH and	
control kidneys	150

Figure 5.13 Contrast enhanced ultrasound results from treated and control kidneys at 330	
minutes of perfusion	2
Figure 5.14 Neutrophil gelatinase-associated lipocalin levels in urine of kidneys treated with	
HDM-FH and control kidneys from 30 minutes to 360 minutes of perfusion15	2
Figure 5.15 Immunofluorescent images of C3 deposition in glomeruli of kidneys treated with	1
HDM-FH and control kidneys at 360 minutes of perfusion15	3
Figure 5.16 C3 deposition in glomeruli of kidneys treated with HDM-FH and control kidneys	
at 360 minutes of perfusion15	4
Figure 5.17 Ratio of C3 alpha chain to C3C alpha chain on Western blot in perfusate from	
kidneys treated with HDM-FH and control kidneys at 360 minutes of perfusion15	5
Figure 5.18 C3a levels in perfusate and urine in perfusate from kidneys treated with HDM-FI	Η
and control kidneys from 30 minutes to 360 minutes of perfusion15	6
Figure 5.19 C5a levels in urine from kidneys treated with HDM-FH and control kidneys at 30	
minutes to 360 minutes of perfusion15	7
Figure 5.20 Immunofluorescent images of Bb deposition in glomeruli of kidneys treated with	1
HDM-FH and control kidneys at 360 minutes of perfusion15	8
Figure 5.21 Bb deposition in glomeruli of kidneys treated with HDM-FH and control kidneys	
at 360 minutes of perfusion15	8
Figure 5.22 FB in perfusate of kidneys treated with HDM-FH and control kidneys from 360	
minutes of perfusion	9
Figure 5.23 Immunofluorescent images of C1q deposition in glomeruli of kidneys treated	
with HDM-FH and control kidneys at 360 minutes of perfusion16	0
Figure 5.24 C1q deposition in glomeruli of kidneys treated with HDM-FH and control kidneys	S
at 360 minutes of perfusion16	0
Figure 5.25 Complement consumption in perfusate of kidneys treated with HDM-FH and	
control kidneys pre-perfusion and at 360 minutes of perfusion16	2
Figure 5.26 IL-6 levels in urine from kidneys treated with HDM-FH and control kidneys from	
30 minutes to 360 minutes of perfusion16	3
Figure 5.27 IL-8 levels in urine from kidneys treated with HDM-FH and control kidneys from	
30 minutes to 360 minutes of perfusion16	4
Figure 5.28 Immunofluorescent images of fibrinogen deposition in glomeruli of kidneys	
treated with HDM-FH and control kidneys at 360 minutes of perfusion16	5
Figure 5.29 Fibrinogen deposition in glomeruli of kidneys treated with HDM-FH and control	
kidneys at 360 minutes of perfusion16	6
Figure 5.30 MSB stained sections of kidneys treated with HDM-FH and kidneys at 360	
minutes of perfusion	7
Figure 5.31 Erythrocyte coverage in kidneys treated with HDM-FH and control kidneys at 36	0
minutes of perfusion	8
Figure 5.32 Hyaluronan levels in perfusate from kidneys treated with HDM-FH and control	
kidneys from 30 minutes to 360 minutes of perfusion16	9
Figure 5.33 Immunofluorescent images of apoptotic bodies in kidneys treated with HDM-FH	
and control kidneys at 360 minutes of perfusion17	0
Figure 5.34 Apoptotic bodies in kidneys treated with HDM-FH and control kidneys taken at	
360 minutes of perfusion	0

Figure 5.35 Immunofluorescent images of CD3ɛ-UNLB positive cells in tissue of kidneys	
treated with HDM-FH and control kidneys at 360 minutes of perfusion	171
Figure 5.36 CD3ε-UNLB positive cells in tissue of kidneys treated with HDM-FH and cont	rol
kidneys at 360 minutes of perfusion	172
Figure 5.37 Immunofluorescent images of CD163 positive cells in tissue of kidneys treat	ed
with HDM-FH and control kidneys at 360 minutes of perfusion	173
Figure 5.38 CD163 positive cells in tissue of kidneys treated with HDM-FH and control	
kidneys at 360 minutes of perfusion	173
Figure 5.39 Immunofluorescent images of neutrophil elastase in tissue from kidneys tre	ated
with HDM-FH and control kidneys at 360 minutes of perfusion	174
Figure 5.40 Neutrophil elastase positive area in tissue from kidneys treated with HDM-F	Н
and control kidneys at 360 minutes of perfusion	175
Figure 6.1 Consequences of complement activation and action of HDM-FH	187
Figure 6.2. Current approved complement inhibitors	189
Figure 6.3 Theoretical multiplex assay to assess decay accelerating activity of HDM-FH o	n the
porcine C3 convertase	193

# **Table of Tables**

Table 1.1 Summary of complement receptors	18
Table 1.2 Summary of negative complement regulators	20
Table 1.3 Summary of FDA approved complement therapeutics (as of October 2024)	22
Table 1.4 Summary of treatments investigated in animal models of renal IRI	30
Table 1.5 Summary of therapeutics assessed during EVNP	41
Table 2.1 Perfusion hardware drugs and fluids	49
Table 2.2 Perfusate biochemical parameters measure throughout perfusion using the	
RAPIDpoint 500e Blood Gas System	51
Table 2.3 Protocol for dewaxing and rehydrating of FFPE sections	52
Table 2.4 Protocol for dehydrating and clearing of FFPE sections	52
Table 2.5 Protocol for Martius Scarlet Blue staining	54
Table 2.6 Reagents used for indirect immunofluorescent staining on FFPE tissue	57
Table 2.7 TUNEL assay procedure	59
Table 2.8 Reagents used for different indirect immunofluorescent staining on frozen OCT	
embedded tissue	62
Table 2.9 Steps to count individual nuclei in Fiji Image J	63
Table 2.10 R&D DuoSet $^{ extsf{TM}}$ details with block buffer and reagent diluent details	65
Table 3.1 Cartridges used to carry out blood analysis	75
Table 3.2 Characteristics of perfused porcine kidney pairs	77
Table 4.1 FH based therapeutics under investigation	

## **Abbreviations**

A2 Annexin 2

AP Alternative pathway

**AAV** ANCA-associated vasculitis

**AAV-HDM-FH** Adeno-associated virus-HDM-FH

**AchR** Acetylcholine receptor antibody

**aHUS** Atypical haemolytic syndrome

**AKI** Acute kidney injury

**AMD** Age related macular degeneration

APC Antigen presenting cell

**AST** Aspartate aminotransferase

ATIII Antithrombin-III (ATIII),

**ATP** Adenosine triphosphate

**AUC** Area under the curve

**AWERB** Animal Welfare Ethical Review Body

**BSA** Bovine serum albumin

**C1-INH** C1 inhibitor

C3aR C3a receptor

C3G C3 glomerulopathy

**C3GN** G3G glomerulonephritis

**C4BP** C4 binding protein

**C5aR** C5a receptor

C5aR1 C5a receptor 1

**CAD** Cold agglutinin disease

**C** Carboxyl

**COHb** Carboxyhaemoglobin

**CIT** Cold ischaemic time

**CHO** Chinese hamster ovary

**CK1** Cytokeratin 1

**CKD** Chronic kidney disease

**CL-11** Collectin-11

**CM5** Carboxymethyl 5

**COVID-19** Coronavirus disease 2019

**CP** Classical pathway (CP).

**CR1** Complement receptor 1 (CR1),

**CRIg** Complement receptor of the immunoglobulin family

**CXCL1** Chemokine CXC ligand 1

CXCL2 Chemokine CXC ligand 2

**DAF** Decay accelerating factor

**DAMP** Danger associated molecular pattern

**DBD** Donation after brainstem death

**DCD** Donation after circulatory death

**DDD** Dense deposit disease

**DGF** Delayed graft function

**DI** Deionised water

**DMEM** Dulbecco's Modified Eagle Medium

**DMSO** Dimethyl sulfoxide

**DPBS** Dulbecco's Phosphate-Buffered Saline

**ECD** Extended criteria donors

**ECMO** Extracorporeal membrane oxygenation

**EDC** 1-Ethyl-3-(3-dimethylaminopropyl) carbodiimide hydrochloride

**EDTA** Ethylenediaminetetraacetic acid

**ELISA** Enzyme-linked Immunosorbent Assays

**EMT** Epithelial–mesenchymal transition

**ESRD** End stage renal disease

**ET-1** Endothelin-1

**EVNP** Ex vivo normothermic perfusion (EVNP)

**FB** Factor B

**FB** Factor D

**FBS** Foetal bovine serum

**FDCs** Dendritic cells

**FFPE** Formalin-fixed paraffin embedded

**FH** Factor H

**FHR1** Factor H related protein 1

FI Factor I

**FHR** Factor-H related protein

**GA** Geographic atrophy

**GAGs** Glycosaminoglycans

**GFR** Glomerular filtration rate

**gMG** Generalised myasthenia gravis

**Hb** Haemoglobin

**HBST** HEPES buffered saline with Tween 20

**HDM-FH** Homodimeric mini-Factor H

**HGF** Hepatocyte growth factor

**HIF** Hypoxia-inducible factor

**HLA** Human leucocyte antigens

**HMOX1** Heme oxygenase 1

**HMP** Hypothermic machine perfusion

**ICAM-1** Intercellular Adhesion Molecule 1

IL Interleukin

IRI Ischaemia reperfusion injury

**LP** Lectin pathway

MAC Membrane attack complex

MAPC Multipotent adult progenitor cell

MASP-1 MBL-associated serine proteases 1

MASP-2 MBL-associated serine proteases 2

MBL Mannan-binding lectin

MCP Membrane cofactor protein

MCP-1 Monocyte Chemoattractant Protein-1

MetHb Methaemoglobin

MHC Major histocompatibility complex

MLKL Mixed lineage kinase domain-like pseudokinase

MPO Myeloperoxidase

**mPTP** Mitochondrial permeability transition pores

MSCs Mesenchymal stem cells

NHS N-hydroxysuccinimide

**NGAL** Neutrophil gelatinase-associated lipocalin

**NMOSD** Neuromyelitis optica spectrum disorder

**OD** Optical density

**PAMP** Pathogen-associated molecular patterns

**PBS** Phosphate buffered saline

**PDGF** Platelet-derived growth factor

**PECAM-1** Platelet endothelial cell adhesion molecule-1

**PEG** Polyethylene glycol

PI3K Phosphatidylinositol 3-kinase

PNH Paroxysmal nocturnal haemoglobinuria

**QAS** Quality assessment score

**RBF** Renal blood flow

**RIPK3** Receptor-interacting protein kinase 3

**ROS** Reactive oxygen species

**RR** Renal resistance

**RU** Resonance units

**S1PR1** Sphingosine-1-phosphate receptor 1

SCD Standard criteria donors

**SCR** Short consensus repeat

**SCS** Static cold storage

**SDS-PAGE** Sodium dodecyl sulphate—polyacrylamide gel electrophoresis

siRNA Silencing RNA

**SPR** Surface plasmon resonance

**SRBC** Sheep red blood cell

**TdT** Terminal Deoxynucleotidyl Transferase

**TGF-β1** Transforming growth factor-beta

TLR Toll-like receptor

**TNF** Tumour necrosis factor

tPA Tissue plasminogen activator

**UW** University of Wisconsin

**VCAM-1** Vascular cell adhesion protein 1

**vWF** Von Willibrand factor

WIT Warm ischaemic time

WT Wild type

#### 1.1 KIDNEY TRANSPLANTATION — CURRENT PRACTICE, CHALLENGES AND UTILISATION

#### 1.1.1 Kidney transplantation – current practice, challenges and utilisation

Chronic kidney disease (CKD) is a condition characterised by diminished kidney function and often manifests with few symptoms, yet poses a significant public health challenge, affecting 8% - 16% of the global population. CKD is a diagnosis that includes a variety of conditions, it is commonly caused by diabetes and hypertension and is a major cause of morbidity and mortality. Additionally, CKD can arise from infections, environmental exposures, and glomerulonephritis, with genetic predisposition further elevating risk (Jha et al., 2013). The diagnosis of CKD is based on three criteria: glomerular filtration rate (GFR) < 60 mL/min/17.3 m<sup>2</sup>, albuminuria of at least 30 mg/24 hours, or signs of kidney damage including structural abnormalities or haematuria for at least three months (Stevens et al., 2024).

CKD affects over 10% of the UK population and is projected to become the fifth leading cause of life years lost worldwide by 2040. The current cost of CKD to the NHS is £1.95 billion annually, with quality of life significantly reduced in patients, dependent on disease stage, treatment option, comorbidities and complications. CKD is graded in stages based on albuminuria and GFR loss which is associated with prognosis (Figure 1.1). CKD stage 3a or above is the main risk factor for end stage renal disease (ESRD) which occurs at stage 5. ESRD requires treatment with renal replacement therapy, dialysis or transplantation (Kidney Research UK, 2023).

			Persistent albuminuria categories  Description and range			
				A1	A2	A3
KDIGO: Prognosis of CKD by GFR and albuminuria categories				Normal to mildly increased	Moderately increased	Severely increased
			<30 mg/g <3 mg/mmol	30–300 mg/g 3–30 mg/mmol	>300 mg/g >30 mg/mmol	
n²)	G1	Normal or high	≥90			
<b>1.73 n</b> nge	G2	Mildly decreased	60–89			
(ml/mir and ra	G3a	Mildly to moderately decreased	45–59			
categories (ml/min/1.7 Description and range	G3b	Moderately to severely decreased	30–44			
GFR categories (ml/min/1.73 m²) Description and range	G4	Severely decreased	15–29			
G.	G5	Kidney failure	<15			

Figure 1.1 CKD stages according to kidney disease improving global outcomes classification.

The clinical stages of CKD graded on the combined severity of albuminuria and GFR. Green indicates low risk (if there are no other markers of kidney disease); Yellow indicates moderately increased risk, orange indicates high risk, red indicates very high risk. Figure is taken from 'KDIGO 2024 Clinical Practice Guideline for the Evaluation and Management of Chronic Kidney Disease' (CKD work group, 2024).

Transplantation is the most optimal treatment for ESRD, as it improves patient quality of life and reduces mortality and risk of cardiac events (Tonelli et al., 2011). Furthermore, after the transplantation procedure and the first year post-transplant, the cost to the NHS is around £25000 less per patient annually than dialysis (NHSBT, 2009). Rejection rates and short-term graft survival of transplanted kidneys have improved following advancements in immunosuppressive strategies, however, improvements in long-term survival have been slower, necessitating the need for ongoing research in the field (Merion et al., 2018). Despite around 5000 people being on the kidney transplant waiting list at any time in the UK, only 3500 transplants are carried out each year (NHSBT, 2023). This disparity between the number of organs required and the number available has led to an increase in the use of organs from donation after circulatory death (DCD) and extended criteria donors (ECD). These organs are

more susceptible to the injury caused by the inevitable period of ischaemia and reperfusion following transplant (Summers et al., 2013).

#### 1.1.2 Living donation, donation after brain death and donation after circulatory death

There are three main categories of donors for transplantation: DCD donors, donation after brainstem death (DBD) donors and living donors. Controlled DCD donors are patients who have undergone irreversible brain injury, but who do not meet brain death criteria. In such cases, life support is withdrawn to allow a natural death. Uncontrolled DCD donors have experienced unexpected cardiac arrest, following which resuscitation is unsuccessful (British Transplant Society, 2021). DCD organs experience a period of warm ischaemia in the time between treatment withdrawal and cold perfusion of organs. Functional warm ischaemia is considered to begin when systolic blood pressure drops below 50 mm Hg for at least two minutes, there is then further warm ischaemia while the aorta is cannulated for cold flush (Ho et al., 2008).

DBD donors are patients who have been confirmed as dead using neurological criteria. The warm ischaemic period for the organs of these donors is minimal, as cold flush of the organs can begin immediately following withdrawal of life support. However, inflammatory events following brain death cause metabolic and hemodynamic changes, with cytokine release and complement activation (Bera et al., 2024).

Living donors donate organs under general anaesthesia and warm ischaemic time is minimal during retrieval as the donor kidney is perfused with the donor's blood until the major renal vessels are clamped. Kidneys from living donors have better outcomes compared with those from deceased donors (Seja et al., 2022).

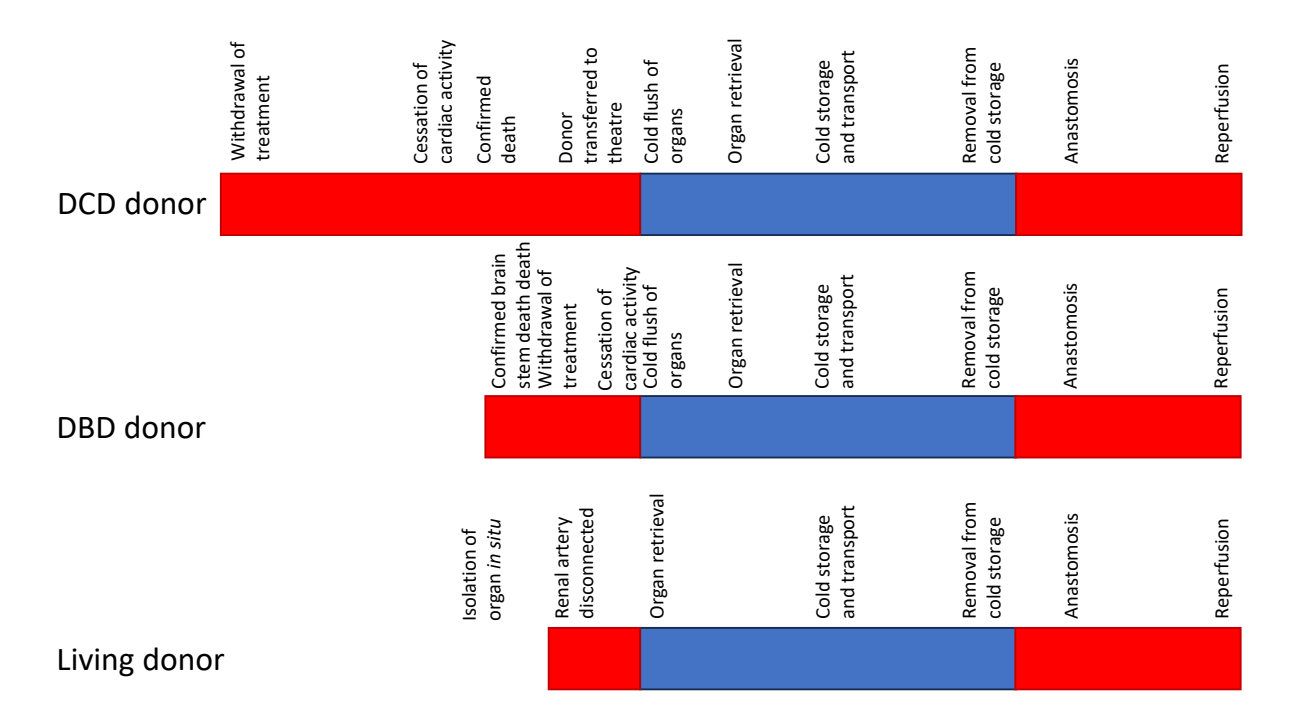


Figure 1.2 Diagram of ischaemic periods during organ retrieval and transplantation.

All organs will undergo a period of warm and cold ischaemia during the retrieval and transplant procedure. These times can differ greatly dependant on donor type and circumstances. Red bars indicate warm ischaemic time, blue bars indicate cold ischaemic time. Adapted from (Aitken et al., 2016).

Organs from living donors have better short and long term outcomes than those from deceased donors, with the 10 year survival rate at 90% for living donor transplantation and 75% following deceased donor transplantation (NHSBT, 2023). While long term outcomes between DCD and DBD donation are similar, DCD organs are more susceptible to delayed graft function (DGF) which is defined as the need for dialysis in the first week post-transplantation (Zens et al., 2018).

## 1.1.3 The use of marginal organs

A scarcity of organs combined with an aging population has resulted in a rise in the utilisation of organs from ECD donors. These donors meet specific criteria which exclude them from being categorised as standard criteria donors (SCD). These criteria include individuals aged 60 years or older, or those aged 50 to 59 years with two of three comorbidities: death by cerebrovascular incident, hypertension or terminal serum creatinine > 133  $\mu$ g/dL (Port et al., 2002). Organs from ECD donors account for around 21% of transplanted organs in the UK (Patel et al., 2023). Due to the nature of transplantation, ischaemia reperfusion injury (IRI) in

transplanted organs is inevitable owing to the period of anoxia and subsequent reperfusion experienced by the organ. IRI leads to acute kidney injury (AKI) and subsequently DGF which is a predictor of inferior graft function and reduced long-term survival. Although ECD transplant is still preferable to dialysis in terms of patient survival, ECD organs are more susceptible to IRI than SCD organs. ECD kidneys experience higher rates of DGF, which is more severe and graft loss is higher when compared with SCD, despite having comparable immediate function (Ponticelli et al., 2022). Furthermore, longer hospital stays and dialysis contribute to significantly higher cost following transplant of ECD kidneys (Saidi et al., 2007).

#### 1.1.4 The effect of transplant parameters on outcomes

The pro-inflammatory environment of the body following death or trauma can have a deleterious effect on organs, worsening outcomes from deceased donors compared to living donors (Seja et al., 2022). Furthermore, differences in warm ischaemic times prior to organ retrieval, static cold storage (SCS) time and anastomosis time have been correlated with DGF and graft loss (Cron et al., 2022, Osband et al., 2016). Longer cold ischaemic time (CIT), indicating the time spent by the kidney at 0°C to 4°C submerged in preservation solution on ice, have been correlated with worse survival rates and increased rates of DGF in ECD and SCD (Peters-Sengers et al., 2019, Nieto-Ríos et al., 2019, Summers et al., 2013, Debout et al., 2015, Lum et al., 2023). These correlations indicate that deleterious processes are occurring during cold storage of kidneys and throughout the rewarming period during anastomosis and that this affects the long-term function of kidneys. This highlights the significance of the ischaemia and reperfusion processes occurring during transplant.

#### 1.2 ISCHAEMIA REPERFUSION INJURY AND THE IMMUNE RESPONSE TO TRANSPLANTATION

IRI is a key mechanism behind immediate non-function, or delayed function following transplantation as it evokes a complex pro-inflammatory response involving cell death, endothelial dysfunction and activation of the innate and adaptive immune systems.

## 1.2.1 Mechanisms and consequences of ischaemia reperfusion injury

During the ischaemic phase, cells are deprived of oxygen and so begin metabolising anaerobically. Anaerobic glycolysis by mitochondria leads to lactic acid formation, and therefore acidosis, which inhibits adenosine triphosphate (ATP) production and leads to the breakdown of ATP to adenosine, inosine, xanthine and hypoxanthine. Acidosis also causes lysosomal leakage, cytoskeleton breakdown and failure of ATP-dependent Na<sup>+</sup>/K<sup>+</sup> pumps. Na<sup>+</sup> ions then accumulate intracellularly, drawing in water and causing cellular oedema (Cowled and Fitridge, 2020).

Aerobic glycolysis can also occur in kidneys through the Warburg effect. The Warburg affect is when glycolysis occurs rather than mitochondrial oxidative phosphorylation despite oxygen being available and has classically been defined as a characteristic of cancer cells (Liberti and Locasale, 2016). Non-cancerous conditions however can also lead to aerobic glycolysis in the kidneys. Elevated fructose levels due to tubular glucose reabsorption or following AKI or intrarenal hypoxia can drive aerobic glycolysis (Andres-Hernando et al., 2017, Park et al., 2017, Mirtschink et al., 2015). Furthermore, following ischaemic injury, proximal tubules can experience fibrosis which alters metabolism, leading to lactate production due to glycolysis through transforming growth factor-beta (TGF-β) signalling (Ding et al., 2017, Lan et al., 2016).

Reperfusion occurs following kidney anastomosis, restoring oxygen and pH. Oxygen influx catalyses the degradation of hypoxanthine to uric acid by xanthine oxidase leading to hydroxyl radical production (Cowled and Fitridge, 2020). During ischaemia, succinate, an intermediate of the citric acid cycle accumulates. Succinate is re-oxidised at reperfusion by succinate dehydrogenase. This drives reverse action of the electron transport at mitochondrial complex 1 during reperfusion, leading to the production of reactive oxygen species (ROS) (Chouchani et al., 2014). ROS formation, mitochondrial dysfunction and calcium overload cause mitochondrial permeability transition pores (mPTP) to open, releasing succinate, mitochondrial DNA, and cytochrome C. These substances can cause necrosis and apoptosis

and can act as danger associated molecular patterns (DAMPs) (Mills et al., 2017, Krysko et al., 2011). These molecular sequalae have a range of downstream consequences.

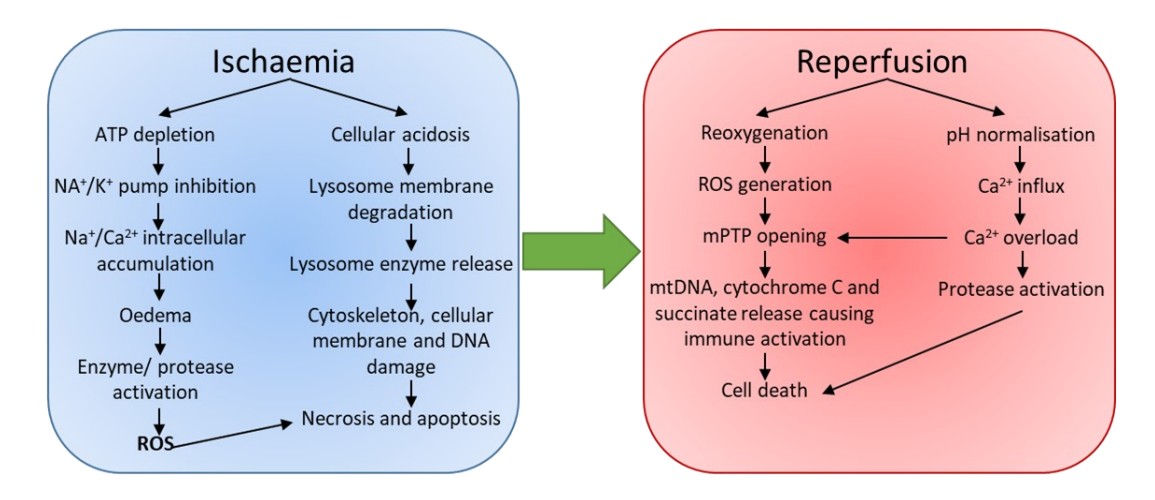


Figure 1.3 Schematic summary of the mechanisms of ischaemia reperfusion injury.

Ischaemia causes ATP depletion, followed by cellular swelling, lysosomal enzyme release and the production of small amounts of ROS. Upon reperfusion, oxygenation leads to further ROS production, mitochondrial dysfunction and protease activation ultimately causing cell death and immune activation. Adapted from (Nieuwenhuijs-Moeke et al., 2020).

#### 1.2.1.1 Cell-death

IRI leads to controlled and uncontrolled cell death. The most uncontrolled form of cell death is necrosis, a process in which cellular oedema causes rupturing of cell membranes and subsequent release of DAMPs into the extracellular space. Necrosis is most often a result of rapid ATP depletion, typically occurring during ischaemia (Hotchkiss et al., 2009).

Apoptosis is a controlled form of cell death where an initiator caspase can activate an effector caspase, such as caspase-3, through proteolytic cleavage following binding to an activator complex. Proteolytic degeneration of intracellular components by caspase-3 or caspase-7 via the executor pathway cause the physical processes of apoptosis including chromatin condensation, cell shrinkage and cytoplasmic bleb formation (Elmore, 2007). Apoptosis occurs via three pathways that all converge at the execution pathway, these are the extrinsic and intrinsic pathways and the perforin/granzyme pathway. The intrinsic pathway is activated via intracellular signals and is mitochondria dependant. The extracellular pathway is activated by extracellular signals and is cell death receptor pathway dependant. In both of these pathways, caspases-3, and -7 are the 'executioner' caspases (Elmore, 2007). The perforin/granzyme pathway is mediated through cytotoxic T-cells which release granzyme A and B enzymes that

induce cell death, with caspase-3 being the 'executioner' caspase (Chowdhury and Lieberman, 2008). The apoptosis pathways and physiological processes of apoptosis are summarised in **Figure 1.4**.

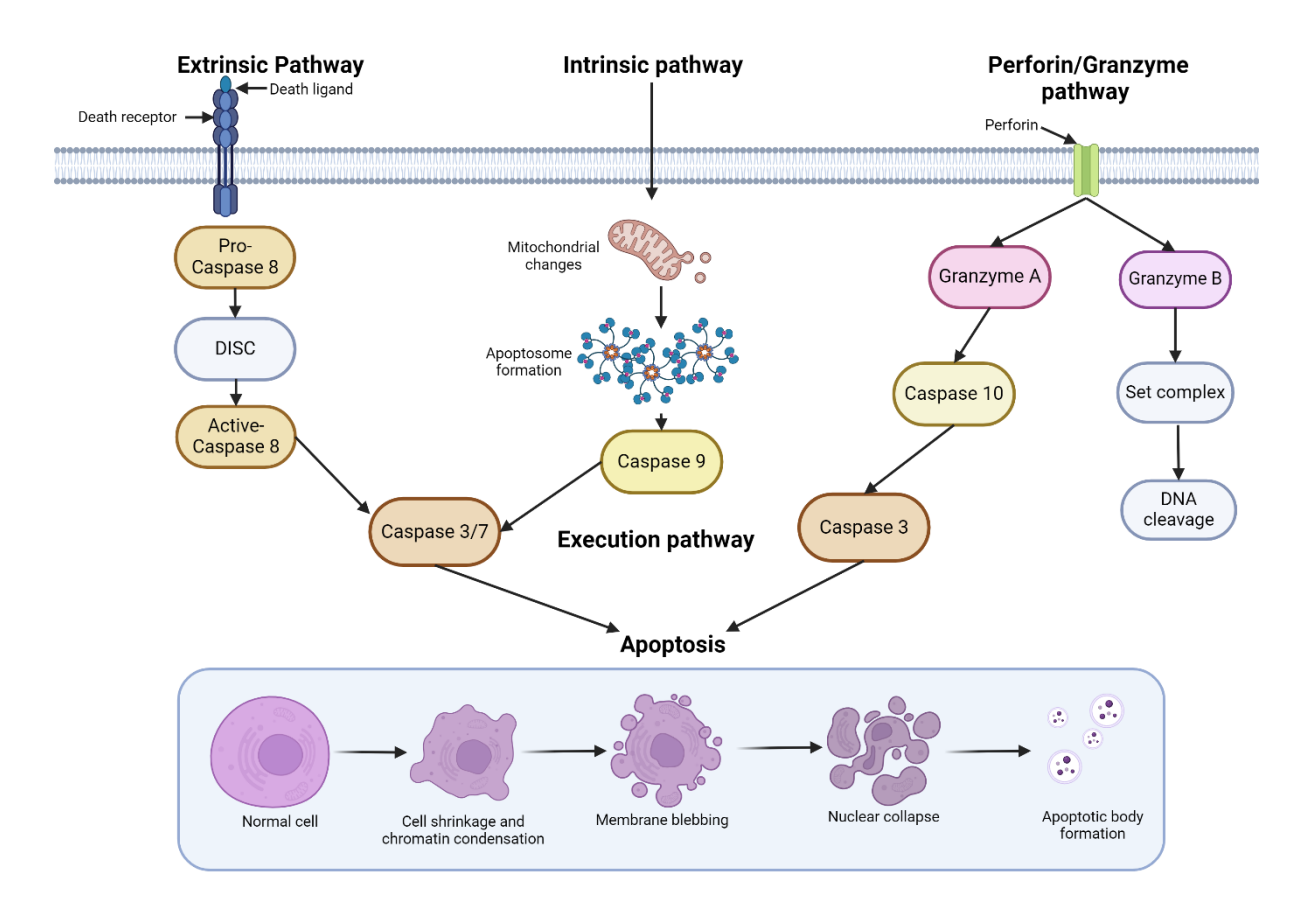


Figure 1.4 The pathways and morphological processes of apoptosis.

The intrinsic and extrinsic pathways are the two main apoptosis pathways, with the perforin/granzyme pathway being the third. The triggering event for each pathway is different and begins an energy dependant cascade through a different initiator caspase (8, 9 and 10). The execution pathway is common to all pathways and leads to the characteristic morphological changes.

Necroptosis is a cell death programme which exhibits morphological features of both necrosis and apoptosis and is mediated by death receptors, toll-like receptors (TLR) and interferon  $\alpha$ ,  $\beta$  and  $\gamma$  (Dempsey, 2013). Necroptosis involves cellular oedema and subsequent rupturing of the cell membrane when the caspase-8 dependant pathway of apoptosis is blocked. Necroptosis relies on activation of receptor-interacting protein kinase 3 (RIPK3) by immune ligands. Activated RIPK3 phosphorylates mixed lineage kinase domain-like pseudokinase (MLKL) which can accumulate at the cellular membrane and bilipid membrane of organelles,

disturbing cellular integrity and leading to the release of DAMPs into the extracellular space (Dhuriya and Sharma, 2018).

Autophagy is a controlled process in which individual damaged cellular components can be removed to prevent cell death. In autophagy, autophagosomes envelop damaged or unused cellular components for transport through the cytoplasm, following which they fuse with lysosomes to degrade cellular components. Autophagy is a process which happens continuously to maintain homeostasis, but can be upregulated following stimulation from ROS, hypoxia, free amino acids and nutrient deprivation (Kroemer et al., 2010). Autophagy can exert protective effects in IRI due to the restoration of homeostasis. However, very severe ischaemic injury can lead to excessive autophagy which can further aggravate injury (Decuypere et al., 2015).

#### 1.2.1.2 Endothelial dysfunction

IRI has a number of effects on the vascular endothelium. Endothelial cells swell, glycocalyx is lost and the cytoskeleton is degraded. Consequentially, intercellular contact between endothelial cells is compromised, leading to increased vascular permeability and fluid leakage into the interstitium (Goligorsky et al., 2004). Vasoconstriction can occur due to the release of vasoactive substances from the endothelium such as endothelin-1 (ET-1) and platelet-derived growth factor (PDGF) and is enhanced by a reduction in nitric oxide during the reperfusion period (Kwon et al., 2009, Faller, 1999).

Enhanced leukocyte-endothelium interaction is also a feature of IRI. Endothelial P-selectin expression is increased during IRI and facilitates leucocyte chemotaxis to the site of injury, followed by 'rolling' on the endothelium through interaction with P-selectin glycoprotein 1 which is expressed on leucocytes. Intracellular adhesion molecule 1 (ICAM-1) expressed on the endothelium enables firm adherence of leucocytes. Transmigration of cells to the interstitium is facilitated by platelet endothelial cell adhesion molecule 1 (PECAM-1). Following this, activated leucocytes will increase oedema, thrombosis, cell death and vascular permeability through the release of substances such as ROS, cytokines and proteases (Nieuwenhuijs-Moeke et al., 2020).

## 1.2.2 The innate immune response to ischaemia reperfusion injury

The innate immune system consists of cellular components such as neutrophils, macrophages, natural killer cells, dendritic cells and soluble serum-based proteins of the complement system (Friedewald and Rabb, 2004). The TLR family of trans-membrane pattern recognition receptors are expressed on innate immune cells where they transduce signals following ligation of DAMPs and pathogen-associated molecular patterns (PAMPs) (Hadley et al., 2007, Yu et al., 2006). DAMPs, which are usually invisible to the immune system, are released from cells and displayed on cell surfaces due to hypoxia during ischaemia. Intracellular and extracellular DAMPs are capable of binding TLRs, with TLR upregulation seen in the ischaemic kidney independent of any immune response (Yu et al., 2010). This interaction stimulates events key to the innate immune response including cytokine and chemokine release and can influence adaptive immunity by promoting antigen uptake and presentation, which in turn modulates T- and B-cell responses of adaptive immunity (Sobek et al., 2004).

Myeloid cells are recruited rapidly to the transplanted organ following reperfusion (Miyazawa et al., 2002, Ysebaert et al., 2000). Within the graft, neutrophils release chemokines which influence T-cell priming and infiltration and other inflammatory mediators such as ROS and proteases (Friedewald and Rabb, 2004). Macrophages constitute a major proportion of infiltrating immune cells following IRI (Li et al., 2008). Classically activated M1 macrophages release pro-inflammatory mediators, whereas alternatively activated M2 macrophages are anti-inflammatory, although can promote fibrosis through the secretion of pro-fibrotic factors (Vernon et al., 2010). In the ischaemically injured organ, pro-inflammatory mediators such as INF-γ polarise infiltrating macrophages which differentiate from monocytes to the M1 form (Gordon, 2003). PAMPs and DAMPs can then activate macrophages through TRL2 and TRL4 to release pro-inflammatory cytokines and chemokines and ROS while inducing renal fibrosis, neutrophil activation and epithelial apoptosis (Shigeoka et al., 2007, Chen et al., 2011).

#### 1.2.3 The adaptive immune response to ischaemia reperfusion injury

The adaptive immune response follows the rapid, non-specific innate immune system and is mediated by lymphoid cells including B- and T-cells. T-cells rapidly infiltrate organs upon reperfusion where they have a pathogenic role causing tissue damage and inflammation (Ascon et al., 2006). T-cells recognize donor cells via their receptors, which bind to major histocompatibility complex (MHC) molecules called human leucocyte antigens (HLA) that are

expressed on donor cells. T-cells are involved in both direct and indirect recognition of HLAs. Direct recognition occurs when T-cell receptors bind intact HLAs expressed on donor cells, while indirect recognition occurs when HLA are peptides presented by antigen presenting cells (APCs) including macrophages, dendritic cells and B-cells. They also recognise intact HLAs presented by dendritic cells which is important in graft rejection in the immediate period post-transplant (Kumbala and Zhang, 2013).

Chemokines cause an accumulation of B-cells in the kidney during IRI, where they are activated by T-cells and complement (Kreimann et al., 2020). The long-term alloimmune response can be modulated by B-cells through activation of memory B-cells, which can rapidly activate and differentiate to plasma cells to produce specific antibodies (Cornell et al., 2008). B-cells also express TLRs which can recognise DAMPs, leading to the previously mentioned inflammatory events (Barr et al., 2007). Following IRI, B-cells can act directly upon kidneys and affect the T-cell response through antigen presentation and production of cytokines.

B-cells also play a major role in chronic and acute antibody mediated rejection (ABMR) caused by donor specific antibodies (DSA). DSAs are antibodies specific to a donor's HLA which can form in the recipient pre- and post-transplant and are present in up to 40% of recipients waiting for a transplant as anti-HLA antibodies (Schmitz et al., 2020). Preformed DSAs in sensitised patients such as those who have been pregnant, had a blood transfusion or a previous transplant can cause hyperacute rejection. DSAs that are formed *de novo* can cause late acute ABMR, chronic ABMR or transplant glomerulopathy.

Interplay between the adaptive and innate immune systems is demonstrated by B-cell binding to fragments of C3, the main component of the complement system, which leads to enhanced B-cell activity through CR1 and CR2 (Dunkelberger and Song, 2010).

#### 1.3 THE COMPLEMENT SYSTEM

The complement system, part of the innate immune system, is the first line of defence following mucus found at mucosal surfaces, in protecting the body from bacteria and removing aberrant host cells. It consists of multiple soluble plasma proteins, mainly produced in the liver, and cell surface membrane proteins that, when activated, work together to produce enzymatic cascades to induce inflammatory pathways. An important consequence of complement is the deposition of complement activation fragments on tissue surfaces in a process called opsonisation, which enables the formation of convertases and assists phagocytosis and the clearance of apoptotic cells. To avoid inappropriate damage to host cells, these cascades are tightly regulated by regulatory plasma and membrane-bound proteins that work at multiple points throughout the cascades. Dysregulation leading to either excessive, or insufficient complement activation can cause harm to the host, leading to autoimmune and inflammatory illness, or increased susceptibility to infection (Barnum and Schein, 2018).

Three main activation pathways exist within the complement system: the alternative, classical and lectin pathways. They mediate a range of immunomodulatory processes, and are classified according to their mechanism of activation, with all three converging on a common terminal complement pathway which ultimately causes cell lysis. Notably, all activation pathways lead to cleavage of the central complement protein, C3.

#### 1.3.1 The classical pathway

The classical pathway (CP) of complement is activated when specific pattern recognition molecules interact with target molecules. C1q, a protein complex, is the recognition molecule of the CP. CP activation occurs when C1q, as part of the C1 complex with C1r and C1s (C1r<sub>2</sub>-C1s<sub>2</sub>), binds to target molecules including immune complex bound IgG and/or IgM. This binding leads to the autoactivation of C1r which then cleaves C1s, activating it. The activated C1s then cleaves C4 and C2 to C4b, C2a, C4a and C2b fragments. C4b and C2a are able to form the C3 convertase C4bC2a on target surfaces which can cleave C3 to C3a and C3b and allowing the formation of the C5 convertase C4bC2aC3b (Barnum and Schein, 2018).

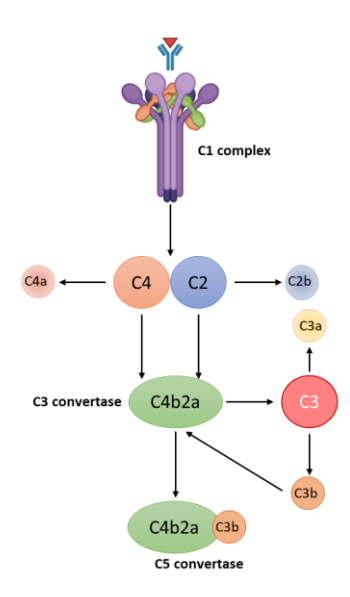


Figure 1.5 The classical pathway of complement activation.

The C1 complex is activated through binding of C1q to target antigen-antibody complexes. This leads to the cleavage of C1s and C1r, activating them and allowing C1s to cleave C4 and C2. C4b and C2a form the C3 convertase C4bC2a. C4bC2a cleaves C3 molecules to C3a and C3b. C3a is an anaphylatoxin while C3b can bind C4bC2a to form the C5 convertase C4bC2aC3b.

## 1.3.2 The lectin pathway

The function of the lectin pathway (LP) is similar to that of the CP in that it is activated through the interaction of specific pattern recognition molecules with their targets, although LP activation is immunoglobulin independent. Macromolecular protein complexes: mannan-binding lectin (MBL), ficolins and collectin are the pattern recognition molecules of the LP. They bind to PAMPs, or to aberrant glycocalyx patterns on necrotic or apoptotic self-cells. These protein complexes are then able to form complexes with MBL-associated serine proteases 1 and 2 (MASP-1 and MASP-2). This is analogous to the binding of C1r and C1s to C1q. MASP-1 activation leads to the activation of MASP-2 and subsequent cleavage of C4 and C2, at which point the lectin pathway follows the same steps as the classical pathway, ending in MAC formation and anaphylatoxin release (Barnum and Schein, 2018).

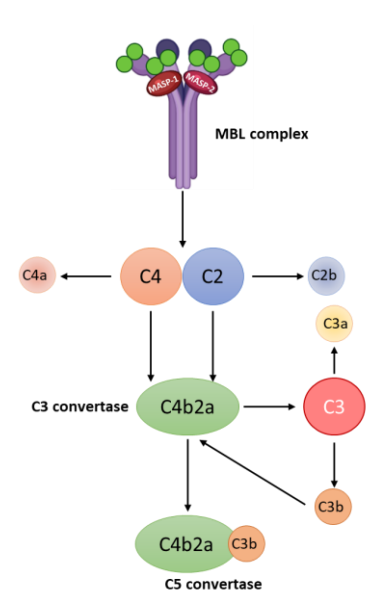


Figure 1.6 The lectin pathway of complement activation.

The lectin pathway is activated through MBL, ficolins or collectins binding to specific sugars on cell membranes. MASP-1 and MASP-2 form a complex with MBL leaving to their cleavage/activation. They then cleave C4 and C2. C4b and C2a form the C3 convertase C4bC2a. C4bC2a cleaves C3 molecules to C3a and C3b. C3a is an anaphylatoxin while C3b can bind C4bC2a to form the C5 convertase C4bC2aC3b.

## 1.3.3 The alternative pathway

The alternative pathway (AP) is constantly activated at a low level in order to maintain homeostasis and monitor for pathogen infiltration. The labile thioester bond of C3 is spontaneously hydrolysed to form C3(H<sub>2</sub>O) in a process known as 'tickover' (Pangburn et al., 1981). The conformational change brought about by this hydrolysis exposes a binding site for factor B (FB). Bound FB is then cleaved by the serine protease factor D (FD) to Bb and Ba, resulting in the formation of the unstable fluid phase C3 convertase C3(H<sub>2</sub>O)Bb (Forneris et al., 2010). C3(H<sub>2</sub>O)Bb cleaves C3 to C3b and C3a. Small quantities of C3b generated in this way bind hydroxyl groups of adjacent surfaces with avidity dependent on surface composition. In the absence of activating surfaces, C3b molecules are degraded (Barnum and Schein, 2018).

When pathogens are present, the fluid phase generated C3b will bind FB after covalently attaching to the activating surface. FB is then cleaved by FD, resulting in the formation of the AP C3 convertase C3bBb which is stabilised by properdin (Fearon and Austen, 1975, Forneris et al., 2010). C3bBb cleaves further C3 molecules to C3b and C3a. These C3b molecules can then go on to form more C3bBb complexes, and so on in the 'amplification loop'. C3b molecules formed by CP and LP activation can also participate in this amplification loop. They can also bind to C3bBb molecules to form the alternative pathway C5 convertase, C3bBb3b (Barnum and Schein, 2018).

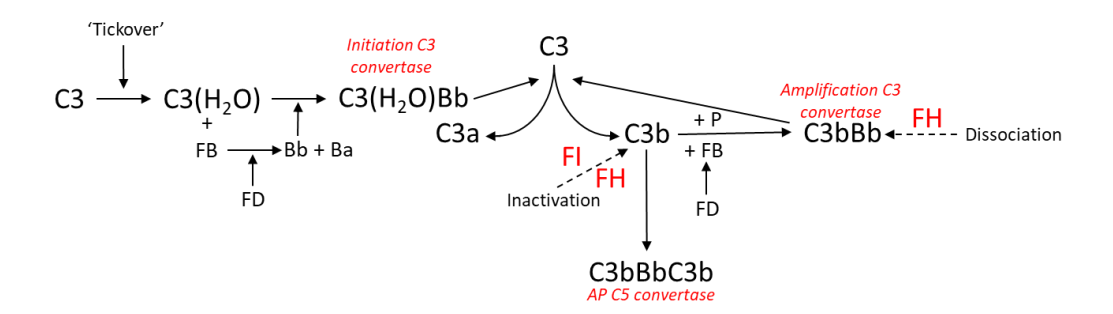


Figure 1.7 The alternative pathway of complement activation.

Spontaneous hydrolysis of C3 to C3( $H_2O$ ) activates the AP. FB bound to C3( $H_2O$ ) is cleaved by FD forming Bb and Ba. Bb binds C3( $H_2O$ ) to form the initiation C3 convertase C3( $H_2O$ )Bb. This convertase cleaves C3 molecules to C3b and C3a. C3b molecules formed this way that attach to an activating surface will bind FB which is cleaved by FD. This convertase is then stabilised by properdin and goes on to cleave more C3 molecules in the 'amplification loop'. These C3b molecules can also form a C5 convertase C3bBbC3b.

It is important to note that the complement pathways do not operate totally independent of each other. The AP plays an important role in the amplification of the CP and LP through the actions of the amplification loop. This occurs as C3b molecules produced through LP and CP activation are able to bind FB, which, through cleavage by FD, forms the AP C3 convertase C3bBb. Furthermore, AP blockade has been demonstrated to lead to a reduction in terminal complement activity of over 80% following activation of the CP (Harboe et al., 2004).

## 1.3.4 The terminal pathway

The C5 convertase cleaves complement protein C5 to C5a and C5b. C5a is a pro-inflammatory anaphylatoxin. Upon cleavage, conformational changes within the C5b fragment allow it to bind C6, followed by C7, leading to the formation of the C5b-7 complex. This complex associates with the surface membrane of target cells. Following incorporation of C8 into the complex, the C8 can penetrate the lipid bilayer of the target surface membrane. Multiple C9 molecules then associate with the C5b-8 complex to begin pore formation, disrupting cell membrane integrity and structure and often leading to cell lysis (Barnum and Schein, 2018).

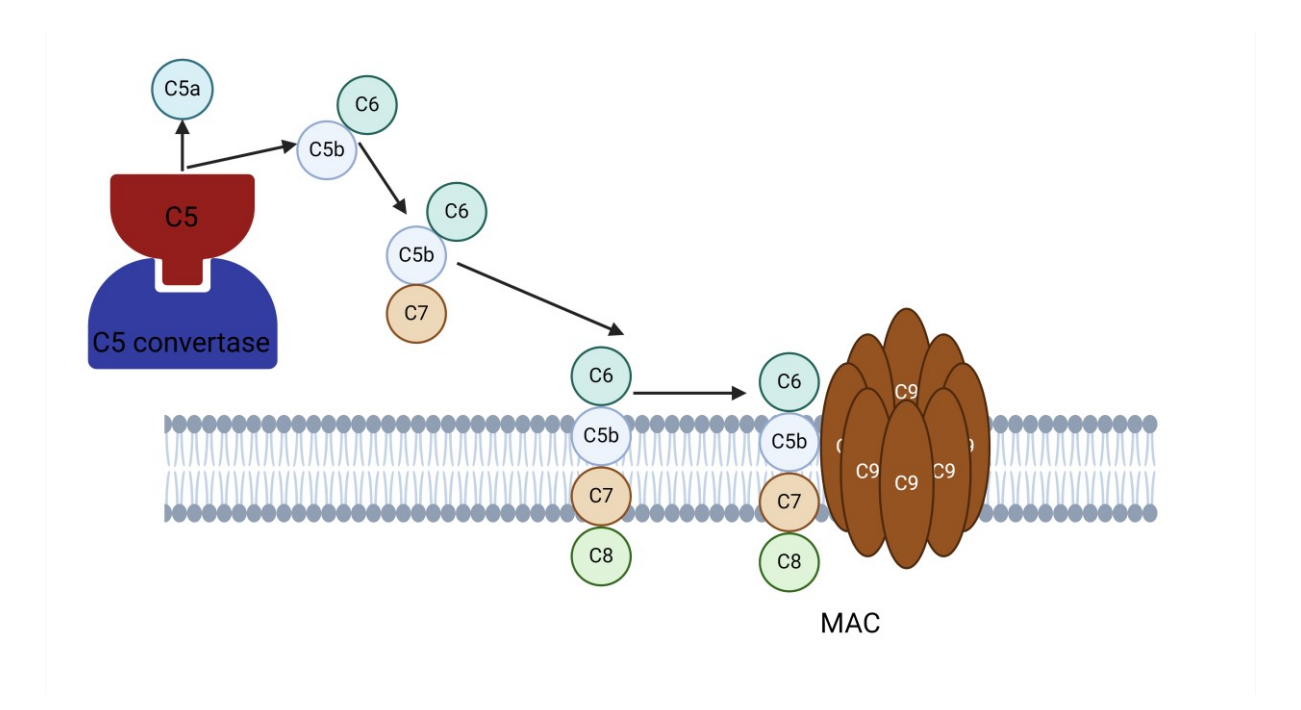


Figure 1.8 The formation of the membrane attack complex.

Complement proteins C5b-C9 form the MAC via the terminal pathway of complement. MAC, anaphylatoxin and opsonin production is a consequence of all three complement activation pathways.

## 1.3.5 Complement receptors

Complement receptors are a group of transmembrane proteins expressed on cells of the innate and adaptive immune system which carry out complement mediated effector responses including, phagocytosis, immune response modulation, and cell adhesion and migration. Activated, proteolytically cleaved complement fragments engage complement receptors such as the C3 active fragments C3b, iC3b and C3dg, and the anaphylatoxins C3a and C5a. The complement receptors fit within four structural categories: short consensus repeat (SCR) domain single-pass transmembrane receptors, G-coupled protein receptors,  $\beta_2$  integrins and complement receptors of the immunoglobulin superfamily (CRIg) (Santos-López et al., 2023, Holers, 2014). The complement receptors are summarised in **Table 1.1**.

Complement	Ligand	Structural class	Function
receptor			
CR1	C3b, C4b, C3	single-pass	Immune regulation, immune
	convertase, C5	transmembrane	complex clearance, phagocytosis
	convertase,	receptors	
	iC3b, C3d(g)		
	MBL, C1q		
CR2	iC3b, C3d(g),	single-pass	B-cell proliferation
		transmembrane	
		receptors	
CR3	iC3b, C3d(g),	β <sub>2</sub> integrin	Phagocytosis, ROS synthesis
	ICAM-1, ICAM-		
	2, fibrinogen,		
	plasminogen		
CR4	iC3b, ICAM-1,	β <sub>2</sub> integrin	Phagocytosis, leucocyte
	VCAM-1,		adherence
	fibrinogen		
C3aR	СЗа	G protein-	Chemotaxis, ROS production
		coupled	
		receptor	
C5aR	C5a	G protein-	Chemotaxis, cytokine release,
		coupled	degranulation, ROS synthesis
		receptor	
C5L2	C5a	G protein-	
		coupled	
		receptor	
CRIg	C3b, ic3b	Immunoglobulin	Immune complex/pathogen
		superfamily	clearance

Table 1.1 Summary of complement receptors.

The ligand, structural family and function of complement receptors are briefly summarised. Abbreviations: Vascular cell adhesion protein 1 (VCAM-1), C3a receptor (C3aR), C5a receptor (C5aR).

## 1.3.6 Complement regulators

Complement activity must be regulated to prevent excessive damage to self-cells. Complement regulators are a group of SCR based proteins (with the exception of CRIg which is made from immunoglobulin domains) that reside at the cell membrane, or are plasma based. At the first stages of complement activation, commonly the recognition of PAMPs and DAMPS, C1 inhibitor (C1INH), a serine protease, can bind to the protease elements of the CP and LP activation complexes, preventing them from cleaving C4. The second level of regulation exists following cleavage of C3 and C4. Factor I (FI) can halt the complement cascade by breaking down C3b and C4b, alongside cofactors; membrane cofactor protein (MCP), complement regulator 1 (CR1), factor H (FH) and C4-binding protein (C4BP). At the third level of complement regulation, the decay of the complement convertases is accelerated by decay accelerating factor (DAF), CR1, C4BP and FH, preventing cleavage of C3 and C5. Finally, CD59, vitronectin and clusterin can prevent formation and insertion of the MAC (West et al., 2024). Negative complement regulatory proteins are summarised in Table 1.2 (Zipfel and Skerka, 2009, Barnum and Schein, 2018).

More recent work has identified the FH related proteins (FHRs) that can act as positive regulators, which are discussed in 1.5.2. Furthermore, properdin is a positive regulator of the AP, stabilising the AP convertase.

Regulator	Location	Function
C1-INH	Plasma	Inactivation of C1r, C1s, MASP-1 and MASP-2
МСР	Cell membrane	Cofactor for FI
DAF	Cell membrane	Decay accelerating activity of the C3 and C5
		convertase of the CP and AP
CR1	Cell membrane	Decay accelerating activity, cofactor for FI
С4ВР	Plasma	Decay accelerating and cofactor for FI
FH	Plasma	Decay accelerating, cofactor for FI
FI	Plasma	C3b and C4b degradation
CD59	Cell membrane	Prevents MAC formation
Vitronectin	Plasma	Prevents MAC formation
Clusterin	Plasma	Prevents MAC formation

Table 1.2 Summary of negative complement regulators.

Table adapted from Noris and Remuzzi, 2019 (Noris and Remuzzi, 2013).

## 1.3.7 Complement therapeutics

Complement dysregulation due to excessive activation or insufficient regulation can cause unwanted inflammation and immune responses which can induce complement-mediated diseases. *De novo* or acquired mutations leading to deficient, reduced or aberrant complement components can cause disease, those most classically associated with complement dysregulation being C3 glomerulopathy (C3G), atypical haemolytic syndrome (aHUS), age-related macular degeneration (AMD) and paroxysmal nocturnal haemoglobinuria (PNH). Sometimes, complement mediated diseases can be triggered by bacterial infections such as Shiga toxin-producing *escherichia coli* haemolytic uremic syndrome (STEC-HUS) or *Pneumococcal* HUS (Wong and Kavanagh, 2018). Furthermore, complement can drive pathology in more common diseases including IRI, coronavirus disease 2019 (COVID-19), rheumatic diseases and atherosclerosis (West et al., 2024).

In complement associated diseases, complement regulating therapeutics can be employed to reduce pathogenic complement activation and associated consequences. The most successful and well-known treatment is Eculizumab, an anti-C5 antibody used to treat atypical aHUS and PNH (Socié et al., 2019). More recently Ravulizumab, an anti-C5 antibody similar to eculizumab

but with a longer half-life due to bioengineered changes that allow recycling from the lysosomal pathway and better residency on neonatal Fc receptors has been developed. It has since been introduced as a replacement to Eculizumab (Kulasekararaj et al., 2022, Syed, 2021). Danicopan, a FD inhibitor was approved for use as an add-on therapy to Eculizumab and Ravulizumab to treat PNH (Lee et al., 2023), while Iptacopan, a FB inhibitor has been approved for use in patients with PNH (Latour et al., 2024). However, despite the success of Eculizumab and clear evidence of complement dysregulation across a broad range of diseases, the number of FDA approved complement regulators remains limited (West et al., 2024). These treatments are summarised in **Table 1.3**.

Therapeutic	Mechanism of action	Target disease
Eculizumab	Anti-C5 antibody	PNH (Hillmen et al., 2006),
		aHUS (Legendre et al., 2013),
		NMOSD (Pittock et al.,
		2022), and adult anti-AchR-
		positive gMG (Howard et al.,
		2017)
Ravulizumab	Anti-C5 antibody	PNH (Kulasekararaj et al.,
		2022), aHUS (Syed, 2021),
		and adult anti-AchR-positive
		gMG (Vu et al., 2023)
Sutimlimab	Anti-C1s antibody	CAD (Röth et al., 2021)
Vilobelimab	Anti-C5a antibody	COVID-19* (Vlaar et al.,
		2022)
Avacopan	C5aR1 antagonist	AAV (Jayne et al., 2021)
Pegcetacoplan	C3 small peptide inhibitor	PNH (de Latour et al., 2022),
		GA secondar to AMD (Heier
		et al., 2023)
Danicopan	Anti-FD antibody	PNH (Lee et al., 2023)
Iptacopan	Anti-FB antibody	PNH (Latour et al., 2024)

Table 1.3 Summary of FDA approved complement therapeutics (as of October 2024).

Abbreviations: Neuromyelitis optica spectrum disorder (NMOSD), acetylcholine receptor antibody (AchR), generalised myasthenia gravis (gMG), cold agglutinin disease (CAD), C5a receptor 1 (C5aR1), ANCA-associated vasculitis (AAV), geographic atrophy (GA).

#### 1.4 COMPLEMENT IN ISCHAEMIA REPERFUSION INJURY

### 1.4.1 Complement activation exacerbates ischaemia reperfusion injury

During IRI, DAMPs are released from damaged tissue while formation of neoantigens and immune complexes also occurs. This can lead to activation of all three complement pathways (Danobeitia et al., 2014). MAC formation causes direct lysis of tubular epithelial cells (Zhou et al., 2000). The anaphylatoxins C3a and C5a cause infiltration of immune cells and proinflammatory cytokine and ROS release, they then cause further activation of the incoming immune cells (Peng et al., 2012). C3aR/C5aR ligation causes activation of the endothelium and tubular epithelium, which alongside activated macrophages, will release pro fibrotic factors TGF- $\beta$  and platelet derived growth factor (PDGF), activating fibroblasts (Boor et al., 2007, Bao et al., 2011). In proximal tubular epithelial cells, TGF- $\beta$  can downregulate C3 and C5 (Gerritsma et al., 1998), however in small airway epithelial cells, it reduces C3aR/C5aR expression(Gu et al., 2014).

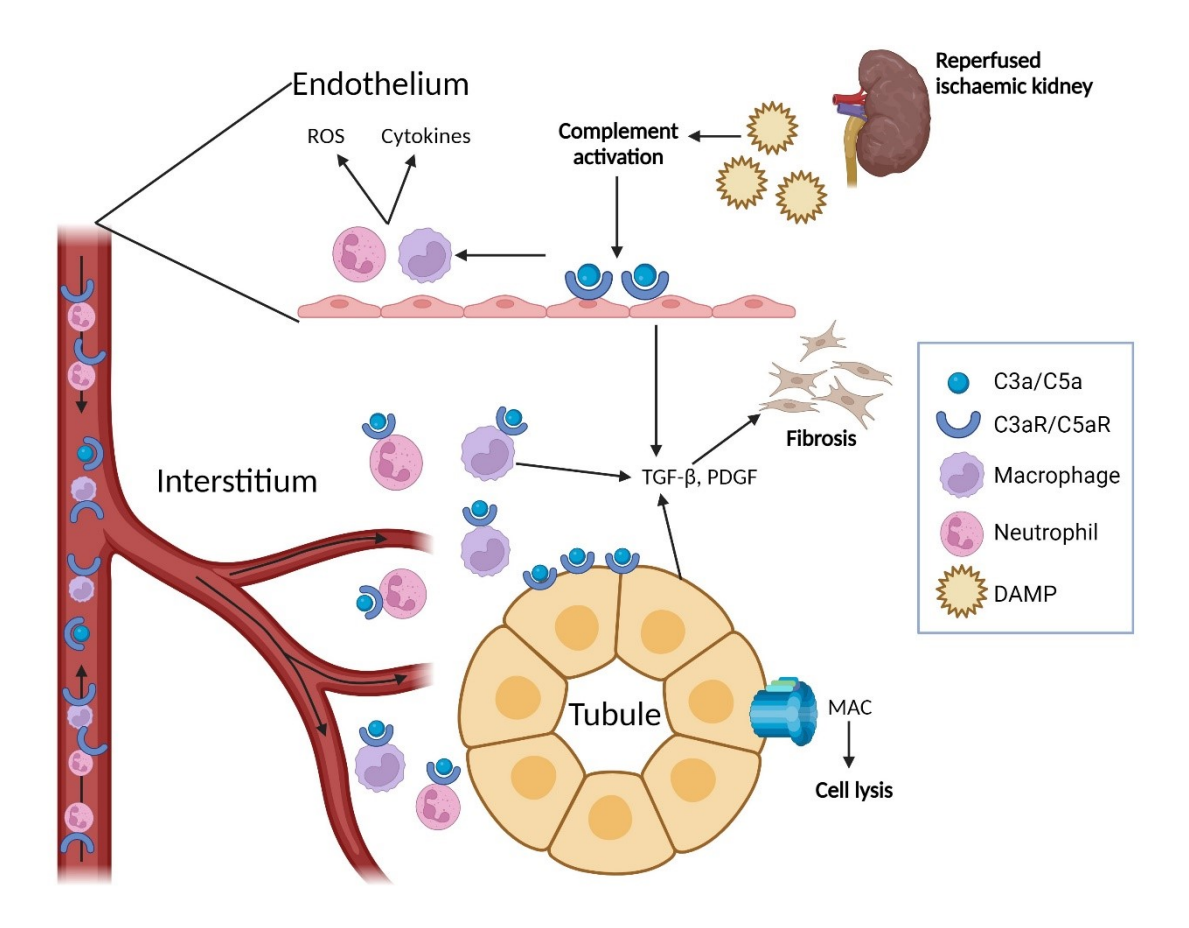


Figure 1.9 The role of the complement system in ischaemia reperfusion injury.

Ischaemically damaged kidneys release DAMPs that activate all three complement pathways. The anaphylatoxins C3a and C5a bind their respective ligands C3aR and C5aR on leucocytes, endothelial cell and tubular epithelial cells leading to the infiltration of leucocytes which release cytokines and ROS. Activated monocytes, tubular epithelial cells and endothelium also release pro-fibrotic factors PDGF and TGF-B Formation of the MAC directly lyses tubular epithelial cells.

During IRI, the complement system plays a crucial role in regulating adaptive immunity. CR2, present on follicular dendritic cells (FDCs) and B-cells, detects antigens opsonised by C3d. The interaction between C3d-opsonised antigen and CR2 aids in retaining the target antigen on FDCs within B-cell zones of lymphoid tissue and enhances the stimulation of B-cells (Carroll and Isenman, 2012). Additionally, the relationship between the complement system and T-cell activity has been demonstrated in mice deficient in DAF who exhibit increased complement activation and heightened T-cell responses upon antigen reintroduction (Liu et al., 2005). Furthermore, C5a can directly bind to C5aR on APCs and T-cells, impacting T-cell immunity (Cravedi et al., 2013, van der Touw et al., 2013).

Complement activation is also linked with the coagulation pathway. When activated, the coagulation pathway ultimately leads to production of factor Xa, which with factor Va, cleaves prothrombin to thrombin. Thrombin converts fibrinogen to fibrin, causing fibrin-mediated blood clots (Grover and Mackman, 2019). The structure of the catalytic domain of thrombin is similar to MASP-1, meaning MASP-1 can also cleave fibrinogen and other components of the coagulation cascade, including factor XIII and thrombin activatable fibrinolysis Inhibitor (Matsushita et al., 2013). Furthermore, MASP-2 can generate thrombin through prothrombin cleavage (Krarup et al., 2007).

Conversely, the coagulation system can lead to activation of the complement system. Kallikrein, a protease of the coagulation system, can release C5a, directly cleave C3 and cleave FB, activating C3 convertase formation (Wiggins et al., 1981, DiScipio, 1982, Thoman et al., 1984). Additionally, thrombin can proteolytically cleave C5, generating C5a and C5b, while coagulation components FIXa, FXa, FXIa, thrombin and plasmin can cleave both C3a and C5a. Furthermore, platelet activation and P-selectin release, downstream effects of the coagulation cascade, can also activate the complement system (Del Conde et al., 2005).

The complement system also has interactions with hypoxia-inducible factor (HIF) which is involved in the protective cellular adaptation to hypoxia. HIF-1 transcription factor activation in hypoxic cells is a key pathway of this protective mechanism (Liu et al., 2022). The subunit HIF-1 $\alpha$  leads to an increase in C3 and C5b-9 deposition on glomerular endothelial cells (Qi et al., 2022).

#### 1.4.2 Clinical evidence of the involvement of complement in ischaemia reperfusion injury

Complement dysregulation has been implicated in the pathogenesis of ischaemia reperfusion injury in the clinical setting. Complement activation begins in the brain-dead donor prior to organ retrieval, with elevated systemic complement activation seen in deceased donors (Damman et al., 2015). This complement activation does have consequences for recipients as donor plasma levels of MAC are associated with acute rejection and worse graft function in the recipient (Damman et al., 2011, Błogowski et al., 2012). More specifically, brain death is associated with increased donor plasma C5a and increased C5aR expression in kidneys, when compared to living donors, which mediates renal inflammation via the C5/C5aR axis (van Werkhoven et al., 2013). Increased expression of complement-regulated genes is also seen in brain dead donors and is correlated with poor graft function (Naesens et al., 2009).

Furthermore, traumatic injury can lead to rapid complement activation and dysfunction in donors which will include a proportion of deceased donors (Burk et al., 2012).

## 1.4.3 Animal models investigating complement and ischaemia reperfusion injury

IRI of the kidney can be modelled in live mice through clamping and then unclamping of renal arteries and veins under anaesthetic. This model has been utilised to evaluate the role of complement in the response to IRI by using mice that lack specific key complement components. Mice deficient in C3 have improved responses to IRI through a reduction in immune cell infiltration and improved kidney function associated with less morphological injury (Zhou et al., 2000, Sheerin et al., 2008, Pratt et al., 2002). However, when C3<sup>-/-</sup> mice receive a kidney transplant from a wild type (wt) mouse, they experience poor graft survival, similar to that seen in wt mice with wt kidneys (Pratt et al., 2002). Conversely, when C3<sup>-/-</sup> kidneys are transplanted into wt mice, they experience full recovery from IRI (Sheerin et al., 2008). These data show that the kidney is an important source of complement in IRI.

The improved kidney function associated with reduced morphological injury and immune cell infiltration noted in C5 and C6 deficient mice following IRI also indicates a role for the MAC in the pathogenesis of IRI (Zhou et al., 2000, Boor et al., 2007). Furthermore, the C3a/C3aR and C5a/C5aR ligand/receptor pairs have also been shown to promote IRI, as C3aR and C5aR deficiency attenuates IRI, with C5aR deficiency granting the most marked improvement, reducing inflammation, fibrosis, immune cell infiltration and improving kidney function (Peng et al., 2012, Bao et al., 2011). Conversely, DAF deficient mice experience enhanced T-cell responses following IRI which exacerbate disease severity, highlighting the importance of complement regulation (Liu et al., 2005).

FB deficient mice also have an improved response to renal IRI with reduced morphological injury, C3 deposition and neutrophil infiltration, implicating a key role for the AP in IRI (Thurman et al., 2003). The LP is also involved in IRI as mice deficient in MBL have reduced kidney injury following IRI with less C3 deposition, C3a (desArg) levels and tubular necrosis compared with wt mice (Møller-Kristensen et al., 2005). More recently, collectin-11 (CL-11), a soluble C-type lectin that binds serine proteases MASP-1, -2 and -3 has been associated strongly with the pathogenesis of IRI, with CL-11 deficient mice experiencing protection from IRI through reduced complement deposition (Farrar et al., 2016). Mice deficient in C4 and IgM

and IgG however, are not protected from IRI, suggesting that the CP, and to some extent the LP are not involved in IRI (Park et al., 2002, Zhou et al., 2000).

#### 1.4.4 Complement therapeutics for ischaemia reperfusion

Few complement inhibitors are approved for use clinically on humans, with none currently available for the treatment of IRI. To date, only three complement inhibitors have been trialled in humans for the prevention of IRI in kidneys. Eculizumab significantly prevents graft loss in patients with aHUS through regulation of uncontrolled complement activation which often is present in these patients (Glover et al., 2023). Furthermore, in a rat model of IRI, Eculizumab improved graft survival and DGF (Yu et al., 2016). However, in a non-aHUS transplantation patients, Eculizumab was unable to prevent DGF or improve graft function following transplantation when added to kidneys 'cold' prior to perfusion (Schröppel et al., 2020). Administration of Mirococept, a complement inhibitor derived from CR1, to kidney transplant recipients was also unsuccessful at improving graft outcomes. However, this could have been due to dosing issues as mirococept was undetectable in patients following transplant (Kassimatis et al., 2021). C1INH has been assessed as a treatment to prevent DGF through administration to transplant patients intraoperatively, then again at 24 hours following transplant. While C1INH administration did not meet the primary endpoint of the study which was a reduction in DGF, significantly fewer dialysis sessions were required in treated patients, while renal function was significantly better at 1-year post transplant. These improvements were most marked in those patients at the highest risk of DGF (Jordan et al., 2018).

A number of therapies have been assessed in animal models of renal IRI. These are summarised in **Table 1.4**. Silencing RNAs (siRNAs) can be used to reduce expression of complement components. C3 and C5aR siRNAs have successfully reduced expression of their respective targets, improving kidney function and morphological injury and reducing immune cell infiltration and inflammatory cytokine levels in mouse models of IRI (Zheng et al., 2006, Zheng et al., 2008). Antagonists targeting C5aR preventing the action of the C5a/C5aR axis have been used in mouse and rat IRI models to prevent injury (Gueler et al., 2008, Arumugam et al., 2003, de Vries et al., 2003a). Antibodies against key components of the complement pathways can be administered to inhibit the action of the complement cascade, as anti-FB and C5 antibodies have successfully ameliorated injury in mouse models of IRI (Thurman et al., 2006, de Vries et al., 2003b). Complement inhibitors have also been administered to kidneys

in a range of models. C1-INH has been administered in mouse and porcine models of IRI, and in a porcine auto transplant model with success improving kidney function, while reducing fibrosis, apoptosis and immune cell infiltration (Castellano et al., 2010, Danobeitia et al., 2017, Delpech et al., 2016). A modified fusion complement inhibitor, CRIg/FH reduced inflammatory cytokine levels, while reducing complement activation and morphological injury in a rat IRI model (Hu et al., 2018). CR1 administered to mice undergoing IRI led to improved renal function, and a reduced T-cell response (Pratt et al., 2003).

Treatment	Treatment	Mechanism of	Treatment outcome
category	name	action	
siRNA	C3 siRNA (Zheng	C3 silencing	Improved renal function, improved
	et al., 2006)		histopathology, ↓ TNF-α
	C5aR siRNA	C5aR silencing	Improved renal function, $\downarrow$ TNF- $\alpha$ ,
	(Zheng et al.,		CXCL2 and CXCL1, reduced neutrophil
	2008)		influx and cell necrosis
Antagonist	C5aR antagonist	Prevents	Reduced monocyte/macrophage and
	(Gueler et al.,	C5a/C5aR	neutrophil infiltration, improved graft
	2008,	binding	survival, kidney function and histology,
	Arumugam et		$\downarrow$ ICAM-1, TNF- $\alpha$ , MPO and AST,
	al., 2003, de		reduced vascular leakage and
	Vries et al.,		haematuria, reduced fibrosis
	2003a, Boor et		
	al., 2007)		
Antibody	Anti-FB	Inhibits FB	↓ C3b deposition and systemic C3a,
	(Thurman et al.,	activity	improved histology and kidney
	2006)		function, reduced apoptosis
	Anti-C5 (de	Inhibits C5	Improved renal function, ↓ MAC
	Vries et al.,	activity	formation and C3 deposition, ↓ CXCL2
	2003b)		and CXCL1, ↓ apoptosis, reduced
			neutrophil infiltration
Complement	C1-INH	Inhibition of C1	Improved renal function, ↓ C5a
inhibitors	(Delpech et al.,		release and C3b deposition, $\downarrow$ TGF- $\beta$ 1,
	2016,		IL-6, CXCL1 and MCP-1, reduced
	Castellano et		fibrosis and apoptosis, reduced
	al., 2010)		macrophage, t-lymphocyte and
			neutrophil infiltration, reduced EMT
	CRIg/FH (Hu et	CP and AP	Reduced apoptosis, improved
	al., 2018, Pratt	inhibition	histology, $\downarrow$ IL-1 $\beta$ , IL-4, IL-12p40, $\uparrow$ IL-
	et al., 2003)		4, TNF- $\alpha$ , IL-10 and IL-5, $\downarrow$ C3d, MAC
			↓ PI3K/Akt signalling

CR1 (Pratt et al.,	Decay	Improved renal function, reduced
2003)	accelerating	rejection and t-cell response, $\downarrow$ MPO,
	and CFA	↓ C3d and MAC

Table 1.4 Summary of treatments investigated in animal models of renal IRI.

Abbreviations: Tumour necrosis factor (TNF), chemokine CXC ligand 2 (CXCL2), chemokine CXC ligand 1 (CXCL1), myeloperoxidase (MPO), aspartate aminotransferase (AST), interleukin (IL), monocyte Chemoattractant Protein-1 (MCP-1), epithelial—mesenchymal transition (EMT), phosphatidylinositol 3-kinase (PI3K).

#### 1.5 FACTOR H

### 1.5.1 Factor H structure and function

As activation of the AP is ubiquitous and C3b deposition is not specific to non-self-cells it must be tightly regulated to avoid damage to the host. FH, the main regulator of the AP, is a soluble plasma glycoprotein containing 20 SCRs. It is synthesised predominantly by the liver and found in concentrations of around 200 -  $700\mu g/mL$  in plasma (Schwaeble et al., 1987, Makou et al., 2013). The gene for FH is on chromosome 1 within the Regulators of Complement (RCA) gene cluster (Rodriguez de Cordoba et al., 1985).

FH regulates the AP in several ways. FH prevents C3bBb formation through binding of C3b, stopping its association with FB. The first four SCRs of the N-terminal domain of FH bind C3b extensively over multiple C3b regions including the thioester domain and CUB domain (Makou et al., 2013). SCRs 19-20 on the carboxyl (C)-terminus are also able to recognise C3b and bind on a region proximal but distinct from that bound by SCRs 1-4, allowing FH to bind the same molecule of C3b at two different points (Morgan et al., 2011). The central region of FH (SCRs 8-15) is able to form a hinge like structure allowing FH to bend back on itself and allowing both SCRs 1-4 and 19-20 to bind C3b simultaneously. The configuration of FH can switch from a preferentially latent form with low C3b affinity, to an active conformation with high C3b affinity in the presence of C3b bound to self-cells (Makou et al., 2013).

FH binds self-cells specifically through SCRs 19-20 and 6-8. SCRs 19-20 recognise and bind both glycosaminoglycans (GAGs) and sialic acids, while SCRs 6-8 can bind only GAGs (Makou et al., 2013, Parente et al., 2017). FH has a higher affinity for C3b found on self/non-complement activator cells due to the presence of polyanions including sialic acid, sulphated heparin and GAGs found in abundance on mammalian cell surfaces. This allows for the continued activation and activity of the AP on activator cells including opsonisation and the formation of C3bBb, while protecting non-activator host cells.

Furthermore, FH disrupts the C3b amplification loop by accelerating decay of C3 and C5 convertases by displacing the C3b bound to Bb through electrostatic repulsion via steric hinderance mechanisms by FH's first four N-terminal complement SCRs (1-4) (Wu et al., 2009a).

FH also regulates AP activity by acting as a cofactor for FI, facilitating the cleavage of C3b to iC3b. The interaction between FH and C3b facilitates binding of the serine protease FI to C3b by providing a large binding surface proximal to the CUB domain, allowing for its proteolytic cleavage (Makou et al., 2013).

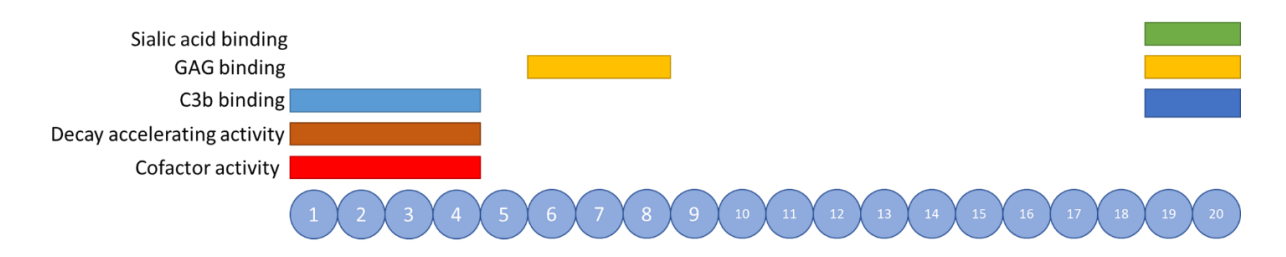


Figure 1.10 The binding sites of factor H.

The 20 contiguous SCRs of FH consist of around 60 amino acids and are connected by linkers. Different regions of the FH protein are responsible for different functional activities including GAG binding, sialic acid binding, C3b binding, decay accelerating activity and cofactor activity.

#### 1.5.2 Factor H related proteins

Five FH related (FHR) proteins exist, FHR-1, FHR-2, FHR-3, FHR-4 and FHR-5 that are encoded by the RCA gene cluster (Cantsilieris et al., 2018). Although the functions of the FHRs are not entirely characterised, their importance is indicated through the relationship between alterations in FHR genes and disease including IgA nephropathy, aHUS, AMD, C3G, and invasive meningococcal disease. The FHRs have homology with the surface recognition domains of FH, allowing them to bind C3 activation products, GAGs and heparin. While some evidence exists that large quantities of FHRs can control complement (Poppelaars et al., 2021), the primary established function of FHRs is antagonism of FH, preventing the complement regulatory activity of FH, enhancing AP activation (Hebecker and Józsi, 2012, Tortajada et al., 2013, Goicoechea de Jorge et al., 2013). FHRs -1, -2 and -5 can form homodimers and heterodimers through a dimerisation motif in their N-terminal domains which aids in the deregulation of FH (Goicoechea de Jorge et al., 2013). These dimers have the ability to bind complement fragments including C3b. C3 fragments which are bound to these dimers/heterodimers rather than FH, continue to be active, leading to dysregulation of complement and uncontrolled AP activation, leading to complement related disease. Patients with mutations altering CHFR genes, including duplicated dimerisation motifs, have an increased rate of deregulation, and can develop C3 glomerulopathy (Goicoechea de Jorge et al., 2013).

#### 1.5.3 Factor H in disease

FH deficiency in humans can lead to kidney disease including aHUS and C3G. Complement mutations account for around 50% of all aHUS cases which present as AKI, thrombocytopenia and microangiopathic haemolytic anaemia due to complement dysregulation (Goodship et al., 2017). Around 25% of complement-mediated aHUS cases stem from inherited FH mutations (Kavanagh et al., 2013). These mutations are generally heterozygous, leading not to a quantitative deficiency, but impaired surface binding of FH to GAGs, sialic acids and C3b due to mutations in the C-terminal domains of FH. The mutations are predisposing rather than directly causative, with penetrance being age related (64% at 70 years of age) (Kavanagh et al., 2013, Wong and Kavanagh, 2018). FH autoantibodies in acquired aHUS similarly predominately affect the FH C-terminal domains (Dragon-Durey et al., 2005).

C3G is an umbrella term encompassing a group of diseases including dense deposit disease (DDD) and C3G glomerulonephritis (C3GN) caused by uncontrolled complement activation leading to complement deposition in the glomerulus. These diseases differ depending on the density and location of complement deposits. Both diseases generally present as proteinuria, haematuria and progressive renal failure. Inherited abnormalities that lead to C3G often cause dysregulation of the AP in the fluid phase through quantitative deficiencies in FH leading to uncontrolled AP activation (Wong and Kavanagh, 2018). FH autoantibodies can also cause C3G and tend to impair FH function by binding the N-terminal domain (Zhang et al., 2012).

Recurrence of disease following transplantation is high in both aHUS and C3G. Eculizumab is currently used to treat complement mediated aHUS with reasonable success and has been shown to be effective in treating C3G in some cases (Licht et al., 2015, Bomback et al., 2012). Due to the role of abnormal FH in the development of aHUS and C3G, FH replacement therapies have the potential to be beneficial therapeutically. Administration of plasma containing functional FH has been previously successful in treating patients with deficiencies in FH. Upon receiving plasma therapy, in general renal function and haematological features of thrombotic microangiopathy improved, only to relapse on cessation of plasma therapy (Licht et al., 2005, Kim et al., 2011).

## 1.5.4 Mini factor H

The key FH SCRs involved in AP regulation and self-recognition in human FH possess the same properties in mouse FH, with high homology between FH of both species (Cheng et al., 2006). Considering the importance of these SCRs, a mini-complement FH construct was generated by Nichols et al., 2015 consisting of SCRs 1-5 of FH bound to SCRs 18-20 (FH<sup>1-5</sup>^18-20), molecular weight ~36-59kDa. This construct bound to both C3b and heparin, a function vital to both complement regulation and self-recognition. FH<sup>1-5</sup>^18-20 was found to protect C3b-coated sheep red blood cells (SRBCs) from lysis when incubated with FI to a greater extent than full length serum derived FH, confirming the ability of FH<sup>1-5</sup>^18-20 to act as a cofactor for FI in the inactivation of C3b. FH<sup>1-5</sup>^18-20 also displayed decay-accelerating activity similar to that of full-length FH through its ability to decay C3bBb, although it did not confer more protection to SRBCs in classical fluid phase assays.

FH<sup>1–5^18–20</sup> did not restore plasma C3 levels in  $CFH^{-/-}$  mice as effectively as full-length FH. A single intraperitoneal injection of 12 nmol increased plasma C3 to levels of around 20% of that seen in wild type animals 6hr post injection, compared with a 60% increase from a 3 nmol injection of FH. However, glomerular C3 staining was significantly reduced upon FH<sup>1–5^18–20</sup> injection with a similar efficacy to FH, although the dose of FH<sup>1–5^18–20</sup> given was 4x higher. A major difference between FH<sup>1–5^18–20</sup> and FH was serum half-life. Plasma FH<sup>1–5^18–20</sup> was only just detectable 6 hours post injection of 12 nmol, compared with FH plasma levels which had reduced only slightly at 6 hours following 3 nmol injection.

Despite having a 50-fold lower half-life than FH, some properties of FH<sup>1-5^18-20</sup> appear to confer positive benefits that could overcome deregulation by FHRs, an issue faced by FH. (Nichols et al., 2015) found that FH<sup>1-5^18-20</sup> is significantly more resistant to deregulation than FH. The occurrence of excessive complement activation in response to aseptic tissue injury in individuals with normally functioning FH indicates that FH can be overwhelmed, or that internal factors impair the ability of FH to regulate AP activation. Annexin 2 (A2) is one such factor. (Renner et al., 2016) identified that A2 binds FH, stopping fluid phase regulation, FI cofactor activity and preventing FH from binding to host surfaces. A2 deposition on tubular epithelial and outer medulla cells is increased following IRI and leads to increased complement activation. A2 - FH binding and inactivation could therefore be a factor in renal injury post-

transplant. A2 binds SCR' 6-8 of FH. Administration of  $FH^{1-5^{18-20}}$  could therefore potentially circumvent A2 – mediated FH binding and uncontrolled complement activation.

## 1.5.5 Homodimeric minimal-factor H

To improve the serum half-life of FH<sup>1-5^18-20</sup>, (Yang et al., 2018) introduced the first two Nterminal domains of FHR1 to either the C-terminus, or N-terminus of FH<sup>1-5^18-20</sup>, creating FH<sup>1-5^18-20R1-2</sup> and FH<sup>R1-21-5^18-20</sup> respectively, which had the potential to self-dimerise. The resulting homodimeric mini-FH (HDM-FH) constructs could be readily produced in CHO cells. Both HDM-FH constructs displayed increased cofactor activity in the fluid phase compared with FH<sup>1-5^18-20</sup> or FH when incubated with C3b and FI, with the greatest activity seen with FH<sup>1-5^18-20R1-2</sup>. The HDM-FH constructs also displayed increased binding avidity to C3b, iC3b, C3d and analogues of GAGs when compared with both FH and FH<sup>1-5^18-20</sup>, with FH<sup>R1-21-5^18-20</sup> consistently showing the highest binding. Furthermore, both constructs conferred protection to human C3b coated SRBCs, indicating an ability to regulate complement activation through cofactor and decay-accelerating activity on surfaces expressing sialic acids similar to those presented on human cell surfaces.

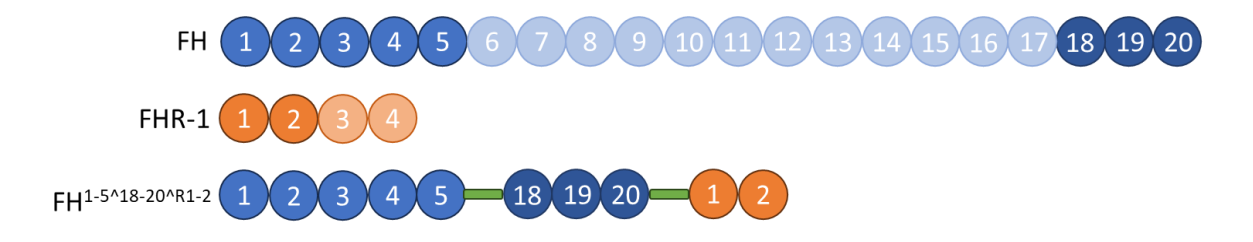


Figure 1.11 The structure of HDM-FH

HDM-FH used in this project (FH<sup>1-5^18-20^R1-2</sup>) consists of SCRs 1-5 and 18-20, with the first two N-terminal domains of FHR-1 joined to the C-terminal. The green bars indicate artificial linkers.

C3 deposits in the kidneys of *CFH*<sup>-/-</sup> mice were reduced to almost background levels 48 hours post intraperitoneal injection of both HDM-FH constructs, with significant improvement in complement regulatory activity when compared with FH<sup>1-5</sup>^18-20 and FH, particularly from FH<sup>1-5</sup>^18-20R1-2; even at doses as low as 0.375 nmol (compared to a dose of 3 nmol of the other proteins). FH<sup>1-5</sup>^18-20R1-2 led to almost complete restoration of plasma C3 24 hr post injection. Furthermore, the HDM-FH constructs were found binding to glomerular C3b fragments 24 hours post injection.

Importantly, the HDM-FH constructs had 5-fold increased serum half-lives compared to  $FH^{1-5^{18-20}}$ , and were still detectable at 48 hours, with  $FH^{1-5^{18-20R1-2}}$  providing a significant reduction in glomerular C3 staining through until 96 hours post injection. The  $T^{1/2}$  of the HDM-FH constructs however were still around half that of FH.

Dimerisation of FH<sup>1–5^18–20</sup> did not cause any significant steric hinderance and in fact increased AP regulation properties such as cofactor activity, decay accelerating activity, recognition of self-cells and binding of C3 fragments. Increased binding avidity to C3 fragments could assist in the homing of HDM-FH constructs to damaged cell surfaces experiencing high levels of complement activation when many of these fragments are present. Increased C3 fragment and GAG binding when compared with FH indicates the potential of the HDM-FH constructs as therapeutic agents inhibiting complement on self-cells.

#### 1.6 MACHINE PERFUSION OF KIDNEYS

Evidence correlating CIT with worse transplant outcomes highlights that despite SCS being standard practice for transport and storage of organs, it is far from ideal. Hypothermia reduces metabolism by 90%-95%, slowing the deleterious processes of ischaemia including ATP depletion, mitochondrial dysfunction and ROS production. However, these processes cannot be totally abolished and can lead to cellular damage. *Ex vivo* machine perfusion was developed not only as an alternative storage method, but as a potential way to recover kidney function prior to transplant.

#### 1.6.1 Hypothermic machine perfusion

Hypothermic machine perfusion (HMP) is a strategy used for organ preservation and restoration. During HMP, kidneys are perfused with acellular preservation solution which provides nutrients and electrolytes at 4°C to 8°C whilst maintaining osmotic balance. This perfusate enters the kidney via a cannula at the renal artery which connects the kidneys to a perfusion device. The pressure at the renal artery is kept at 25 to 30 mm Hg to avoid endothelial injury and oedema (Radi, 2023). As cellular metabolism is still occurring during hypothermia, albeit at a slower pace, oxygenated hypothermic perfusion is also possible, to restore depleted ATP levels via aerobic metabolism (Patel et al., 2019, Thuillier et al., 2013).

HMP as an alternative to SCS can reduce rates of DGF in DBD and DCD kidneys (Tingle et al., 2019), and improve 3-year graft survival (Peng et al., 2019). Active metabolism can be maintained during HMP, as evidenced by increased metabolites including glutamate, lactate, fumarate, acetate and aspartate in grafts following HMP (Nath et al., 2017). HMP can improve microvascular perfusion through upregulation of nitric oxide synthase and Kruppel-like 2 transcription factor and downregulation of ET-1 (Chatauret et al., 2014). Inflammatory cytokine release through ICAM-1 expression is also reduced by HMP, while apoptosis and caspase-3 production can be reduced through the ezrin/AKT pathway (Zhang et al., 2016, Tozzi et al., 2013).

### 1.6.2 Ex vivo normothermic perfusion

Ex vivo normothermic perfusion (EVNP) is an organ preservation technique that is more physiological than HMP. During EVNP kidneys are perfused with an oxygen carrying solution, often packed red blood cells suspended in crystalloid containing additives that can include

insulin, glucose, dexamethasone, mannitol, epoprostenol, sodium bicarbonate and antibiotics. This solution is oxygenated using extracorporeal membrane oxygenation (ECMO) and warmed to 37°C. The kidney is connected to a perfusion circuit which will pump the perfusate solution at physiological pressures via the renal artery. Cellular metabolism can be entirely restored during EVNP, allowing assessment of kidney function.

The current technique for EVNP of large animal/human organs was first described in 2008 by (Bagul et al., 2008). This study describes the ability of EVNP to restore metabolism and improve kidney function as an alternative storage method to SCS. Despite promising early studies indicating that EVNP was a safe and feasible alternative preservation method that may improve graft outcomes (Hosgood and Nicholson, 2011, Nicholson and Hosgood, 2013), a recent multi-centre clinical trial did not achieve its primary endpoint goal of reducing DGF when EVNP was used in addition to SCS (Hosgood et al., 2023). Although EVNP can restore cellular metabolism and improve kidney function upon reperfusion, the EVNP circuit itself is a pro-inflammatory environment, leading to increased cytokine release, without necessarily improving downstream key ischaemic/kidney injury markers (Hosgood et al., 2013).

EVNP has also been used as a method to assess the suitability of kidneys for transplant to widen the donor pool. A quality assessment score (QAS) was devised to grade kidneys undergoing EVNP based on macroscopic perfusion, renal blood flow and urine output. A number of kidneys that would have otherwise been declined for transplant, largely due to poor *in situ* flushing were successfully transplanted following a good QAS (Hosgood et al., 2018).

#### 1.6.3 Therapies administered during ex vivo normothermic perfusion

As EVNP closely mirrors physiological conditions, it provides an excellent platform in which to test novel therapeutics. EVNP is a unique system as a whole, metabolically active, isolated organ can be directly administered with a therapeutic agent. Organ function can then be monitored in real time, with tissue, perfusate and urine samples collected for downstream analysis. Currently a number of different therapies have been administered and assessed during EVNP. These are summarised in **Table 1.5**.

Multiple studies have administered mesenchymal stem cells (MSCs) to kidneys during EVNP due to their immunomodulatory properties. MSCs do not appear to illicit a change in perfusion

haemodynamics or urine output. Some studies did however observe a reduction in inflammatory cytokine release and tubular injury marker neutrophil gelatinase-associated lipocalin (NGAL) (Pool et al., 2020), while others observed no difference in injury markers and an increase in inflammatory cytokines (Lohmann et al., 2021, Pool et al., 2019). More positive results were seen following perfusion with Multipotent Adult Progenitor Cells (MAPCs), a cell type similar to MSCs, as they are derived from the same source, but that have different culture and expansion characteristics. Perfusion with MAPCs led to improved microvascular flow, urine output, and lowered NGAL and inflammatory cytokine levels (Thompson et al., 2021).

Bioengineered nanoparticles encapsulate drugs that are released slowly during nanoparticle hydrolysis. Administration directly to kidneys caused microvascular obstruction due to accumulation within poorly perfused regions of the vasculature (Tietjen et al., 2017). To circumvent this, lysis of microvasculature obstructions was attempted. Treatment with plasminogen and tissue plasminogen activator (tPA) clears microvasculature plugs of red cell aggregates that are triggered by EVNP, improving nanoparticle vascular targeting and perfusion haemodynamics (DiRito et al., 2021). Treatment with tPA and plasminogen plus thrombin and platelet inhibitor further improves haemodynamics (Olausson et al., 2022).

A Caspase-3 siRNA delivered during EVNP reduced tissue apoptosis and improved kidney function and haemodynamics during EVNP (Yang et al., 2011), while an anti-CD47 antibody improved haemodynamics, oxidative stress and histological damage (Hameed et al., 2020). Conversely, treatment with an antagomir against mir-24-3p and a recombinant complement receptor 1 had no beneficial effect when administered during EVNP (Thompson et al., 2022, Kassimatis et al., 2021).

These studies demonstrate that EVNP is a feasible platform for the delivery of therapeutics, with many different categories of treatment successfully reaching and remaining within kidney vasculature, exerting a range of effects on function and downstream parameters.

Therapy	Author	Model	Effects of therapy
MSC	Pool et al.,	Porcine EVNP, 7	No changes
	2019 (Pool et	hours	
	al., 2019)		
MSC	Lohmann et	Porcine EVNP, 4	No changes
	al., 2020	hours following	
	(Lohmann et	14 hours	
	al., 2021)	oxygenated HMP	
MSC	Pool et al.,	Porcine EVNP, 7	↓ Lactate dehydrogenase and NGAL,
	2020 (Pool et	hours	↑ human HGF, IL-6, IL-8
	al., 2020)		
MAPC	Thompson et	Human EVNP, 7	$\downarrow$ NGAL, IL-1 $\beta$ , $\uparrow$ IL-10, Indolamine-2,
	al., 2020	hours	3-dioxygenase, microvascular
	(Thompson et		perfusion, urine output
	al., 2021)		
Nanoparticles	Tietjen et al,	Human EVNP, 4	Widespread vessel plugging and poor
	2017 (Tietjen	hours	perfusion
	et al., 2017)		
Plasminogen	DiRito et al.,	Human EVNP, 90	Lysis of microvascular obstructions, $\downarrow$
and tPA, plus	2020 (DiRito	minutes	NGAL, IL-6, ICAM-1, 个 urine output.
nanoparticles	et al., 2021)		Although nanoparticle targeting was
			improved, the nanoparticles had no
			effect
Lys-	Olausson et	Porcine EVNP, 3	↓ Vascular resistance, ↑ Arterial flow
plasminogen,	al., 2022	hours	
ATIII and tPA	(Olausson et		
	al., 2022)		
Caspase-3	Yang et al.,	Porcine EVNP, 3	↓ Apoptosis, ↑ oxygen consumption
siRNA	2011 (Yang et	hours	and blood flow
	al., 2011)		
αCD47	Hameed et	Porcine EVNP, 1	$\uparrow$ Blood flow, $\downarrow$ oxidative stress and
antibody	al.,	hour	histological damage

Mirococept (recombinant CR1)	2020(Hameed et al., 2020)  Kassimatis et al., 2020 (Kassimatis et al., 2021)	Porcine EVNP, 3 hours	No effect
Mir-24-3p antagonist	Thompson et al., 2021 (Thompson et al., 2022)	Human EVNP, 6 hours	个 HMOX1 and S1PR1 gene expression

Table 1.5 Summary of therapeutics assessed during EVNP.

Abbreviations: Hepatocyte growth factor (HGF), tissue plasminogen activator (tPA), antithrombin-III (ATIII), complement receptor 1 (CR1), heme oxygenase 1 (HMOX1), sphingosine-1-phosphate receptor 1 (S1PR1).

## 1.7 HYPOTHESIS

Extending the warm and cold ischaemic times of porcine kidneys will lead to complement activation and ischaemic injury. HDM-FH, when administered to ischaemically injured kidneys during EVNP, will bind avidly to sites of complement deposition, regulating complement activation and reducing downstream ischaemic injury.

## 1.8 AIMS AND OBJECTIVES

The role of complement in the pathogenesis of IRI is clear, with HDM-FH successfully inhibiting uncontrolled activation in mice, while other complement inhibitors have successfully ameliorated IRI in animal models. Complement inhibitors have been successful in treating complement mediated diseases clinically such as aHUS and PNH, however no therapeutic has yet been approved for the treatment of IRI. EVNP provides a useful platform on which to assess novel therapeutics which can be directly administered to organs while mirroring IRI. The overarching aim of this project is to assess the effect of HDM-FH as a treatment for IRI.

Specific project aims will be addressed in three results chapters. These are to:

- Establish a model of porcine EVNP with elevated complement and ischaemic injury to facilitate HDM-FH binding and assessment.
- Produce HDM-FH and validate binding and complement inhibitory activity in vitro.
- Administer HDM-FH to kidneys during EVNP and assess the effect it has on complement activation and downstream ischaemic injury.

#### 2.1 ETHICS

Animals were euthanised according to Home Office Schedule regulations at Newcastle University Cockle Park Farm facility by trained animal technicians under Animal Welfare and Ethics Review Board (AWERB) number 854, study plan 38.

#### 2.2 NORMOTHERMIC MACHINE PERFUSION OF PORCINE KIDNEYS

# 2.2.1 Retrieval of porcine kidneys.

Organs from 16-week-old female white landrace pigs weighing approximately 60 kg were used in this study and were euthanised following Home Office schedule 1 regulations. Mr Balaji Mahendran or Mr Sam Tingle led and performed the kidney retrieval and benching with assistance from me. Animals were housed in Newcastle University Cockle Park Farm facility. The pigs were moved to holding pens closer to the surgical facility at least 1 week before the procedure to acclimatise and were always kept with other animals to reduce stress. On the day of retrieval, pigs were sedated by a trained animal technician via intramuscular injection of 5 mL Tiletamine & Zolazepam (Zoletil<sup>TM</sup>, Virbac) inside of their holding pens. When fully sedated, they were transported to the farm surgical facility, and lifted onto a surgical table where the same technician administered 25 mL Pentobarbital Sodium (Euthatal<sup>TM</sup>, Dopharma Research B.V.) intravenously via an ear vein causing cardiorespiratory arrest. Following confirmation of asystole on cardiac auscultation, a rapid midline laparotomy was performed.

The inferior vena cava was exposed and cannulated with two clinical blood bags (Troge). The blood bags had been depleted of citrate-based anticoagulant, rinsed three times using saline (Fresenius Kabi), then spiked with 10000 I.U. sodium heparin (Panpharma) and 50 mL saline. At least 250 mL blood was collected into each blood bag, then the pig was exsanguinated via the inferior vena cava using a SAM Medical Aspirator (MGE worldwide).

Bilateral donor nephrectomy was performed akin to clinical retrieval. This involves retrieving the renal artery in its entirety with a patch of aorta; ureter and renal veins were preserved. After a predetermined amount of time (see chapters 3 and 5), the kidneys were removed from the cavity of the pig and placed onto a surgical bag over ice on the back bench. Kidneys were flushed with 1 L of 4°C University of Wisconsin (UW) (Bridge to life) containing 25000 I.U.

sodium heparin via the renal artery to remove all blood. Kidneys were then stored in a surgical bag containing UW on ice in an insulated box for a predetermined amount of time (see chapters 3 and 5).

### 2.2.2 Normothermic machine perfusion

The perfusion was set up and carried out by a core team consisting of myself, Dr Beth Gibson, Mr Balaji Mahendran and Mr Sam Tingle. The disposable individual custom perfusion circuits based on a paediatric cardiopulmonary bypass technology perfusion circuit (M449802B, Medtronic) was set up attached to a flow probe, centrifugal pump, heat exchanger and glass dish (Figure 2.1 and Table 2.1). The circuit was primed with the perfusate components outlined in Table 2.2. The perfusate components were heated to 37°C via a heat exchanger continuously flowing warmed water through the oxygenator component of the circuit. The perfusate was oxygenated via extra corporeal membrane oxygenation using a gas mixture of 95% O<sub>2</sub> and 5% CO<sub>2</sub> flowing at 100 mL/min.

Renal arteries were cannulated with a 12 Fr cannula (77012, Medtronic), ureters were cannulated with enteral feeding tubes (Vygon) to allow for urine collection and the renal vein was left to free drain. 4°C UW solution was flushed from the kidneys using approximately 500 mL saline via the arterial cannula. Kidneys were sat on mesh inserts on custom blown glass dishes that connected to the venous limb of the circuit (Cambridge glass blowing company). Kidneys were then connected via the renal artery (Figure 2.1) to the perfusion circuit. Urine was collected in a urometer. Upon connection of the renal artery to the circuit, the centrifugal pump speed was gradually increased via the bio-console to achieve a mean arterial pressure (MAP) of 75 mmHg.

Connection of kidneys to the circuit was staggered by 5 minutes to allow time for sampling. The reservoir volume was kept constant during the entire perfusion through the addition of Ringers solution (Aquapharm no.9, Animalcare Ltd) to replace fluid loss via urine. The pH of the perfusate was kept within physiological limits between 7.35 and 7.45 through the addition of sodium bicarbonate solution (Freeflex).

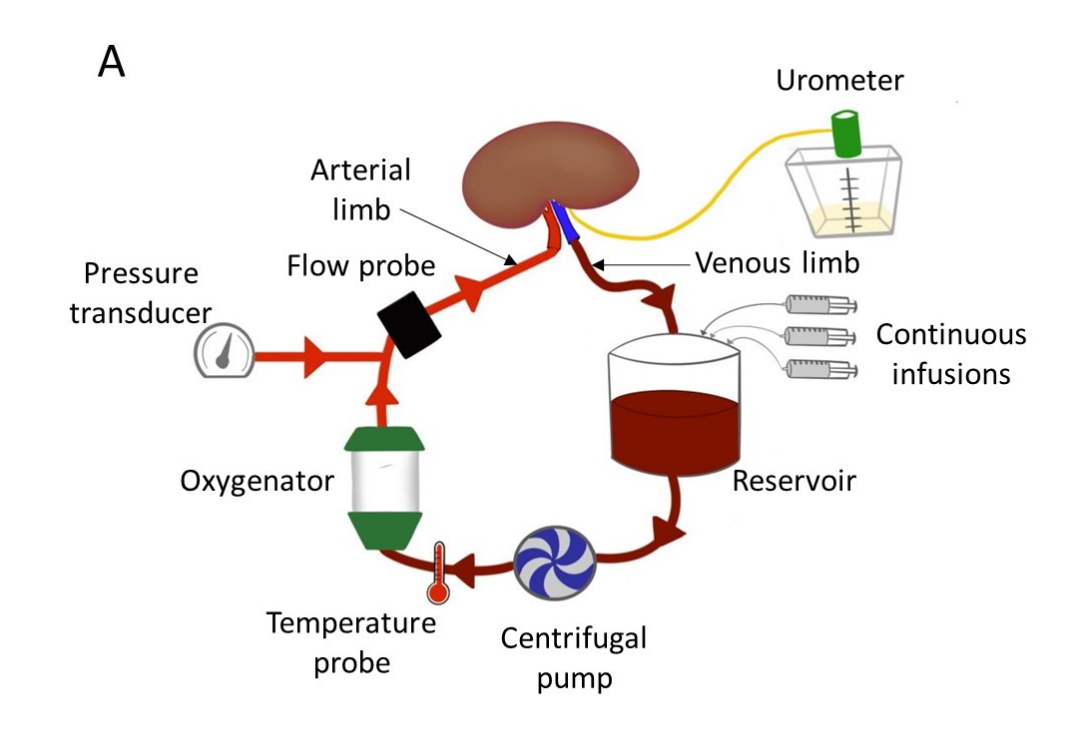




Figure 2.1 Diagram of EVNP circuit.

A – schematic depicting EVNP. Perfusate from the renal vein free drains into the reservoir. Key infusions of glucose, epoprostenol, amino acids and vitamins are continuously pumped into the circuit using syringe drivers. Perfusate from the reservoir is pumped around the circuit by a centrifugal pump. The temperature of the circuit maintained via a heat exchanger, and the blood is oxygenated. The pressure and flow of the arterial limb is read before blood returns to the kidney via an arterial cannula. B-A photograph of a pair of porcine kidneys perfusing side by side.

Perfusion circuit and hardware	• Perfusion circuit (Medtronic –
	M449802B)
	• Motor 560A external drive
	(Medtronic)
	Heater exchanger (Hico-variotherm
	550, Hico)
	Flow probe (TX50P flow transducer,
	Medtronic)
	• Bio-console (Bio-console 560,
	Medtronic)
	3 Syringe drivers (Graseby)
Perfusate components	250 mL autologous whole blood
	containing 10000 I.U. sodium
	heparin (Panpharma)
	• 300 mL Aquapharm no.9 Ringers
	Solution (Animalcare Ltd)
	• 20 mL 10% mannitol solution
	(Polyfusor)
	3.75mg dexamethasone (Hameln)
	• 10 mL 8.4% sodium bicarbonate
	solution (Freeflex)
	40 mg Papaverine Hydrochloride
	0.056g Creatinine (Sigma)
Continuous infusions	• 5% glucose solution at 5 mL/hr
	(Freeflex)
	● Epoprostenol (Flolan <sup>TM,</sup>
	MercuryPharma) at 4 mL/hr
	1 full vial multivitamins (cernevit,
	Baxter) reconstituted in amino acid

solution (Synthamin, Baxter) 17 at
20 mL/hr
Aquapharm no.9 Ringers Solution
(Animalcare Ltd) matching fluid loss

Table 2.1 Perfusion hardware drugs and fluids.

# 2.2.3 Collection and processing of samples

Serum and plasma samples were taken during the kidney retrieval in standard falcon tubes and in BD Vacutainer<sup>TM</sup> Ethylenediaminetetraacetic acid (EDTA) tubes. Perfusate samples were taken prior to the start of the perfusion and at various time points during the perfusion in both plastic falcon tubes (5 mL) and BD Vacutainer<sup>TM</sup> EDTA tubes. 3 mL of blood was collected in the EDTA tubes to ensure consistent EDTA concentrations. EDTA samples were taken to allow to analysis of activated complement components (Mollnes et al., 1988). Urine samples were collected periodically throughout the perfusion in plastic falcon tubes (6 mL). All blood and perfusate samples were immediately placed on ice, then spun at 2000 g for 10 minutes at 4°C to remove cells and cellular debris. The supernatant was then aliquoted and stored at -80°C.

19 mm core biopsies were taken with an 18-gauge BioPince<sup>™</sup> core biopsy instrument (Argon Medical) at the farm after kidney retrieval pre- and post-UW flush, prior to perfusion and throughout the perfusion. Three core biopsies were taken at 30 minutes, 120 minutes, 240 minutes and 360 minutes, with excision biopsies of cortex and medulla taken at the end of perfusion. One core biopsy from each time point was fixed in formalin for 24 hours prior to embedding in wax according to established protocols by Cellular Pathology at the Royal Victoria Infirmary, Newcastle. Excision biopsies were fixed in formalin for 48 hours prior to embedding. One biopsy from each time point was snap frozen in liquid nitrogen, to be later embedded in OCT. The remaining biopsy was placed in RNAlater<sup>™</sup> Solution (Invitrogen) and moved to -80°C for long term storage. The sampling protocol is outlined in **Figure 2.2**.

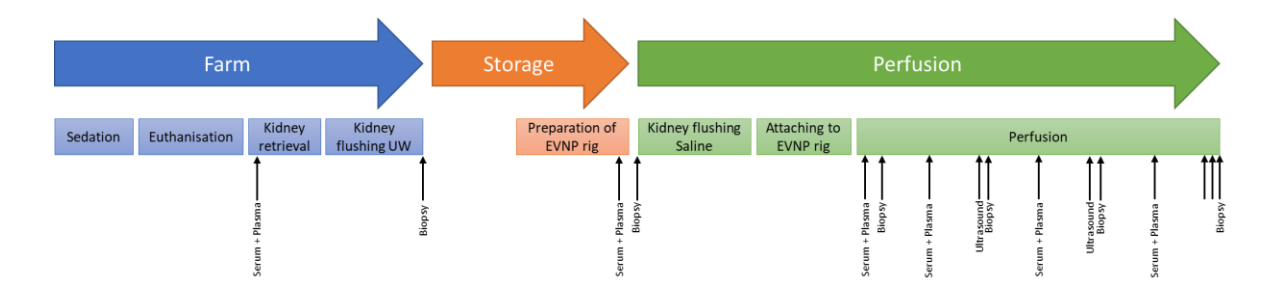


Figure 2.2 Diagram of experimental timeline with sampling schedule.

Various blood, tissue and urine samples were collected throughout the retrieval and perfusion process.

# 2.2.4 Perfusate blood gas analysis

The gas/electrolyte composition of the perfusate was measured prior to perfusion, then at 30 minutes, 60 minutes, 120 minutes, 180 minutes, 240 minutes, 300 minutes and 360 minutes using a RAPIDpoint 500e Blood Gas System (Siemens). Perfusate composition was recorded from samples taken from the arterial limb of the circuit (**Table 2.2**). Perfusate samples were taken from the venous limb to calculate oxygen consumption only. Oxygen consumption was calculated by multiplying the difference in arterial and venous oxygen content by the total renal blood flow (RBF). This value was normalised for kidney weight to give oxygen consumption/100 g. The following equation was used to calculate oxygen content (Mairbäurl and Weber, 2012):

$$\begin{array}{l} (0.134 \times [\text{Hemoglobin in g/L}] \times (02 \text{Hb\%} \div 100)) \\ + (\text{p02 in kPa} \times 0.0225) \end{array}$$

Parameters	Analyte	
Blood Gas	рН	
	pCO <sub>2</sub>	
	pO <sub>2</sub>	
Electrolytes	Na <sup>+</sup>	
	K <sup>+</sup>	
	Ca <sup>++</sup>	
	CI <sup>-</sup>	
Metabolites	Glucose	
	Lactate	
CO-oximetry	tHb	
	sO <sub>2</sub>	
	O <sub>2</sub> Hb	
	СОНЬ	
	MetHb	

Table 2.2 Perfusate biochemical parameters measure throughout perfusion using the RAPIDpoint 500e Blood Gas System.

Abbreviations: Haemoglobin (Hb), Carboxyhemoglobin (COHb), Methaemoglobin (MetHb)

#### 2.2.5 Functional parameters

To assess glomerular function and renal resistance (RR), urine output, RBF and MAP were recorded throughout perfusion. RR was calculated by dividing the MAP by the flow rate. Glomerular filtration was assessed by assessing creatinine levels in the perfusate. 0.056g creatinine (Sigma Aldrich) was added to the perfusate prior to the start of the kidney perfusion. Creatinine levels were measured from samples taken at 5 minutes, 30 minutes, 60 minutes, 120 minutes and 180 minutes at the Blood Sciences department of the Royal Victoria Infirmary. A decay curve over time was plotted and the area under the curve was calculated to determine how quickly creatinine was cleared from the circuit.

### 2.3 HISTOLOGY AND IMMUNOFLUORESCENT STAINING

All histological and immunofluorescent techniques were performed on 4 - 6  $\mu$ m formalin-fixed paraffin-embedded (FFPE) sections or cryosections.

All FFPE tissue sections used were dewaxed and rehydrated using xylene and graded alcohol following the protocol outlined in **Table 2.3**.

Step	Time
Xylene (Honeywell)	5 minutes
Xylene (Honeywell)	5 minutes
100% Ethanol	3 minutes
100% Ethanol	3 minutes
90% Ethanol	3 minutes
70% Ethanol	3 minutes
Running deionised (DI) water	3 minutes

Table 2.3 Protocol for dewaxing and rehydrating of FFPE sections.

Following histological staining, all FFPE sections were dehydrated and cleared following the protocol outlined in **Table 2.4**. Following dehydration and clearing they were mounted using a glass coverslip with non-aqueous DPX mounting media (Sigma).

Step	Time
70% Ethanol	3 minutes
90% Ethanol	3 minutes
100% Ethanol	3 minutes
100% Ethanol	3 minutes
Xylene (Honeywell)	5 minutes
Xylene (Honeywell)	5 minutes

Table 2.4 Protocol for dehydrating and clearing of FFPE sections.

# 2.3.1 Haematoxylin and Eosin staining

Haematoxylin and eosin staining was used to visualise kidney morphology. Following dewaxing and rehydration (**Table 2.3**), nuclei were stained using Mayer's haematoxylin (Sigma) for 4 minutes then rinsed in alkaline tap water to 'blue' the haematoxylin. Eosin Y (Sigma) was then applied to slides for 80 seconds before a brief rinse with DI water. Slides were then dehydrated and mounted (**Table 2.4**). Brightfield images of sections were then taken using the CMOC colour camera SC50 (Olympus) and Cellsens Standard software (Olympus).

# 2.3.2 Periodic acid-Schiff staining

Periodic acid-Schiff staining was used to visualise basement membranes and tubular brush borders. Following dewaxing and rehydration (**Table 2.3**), tissue was oxidised in 0.5% periodic acid solution (Sigma) for 5 minutes then rinsed in DI water. Slides were then immersed in Schiff reagent (VWR) for 15 minutes and rinsed in DI water to develop the stain. Nuclei were counter stained using Mayer's Haematoxylin for 1 minute then rinsed in DI water. Slides were then dehydrated and mounted (**Table 2.4**). Brightfield images of sections were taken using the CMOC colour camera SC50 and Cellsens Standard software.

### 2.3.3 Martius Scarlet Blue staining

Martius Scarlet Blue (MSB) staining was used to visualise erythrocytes, red cells, fibrin and collagen. Following dewaxing and rehydration (**Table 2.3**), tissue was stained using a Martius Scarlet Blue Stain Kit (Atom Scientific) as detailed in **Table 2.5**. Following this, slides were dehydrated and mounted (**Table 2.4**). Brightfield images of sections were then taken using the CMOC colour camera SC50 and Cellsens Standard software.

Step	Time
Bouin's solution 56°C (Sigma)	1 hour
Wiegerts Iron haematoxylin	10 minutes
DI water rinse	10 seconds
1% Acid alcohol solution (1% hydrochloric	10 seconds
acid in 70% ethanol)	
DI water rinse	3 minutes
95% Ethanol	10 seconds
Martius yellow solution	5 minutes
DI water rinse	5 minutes
Crystal Scarlet Solution	5 minutes
DI water rinse	5 minutes
Phosphotungstic acid solution	10 minutes
DI water rinse	5 minutes
Aniline blue solution	5 minutes
DI water rinse	5 minutes

Table 2.5 Protocol for Martius Scarlet Blue staining

### 2.3.3.1 Quantification of erythrocytes in Martius scarlet blue stained sections

Ten 200x regions of MSB stained tissue containing at least one glomerulus were imaged. LABKIT, a Fiji Image J plugin for segmentation of microscopy images was used to create a pixel classifier (Arzt et al., 2022). The classifier was trained to segment the image, recognising erythrocytes within the section as 'foreground' and all other structures/empty space as 'background' by manually labelling small sections of relevant areas as such. One image per section was used to train a classifier, as staining was consistent across sections but not between organs. Images were then batch segmented by applying the trained classifier to all images from the same section.

Mr George Kourounis further processed the segmented image. A binary mask was created for each image, showing areas of 'background' and 'foreground' only (Figure 2.3). Using Python, along with the OpenCV and pandas libraries, we analysed the images to determine the percentages of the 'background' and 'foreground' areas. The portion of the image covered by

the 'foreground' mask indicated the percentage of erythrocyte coverage in each 200x magnification field of view.

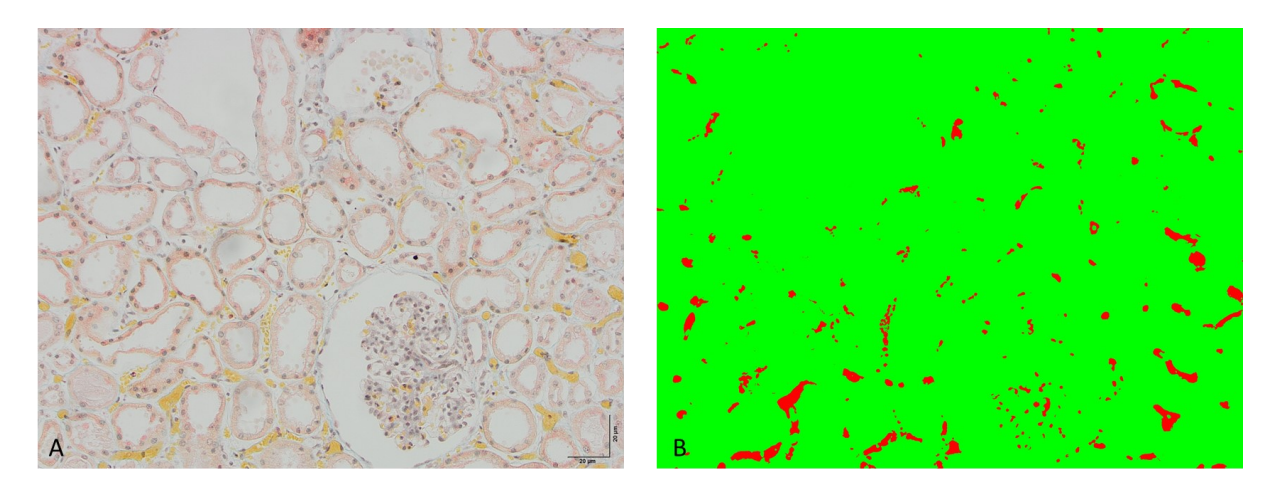


Figure 2.3 LABKIT mask identifying erythrocytes.

A) shows a 200x image of an FFPE MSB stained kidney section. B) shows the mask generated from a trained classifier selecting erythrocytes as 'foreground' in red.

### 2.3.4 Immunofluorescent staining of FFPE sections

# 2.3.4.1 Indirect immunostaining

FFPE sections were dewaxed and rehydrated as outlined in **Table 2.3**. FFPE sections were used preferentially due to preserved morphology as frozen sections can contain ice crystal artefacts. As formalin fixation masks antigens/epitopes in tissue, antigen retrieval was required to break these protein cross-links. Heat-induced antigen retrieval (HIER) was therefore performed. For HIER, sections were boiled in antigen retrieval solution (**Table 2.6**) in an InstantPot<sup>TM</sup> at 82 kPa for 3 minutes. Following antigen retrieval, sections were washed by immersion in PBS-T (Phosphate-Buffered Saline (Merck), 0.05% Tween\* 20 Detergent (Sigma)) 3 times for 5 minutes. A hydrophobic barrier was then drawn around tissue sections with a hydrophobic barrier PAP pen. A blocking solution (**Table 2.6**) was added to the tissue and incubated for 30 minutes.

Primary antibody (**Table 2.6**) diluted in PBS was then applied directly to sections and incubated overnight at 4°C. A 'no primary' negative control section was incubated overnight with PBS only. Slides were then washed in PBS-T 3 times for 5 minutes. The secondary antibody (**Table 2.6**) diluted in PBS was then applied to the section and incubated for 1 hour. Slides were washed in PBS-T 3 times for 5 minutes, then washed in 0.1% Sudan Black-B (Sigma) in 70%

ethanol for 20 minutes to quench autofluorescence. Slides were washed again in PBS-T 3 times for 5 minutes. Excess PBS-T was tapped off, and sections were mounted with a glass coverslip using aqueous VECTASHIELD mounting medium with DAPI (Vector labs). All sections were then imaged using the LEICA DM2000 LED microscope and processed using LAS X software.

Primary	Primary	Antigen	Blocking	Secondary	Secondary
antibody	antibody	retrieval	solution	antibody	antibody
	dilution	solution			dilution
Anti-Pig C3	1:50	Tris-EDTA	10% normal	Alexa Fluor™	1:200
Rabbit IgG		Buffer (10mM	goat serum	488 Goat anti-	
polyclonal		Tris Base	in PBS	Rabbit IgG (H+L)	
(ab180640,		(Sigma), 1mM		(A-11008,	
abcam)		EDTA		ThermoFisher)	
		Solution,			
		0.05% Tween			
		20, pH 9.0			
Anti-Human	1:200	Citrate Buffer	10% normal	Alexa Fluor™	1:200
fibrinogen		(10mM Citric	rabbit	555 Rabbit anti-	
Sheep IgG		Acid (Sigma),	serum in	Sheep IgG (H+L)	
polyclonal		0.05% Tween	PBS	(ab150182,	
(4440-8004,		20, pH 6.0		abcam)	
BioRad)					
Anti-Human	1:50	Citrate Buffer	10% normal	Alexa Fluor™	1:200
neutrophil		(10mM Citric	goat serum	488 Goat anti-	
elastase		Acid, 0.05%	in PBS	Rabbit IgG (H+L)	
Rabbit IgG		Tween 20, pH		(A-11008,	
polyclonal		6.0		ThermoFisher)	
(ab21595,					
abcam)					
Anti-Human-	1:50	Tris-EDTA	10% normal	Alexa Fluor™	1:50
Factor B		Buffer (10mM	goat serum	488 Goat anti-	
Mouse IgG <sub>1</sub>		Tris Base,	in PBS	Mouse IgG (H+L)	
monoclonal		1mM EDTA		(A-11001,	
(sc-271636,		Solution,		ThermoFisher)	
Santa Cruz)		0.05% Tween			
		20, pH 9.0			

Table 2.6 Reagents used for indirect immunofluorescent staining on FFPE tissue.

# 2.3.4.2 TdT-mediated dUTP Nick-End Labelling

A TUNEL (TdT-mediated dUTP Nick-End Labelling) assay identifies cell-death in tissue sections by binding to fragmented DNA. Fluorescin-12-dUTP is incorporated at 3′-OH DNA ends using Terminal Deoxynucleotidyl Transferase (TdT) which forms a polymeric tail enabling the fluorescein-12-dUTP-labeled DNA to be visualised using fluorescent microscopy.

The DeadEnd™ Fluorometric TUNEL System (Promega) was carried out according to manufacturer's instructions (**Table 2.7**) following dewaxing and dehydration of FFPE sections (**Table 2.3** and **Table 2.4**). Sections were then mounted with a glass coverslip using aqueous VECTASHIELD mounting medium with DAPI (Vector labs). All sections were then imaged using the LEICA DM2000 LED microscope and processed using LAS X software.

Step	Time
0.85% NaCl	5 minutes
PBS	5 minutes
4% PFA in PBS	15 minutes
PBS	5 minutes
PBS	5 minutes
20 μg/mL Proteinase K in PBS	8 minutes
PBS	5 minutes
4% PFA in PBS	5 minutes
PBS	5 minutes
Equilibration buffer	5 – 10 minutes
Nucleotide mix (45μL Equilibration buffer,	60 minutes at 37°C protected from light
5μL Nucleotide mix, 1μL TdT enzyme /	
section)*	
2x Saline-sodium Citrate buffer	15 minutes
PBS	5 minutes
PBS	5 minutes
PBS	5 minutes

Table 2.7 TUNEL assay procedure.

# 2.3.5 Immunofluorescent staining of cryosections

# 2.3.5.1 Indirect immunostaining

Cryosections were defrosted for 30 minutes and fixed in ice-cold acetone for 10 minutes. Sections were then washed in PBS. A hydrophobic barrier was then drawn around tissue sections, blocking solution (**Table 2.8**) was applied and then incubated for 30 minutes. Primary antibody (**Table 2.8**) diluted in PBS was then applied and incubated overnight at 4°C. A negative control section was incubated overnight with PBS only. Slides were then washed in PBS 3 times for 5 minutes. The secondary antibody (**Table 2.8**) diluted in PBS was then applied to the section and incubated for 1 hour at room temperature. Slides were washed in PBS 3 times for 5 minutes. Where an individual section was stained with multiple antibodies, the

<sup>\*</sup>Negative control was prepared without TdT enzyme

next primary antibody was then applied, and the process repeated. Slides were then washed in 0.1% Sudan Black-B (Sigma) in 70% ethanol for 20 minutes to quench autofluorescence. Slides were washed again in PBS-T 3 times for 5 minutes. Excess PBS-T was tapped off, then sections were mounted with a glass coverslip using VECTASHIELD mounting medium with DAPI (Vector labs). Sections were then imaged using the LEICA DM2000 LED microscope or the Leica SP8 point scanning confocal microscope and processed using LAS X software.

Primary antibody	Primary antibody	Blocking solution	Secondary antibody	Secondary antibody
	dilution			dilution
Anti-FH Mouse	1:200	10%	Alexa Fluor™ 594 Goat anti-	1:200
monoclonal IgG <sub>1</sub>		normal	mouse IgG <sub>1</sub> (A-21125,	
(OX-24 antibody		goat	ThermoFisher / Alexa	
produced in house		serum in	Fluor™ 488 Goat anti-	
at 1mg/mL)		PBS	Mouse IgG (H+L) (A-11001,	
			ThermoFisher)	
Anti-Pig CD163	1:50	10%	Alexa Fluor™ 488 Goat anti-	1:200
Mouse monoclonal		normal	rabbit IgG (H+L) (A-11008,	
IgG <sub>1</sub> (MCA2311GA,		rabbit	ThermoFisher)	
BioRad)		serum in		
		PBS		
Anti-Pig CD3ε-APC	1:50	10%	Alexa Fluor™ 488 Goat anti-	1:200
Mouse monoclonal		normal	rabbit IgG (H+L) (A-11008,	
IgG <sub>1</sub> (4501-11,		goat	ThermoFisher)	
Southern Biotech)		serum in		
		PBS		
Anti-WT1 Mouse	1:50	10%	Alexa Fluor™ 488 Goat anti-	1:200
monoclonal IgΜκ		normal	mouse IgM (Heavy chain)	
(sc-393498, Santa		goat	(A-21042, ThermoFisher)	
Cruz Biotechnology)		serum in		
		PBS		
Anti-laminin Rabbit	1:200	10%	DyLight® 550 Goat anti-	1:200
polyclonal IgG		normal	Rabbit IgG (H+L) (GtxRb-	
(L9393, Sigma-		goat	003-F550NHSX,	
Aldrich)		serum in	ImmunoReagents)	
		PBS		
Anti-Pig CD31 Rat	1:200	10%	DyLight® 650 Goat anti-Rat	1:200
monoclonal IgG <sub>1</sub>		normal	IgG (H+L) (GtxRt-003-	
		goat		

(MAB33871 R&D	seri	m in	D650NHSX	
Systems)	PBS		ImmunoReagents)	

Table 2.8 Reagents used for different indirect immunofluorescent staining on frozen OCT embedded tissue.

# 2.3.6 Quantification of immunofluorescent staining

C3, Fibrinogen, C1q and FB levels were measured in glomeruli. Ten 200x magnification images with each including at least 1 glomerulus were taken per stained section. Background fluorescence was subtracted from each image in LAS X using the negative control section. LIF files were exported to TIFF files for analysis in Adobe Photoshop. Images were converted to 8-bit and grayscale. Glomeruli were drawn around using the lasso tool and the pixel count of the area recorded. 'Highlights' were selected, outlining positively stained regions. The pixel count of these highlights was then measured. The pixel count of highlighted areas was divided by the pixel area of the entire glomeruli to give percentage of glomerular area stained.

CD163 positive macrophages, neutrophil elastase and CD3 $\epsilon$  positive cells were measured in all tissue components. Ten 200x magnification images were taken per section. Background fluorescence was subtracted from each image in LAS X using the negative control section. LIF. files were exported to TIFF files for analysis. For quantification of CD163 and neutrophil elastase, positively stained areas were selected and positively stained % area calculated by QuPath software. CD3 $\epsilon$  positive cells were manually counted individually using the multi-point tool in Fiji image J software.

Apoptotic bodies were measured in all tissue components. Ten 200x magnification images were taken per section. Background fluorescence was subtracted from each image in LAS X using the negative control section. LIF. files were exported to TIFF files for analysis. Apoptotic bodies were manually counted individually using the multi-point tool in Fiji image J software (Schindelin et al., 2012). Nuclei stained with DAPI were also imaged and quantified on each imaged section. Nuclei were quantified using Fiji ImageJ software using the following steps outlined in **Table 2.9**.

Step	Process
Change image to 8 bit and black and white	Image< Type< 8bit
	Edit < Invert
Threshold image and convert to binary	Image < Adjust < Threshold <
	Change settings from Default to Triangle
	Threshold slider changed until all nuclei are
	red, apply
Modify image so individual nuclei can be	Process < Binary < Fill holes
quantified	Process < Noise < Despeckle
	Process < Binary < watershed separation
Analyse nuclei number	Analyse < Analyse particles <
	Size (pixel^2) = 0.5-infin
	Circularity = 0.30-1.00
	Show = overlay
	Ensure selected: Display results, Clear
	results, Summaries, Include holes, In situ
	show
	Select ok, 'count' gives number of individual
	nuclei

Table 2.9 Steps to count individual nuclei in Fiji Image J.

### 2.4 PROTEIN ANALYSIS

#### 2.4.1 Enzyme-linked Immunosorbent Assays

Sandwich Enzyme-linked Immunosorbent Assays (ELISAs) were used to detect concentrations of various proteins in both perfusate and urine samples. In sandwich ELISAs, a capture antibody is coated onto a 96-well plate that will bind an antigenic site on the protein of interest in samples. A second antibody is then added that will bind a different antigenic site on the protein of interest. This second antibody is directly enzyme linked to allow detection after addition of a developing solution.

Cytokine levels in urine and hyaluronan levels in perfusate were measures using DuoSet<sup>TM</sup> ELISA kits (R&D Systems) (**Table 2.10**). ELISA reagents were diluted to the working concentration stated on the individual kit certificate of analysis immediately prior to use. The capture antibodies were diluted in PBS, detection antibodies and streptavidin-horse radish peroxidase (HRP) were diluted in reagent diluent (**Table 2.10**). A range of standards of known protein concentration were made by serially diluting the reconstituted standard using reagent diluent. Substrate solution was prepared by mixing equal parts of Colour Reagent A (H<sub>2</sub>O<sub>2</sub>, Sigma) and Colour Reagent B (Tetramethylbenzidine, R&D systems). Appropriate sample dilutions were identified by testing a range of dilutions in reagent diluent.

An adsorption immunoassay 96-well Plate (ThermoFisher) was coated with 100  $\mu$ L capture antibody, then sealed with an adhesive cover and incubated overnight. The capture antibody was aspirated, and the plate washed with 300  $\mu$ L PBS-T 3 times. The plate was then blocked by adding 300  $\mu$ L blocking buffer (**Table 2.10**) to wells, sealed with an adhesive cover and incubated for 1 hour. The plate was then washed/aspirated before 100  $\mu$ L of either the samples or the standards were added to the appropriate wells in duplicate. The plate was then sealed with an adhesive cover and incubated for 2 hours. The plate was aspirated/washed before 100  $\mu$ L of the detection antibody was added to wells, the plate was sealed with an adhesive cover and incubated for 2 hours. The plate was aspirated/washed, then 100  $\mu$ L of streptavidin-HRP added. The plate was sealed with an adhesive cover and incubated for 20 minutes out of direct light. The plate was aspirated/washed, and 100  $\mu$ L substrate solution added, sealed with an adhesive cover and incubated for 20 minutes out of direct light. The reaction was quenched through the addition of 50  $\mu$ L stop solution (10% H<sub>2</sub>SO<sub>4</sub> in DI H<sub>2</sub>O) to the wells.

Optical density (OD) at 450 nm was measured using a micro plate reader (Biotek synergy). The OD of the 'blank' well was subtracted from all other values. A standard curve was constructed by plotting the standard OD values against known concentrations. Protein concentrations of samples were extrapolated from the standard curve and multiplied by the dilution factor to calculate original concentration.

Protein target	Block buffer	Reagent Diluent
IL-8 (DY535)	1% bovine serum albumin	1% BSA in PBS, pH 7.2-7.4,
	(BSA, (Sigma)) in PBS, pH 7.2-	0.2 μm filtered
	7.4, 0.2 μm filtered	
IL-6 (DY686)	1% BSA in PBS, pH 7.2-7.4,	1% BSA in PBS, pH 7.2-7.4,
	0.2 μm filtered	0.2 μm filtered
IL-1 beta (DY681)	1% BSA in PBS, pH 7.2-7.4,	0.1% BSA, 0.05% Tween 20 in
	0.2 μm filter	Tris-buffered Saline (20 mM
		Trizma base, 150 mM NaCl)
		pH 7.2-7.4, 0.2 μm filtered
Hyaluronan (DY3614)	5% Tween 20 in PBS, 7.2-7.4,	or 5% Tween 20 in PBS, 7.2-
	0.2 μm filtered	7.4, 0.2 μm filtered

Table 2.10 R&D DuoSet<sup>™</sup> details with block buffer and reagent diluent details.

C5a concentrations in urine and FB concentrations in perfusate were measured using precoated sandwich ELISA kits from Abbexa following manufacturers protocol (C5a – abx154898, Factor B - abx570475). Detection reagent A and detection reagent B were diluted with relevant buffers provided in the kit to form working solutions. A range of standards of known protein concentration were made by serially diluting the reconstituted standard using standard diluent buffer. Appropriate sample dilutions were identified by testing a range of dilutions in diluent buffer.

100  $\mu L$  of standard or samples were added to the appropriate wells in duplicate, including a 'blank' well of standard diluent only. The plate was sealed with an adhesive cover and incubated for 1 hour at 37°C. The plate was aspirated, and 100  $\mu L$  of detection reagent A working solution added to each well. The plate was sealed with an adhesive cover and incubated 1 hour at 37°C. The plate was aspirated and washed 3 times with 300  $\mu L$  wash

buffer. 100  $\mu$ L of detection reagent B working solution was added to wells, the plate was sealed with an adhesive cover and incubated for 30 minutes at 37°C. The plate was aspirated and washed 5 times with 300  $\mu$ L wash buffer. 90  $\mu$ L TMB substrate was added to each well. The plate was sealed with an adhesive cover and incubated for 10-20 minutes at 37°C out of direct light. 50  $\mu$ L stop solution was added to each well.

Optical density (OD) at 450 nm was measured using a micro plate reader. The OD of the 'blank' well was subtracted from all other values. A standard curve was constructed by plotting the standard OD values against know concentrations. Protein concentrations were extrapolated from the standard curve and multiplied by the dilution factor to calculate original concentration.

NGAL concentrations in urine were measured using a pre-coated sandwich ELISA kit (ab207924 – abcam). The wash solution and sample diluent were diluted in deionised water to the working concentration. All other reagents were provided at working concentration. Appropriate sample dilutions were identified by testing a range of dilutions in sample diluent.

100  $\mu$ L of standard or samples were added to the appropriate wells in duplicate, including a 'blank' well of standard diluent only. The plate was sealed with an adhesive cover and incubated for 1 hour on a shaking platform set at 200 rpm. The plate was aspirated and washed 3 times with 300  $\mu$ L wash buffer. 100  $\mu$ L of Biotinylated Pig-NGAL antibody was added to wells then the plate was sealed with an adhesive cover and incubated for 1 hour on a shaking platform set at 200 rpm. The plate was aspirated/washed, then 100  $\mu$ L HRP-Streptavidin solution added. The plate was sealed with an adhesive cover and incubated for 1 hour with agitation (200 rpm). The plate was aspirated and washed and then 100  $\mu$ L TMB substrate was added to all wells. The plate was sealed with an adhesive cover and incubated for 10 minutes out of direct light at which point 100  $\mu$ L of stop solution was added to all wells.

Optical density (OD) at 450 nm was measured using a micro plate reader. The OD of the 'blank' well was subtracted from all other values. A standard curve was constructed by plotting the standard OD values against know concentrations. Protein concentrations of diluted were extrapolated from the standard curve and multiplied by the dilution factor to calculate original concentration.

C3a levels in both perfusate and urine were measured in Norway by Professor Tom Eirik Mollnes research group using in-house porcine specific ELISAs.

### 2.5 CLASSICAL HAEMOLYTIC ASSAYS

Haemolytic assays assess the function activity of complement in samples. The capacity of the complement components in serum to lyse antibody-coated sheep red blood cells (SRBCs) is given as the CH<sub>50</sub> (**Table 2.4**).

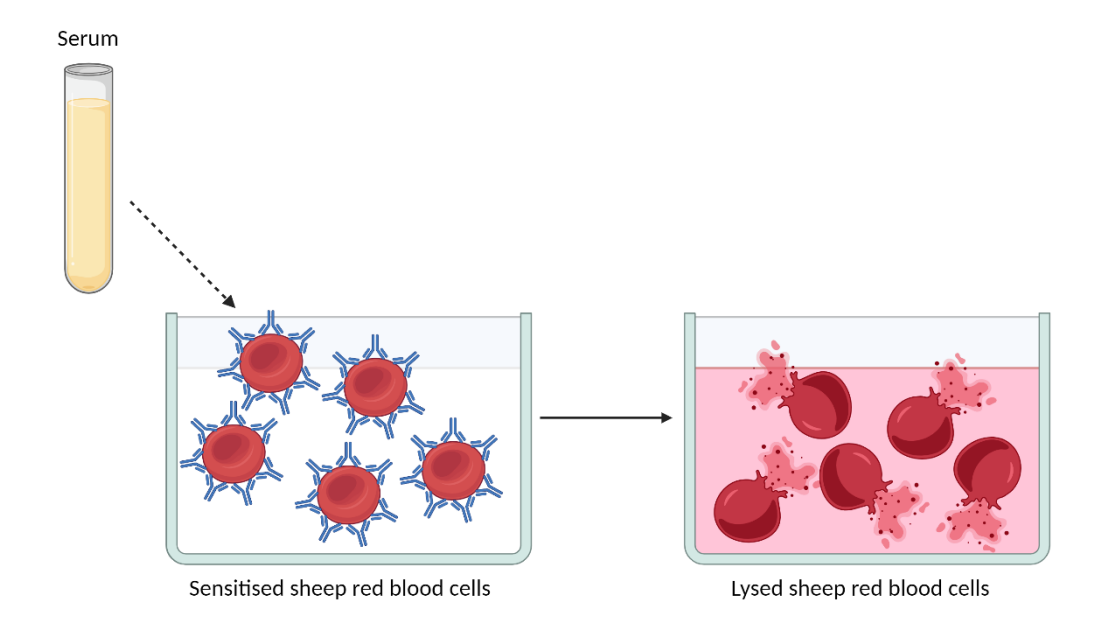


Figure 2.4 Schematic showing lysis of sensitised sheep red blood cells following the addition of serum.

1 mL SRBCs in Alsever's solution (TCS biosciences) was added to 20 mL Dulbecco's Phosphate Buffered Saline (DPBS) (Gibco) and washed by centrifuging at 800 g for 5 minutes at 4°C 3 times. After each wash, the cells form a pellet, the DPBS was removed, and the pellet was agitated by manually applying force to the bottom of the falcon. SRBCs were then washed in 20 mL HEPES buffered saline (0.01 M HEPES, 0.15M NaCl, 135nM CaCl2, 1mM MgCl2, pH 7.4) and centrifuged at 800 g for 5 minutes at 4°C 3 times. 60  $\mu$ L Rabbit anti-Sheep Red Blood Cell Stroma (Merck) was added to the SRBC pellet and incubated for 30 minutes at room temperature on a rotating platform. SRBCs were then washed in 20 mL HEPES buffered saline, centrifuged at 800 g for 5 minutes at 4°C 3 times then resuspended in 15 mL HEPES buffered saline.

Serum was serially titrated in HEPES buffered saline in triplicate in a pre-chilled clear flat bottomed 96 well-plate (ThermoFisher) giving a total volume of 50  $\mu$ L. The 96-well plate was kept on ice for the following steps. Control wells were set up with 50 mM EDTA. 50  $\mu$ L H<sub>2</sub>O was added in triplicate to wells to measure '100% lysis', 50  $\mu$ L HEPES buffered saline was

added in triplicate to wells to measure '0% lysis'. 50  $\mu$ L sensitised SRBCs were added to each well and mixed by gently pipetting up and down. The plate was sealed with an adhesive strip and incubated at 37°C for 1 hour. The whole plate was spun at 800 g for 5 minutes at 4°C to stop the reaction. 80  $\mu$ L from each well was transferred to a 96-well round bottomed plate (ThermoFisher). Optical density (OD) was measured by using a micro plate reader (TECANSpark 20m) at 412nm (reference 660nm). An average value was calculated from the triplicate wells.

Total lysis from each dilution was calculated using the following formula:

$$\left(\frac{Sample\ OD}{'100\%\ lysis'OD - '0\%\ lysis'OD}\right)$$
 X 100

The sample dilution that achieved 50% the OD of the '100% lysis' wells was identified.

#### 3.1 Introduction

For patients with end-stage renal failure, a kidney transplant is the optimal treatment option. Due to a shortage of kidneys suitable for transplant however, patients in the UK wait 3 years on average for a kidney from a deceased donor, with 12% of patients removed from the waiting list during this time due to death or illness (Summers et al., 2015). This has led to an increase in the use of kidneys from marginal, extended criteria and DCD donors who are more susceptible to DGF (Yarlagadda et al., 2008).

IRI contributes to the development of DGF and other forms of AKI (Situmorang and Sheerin, 2019). IRI occurs when restoration of oxygenated blood supply follows a sudden disruption in blood flow, as is seen in the setting of transplantation. IRI leads to microvascular damage and cell death, primarily affecting tubular structure causing poor metabolic function, inflammation and neutrophil activation, while production of ROS occurs upon restoration of circulation. These factors exacerbate damage caused by oxygen and ATP depletion experienced during the initial ischaemic insult on the organ following retrieval (Ponticelli, 2013).

The standard technique to preserve kidneys before transplant is SCS. Hypothermia reduces cellular metabolism, slowing ATP depletion to maintain cellular viability. Furthermore, it is a cheap and convenient method. However, prolonged storage times lead to tubular injury, DGF and complement activation (Troppmann et al., 1995, Lo et al., 2021, Tozzi et al., 2013, Summers et al., 2015) . EVNP is an alternative storage method in which organ metabolism is maintained using extracorporeal membrane oxygenation under normothermic conditions (Hosgood and Nicholson, 2011).

EVNP provides a platform to deliver therapeutics directly to the kidney, avoiding potential complications from systemic delivery of drugs (Hume, 2006). Therapies administered during EVNP can be monitored closely in real time and through the collection and analysis of tissue, perfusate and urine. Various therapies have previously been administered to kidneys using the EVNP platform including gene therapies, stem cells and nanoparticles (Hosgood et al., 2021). Although results from these studies show promising results and indicate the viability of therapeutic administration during EVNP, they are yet to make the transit to use in clinical practice and the field is still in relative infancy. The limited clinical success of existing

complement inhibitors at preventing IRI means investigations into new inhibitors with different mechanisms of action is warranted.

As activation of the alternative pathway is ubiquitous and C3b deposition is not specific to non-self-cells it must be regulated, as to not cause damage to the host. FH can recognise, and control complement on self surfaces as it binds deposited C3b alongside specific host cell markers. This also applies to HDM-FH which avidly binds C3b and GAGs (Yang et al., 2018). It is therefore predicted that when applying HDM-FH as a therapy *ex vivo*, having C3b deposition on the target surface would be advantageous. Furthermore, to assess the potential efficacy of HDM-FH in ameliorating downstream ischemic injury, it is important for organs to have sustained some level of damage and complement activation, similar to the clinical situation (Damman et al., 2011, van Werkhoven et al., 2013).

Whole porcine organs have been utilised in a number of studies investigating IRI interventions due to their similar size, physiology and anatomy to human organs, as supply of human organs available for research can be inconsistent and unpredictable. A range of factors including donor age, genetics, lifestyle, and warm and cold ischaemic times lead to large heterogeneity between organs. Outbred pigs from the same stock can be bred to be very genetically similar, reducing this variability. The kidney anatomy of pigs is highly similar, although not identical to that of humans, being multilobular, with similar venous, arterial and urinary collecting systems (Pereira-Sampaio et al., 2004, Bagetti Filho et al., 2008). The pig also has high chromosome structural homology with humans (Lunney, 2007, Groenen et al., 2012). Furthermore, experimental animals can be of the same age, and the warm and cold ischaemic times can be controlled so they have received the same ischaemic insult. This highly controlled environment provides an ideal model in which to test therapeutics.

A caveat of using porcine organs is that they are not necessarily representative of human organs available for transplant. Kidneys from young pigs are generally used in porcine models, whereas kidneys for transplantation come from donors with a range of ages, with 37% of deceased donor kidneys coming from donors over 60 years old (NHS Blood and Transplant, 2023). Young pigs also don't have comorbidities such as hypertension. This necessitates

investigations into methods of inducing ischaemic injury to porcine organs so that they more closely mirror human organs.

Extended SCS times have been associated with increased incidences of delayed graft function, affecting DCD organs and organs from older donors to a greater extent (Peters-Sengers et al., 2019, Nieto-Ríos et al., 2019, Summers et al., 2015). Cumulative deleterious effects have been observed with each additional hour of SCS, with some studies also showing a correlation between SCS times and graft loss (Debout et al., 2015, Lum et al., 2023). DGF has also been associated with increased complement activation, although it is likely that complement both contributes to DGF and is activated by other DGF-causing factors (Arias-Cabrales et al., 2021). Extending SCS times of porcine kidneys may therefore cause additional ischaemic injury and complement activation, providing a more appropriate setting to deliver and assess the efficacy of HDM-FH.

### This chapter aims to:

- Carry out stepwise changes to an established porcine kidney retrieval and EVNP model.
- Extend retrieval and SCS times of porcine kidneys to induce complement activation and ischaemic injury.

# 3.2 SPECIFIC METHODS

### 3.2.1 Initial changes to an established porcine EVNP model

A model of porcine EVNP had previously been established at Newcastle by Ms Emily Thompson. However, further optimisation was required for this model. The aim being to activate complement and induce ischaemic injury to kidneys without causing damage to the extent that the organs could not be perfused. Changes were made in a stepwise manner in the first stage of optimisation as a new retrieval and perfusion team was in place (**Figure 3.1**).

Changing one condition per experiment compared with the established model would ensure that variation was due to changing conditions, not human factors. Changes were made to one kidney from each perfused pair, while the other was treated as a control. A 'pass' was defined as renal blood flow > 50 mL/min/100g and urine output > 43 mL/hr (Hosgood et al., 2015). If kidneys 'passed', then another condition would be changed during the next perfusion in addition to the previously investigated change so that in the last step, the cumulative effect of all changes could be investigated (**Figure 3.1**).

Either standard clinical blood bags (Troge) with 100 mL CDPA-1 solution, or standard clinical blood bags depleted of CDPA-1, washed with saline (Fresenius Kabi) and then filled with 10000 IU heparin (Panpharma) with 50 mL saline were used to collect blood. In all cases, kidneys were perfused with blood taken from the same pig. To deplete leukocytes, blood was passed through a leukocyte filter (Haemonetics) prior to addition to the EVNP circuit. For 'whole' blood, the leukocytes were not depleted. An additional secondary period of warm ischaemia was induced by placing kidneys in storage bags into a water bath at 25° C for either 20 or 40 minutes prior to perfusion.

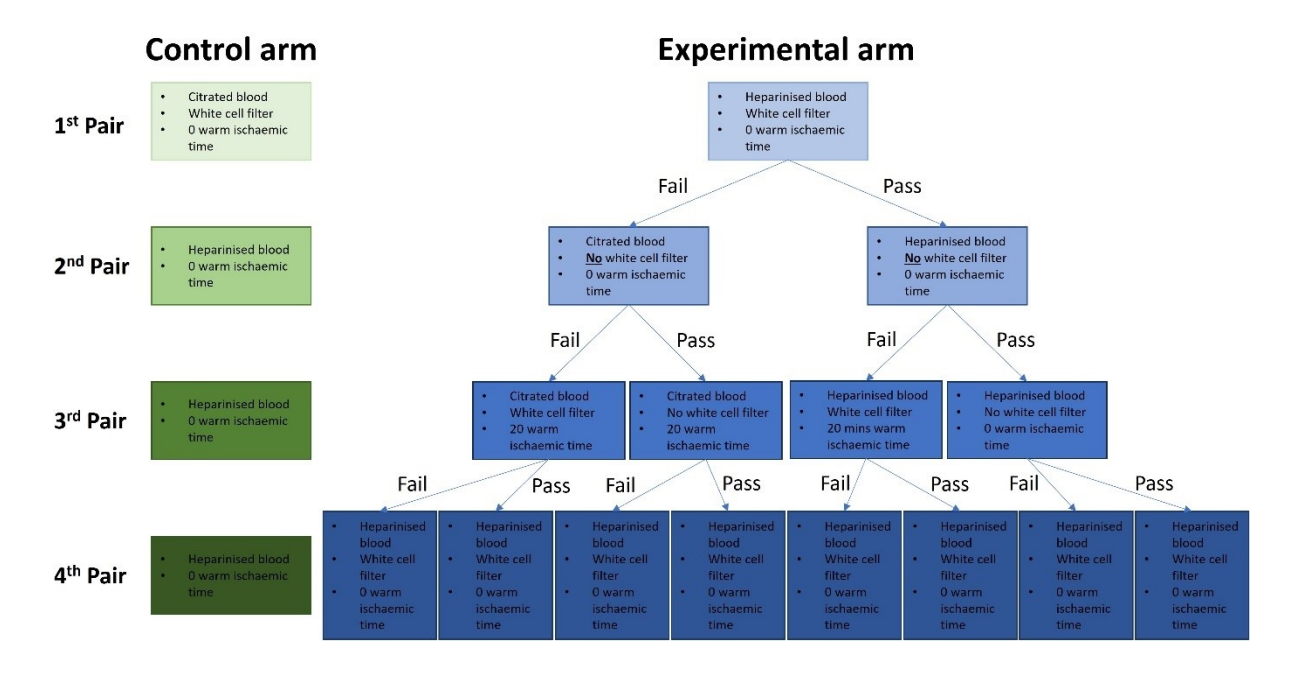


Figure 3.1 Flow chart to determine EVNP conditions in the first stage of model optimisations.

In the previously established porcine EVNP model at Newcastle, citrated autologous blood was collected. To investigate whether EVNP was possible with heparinised blood, each kidney from one pig was perfused with either heparinised or citrated blood. If the experimental arm 'passed' and perfused sufficiently, the next experimental arm would investigate whether kidneys would perfuse sufficiently with whole blood, rather than white cell depleted blood. Following a pass, an additional secondary warm ischaemic time would be introduced, which would be lengthened if it was tolerated by the kidneys. In the event of a 'fail' induced by a step change, a different parameter would be changed and investigated.

Experiments in this chapter were carried out before the RAPIDpoint 500e Blood Gas System described in chapter 2 was available. Blood gas readings were therefore taken using the i-STAT handheld blood analyser (Abbott) using specific CG4+, CG8+ and C3+ cartridges (Abbott) described in **Table 3.1**.

Reading	CG4+	CG8+	G3+	
рН			х	
Venous pO <sub>2</sub>			х	
Arterial pO <sub>2</sub>		х		
Lactate	x			
K <sup>+</sup>		х		
Na <sup>+</sup>		х		
iCa		х		

Table 3.1 Cartridges used to carry out blood analysis.

### 3.2.2 Extension and standardisation of warm and cold ischaemic times

In the second stage of optimisation, the initial warm ischaemic time (WIT) of the kidneys (the time spent warm within the pig following the cessation of cardiac output) was standardised. To achieve this, kidneys were dissected around, and then left in the cavity of the pig for either 20 or 25 minutes from confirmed cessation of cardiac output. Following this, they were removed, immediately flushed with 1 L of cold heparinised UW solution (Bridge to life), and then stored at  $4^{\circ}$ C on ice submerged in UW solution for 16 hours standardised cold ischaemic time (CIT). EVNP was then commenced. The outcomes from these kidneys were then compared with kidneys perfused in the first optimisation stage (3.2.1), which were perfused with whole heparinised blood, did not experience a secondary WIT, and had retrieval times of between 14 - 22 minutes and SCS of 120 - 158 minutes (Table 3.2).

### 3.2.3 Comparison of EVNP with and without a kidney

To investigate complement consumption in whole blood on an EVNP rig without a kidney, blood and kidneys were retrieved as standard with 25 minutes WIT and 16 hours CIT. An EVNP circuit was then set up with the kidney omitted, but all standard perfusate components included. The arterial limb of the circuit was set up to run straight into the venous limb. One kidney was perfused in parallel as standard as a control.

### 3.3 RESULTS

#### 3.3.1 Stepwise changes to perfusion set up

During the first kidney retrieval the renal artery of one kidney was dissected and so could not be flushed with heparinised UW. It was therefore decided to abandon perfusion of that kidney. The remaining kidney was successfully perfused with heparinised blood and so we progressed to the next stage of optimisation using heparinised, whole, non-white cell depleted blood. As there was no control arm for this first pair analysis has been omitted.

The use of heparinised whole blood within the EVNP circuit (second pair) was well tolerated by the kidneys (RBF remained above >50mL/min/100g and urine output was above 43mL/hr). Following this, 20 minutes secondary WIT was introduced to the next experimental kidney (third pair) alongside the use of heparinised whole blood. After this initial shorter secondary WIT was tolerated, it was increased to 40 minutes (fourth pair) (Figure 3.2). The pre-perfusion parameters for each kidney are shown in Table 3.2.

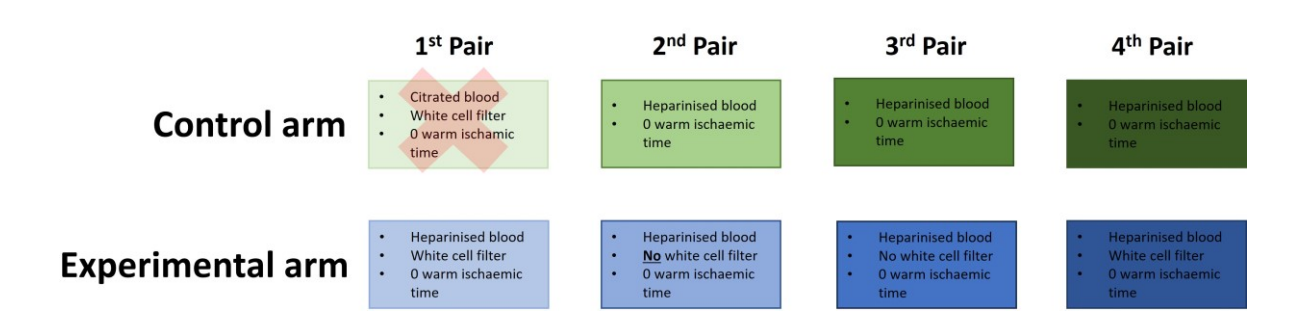


Figure 3.2 Flow chart showing successful porcine EVNP optimisation.

Stepwise changes made to the EVNP model are outlined. Changes were made to one randomised kidney in each pair. The other kidney from the same pair was used as a control. The control kidney from the first pair could not be used due to a retrieval injury.

Pig	Kidney	Initial WIT	CIT (minutes)	Second WIT	Perfusate type
number	pair	(minutes)		(minutes)	
1	First, A	20	117	0	Leukocyte
					depleted
					(heparinised)
1	First, B	22	-	-	-
2	Second,	18	150	0	Leukocyte
	Α				depleted
					(heparinised)
2	Second, B	22	170	0	Whole blood
					(heparinised)
3	Third, A	22	168	0	Whole blood
					(heparinised)
3	Third, B	20	134	20	Whole blood
					(heparinised)
4	Fourth, A	14	126	0	Whole blood
					(heparinised)
4	Fourth, B	17	108	40	Whole blood
					(heparinised)

Table 3.2 Characteristics of perfused porcine kidney pairs.

Initial WIT indicates the time taken from confirmation of cessation of cardiopulmonary effort to the removal of the kidney from the body of the pig. CIT indicates the time from when the kidney is placed on ice for flushing and then into an ice box, to the start of perfusion. Secondary WIT indicates the time spent in a 25° C water bath following removal from ice.

### 3.3.1.1 Physiological parameters and kidney function

Physiological parameters during EVNP were measured as an immediate indicator of kidney function that could be indicative of long-term outcomes (Hosgood et al., 2018). There was no difference in RR, RBF or urine output between kidney pairs. All physiological parameters were worse in the kidneys from the third pair when compared with the second and fourth pair (Figure 3.3).

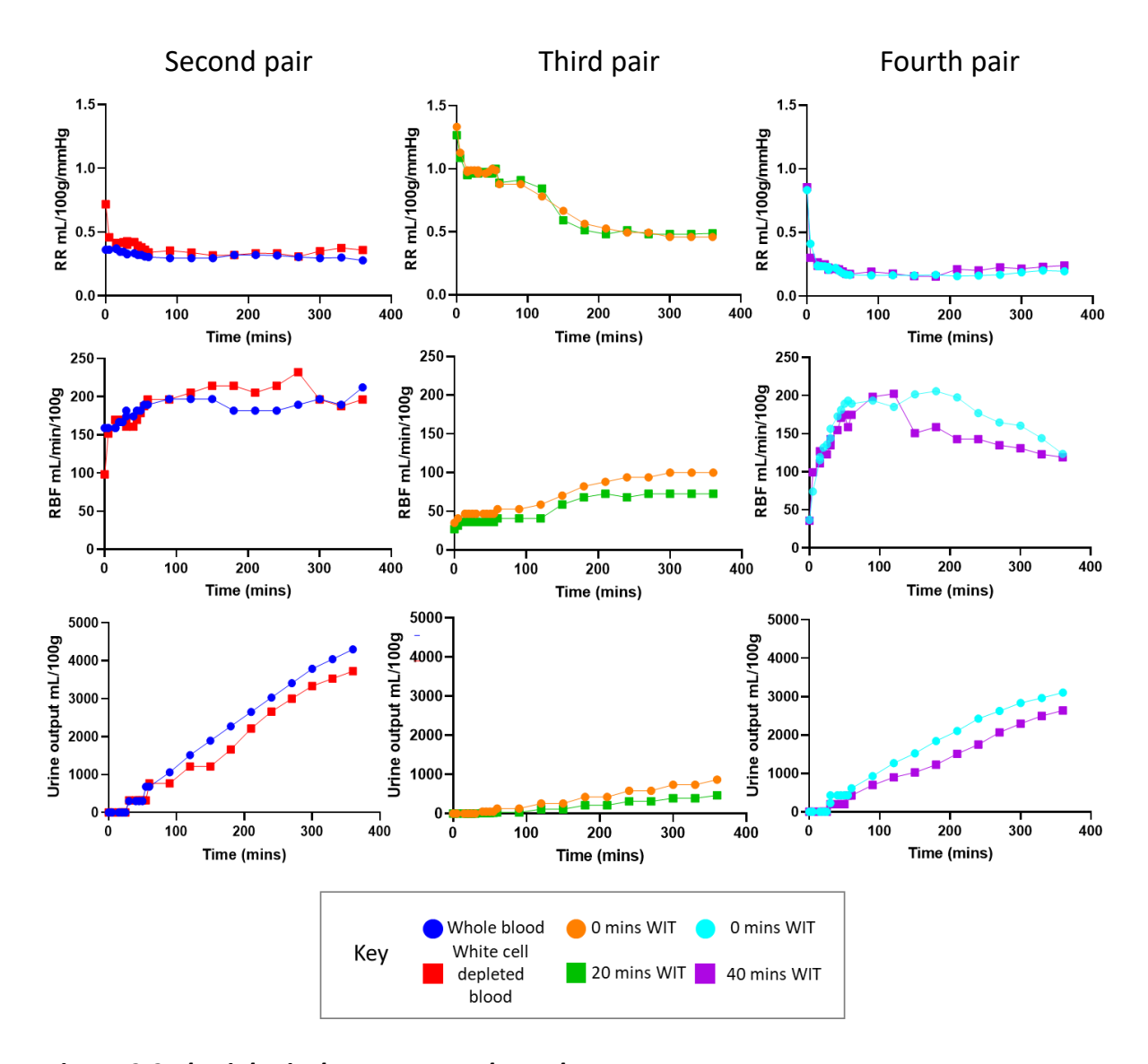


Figure 3.3 Physiological parameters throughout EVNP.

Renal resistance, renal blood flow and urine output were measured from 0 minutes to 360 minutes of perfusion, N=1 (three separate kidney pairs are presented). Individual values are presented.

Plasma creatinine was measured to indicate creatinine clearance by the kidneys as an estimate of GFR. The levels of creatinine in the perfusate dropped over the first three hours of perfusion. There was no difference in plasma creatinine levels within kidney pairs (**Figure 3.4**).

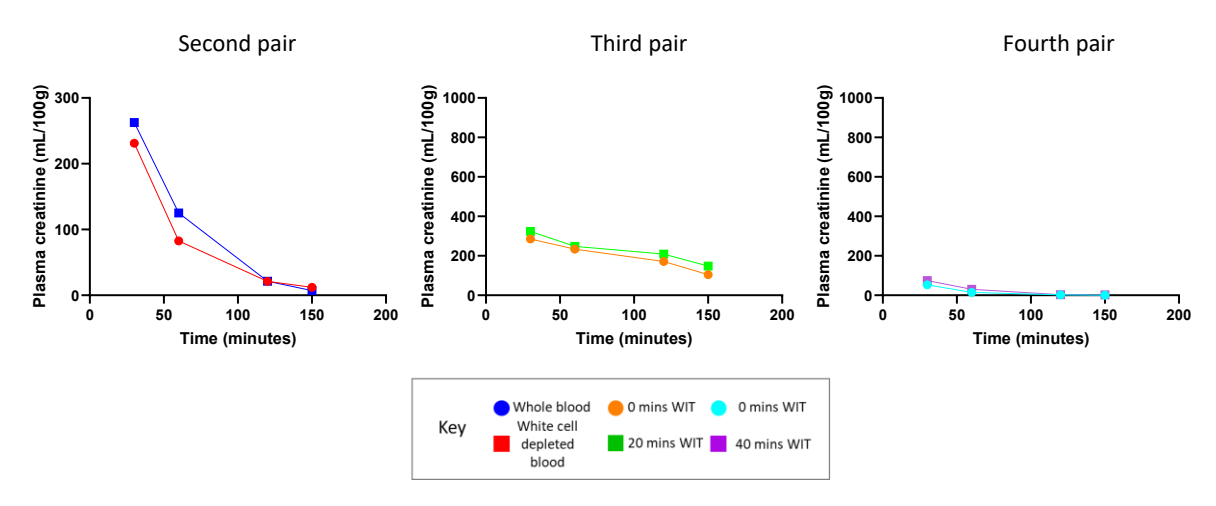


Figure 3.4 Plasma creatinine throughout EVNP.

Creatinine was measured in perfusate from 30 minutes to 150 minutes of perfusion and normalised for kidney weight, N=1 (three separate kidney pairs are presented). Individual values are presented.

### 3.3.1.2 Complement activation

Complement activation, when excessive or unregulated, can lead to C3 glomeruli deposition. C3 deposition in glomeruli was therefore measured as an indicator of complement activation (Pickering et al., 2002, Goodship et al., 2017). C3 deposition within glomeruli increased in all kidneys perfused with whole, non-leukocyte depleted blood over the course of the perfusion. An additional period of warm ischaemia did not increase C3 deposition, with around 3-fold more C3 deposition at the end of perfusion seen in the control kidney of the fourth pair when compared with the experimental kidney with 40 minutes additional secondary WIT (**Figure 3.5**).

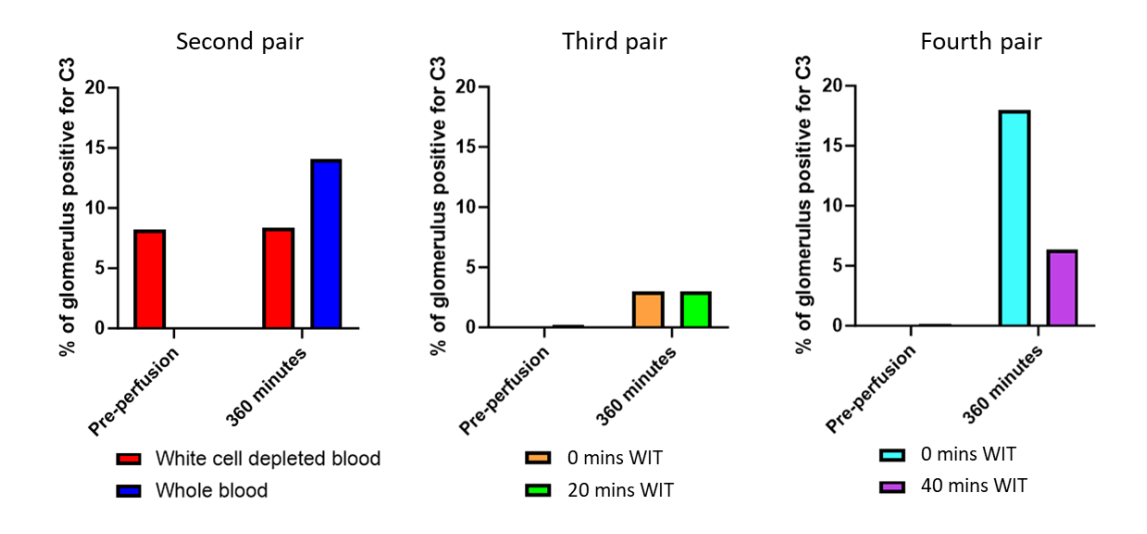


Figure 3.5 C3 deposition in glomeruli pre-perfusion and at 360 minutes of perfusion.

FFPE wedge biopsies taken pre-perfusion and at 360 minutes of perfusion were stained with an anti-C3 antibody. Sections were then imaged using the LEICA DM2000 LED microscope and processed using LAS X software. The percentage area of positive C3 signal of 10 glomeruli was measured from each biopsy, N=1 (three separate kidney pairs are presented). Mean values are presented.

C3a was measured in perfusate to assess C3 activation throughout perfusion. C3a levels dropped throughout perfusion in all kidney pairs (Figure 3.6).

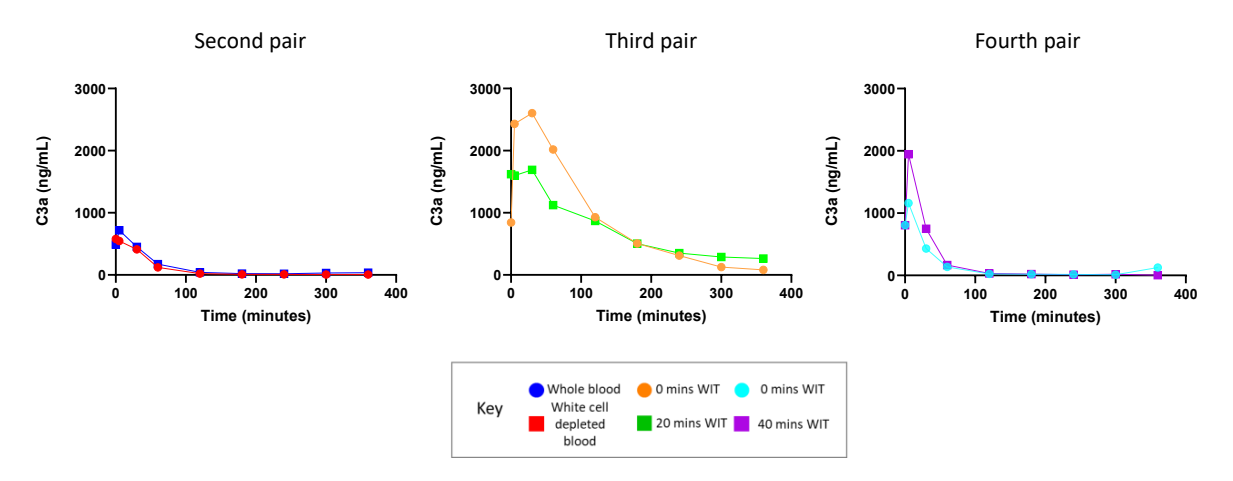


Figure 3.6 C3a levels in perfusate throughout perfusion.

C3a levels were measured in perfusate from 0 to 360 minutes of perfusion using ELISA. Individual values are presented, N=1 (three separate kidney pairs are presented).

# 3.3.2 Extension of cold ischaemic times

Following work carried out in the first stage of optimisation, it was determined that the addition of a secondary WIT after SCS prior to EVNP, while tolerated, did not greatly affect kidney function or complement activation.

Following the first three porcine perfusions, which had slightly varying retrieval and SCS times, it was decided that these times should be standardised to allow for better comparison between different experiments, and to remove sources of variation between pigs in future experiments. Kidneys were therefore subject to retrieval times (WIT) of 20 or 25 minutes, followed by 16 hours SCS (CIT). Three pairs of kidneys were perfused. Kidneys that had undergone approximately 20 minutes retrieval time, 2 hours CIT, and no secondary warm ischaemic time that were perfused with whole, heparinised blood (N=3) from the first stage of optimisations outlined in 3.3.1, were compared with kidneys undergoing 20 minutes of WIT with 16-hour CIT (n=3) and 25 minutes WIT and 16 hours CIT (N=3).

### 3.3.2.1 Renal physiology

Renal physiological parameters were measured to assess if extended initial WIT and CIT affected immediate kidney function. WIT and CIT did not affect RR or RBF (**Figure 3.7** and **Figure 3.8**). Kidneys with an extended CIT of 16 hours had two-fold less urine output compared to kidneys with 2-hour CIT (**Figure 3.9**).

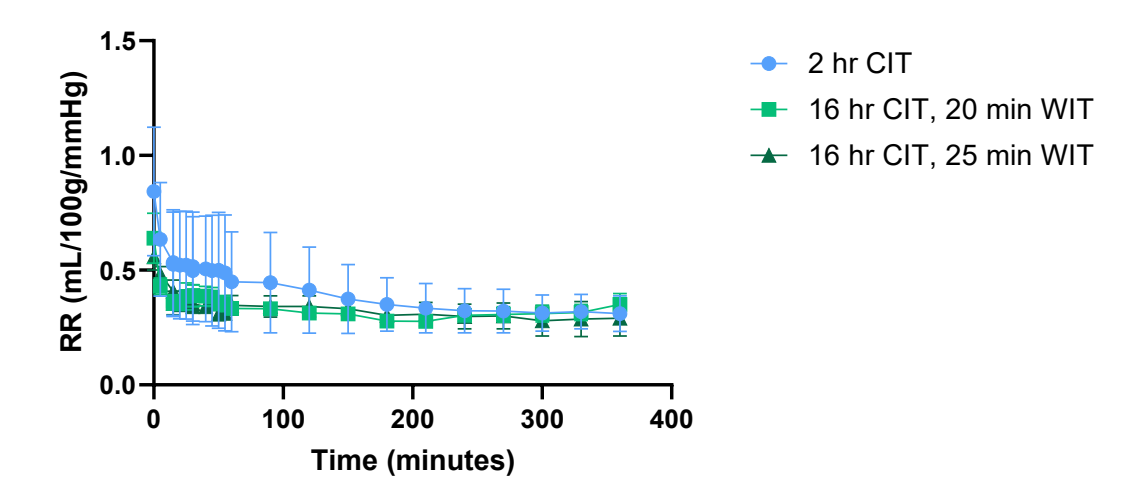


Figure 3.7 Renal resistance in kidneys with 2-hour and 16-hour cold ischaemic times throughout perfusion.

Renal resistance was measured from 0 minutes to 360 minutes of perfusion and normalised for kidney weight, N=3 Mean is presented with SEM. Two-way ANOVA was used to calculate statistical significance.

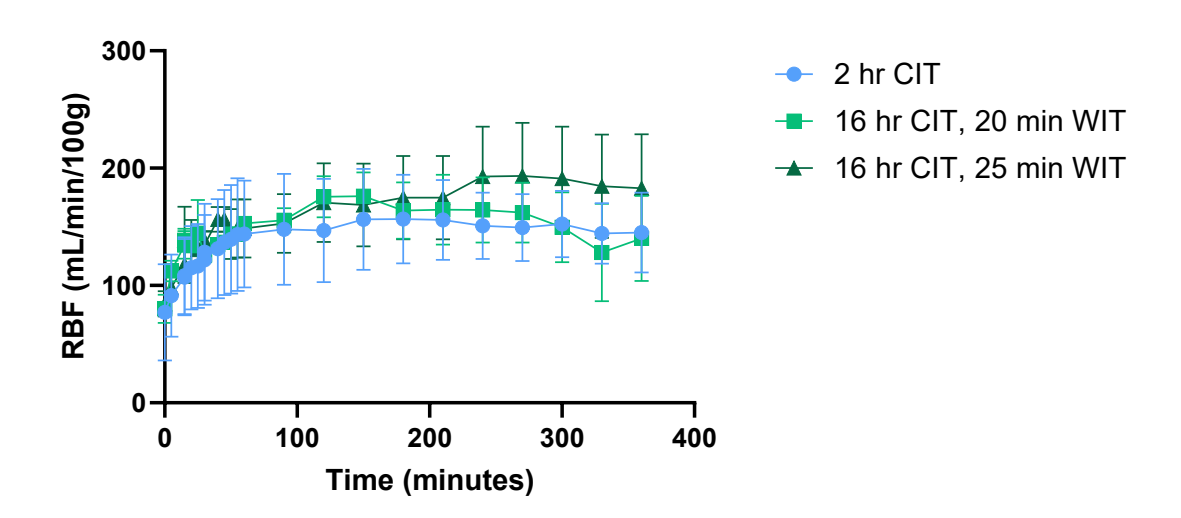


Figure 3.8 Renal blood flow in kidneys with 2-hour and 16-hour cold ischaemic times throughout perfusion.

Renal blood flow was measured from 0 minutes to 360 minutes of perfusion and normalised for kidney weight, N=3. Mean is presented with SEM. Two-way ANOVA was used to calculate statistical significance.

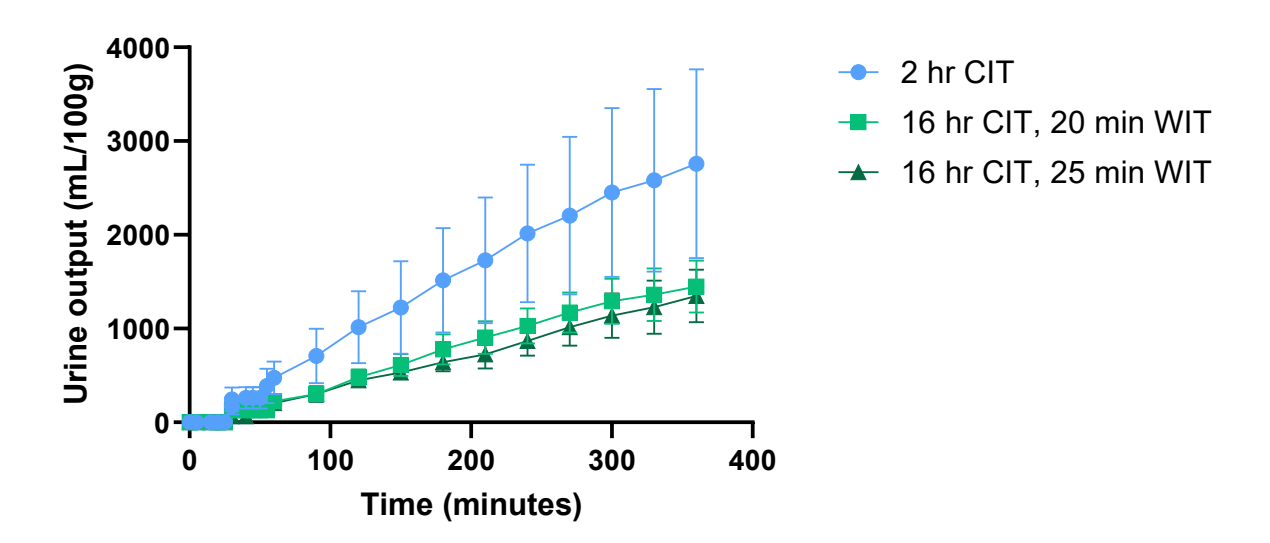


Figure 3.9 Urine output in kidneys with 2-hour and 16-hour cold ischaemic times throughout perfusion.

Urine output was measured from 0 minutes to 360 minutes of perfusion and normalised for kidney weight, N=3. Mean is presented with SEM. Two-way ANOVA was used to calculate statistical significance.

# 3.3.2.2 Cellular metabolism and function

Electrolytes were measured throughout perfusion from arterial perfusate. WIT and CIT did not affect ionised calcium, potassium, sodium or lactate levels throughout perfusion (**Figure 3.10**).

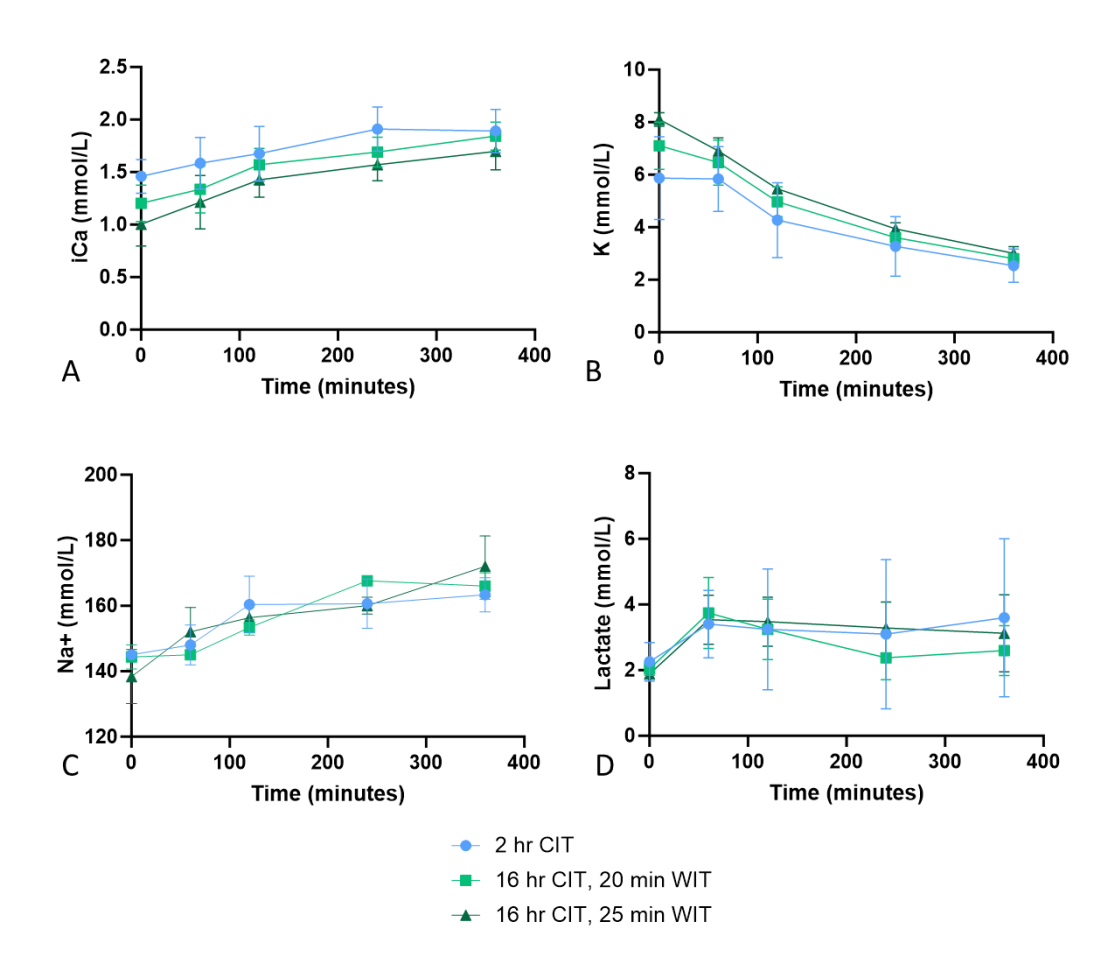


Figure 3.10 Electrolyte levels in kidneys with 2-hour and 16-hour cold ischaemic times throughout perfusion.

Electrolytes were measured from arterial perfusate samples using the i-STAT blood analyser from 0 minutes to 360 minutes of perfusion, N=3. Mean is presented with SEM. Two-way ANOVA was used to calculate statistical significance.

The clearance of creatinine from perfusate was measured as an estimate of GFR. The area under the curve (AUC) value for creatinine clearance for perfusion was 2-fold higher in kidney with 25 minutes WIT and 16 hours CIT compared to kidneys with 2-hour CIT (**Figure 3.11**).

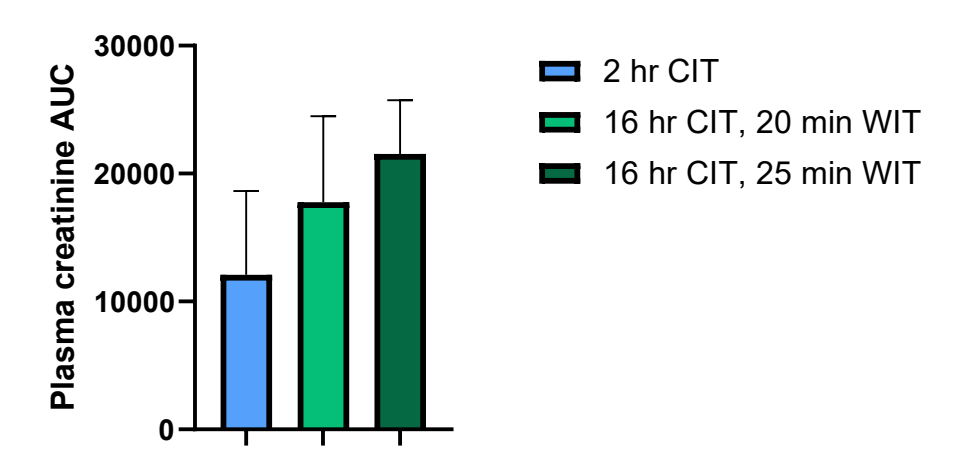


Figure 3.11 Creatinine clearance from perfusate over the first three hours of perfusion.

Creatine levels were measured in perfusate from 30 minutes to 150 minutes of perfusion and normalised for kidney weight. An AUC value was calculated, N=3. Mean is presented with SEM. Unpaired t-test was used to calculate statistical significance.

# 3.3.2.3 Histology

PAS staining was used to visualise kidney morphology. All kidney cohorts showed more morphological signs of damage at the end of perfusion including loss of brush border integrity and shearing of tubular cells, while there appeared to be more signs of damage in kidneys with extended CIT (**Figure 4.12**). In kidneys with 2-hour CIT, good brush border integrity can be seen at the start of perfusion. Over the course of perfusion, brush border integrity is lost in all cohorts of kidneys, this being more severe in kidneys with 16-hour CIT. All cohorts of kidneys also experience shearing of tubular cells into the tubular lumen by the end of perfusion. Over perfusion, kidneys with 16-hour CIT also experienced cast formation.

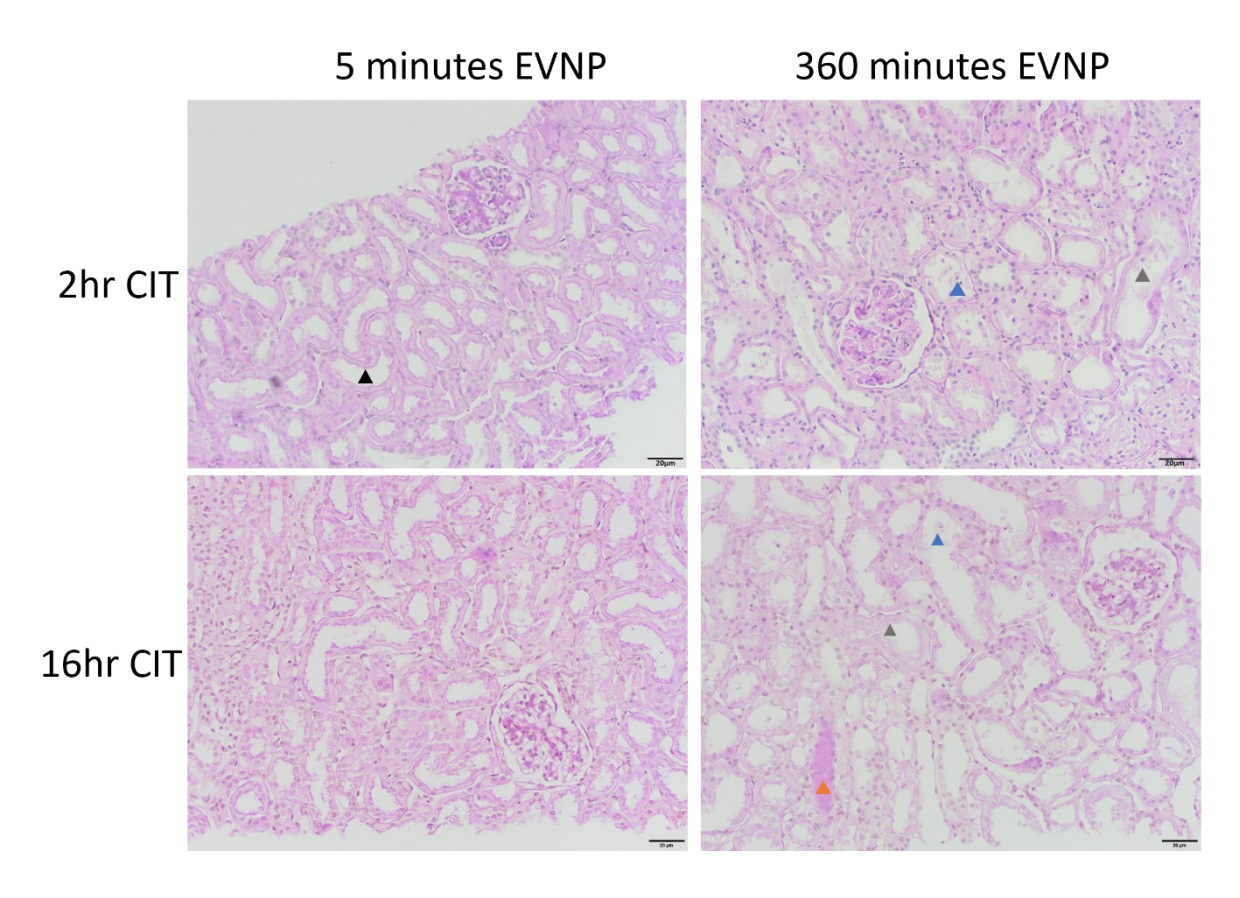
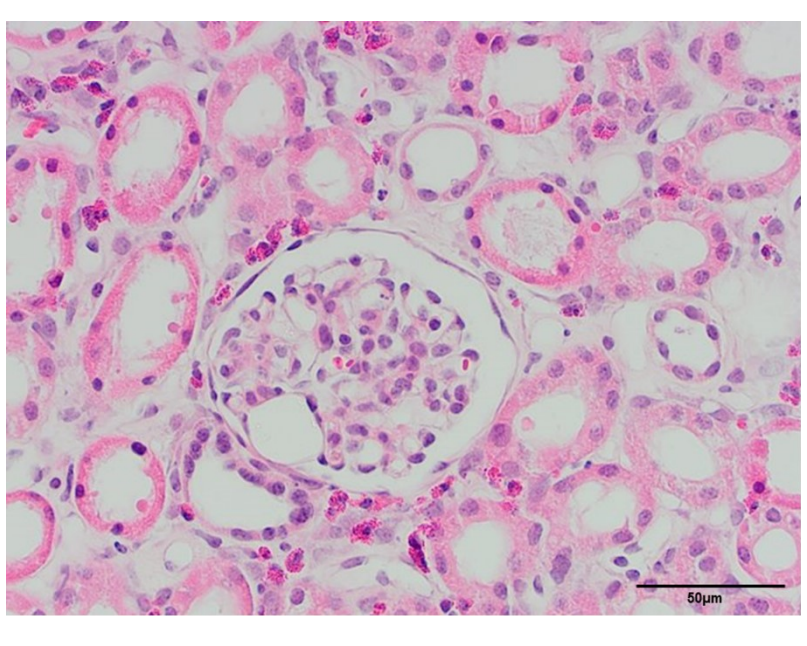


Figure 3.12 Periodic acid-Schiff-stained kidney section from 2-hour CIT kidneys and 16-hour CIT kidneys taken at 5 minutes and 360 minutes of perfusion.

FFPE sections taken at 5 minutes and 360 minutes of perfusion were stained with periodic acid-Schiff, haematoxylin was used as a counterstain. Brightfield images of sections were then taken using the CMOC colour camera SC50 and processes using Cellsens Standard software. Brush border integrity (black arrowhead) can be seen at the start of perfusion in kidneys with 2hr CIT. Shearing of tubular cells into tubular lumens (blue arrowhead), and loss of brush border integrity (grey arrowhead) can be seen at the end of perfusion in all cohorts. Cast formation (orange arrowhead) can be seen only in kidneys with 16-hour CIT at the end of perfusion.

Haematoxylin and eosin staining allowed us to confirm the presence of immune cells in kidney biopsies. Neutrophils could be identified due to their spherical shape and multilobed nuclei. Eosinophils could be identified by their bilobed nuclei, and many granules (Elgert, 1996) (Figure 3.13).



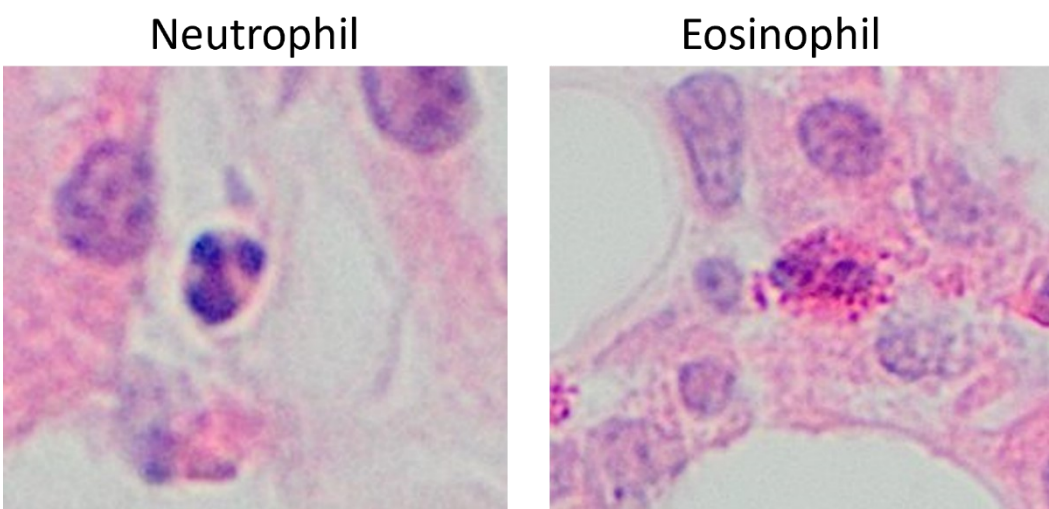


Figure 3.13 Haematoxylin & eosin-stained kidney section taken at 360 minutes of perfusion showing an influx of immune cells.

An FFPE section from the end of perfusion was stained with haematoxylin and eosin. Brightfield images of sections were then taken using the CMOC colour camera SC50 and processed using Cellsens Standard software. Neutrophils and eosinophils can be seen in the kidney interstitium in a H&E-stained biopsy taken at the end of perfusion.

# 3.3.2.4 Immunofluorescence

Fibrinogen deposition within glomeruli was measured to assess the effect of extended CIT and WIT on fibrinogen release at the start and end of perfusion. Fibrinogen detected in the glomeruli was increased by approximately 150-fold at the end of perfusion compared with pre-perfusion in all cohorts (**Figure 3.14** and **Figure 3.15**).

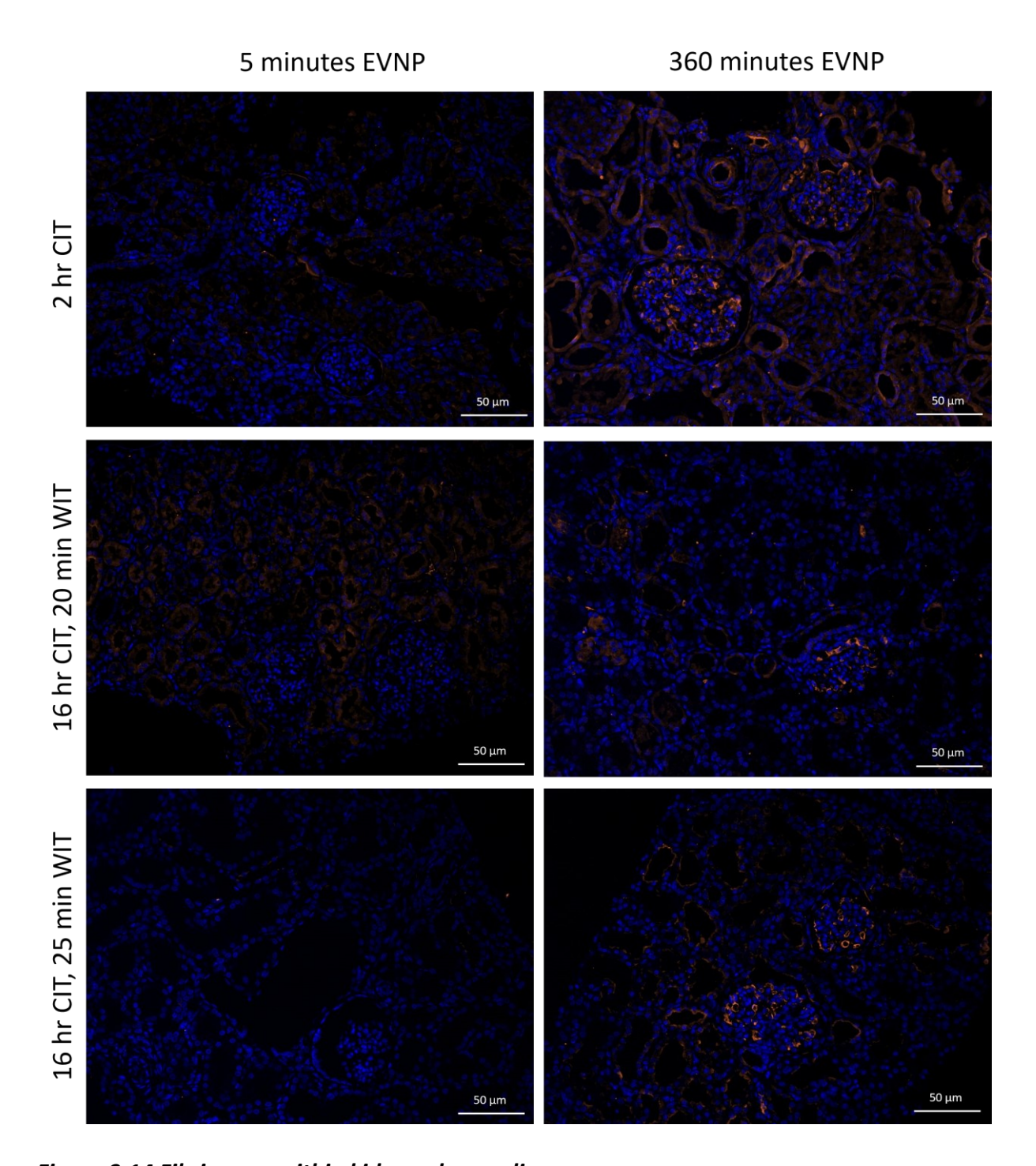


Figure 3.14 Fibrinogen within kidney glomeruli.

FFPE wedge biopsies were stained with an anti-fibrinogen antibody, DAPI was used as a counterstain. Sections were then imaged using the LEICA DM2000 LED microscope and processed using LAS X software. Fibrinogen is shown in orange, DAPI is shown in blue.

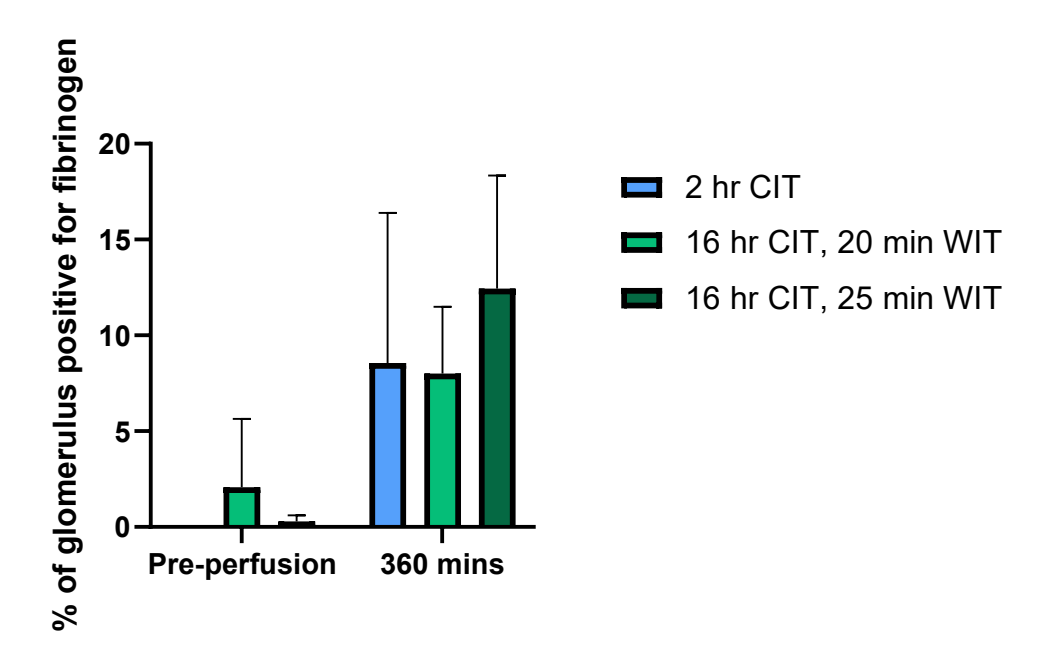


Figure 3.15 Glomerular deposition of fibrinogen pre-perfusion and at 360 minutes of perfusion.

FFPE wedge biopsies taken pre-perfusion and at 360 minutes of perfusion were stained with an anti-fibrinogen antibody. Sections were then imaged using the LEICA DM2000 LED microscope and processed using LAS X software. The percentage area of positive fibrinogen signal of 10 glomeruli was measured from each biopsy, N=3. Mean is presented with SEM. Two-way ANOVA was used to calculate statistical significance.

A TUNEL assay was used to detect apoptotic cells in tissue through binding to fragmented nuclear DNA. Apoptosis increased in all kidney cohorts at the end of perfusion compared with pre-perfusion. Apoptosis was 20-fold higher at the end of perfusion in kidneys with 16 hours CIT and 25 minutes WIT at the end of perfusion compared with the start. End of perfusion apoptosis was 4-fold higher in kidneys with 16 hours CIT and 25 minutes WIT than in kidneys with 2 hours CIT (Figure 3.16 and Figure 3.17).

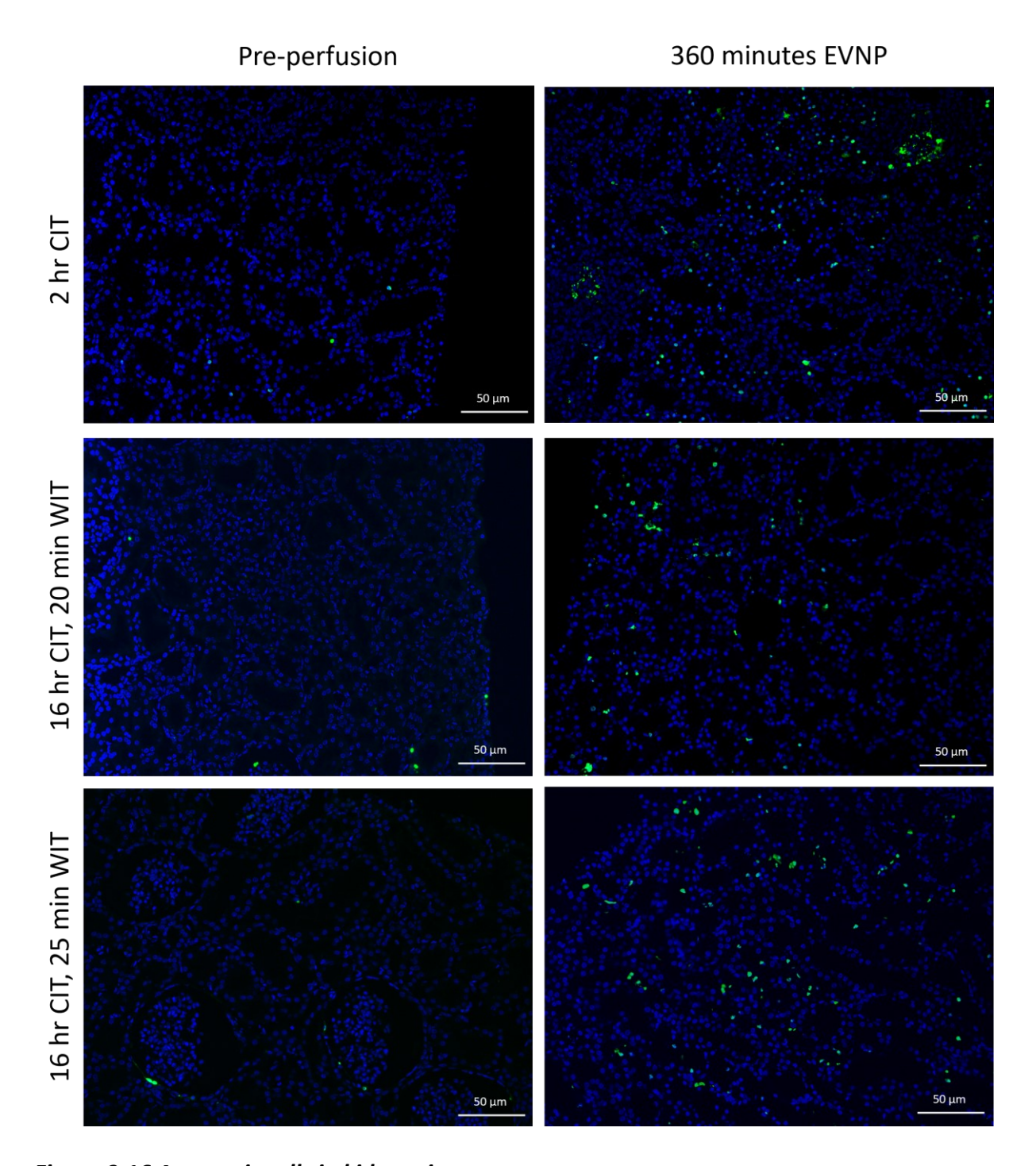


Figure 3.16 Apoptotic cells in kidney tissue.

FFPE wedge biopsies were stained with a TdT-mediated dUTP Nick-End Labelling assay, DAPI was used as a counterstain. Sections were then imaged using the LEICA DM2000 LED microscope and processed using LAS X software. Apoptotic bodies are shown in green, DAPI is shown in blue.

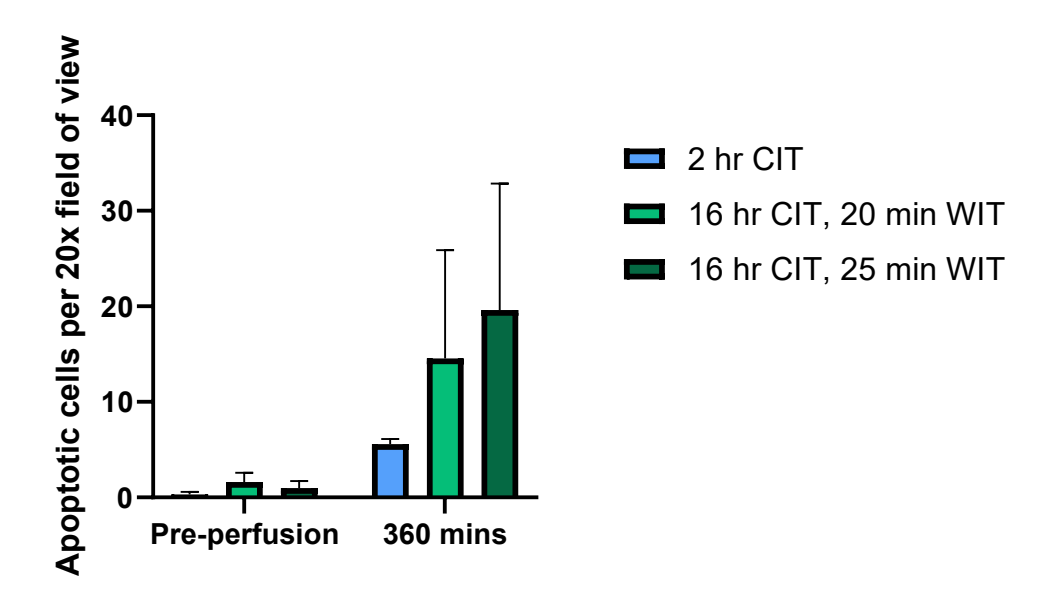


Figure 3.17 Percentage of apoptotic cells in kidney sections pre-perfusion and at 360 minutes of perfusion.

FFPE wedge biopsies taken pre-perfusion and at 360 minutes of perfusion were stained with a TdT-mediated dUTP Nick-End Labelling assay. Sections were then imaged using the LEICA DM2000 LED microscope and processed using LAS X software. Apoptotic bodies and nuclei were counted individually 10 20x magnification images. These values were used to calculate a percentage of apoptotic bodies per 20x field of view, N=3. Mean is presented with SEM. Two-way ANOVA was used to calculate statistical significance.

In kidneys with 16-hour CIT, glomerular C3 deposition was seen pre-perfusion. In all kidney cohorts, C3 was significantly up regulated over the time of perfusion. There was significantly higher C3 deposition in kidneys with the 25 minutes WIT and 16 hours CIT, compared to those with 2 hours CIT, both prior to and at the end of perfusion (Figure 3.18 and Figure 3.19).

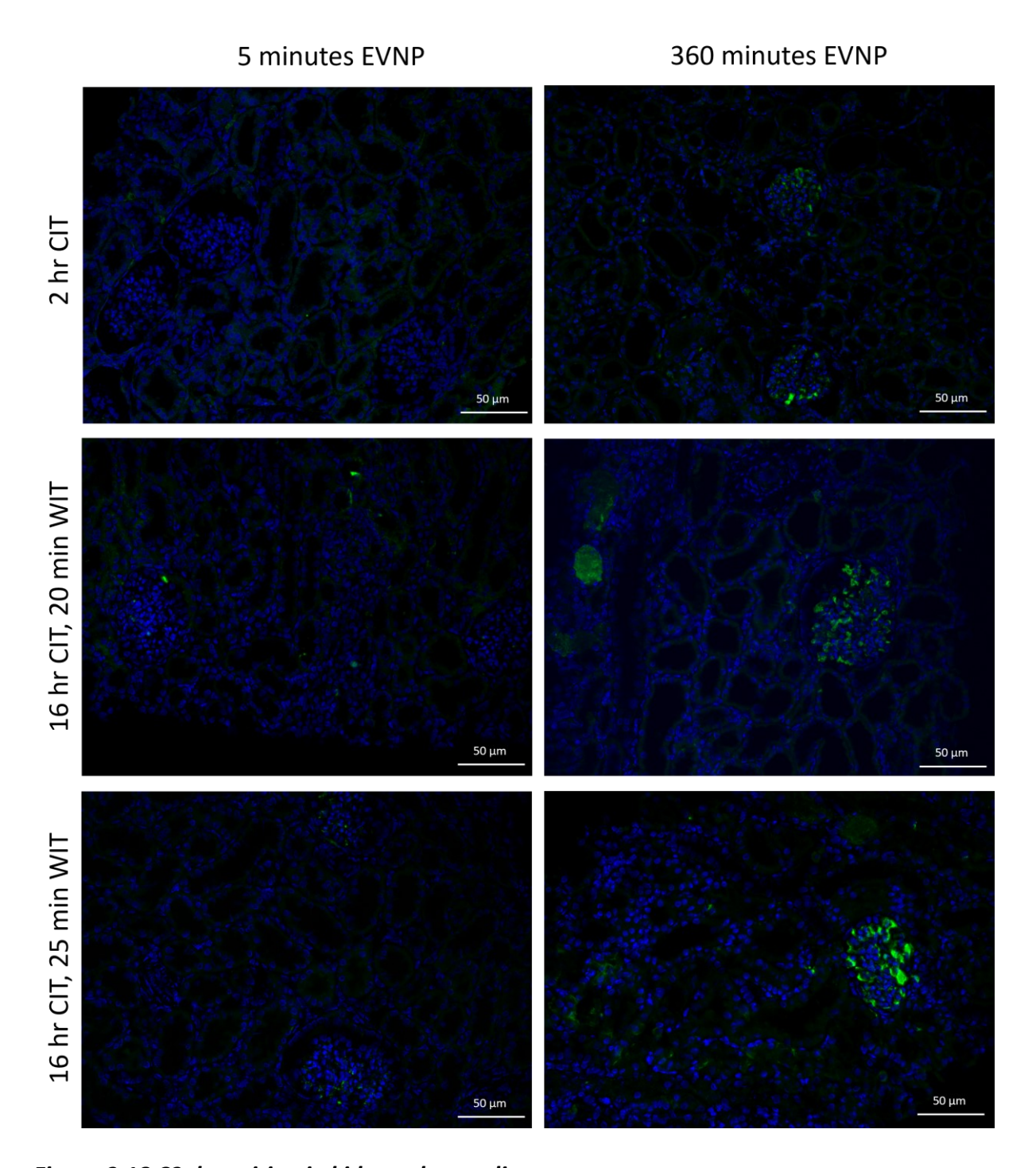


Figure 3.18 C3 deposition in kidney glomeruli.

FFPE wedge biopsies were stained with an anti-C3 antibody, DAPI was used as a counterstain. Sections were then imaged using the LEICA DM2000 LED microscope and processed using LAS X software. C3 is shown in green, DAPI is shown in blue. C3 can be seen within the glomeruli.

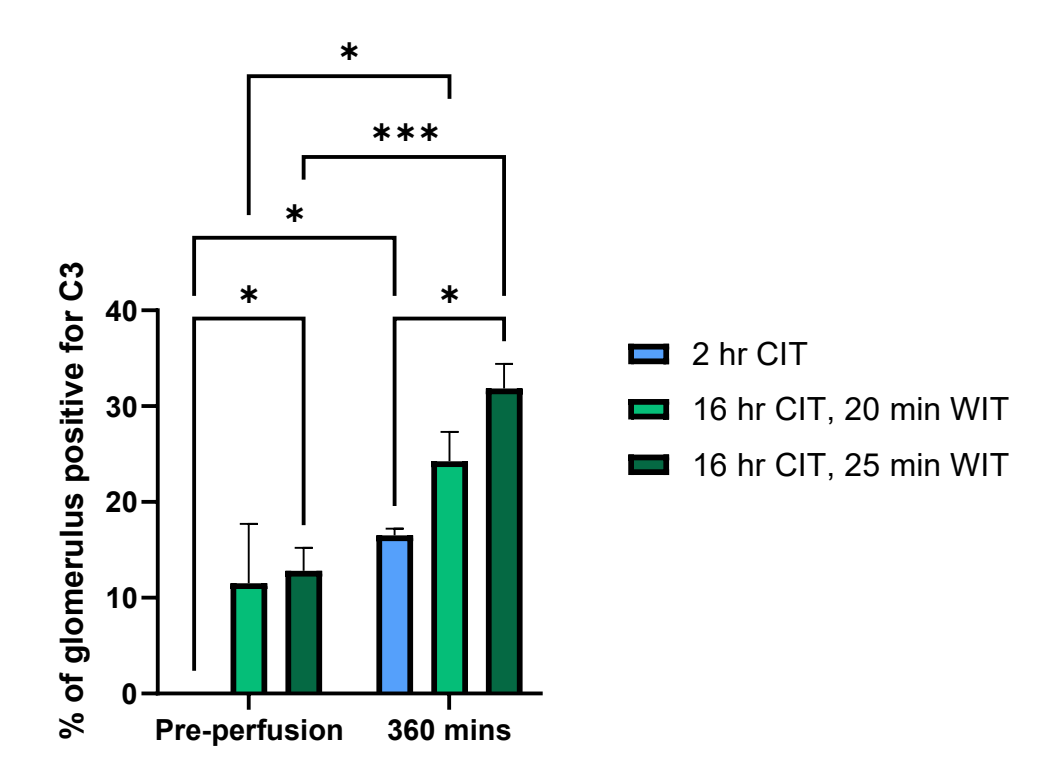


Figure 3.19 Glomerular deposition of C3 pre-perfusion and at 360 minutes of perfusion.

FFPE wedge biopsies taken pre-perfusion and at 360 minutes of perfusion were stained with an anti-C3 antibody. Sections were then imaged using the LEICA DM2000 LED microscope and processed using LAS X software. The percentage area of positive C3 signal of 10 glomeruli was measured from each biopsy, N=3. Mean is presented with SEM. Two-way ANOVA was used to calculate statistical significance. \*p<0.05, \*\*\*p<0.001.

#### 3.3.2.5 Perfusate and urine composition

C3a levels in perfusate were compared between cohorts to assess the effect of WIT and CIT on C3 breakdown. At 5 minutes of perfusion, C3a was two-fold higher in kidneys with 20 minutes WIT and 16-hour CIT than kidneys with 2-hour CIT. By 30 minutes of perfusion there was no difference in C3a levels between cohorts. C3a levels in perfusate dropped over the 6 hours of perfusion in all cohorts (**Figure 3.20**).

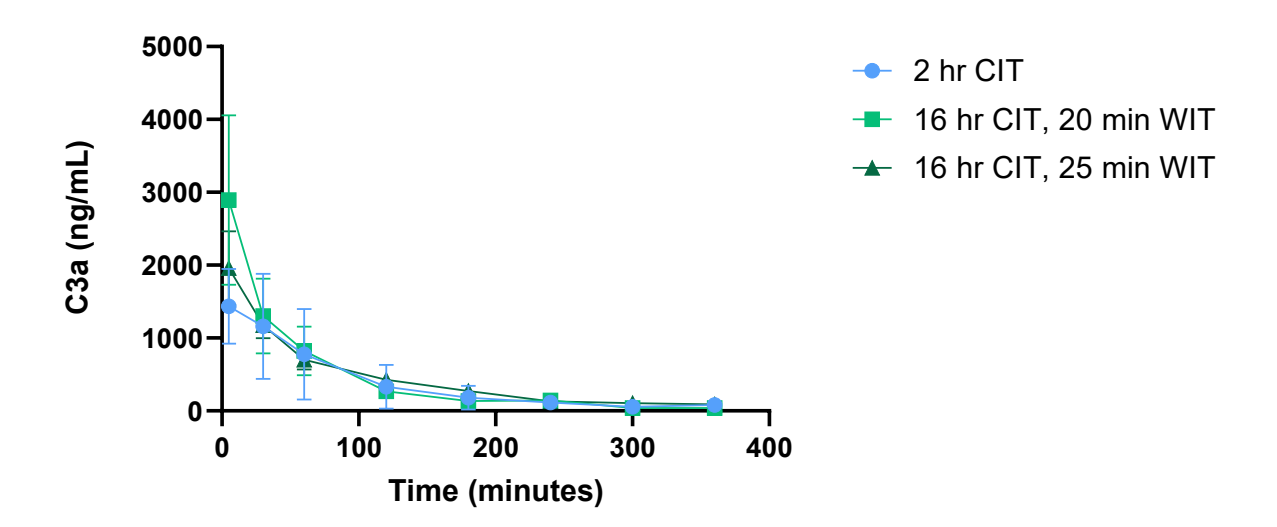


Figure 3.20 C3a levels in perfusate from 5 minutes to 360 minutes of perfusion.

C3a levels were measured in perfusate from 5 minutes to 360 minutes of perfusion using ELISA, N=3. Mean is presented with SEM. Two-way ANOVA was used to calculate statistical significance.

Hyaluronan was measured in EVNP perfusate as a marker of endothelial activation leading to glycocalyx shedding. Hyaluronan levels rose in all kidney cohorts over the course of the perfusion by approximately 2-fold. This difference was significant in the 16-hour CIT, 25-minute WIT kidneys (Figure 3.21.

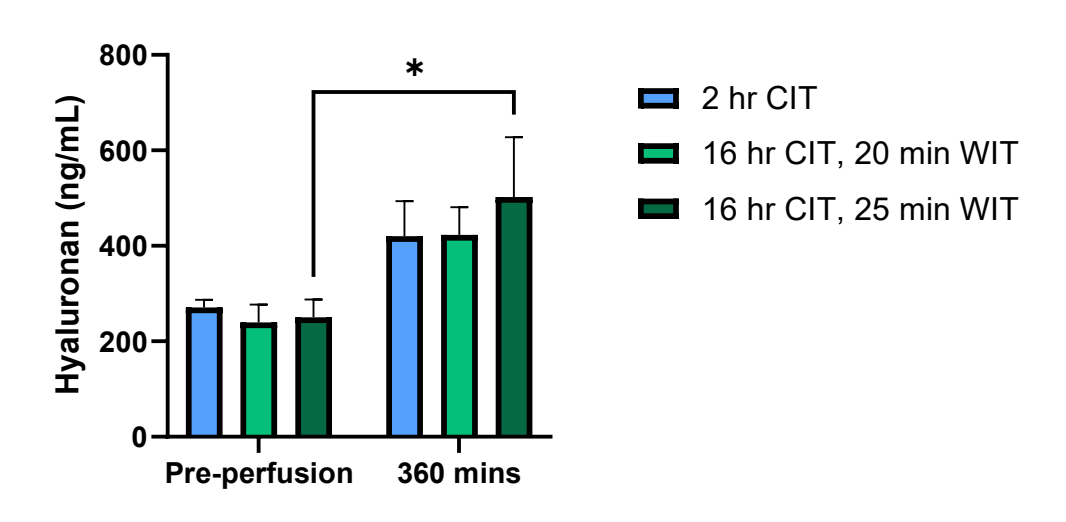


Figure 3.21 Hyaluronan levels in perfusate pre-perfusion and at 360 minutes of perfusion.

Hyaluronan concentrations in perfusate samples taken from the EVNP circuit pre-perfusion and at 360 minutes of perfusion were measured using ELISA, N=3. Mean and SEM are presented. Two-way ANOVA was used to calculate statistical significance. \*p<0.05.

IL-6 and IL-8 were measured in urine produced by kidneys during EVNP as markers of inflammation. In all cohorts, IL-6 and IL-8 increased over the course of the perfusion. There was around a 40-fold increase in IL-6 at the end of perfusion compared with 30 minutes of perfusion in the 16 hour CIT 25 minute WIT kidneys and a 1000-fold increase in IL-8 at the end of perfusion compared with 30 minutes of perfusion (Figure 3.22 and Figure 3.23).

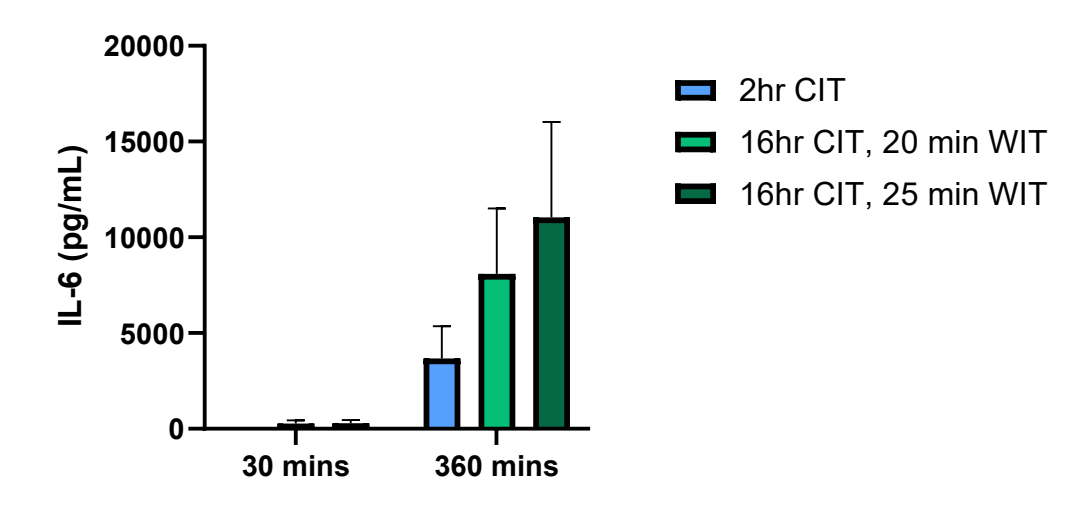


Figure 3.22 IL-6 levels in urine at 30 and 360 minutes of perfusion.

IL-6 concentrations in urine samples taken at 30 minutes and at 360 minutes of perfusion were measured using ELISA N=3. Mean is presented with SEM. Two-way ANOVA was used to calculate statistical significance.

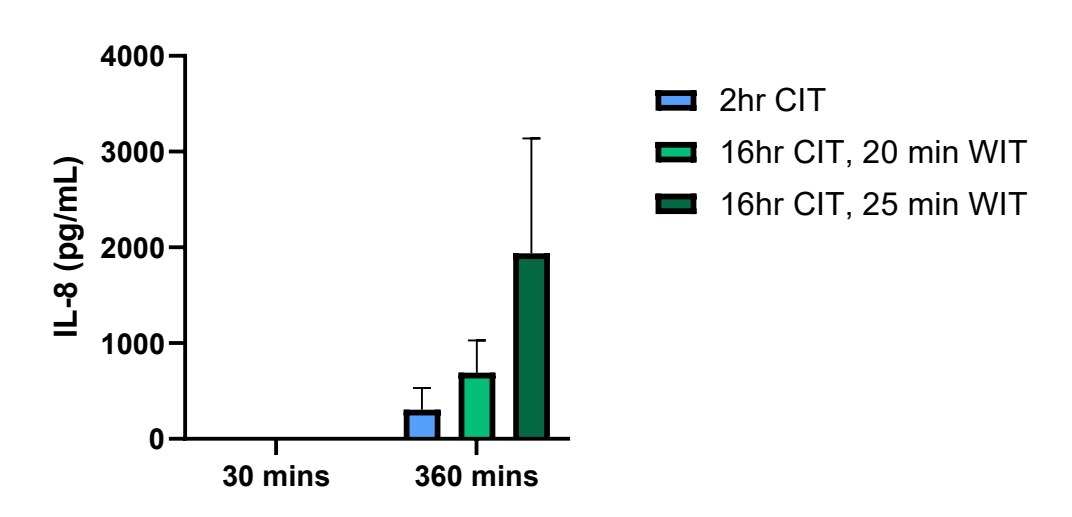


Figure 3.23 IL-8 levels in urine at 30 and 360 minutes of perfusion.

IL-8 concentrations in urine samples taken at 30 minutes and at 360 minutes of perfusion were measured using ELISA, N=3. Mean is presented with SEM. Two-way ANOVA was used to calculate statistical significance.

# 3.3.3 Blood only perfusion experiment showing complement activity in EVNP system

Classical haemolytic assays were used to measure complement consumption in perfusate. If a higher sample concentration is required to lyse sensitised sheep red blood cells to achieve  $CH_{50}$ , this indicates that the active complement components in the sample have been consumed due to complement activation. The  $CH_{50}$  was measured in samples taken from perfusate from:

- An EVNP rig with standard blood and perfusate and a kidney attached that has had
   16-hour CIT and 25 minutes WIT.
- An EVNP rig with standard blood and perfusate with no kidney attached.

Complement consumption increased linearly over time in the EVNP rig with no kidney in a pattern similar to that in a rig with a kidney (Figure 3.24).

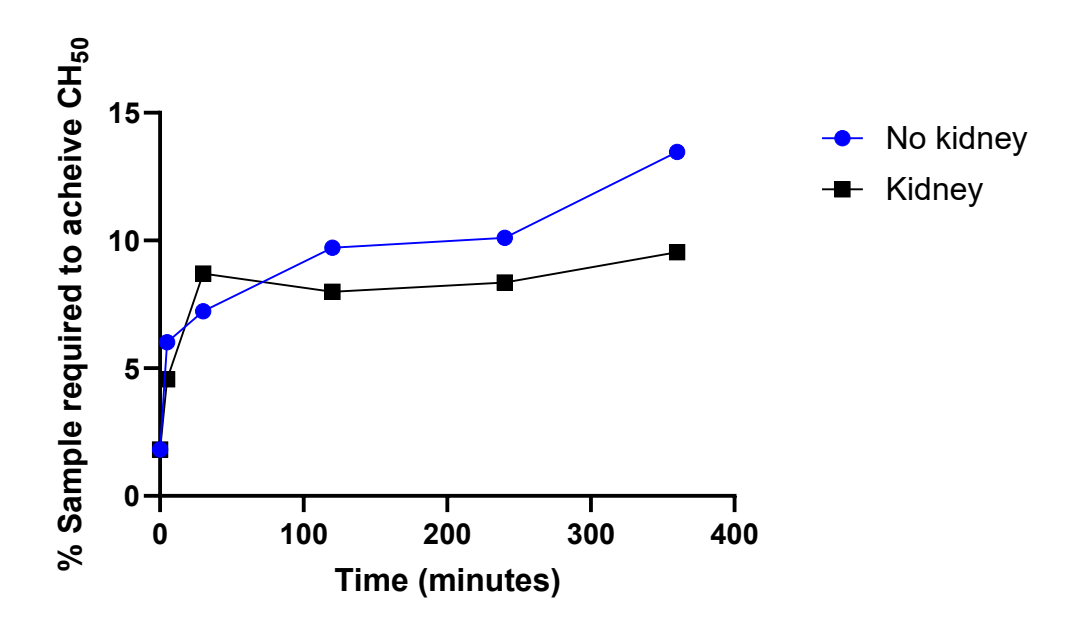


Figure 3.24 Complement consumption in an EVNP circuit with and without a kidney throughout perfusion.

The percentage dilution of samples taken from 0 minutes to 360 minutes of perfusion in an EVNP circuit with and without a kidney required to achieve  $CH_{50}$  was found using classical haemolytic assays, N=1. Individual values are presented.

C3a was measured in perfusate to assess C3 breakdown in an EVNP circuit with and without a kidney. While the C3a levels in the EVNP circuit with a kidney drop and plateau at around 120 minutes, C3a levels remain steady at around 46-fold higher in the circuit without a kidney than in the EVNP circuit with a kidney (**Figure 3.25**).

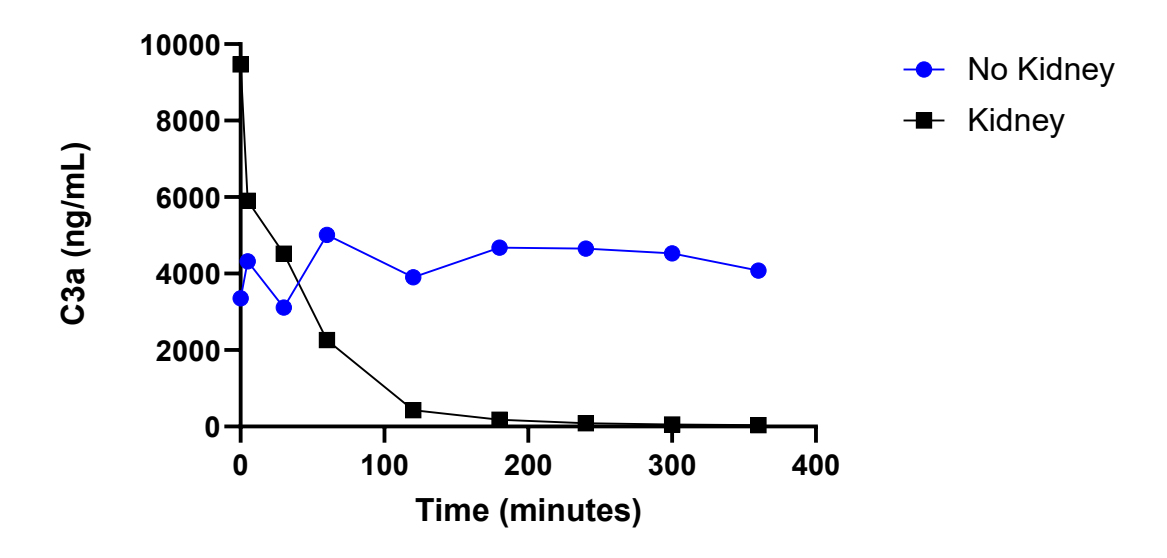


Figure 3.25 C3a levels in an EVNP circuit with and without a kidney throughout perfusion.

C3a levels were measured in perfusate taken throughout perfusion using ELISA, N=1. Individual values are presented.

#### 3.4 Discussion

While benefits of a porcine EVNP model include predictable availability, a homogenous sample cohort and the ability to standardise the ischaemic insult, porcine organs aren't always representative of human organs clinically available for transplant. Additionally, HDM-FH likely requires complement activation fragments for adequate or optimal binding. Work in this chapter aimed to optimise a porcine model of EVNP in which kidneys sustained ischaemic injury and in which complement is activated. This was so that in future work the efficacy of HDM-FH in preventing ischaemic injury could be tested. It would also make the model more clinically relevant.

Before the effects of extended SCS could be investigated, key changes were required to alter the porcine EVNP model established at Newcastle by Ms Emily Thompson in 2018. Previously, a citrate based anticoagulant CDPA-1 provided inside standard clinical blood bags was used to prevent clotting. However, due to the ability of citrate to reduce complement activation in blood (Huang et al., 2015), this was replaced by heparin. The depletion of leukocytes from porcine blood prior to perfusion has been shown to improve kidney function and improve tubular damage (Harper et al., 2006). Leukocyte depletion using a leukocyte filter was therefore previously carried out at Newcastle. However, a unique benefit of porcine EVNP is the availability of whole blood, which is logistically difficult to source for human experiments.

Plasma and immune cells are an important source of complement, while complement activation can also influence immune cell migration from blood to kidneys (Dunkelberger and Song, 2010). Therefore, in this work leukocytes would be beneficial not only due to the injury they cause, but because they would allow downstream assessment of the effects of HDM-FH on leukocyte infiltration. Following these changes in the first stage of optimisations, an additional secondary period of warm ischaemia was included by placing kidneys, while in storage bags, into a water bath 25° C for either 20 or 40 minutes prior to perfusion as an additional ischaemic insult.

Changes were made in a stepwise manner to investigate the effects of each change individually and then cumulatively. All initial changes were well tolerated by kidneys with functional parameters of urine output and blood flow measured in real time. All kidneys perfused with whole, non-white cell depleted blood experienced an increase in C3 deposition over the course of the perfusion. The addition of a secondary warm ischaemic time did not

appear to affect kidney function or complement activation, it was therefore decided to move to the next stage of optimisation.

To improve reproducibility, the initial WIT of the kidneys was standardised as retrieval time affects transplant outcomes, with longer retrieval times associated with DGF and primary nonfunction (Osband et al., 2016). Clinically, upon confirmation of death following the withdrawal of life support, organs are flushed with cold preservation solution beginning the cold ischaemic time. However functional warm ischaemia can begin before confirmation of death and is clinically defined as starting when systolic blood pressure goes below 50 mmHg and/or oxygen consumption below 70% (Gunning, 2010). This is the period of time mirrored during the 'initial warm ischaemic time'. The length of SCS which is the CIT of kidneys was also standardised.

Urine output is a used as an indicator of kidney function following transplantation, with low output indicating kidney injury, and is associated with mortality in transplant patients, so is an indicator of kidney function at the most basic level (Ralib et al., 2013). Reduced urine output in kidneys with extended CIT indicates that kidney injury occurs over SCS. This indicates that deleterious processes are occurring during retrieval and SCS that affect the ability of kidneys to perform their basic filtrating function. In addition to urine output, creatinine clearance is a well-documented measurement of kidney function. It measures how well the kidney is able to clear creatinine from blood plasma, giving an indication of the GFR, with low creatinine clearance indicating renal damage (Shahbaz and Gupta, 2021). Creatinine levels in plasma were measured in this model as an indicator of creatinine clearance. Creatinine clearance from plasma was approximately 2-fold lower in kidneys with the shortest CIT and WIT compared with those with the longest, supporting the urine output data in suggesting a reduction in kidney function due to extended CIT and WIT. The elevation in lactate over the first hour or perfusion despite oxygen being present suggests that aerobic glycolysis is occurring. This may be driven by TGF- β signalling which could also play a role in the increase in fibrin/fibrinogen observed (Lan et al., 2016).

PAS staining was used to visualise kidney morphology. Certain obvious morphological features that indicate kidney damage were observed in sections taken from different kidney cohorts at the start and end of perfusion. In kidneys with shorter CIT, good brush border integrity can be seen at the start of perfusion. Over the course of perfusion, brush border integrity is lost in all

cohorts of kidneys, this being more severe in kidneys with longer CIT. All cohorts of kidneys also experience shearing of tubular cells into the tubular lumen by the end of perfusion. Over perfusion, kidneys with longer CIT also experience cast formation. This histological data is consistent with findings that show increased morphological injury following IRI (Aitken et al., 2016, Zhou et al., 2000). Furthermore, in the setting of EVNP, a significant overall worsening of kidney morphology has been observed after 6 hours of perfusion (Harper et al., 2006).

Immune cells including eosinophils and neutrophils were observed within the interstitium of kidneys on H&E-stained sections at the end of perfusion. The presence of immune cells on H&E-stained sections indicates that downstream analysis of the effects of HDM-FH on immune cell infiltration is possible.

The glycocalyx is a carbohydrate rich layer lining vascular endothelium. It is highly susceptible to deleterious processes including inflammation and ischaemia reperfusion, with damage indicating vascular and endothelial dysfunction. The glycocalyx is prone to shedding when damaged by matrix proteinases in a process driven by TNF-alpha signalling and is observed in association with IRI (Rehm et al., 2007, Duni et al., 2021). Hyaluronan is a glycocalyx component, with increased circulating levels indicating loss of glycocalyx structure and therefore endothelial dysfunction. An accumulation of hyaluronan can also exacerbate inflammation and fibrosis through leukocyte recruitment and enhancement of the TGF- $\beta$  pathway following ligation to CD44, which is found on damaged tubular cells and immune cells (Colombaro et al., 2013, Rouschop et al., 2004, Declèves et al., 2006).

Hyaluronan levels in kidney perfusate were measured by ELISA. Hyaluronan levels increased over the course of perfusion in all kidney cohorts, this was significant in kidneys with the most extended CIT and WIT suggesting that these factors lead to endothelial dysfunction.

Inflammatory cytokines in urine are used as markers for AKI and DGF. They are known to be upregulated in response to IRI and have a significant role in the inflammatory process following reperfusion. Tubular epithelial cells and macrophages experiencing hypoxia will express cytokines including IL-6 and IL-8 in response to C3a and C5a signalling. Activated neutrophils that have migrated to the site of injury will also release pro-inflammatory cytokines (Akcay et al., 2009, Peng et al., 2012). Urinary IL-6 and IL-8 levels were measured in urine. In all kidney cohorts, levels of both were upregulated over the course of perfusion. Due to the association of IL-6 and IL-8 with renal dysfunction and ischaemic injury, these results

show that EVNP is a proinflammatory environment, in line with data from other EVNP models (Nath et al., 2017, Hosgood et al., 2017, Hameed et al., 2020, Jager et al., 2022).

Elevated cytokine levels could be due to neutrophil recruitment from the circulating whole blood to into the kidney, and ongoing complement activation by DAMPs. High cytokine levels in kidneys with extended CIT and WIT suggests that during both of these ischaemic phases, TECs and macrophages could be activated as cold storage followed by rewarming has been seen to trigger cytokine production (Lo et al., 2021), with extended WIT exposing kidneys to a pro-inflammatory environment for a greater time.

An anti-fibrinogen antibody was used to stain for fibrinogen/fibrin in kidney biopsies. As kidneys were perfused with whole blood, fibrinogen present could have been cleaved to fibrin through thrombin mediated cleavage, although to a limited extent as the liver is the primary source of thrombin (Narayanan, 1999). Furthermore, the oxygenator and reservoir components of the EVNP circuit are coated with negatively charged sulphonated polymers which bind antithrombin, inhibiting the action of thrombin (Silver et al., 1992). In kidneys with extended cold times, fibrinogen was detected in the glomeruli of biopsies taken prior to reperfusion, after SCS. Recent work in a serum free EVNP system suggests that extra-hepatic fibrinogen is produced by the kidney in response to hypoxia and may influence the effect cold storage has on kidneys (DiRito et al., 2021).

Apoptosis is a regulated, ATP controlled, form of cell death that occurs following hypoxia and ROS production. Following apoptosis, a cell is fragmented into distinct apoptotic bodies that are phagocytosed/digested by surrounding cells and macrophages. This controlled cell death invokes less inflammatory response compared with necrosis, which is uncontrolled, due to the containment of apoptotic bodies within a cell membrane and their quick removal. However, in circumstances such as IRI, apoptosis can become excessive. If apoptotic cells aren't rapidly cleared due to an overwhelming of phagocytes, they can release DAMPs as they lose plasma membrane integrity through secondary necrosis (Kono and Rock, 2008). Endogenous ligands presented on apoptotic cells can also lead to the activation of complement through binding C1q and MBL which leads to their clearance (Gasque, 2004). Furthermore, DAMP release from apoptotic cells can lead to complement activation. This can subsequently lead to more apoptosis through MAC formation, with C5 inhibition leading to reductions in apoptosis in a murine model of IRI (de Vries et al., 2003b).

A feature of apoptosis is the formation of DNA fragments by endogenous endonucleases. These fragments can be detected using TUNEL staining which binds them with a fluorescent tag. Kidney biopsies were stained using a fluorometric TUNEL system, and the percentage of apoptotic cells was calculated. Apoptosis increased in all kidney cohorts over perfusion. This indicates that cellular damage occurs over the course of EVNP, with damaged cells then undergoing programmed cell death which may indicate a potential role for EVNP in clearing aberrant cells prior to transplant. However inappropriate apoptosis may lead to excessive clearance of parenchyma, a process indicated in the loss of tubular cells shown in PAS-stained sections.

The kidney is a major source of extra-hepatic C3 (Sheerin et al., 2008). Proximal tubular epithelial cells, glomerular parietal and mesangial cells, vessels and infiltrating monocytes and macrophages synthesise C3 through increased expression of complement mRNA in a process regulated by cytokines and induced following hypoxia. This synthesis is seen to be upregulated during allograft rejection, with kidney derived, rather than circulating C3 being a major source of complement mediated damage (Pratt et al., 2000).

Complement activation in kidneys was assessed by measuring C3 deposition in the glomeruli of kidneys. C3 glomerular deposition, quantified from immunofluorescent staining, was significantly upregulated in all kidney cohorts at the end of perfusion compared with preperfusion. This is in agreement with previous data showing that EVNP activates the complement system (Jager et al., 2022). IRI can induce complement activation on the endothelium with deposition of C3 activation products, C4d and MAC (Castellano et al., 2010, Peng et al., 2012). Furthermore, endothelial oxidative stress leads to increased expression of cytokeratin 1 (CK1) which binds MBL leading to LP activation causing C3 deposition (Collard et al., 2001). C3a and C5a also activate the endothelium in IRI which leads to leukocyte recruitment through C3aR/C5aR signalling (Peng et al., 2012).

As reperfusion of the kidney with whole blood occurs, incoming innate immune cells can be activated by DAMPs presented on ischaemic tissue, exacerbating inflammation through cytokine production. This leads to complement activation through endogenous C3 production, and cleavage of components in complement cascades (Lo et al., 2021). This complement activation may have driven some of the observed glycocalyx shedding as TNF-alpha is

expressed in response to C3a and C5a stimulation of macrophages and TECs (de Vries et al., 2003b)

C3 deposition was significantly higher pre-perfusion in kidneys with the longest CIT compared to those with the shortest. C3 cleavage, but not gene expression, has been observed to be upregulated in response to cold storage in animal transplant studies (Lo et al., 2021). C3 cleavage during SCS would lead to further complement activation upon the restoration of blood flow due to increased availability of C3 (C3a and C3b), priming the kidney for additional complement activity upon reperfusion, further explaining the significantly higher C3 deposition at the end of perfusion in kidneys with extended CIT compared to those with short CIT. Equally, kidneys with extended CIT showed increased complement deposition preperfusion. As the antibody used detects C3 fragments as well as intact C3, this may be picking up multiple C3 fragments formed during SCS.

Furthermore, C3 deposition was higher in kidneys with extended WIT when CIT was identical. Extended warm time allows physiological processes and complement activation to continue while the organ is deprived of oxygen. This anaerobic metabolism leads to ATP depletion, acidosis and lactate build up driving general inflammation and therefore complement activation (Danobeitia et al., 2014).

Complement activation triggered by the EVNP environment alone was investigated by running an EVNP rig primed as standard with whole blood and perfusate components without a kidney. An EVNP rig with a kidney was ran at the same time – with blood from the same pig and the same perfusion components. Classical haemolytic assays were used to measure complement consumption.

Complement consumption increased linearly over time in the EVNP rig with no kidney in a pattern similar to the rig run with a kidney. This shows that complement is activated/consumed in perfusate due the EVNP environment itself. Complement is activated during haemodialysis, both in the fluid phase in plasma indicated by increased soluble MAC and C3d/C3 ratios (Hempel et al., 2016), and in the solid phase on the dialysis membrane which binds MCL, ficolin, C3c and properdin (Mares et al., 2010). Similar activation could have occurred due to the perfusion consumables used in this project.

There are some caveats to using haemolytic assays to assess complement activation in this system as the kidney is a major source of complement. Complement consumption as

measured via haemolytic assay in the rig with the kidney may be underestimated due to continuous production of complement components (Sheerin et al., 2008). A reduction in C3a levels in perfusate throughout perfusion however indicates that the complement in the EVNP system is being consumed through activation more quickly than it can be produced.

Through the work reported in this chapter, it is clearly possible to induce injury to porcine kidneys by extending warm and cold storage times that is exacerbated during EVNP. The increase in ischaemic injury markers over the course of EVNP indicate that it will be a useful model in which to test therapeutics as it is clearly a pro-inflammatory environment. Most importantly, C3 deposition indicates complement activation pre- and post-perfusion in kidneys with extended cold ischaemic times. Activated complement components present on cell surfaces provide an ideal surface to which HDM-FH can bind, potentially regulating complement during EVNP.

#### 4.1 Introduction

Patients with deficiencies in FH or who have autoantibodies against FH can have impaired complement regulation leading to diseases such as aHUS and MGPN, which are rare but severe renal diseases (Wong and Kavanagh, 2018). Additionally, patients with FH functional deficits are at risk for AMD which is the main cause of irreversible vision loss in the world (Tzoumas et al., 2021). Due to this, FH was given orphan drug designation in 2009 for the treatment of aHUS, with human plasma derived FH being the only therapeutic source available (Büttner-Mainik et al., 2011).

It has since become standard clinical practice to administer Eculizumab to aHUS patients, with Eculizumab recovering renal function more successfully than plasma exchange (Brocklebank et al., 2017). This followed work that showed that C5/terminal pathway inhibition was transformative in PNH, another rare complement mediated disease (Hillmen et al., 2024). Despite the success of Eculizumab in PNH it only targets one element of the complement cascade, C5, and it has since become apparent that targeting at the level of C3, to control extravascular haemolysis, is of significant benefit to certain patients (de Latour et al., 2022, Hillmen et al., 2021). Development of FH or a FH derived therapy which would target complement at the level of C3 and C5 therefore remains an active area of interest.

Full length FH has been produced in various expression systems including insect cells, mammalian cells and transgenic moss with comparable complement regulatory activity compared with FH purified from plasma. However, the production of recombinant FH at sufficient quantity for clinical application poses several challenges due to its large size, complex structure, and extensive glycosylation. FH yield from these systems has historically been low, with the resulting FH having not been fully biophysically characterized, although higher production levels have been achieved in yeast cells (Sharma and Pangburn, 1994, Büttner-Mainik et al., 2011, Schmidt et al., 2011, Sanchez-Corral et al., 2002).

Therapeutically, the required dose of FH is in the range of hundreds of milligrams, due to its high circulating concentration in healthy individuals. As a result, low production yields represent a significant limitation in meeting therapeutic demand (Schmidt et al., 2011). Moreover, human plasma derived FH poses potential safety issues due to adverse reactions

and the risk of pathogen transmission (Carbone, 2007). To overcome these issues, recombinant fusion FH proteins have been developed. Investigated FH based therapeutics including 'mini' FH constructs lacking certain SCRs and FH 'fusion' constructs are summarised in **Table 4.1**.

FH therapeutic	Structure	References
Mini-FH	FH SCRs 1-4 and FH SCRs 19-	(Hebecker et al., 2013,
	20	Schmidt et al., 2013, Schmidt
		et al., 2016, Xue et al., 2017,
		Harder et al., 2016, Kozma et
		al., 2021)
Mini FH	FH SCRs 1-5 and FH SCRs 18-	(Schmidt et al., 2016, Nichols
	20	et al., 2015)
FH-CR2	FH SCR 1-5, CR2 1-4	(Schmidt et al., 2016, Rohrer
		et al., 2009, Risitano et al.,
		2012, Woodell et al., 2016,
		Fridkis-Hareli et al., 2011,
		Atkinson et al., 2010, Yu et
		al., 2016)
FH <sup>Δ10–15</sup>	FH SCRs 1-9 and FH SCRs 16-	(Harder et al., 2016)
	20	
midiFH	FH SCRs 1-4 and FH SCRs 19-	(Harder et al., 2016)
	20, duplicated	
HDM-FH	FH SCRs 1-5, FH SCRs 18-20,	(Yang et al., 2018, Kamala et
	FHR1 SRCs 1-2	al., 2021)
AAV-HDM-FH	AAV gene delivery of HDM-	(Kamala et al., 2021)
	FH	
CRIg/FH	FH SCRs 1-5 and CRIg	(Hu et al., 2018, Qiao et al.,
		2014, Shi et al., 2019)
B4-scFv-fH	FH SCRs 1-5 and single-chain	(Annamalai et al., 2021)
	variable fragment of self-	
	reactive pathogenic B4 (B4-	
	scFv)	
IgG-FH <sup>1-5</sup>	FH SCRs 1-5 and non-	(Gilmore et al., 2021)
	targeting mouse IgG	
Anti-P-FH <sup>1-5</sup>	FH SCRs 1-5 and properdin	(Gilmore et al., 2021)

sMAP-FH	FH SCRs 1-5 and small (Takasumi et al., 2020)
	mannose-binding lectin-
	associated protein
MAp44-FH	FH SCRs 1-5 and MBL- (Takasumi et al., 2020)
	associated protein 1; MAP-
	1

Table 4.1 FH based therapeutics under investigation.

FH-based therapeutics designed to reduce complement activation are summarised. Abbreviations: Adeno-associated virus-HDM-FH (AAV-HDM-FH).

HDM-FH consists of the key complement regulatory domains of FH, SCRs 1-4, with the addition of SCR 5. SCR 5 has been found to enhance complement regulatory activity and enables purification and recognition by the OX-24 antibody which binds SCR 5 (Dopler et al., 2019, Sim et al., 1983, Nichols et al., 2015). These domains are fused to the key self-recognition SCRs 19-20 with the addition of SCR 18 to improve spacing and flexibility. To improve the half-life of the construct, the first two N-terminal domains of FHR-1 were added to the C-terminus of FH causing it to dimerise (Yang et al., 2018, Jozsi et al., 2015). Furthermore, SCRs 1-2 of FHR1 do not interact with C5 or C3b in a way that abrogates HDM-FH function. The resultant HDM-FH glycoprotein is 159–165 kDa as a dimer (including 22-25 kDa of glycosyl groups). The cofactor activity for FI mediated cleavage of C3b of HDM-FH is approximately 50% greater than full length FH. Furthermore, HDM-FH has 33-fold greater decay accelerating activity and increased binding to C3b measured at a 40-fold lower concentration than FH. Finally, HDM-FH binds with much greater affinity to GAGs than full length FH or other minimal FH constructs.

The molecular cloning and functional characterisation of porcine FH was carried out by (Hegasy et al., 2003) and was found to be 62% identical to human FH on the amino acid level. The porcine SCRs 1-4 were found to have strong binding to human C3b, while SCRs 15-20 showed limited binding to heparin, and can bind to human endothelial cells. Porcine FH was also seen to exhibit cofactor activity and decay accelerating activity through SCRs 1-4, although at a lower level than human FH. Due to these differences, the decision was made to produce a porcine specific HDM-FH for administration to pigs in this project. The porcine construct contains porcine FH SCRs 1-5 fused to porcine FH SCRs 18-20, with the addition of human FHR SCRs 1-2 at the C-terminus. While a porcine FHR1 like protein was identified, it did

not contain a dimerisation motif, as was identified in murine FHR1 (Kamala et al., 2021). As dimerisation was key to extending the half-life of HDM-FH, the decision was made to add human FHR1 due to its dimerisation motif.

# This chapter aims to:

- Produce HDM-FH in transfected CHO cells.
- Purify and quantify HDM-FH.
- Test the efficacy of HDM-FH in a porcine system *in vitro*.

#### 4.2 METHODS

## 4.2.1 HDM-FH production in mammalian cells

The following methods describe the production of both a porcine specific HDM-FH (porcine FH SCRs 1-5 and 18-20 and human FRH1 SCRs 1-2) and a human specific HDM-FH (human FH SCRs 1-5 and 18-20 and human FRH1 SCRs 1-2). Production of HDM-FH was carried out by Dr Beth Gibson, Harriet Denton and myself.

#### 4.2.1.1 Cell maintenance and subculture

Chinese hamster ovary (CHO) cells were grown in a humidified incubator at 37°C and 5% CO<sub>2</sub> using Dulbecco's Modified Eagle Medium/Nutrient Mixture media (1:1 DMEM/F-12) (Gibco) supplemented with 10% heat-inactivated foetal bovine serum (FBS) (Gibco) 1% penicillin-streptomycin-glutamine (Gibco) and 0.2mg/ml hygromycin (Sigma) (complete media) for selection of HDM-FH expressing cells. Cells were grown to 80% confluency and subcultured under sterile conditions using a BioMat class 2 microbiological safety cabinet.

For subculture, media and cells were washed gently with DPBS to remove media. 0.5% Trypsin-EDTA (Gibco) was then added to cells and incubated for approximately 5 minutes at  $37^{\circ}$ C until cells were detached. An equal volume of complete media was then added, as FBS inhibits the action of trypsin. The cell suspension was removed from the flask, transferred to a sterile falcon tube and spun at 400~g for 5 minutes. The trypsin/media supernatant was then discarded and the cell pellet resuspended in fresh complete media and added to a new flask containing complete media at a ratio of 1:10.

#### 4.2.1.2 Cell counting

Cells were counted when a specific seeding density was required. Cells were detached from the flask as described in 4.2.1.1, then centrifuged at 400 g for 5 minutes. The cell pellet was then resuspended in 5 mL of media. 10  $\mu$ L of 0.4% trypan blue (Sigma) was added to 10  $\mu$ L of resuspended cells for exclusion of dead cells and cellular debris. This mixture was loaded into a Neubauer haemocytometer, and cells visualised using a brightfield inverted microscope. Cells were then manually counted using the following formula:

$$Total \frac{cells}{mL} = no. of cells per central gridded square \times 10^4$$

# 4.2.1.3 Cryopreservation

Cells were detached and pelleted as outlined in 4.2.1.1 when at 90%-100% confluency. The pellet was then resuspended in FBS with 10% dimethyl sulfoxide (DMSO) (Sigma) as a cryoprotectant and added to a cryovial. Cryovials were then placed in a Mr Frosty<sup>TM</sup> (Nalgene) filled with room temperature isopropanol (ThermoFisher Scientific) which was then stored at -80°C, designed to allow the vials/cells to cool at a rate of -1°C/minute until they reach -80°C. For long term storage cells were moved to liquid nitrogen.

#### 4.2.1.4 Chinese Hamster Ovary Cell transfection

The human HDM-FH construct was designed prior to the start of this study and is outlined in the paper first describing HDM-FH by (Yang et al., 2018) (Figure 4.1). A porcine HDM-FH construct was also designed for this study by Professor Kevin Marchbank and produced by VectorBuilder (Figure 4.2). The method for cell transfection was the same for both vectors, however the human HDM-FH construct was stably transfected and cloned prior to the start of this project by Dr Yi Yang. Dr Beth Gibson carried out porcine HDM-FH CHO cell transfection and purification.

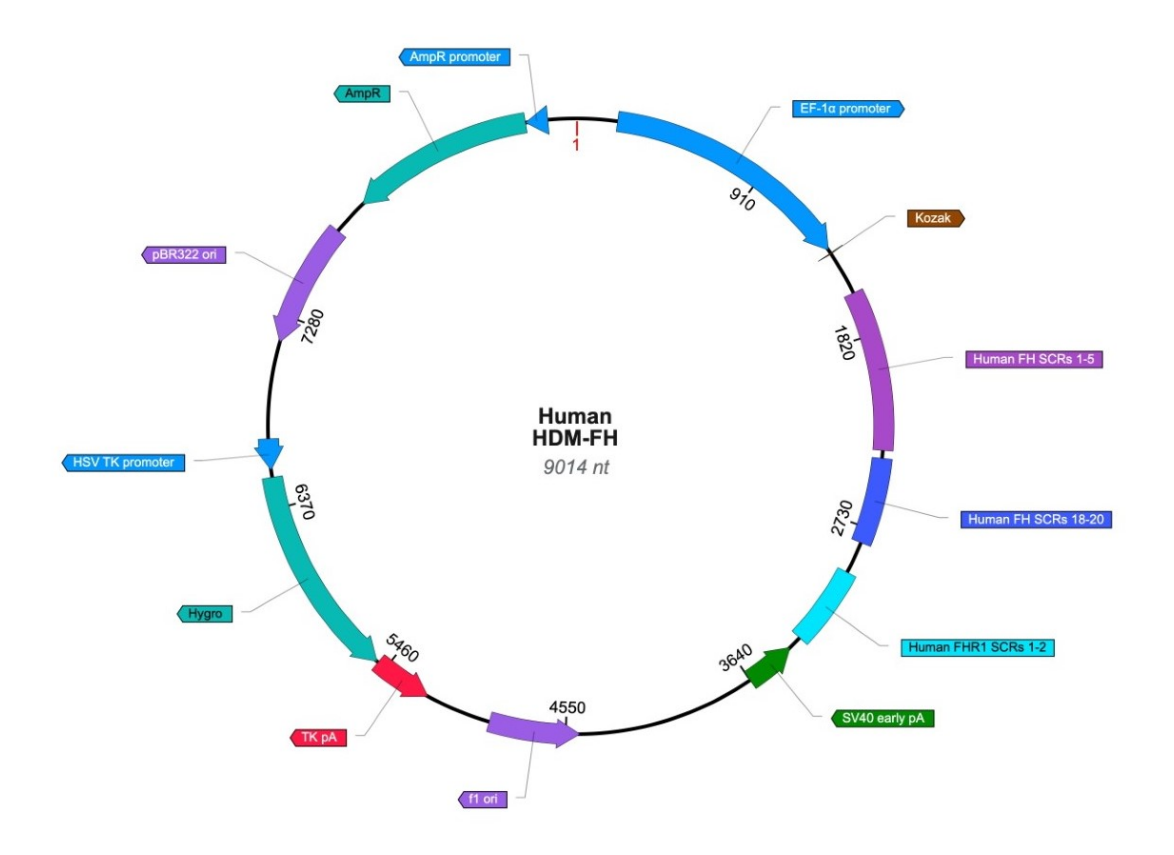


Figure 4.1 Vector map for human HDM-FH.

A vector map for human HDM-FH is shown illustrating different features of the vector. The sequences of human FH SCRs 1-5 and 18-20 are included, alongside the sequence of SCRs 1-2 of human FHR1. A hygromycin resistance gene allowed clonal selection.

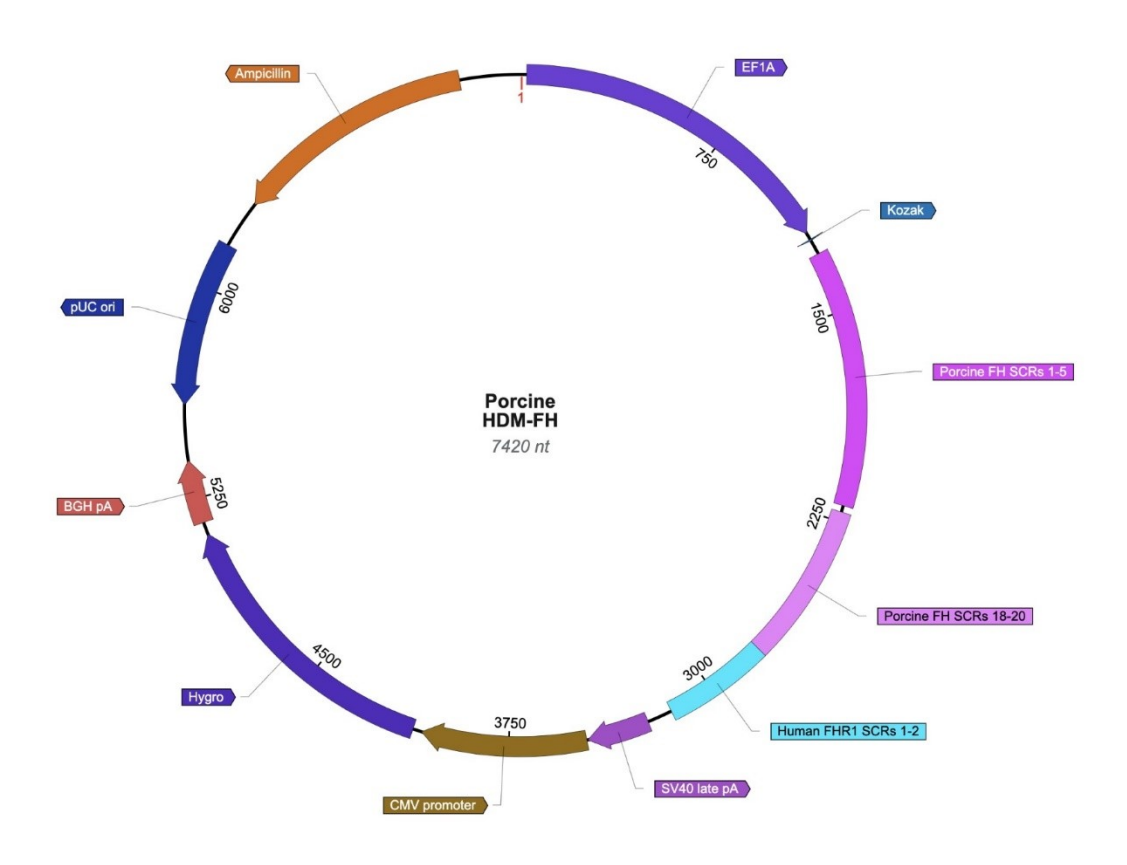


Figure 4.2 Vector map for porcine HDM-FH.

A vector map for porcine HDM-FH is shown illustrating different features of the vector. The sequences of porcine FH SCRs 1-5 and 18-20 are included, alongside the sequence of SCRs 1-2 of human FHR1. A hygromycin resistance gene allowed clonal selection. A His tag allowed purification using metal chelation (Nickel or Cobalt) fast flow sepharose columns.

For transfection of porcine HDM-FH, the JetPEI<sup>TM</sup> DNA transfectant reagent (Polyplus) was used to transfect CHO cells according to manufactures instructions. 2  $\mu$ g vector DNA was diluted in 150 mM NaCl to give a final volume of 50  $\mu$ L and vortexed gently then briefly pulse spun. The JetPEI<sup>TM</sup> reagent (Polyplus) was vortexed for 5 seconds and then pulse spun. 2  $\mu$ L JetPEI<sup>TM</sup> reagent was then added to 48  $\mu$ L 150 mM NaCl, gently vortexed and pulse spun. This solution was added to the DNA solution, then gently vortexed and pulse spun and incubated at room temperature for 15-30 minutes.

CHO cells were seeded at a density of 150000 cells per well in a 12 well plate (Greiner Bio-One) in 1 ml of media per well and grown to 50%-70% confluency. 100  $\mu$ L JetPEI<sup>TM</sup>/DNA solution was added dropwise to each well and mixed with gentle swirling of the plate. The plate was then incubated at 37°C with 5% CO<sub>2</sub> for 2-3 hours. Media was removed, and 1 mL

fresh media was added. The plate was then incubated for 3-4 days. Cells were detached and resuspended as described in 4.2.1.1 and transferred to a 6-well plate (Greiner Bio-One) with media containing hygromycin at 0.2 mg/mL. This was done to select correctly transfected cells based on the hygromycin resistance conferred by the HDM FH construct. Cells were maintained for ten days, with media changed routinely (no less than every 72 hours) to maintain active hygromycin levels. At 80% confluency, cells were transferred to larger flasks. Polyclonal cell lines were frozen down to be used for clonal selection.

#### 4.2.1.5 Monoclonal selection and expansion

The most highly expressing clone was identified and isolated through limiting dilution in a 96-well plate. Cells were diluted to 10 cells/mL. 100  $\mu$ L of cell solution was added to each well of a 96-well plate to seed at ~1 cell per well. The plate was incubated for 18 hours and cells containing only one cell were noted. Cells were detached and resuspended as described in 4.2.1.1 and transferred to a 12-well plate when 80% confluent.

Protein expression of individual colonies was assessed using sodium dodecyl sulphate—polyacrylamide gel electrophoresis (SDS-PAGE). 5 μL media was boiled at 95°C for 5 minutes with 4x reducing Laemmli sample buffer (Merck). 20 μL sample was loaded into separate wells of a Novex<sup>TM</sup> WedgeWell<sup>TM</sup> 10-20% Tris-Glycine 1.0 mm gel (Invitrogen) alongside 5 μL of PageRuler<sup>TM</sup> Plus Prestained Protein Ladder, 10 to 250 kDa (ThermoFisher Scientific). The gel was run in running buffer (2.5 mM Tris, 19 mM glycine, 0.1% SDS, pH 8.3) at 200 V until the visible dye reached the end of the gel. The gel was then stained for 15 minutes using InstantBlue<sup>TM</sup> protein stain (Sigma). The cell colony with the highest protein expression was transferred to larger flasks and expanded for protein production.

#### 4.2.1.6 Cell expansion in roller bottles

The highest porcine HDM-FH expressing cell line, and a previously transfected HDM-FH expressing line were scaled to 1 L roller bottles. Cells from two T175 flasks were detached and resuspended when at 80% confluency as outlined in 4.2.1.1 and transferred to a 1L sterile Duran bottle with 100 mL complete media (without hygromycin). The cells were equilibrated in a sterile incubator at  $37^{\circ}$ C with 5% CO<sub>2</sub> for 4 hours, then transferred to a roller bottle rig (Bellco Biotchnology) spinning at 1 rpm at  $37^{\circ}$ C and incubated for 9 days. The media was collected, centrifuged at  $4000 \ g$  for 10 minutes to remove cellular debris and stored at  $-20^{\circ}$ C. Fresh media was then added to the cells and incubated for a further 9 days before a second

supernatant harvest. The supernatant was stored at -20°C until used for purification of HDM-FH.

#### 4.2.2 Protein purification and concentration

#### 4.2.2.1 Generation of an OX-24 protein G column

The HiTrap NHS-activated HP column (Cytiva) is prepacked with NHS-activated Sepharose™ High Performance which is specifically designed for covalent ligand coupling. By covalently coupling a purified monoclonal antibody to agarose beads activated by N-hydroxysuccinimide (NHS), an affinity column is created. This column, with bound immunoglobulin, can then be utilised to capture target antigens through immunoaffinity chromatography. The OX-24 antibody binds SCR 5 of human FH, and so was coupled to the agarose beads and used to purify human HDM-FH (Sim et al., 1983, Sakari Jokiranta et al., 1996). The OX-24 column used in this work was previously made by Harriet Denton.

OX-24 antibody in PBS was concentrated using a 30000 kDa molecular weight cut off Vivaspin protein concentrator spin column (Sartorius) to 7 mg/mL. Concentrated OX-24 antibody then was buffer exchanged into coupling solution (0.2 M sodium carbonate and 0.5 M NaCl, pH 8.3) using a PD-10 desalting column containing Sephadex G-25 resin (Cytiva). All buffers in sections 4.2.1, 4.2.2, 4.2.3 and were prepared using a 0.22 µm filter

The following steps were carried out using the ÄKTAPure protein purification system. To maintain the activity of the 5 mL HiTrap NHS-activated HP column, 5 column volumes of ice cold 1 mM HCl was used to wash out the isopropanol column storage solution. 5 mL of OX-24 was then loaded onto the column and incubated for 30 minutes at room temperature. 5 column volumes of buffer A (0.5 M ethanolamine and 0.5M NaCl, pH 8.30 and buffer B (0.1 M sodium acetate and 0.5 M NaCl, pH 4.0) were washed through the column alternatively 3 times. Following the second wash with buffer A, the column was incubated at room temperature for 30 minutes. The column was then washed with PBS, washed with PBS azide (Sigma) 0.1% w/v and stored at 4°C until used to purify HDM-FH.

# 4.2.2.2 Affinity purification, metal ion affinity chromatography purification, concentration and buffer exchange of HDM-FH

A 5 mL HiTrap NHS-activated HP column with bound OX-24 antibody was used for purification of human HDM-FH. A HisTrap™ HP column (Cytiva) was used for porcine HDM-FH purification.

Each column was equilibrated with 5 column volumes of PBS. The cell culture supernatant collected from the transfected CHO cells was spun at 3500 rpm for 30 minutes to remove cryoprecipitate. Supernatant was then diluted with 4x PBS, prepared using a 0.22  $\mu$ m filter and applied to the column using the ÄKTAPure protein purification system. The column was then washed with 5 column volumes of PBS, then HDM-FH bound to the column was eluted using an elution buffer (0.1 M glycine-HCl pH 2.7) and collected into 500  $\mu$ L fractions. 80  $\mu$ L 1 M Tris pH 9.0 was used to immediately neutralise the eluted fractions. SDS-PAGE was used to evaluate fractions for HDM-FH as described in 4.2.1.5. Protein concentrations of fractions containing HDM-FH were then measured using NanoDrop spectrophotometer.

Eluted fractions containing HDM FH were then pooled, concentrated and buffer exchanged into PBS using 30000 kDa molecular weight cut off Vivaspin protein concentrator spin columns.

#### 4.2.2.3 Triton X-114 assisted endotoxin removal

Purified, concentrated HDM-FH fractions in PBS were cooled on ice. Triton X-114 (Sigma) was then added to fractions to give a final Triton X-114 concentration of 1%. The solution was then mixed by vigorous vortexing and placed back on ice for 5 minutes. Samples were vortexed again, incubated at 37°C for 5 minutes to allow two phases to form and incubated at 42°C for 1 minute. The solution was then pulse spun for 7 seconds to pellet the detergent phase. The upper aqueous phase containing HDM FH was carefully removed, and stored at -80°C.

#### 4.2.3 Surface plasmon resonance

Surface plasmon resonance (SPR) is used to measure the affinity of interactions between molecules in real time, without labels. Experiments were carried out essentially as previously described in (Yang et al., 2018). A specific ligand of interest, i.e. porcine or human C3b, is immobilised on the surface of a gold coated chip. An analyte of interest, in this case human FH or HDM-FH is flowed over the chip to bind to the ligand. Plane-polarised light is directed at the chip, the binding of the analyte will cause a change in the refractive index of the sensor chip. The affinity of the binding, as well as the association and dissociation rates in resonance units (RU) is measured based on the mass bound on the chip surface.

# 4.2.3.1 Extraction of porcine and human C3 and conversion of C3 to C3b

Porcine and human C3 were isolated using ion exchange chromatography prior to the start of the project by Dr Kate Smith-Jackson who adapted a published method (Ruseva and Heurich, 2014). Porcine and human C3 were converted to C3b through 10 freeze-thaw cycles.

#### 4.2.3.2 Immobilisation of porcine and human C3b onto a Sensor Chip CM5

Carboxymethyl-dextran matrix coats the gold surface a Carboxymethyl 5 (CM5) Sensor Chip (GE). This provides a suitable inert hydrophilic surface for the ligand to attach to. Using a BIAcore S200 (GE), 1-Ethyl-3-(3-dimethylaminopropyl) carbodiimide hydrochloride (EDC) and (NHS) was flowed over the chip to create a negatively charged surface, activating the surface for amine coupling. This allows C3b in a low pH buffer to covalently bond to the surface through its amine groups.

Porcine C3b and human C3b at 5  $\mu$ g/mL in 10 mM sodium acetate at pH 5 were flowed over a flow cell of the chip using the BIAcore S200 over multiple intervals. 900 resonance units (RU) of C3b were immobilised onto the chip measured by SPR (**Figure 4.3**). The running buffer used in all SPR experiments was HEPES buffered saline with Tween 20 (HBST) (10 mM HEPES, 150 mM NaCl, and 0.005% Tween 20, pH 7.4). All solutions were prepared using ultrapure water and 0.45  $\mu$ M filtered. Any remaining binding sites were blocked through deactivation of unbound NHS ester by flowing 1 M ethanolamine-HCl pH 8.5 over the flow cell. Reference flow cells without C3b bound were also activated and blocked in the same process so that they would have approximately the same background charge to be used as blanks.

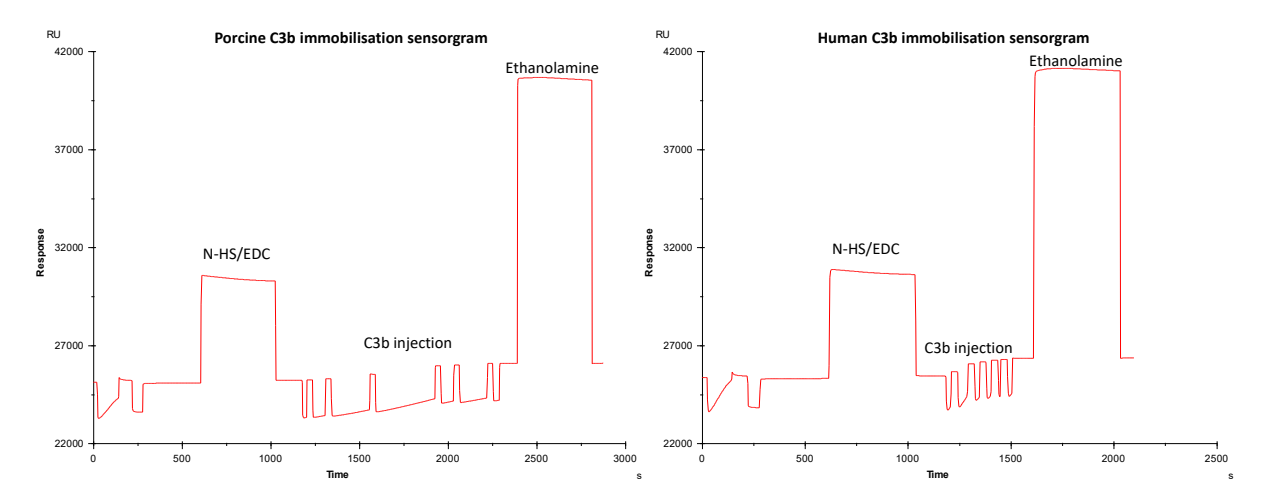


Figure 4.3 Sensorgram of amine coupling of porcine and human C3b on a CM5 Sensor Chip surface.

A sensorgram graph was generated by the BIAevaluation software S200 showing the immobilisation of C3b onto a CM5 Sensor Chip following activation of the chip by NHS and EDC. The X-axis shows the RU following subtraction of the RU values from the immobilisation of the blank flow cells over time (Y-axis). C3b was injected in separate individual flow periods until the target RU was reached.

# 4.2.3.3 Affinity analysis of HDM-FH to porcine and human C3b

The affinity of human HDM-FH and human FH to human and porcine C3b amine coupled to the chip surface was assessed using the Biacore S200. The analytes of interest, HDM-FH (produced as described above) and human FH (A137, Comptech) were diluted to a top concentration of 1000 nM in HBST, then serially diluted in HBST to achieve a concentration range of 1000 nM to 3.9065 nM. In separate experiments, the analytes were then flowed over the surface of the flow cells with porcine and human C3b and the blank flow cells. The chip surface was cleaned with regeneration buffer (10 mM sodium acetate,1 M NaCl, pH 4.0) after each construct injection. The steady state binding responses of the range of concentrations of both analytes with the binding responses from the blank flow cells subtracted were plotted as RU against time by the BIAevaluation software S200 (GE).

# 4.2.4 Administration of human HDM-FH to porcine kidneys

Kidneys were retrieved as described in chapter 2 following 25 minutes of initial WIT, then coldstored as standard for 16 hours. The control kidney was cannulated at the artery with a 12 Fr cannula (77012, Medtronic) and vein with a 24 Fr cannula (76024, Medtronic) and flushed with 10 μg/mL methylene blue (Sigma) in 4°C saline via the arterial cannula while placed in

ice. Flow through from the renal vein was collected until it turned blue, and the volume recorded to calculate the minimum column volume of the kidney. 500 mL 4°C UW with 8 µg/mL HDM-FH was flushed through the renal artery of the experimental kidney which was placed on ice. The cannulated renal vein was then clamped, and the kidney left for 1 hour on ice. The kidney was then flushed with 500 mL cold saline to remove all UW and HDM-FH in the vasculature. Snap-frozen wedge biopsies were then taken from various areas of the kidney. Control kidneys were kept stored at 4°C in UW solution for 1 hour then flushed with saline and snap-frozen wedge biopsies taken. The OX-24 antibody was used to detect HDM-FH in tissue by immunofluorescence as described in chapter 2.

# 4.2.5 Testing HDM-FH using classical haemolytic assay

The efficacy of HDM-FH in inhibiting lysis of sheep RBCs coated with anti-sheep antibodies by both porcine and human serum was assessed. SRBCs were sensitised as outlined in chapter 2.

A clear flat bottomed 96 well-plate was pre-chilled on ice. HDM-FH was titrated from 64  $\mu$ g/mL – 0  $\mu$ g/mL in PBS in the plate in triplicate leaving at final volume of 25  $\mu$ L. 25  $\mu$ L serum diluted 1:30 in HEPES buffered saline was added to wells, followed by 50  $\mu$ L sensitised sheep red blood cells. Wells were mixed by gently pipetting up and down. The plate was sealed with an adhesive strip and incubated at 37°C for 1 hour. The whole plate was spun at 800 g for 5 minutes at 4°C to stop the reaction. 80  $\mu$ L from each well was transferred to a 96-well round bottomed plate (ThermoFisher). Optical density (OD) was measured by using a micro plate reader (TECANSpark 20m) at 412nm (reference 660nm).

Protection from lysis by HDM-FH was calculated using the following formula and was plotted as % protection from lysis:

$$\left(\frac{Sample\ OD}{0\ ng/mL\ sample\ OD}\right)\ X\ 100$$

#### 4.3 RESULTS

## 4.3.1 Size and purity of construct

Figure 4.4 shows SDS-PAGE gels with eluted fractions of porcine and human HDM-FH following the same preparation indicating that the porcine HDM-FH construct could not be produced in sufficient quantities or purity for the subsequent study in the time constraints. Fewer porcine HDM-FH fractions contained proteins, and more contaminants were present when compared with human HDM-FH fractions. Due to time and financial constraints, it was decided to abandon production of the porcine HDM-FH and continue with human HDM-FH production.

Figure 4.5 shows a chromatogram of HDM-FH elution generated by the ÄKTAPure.

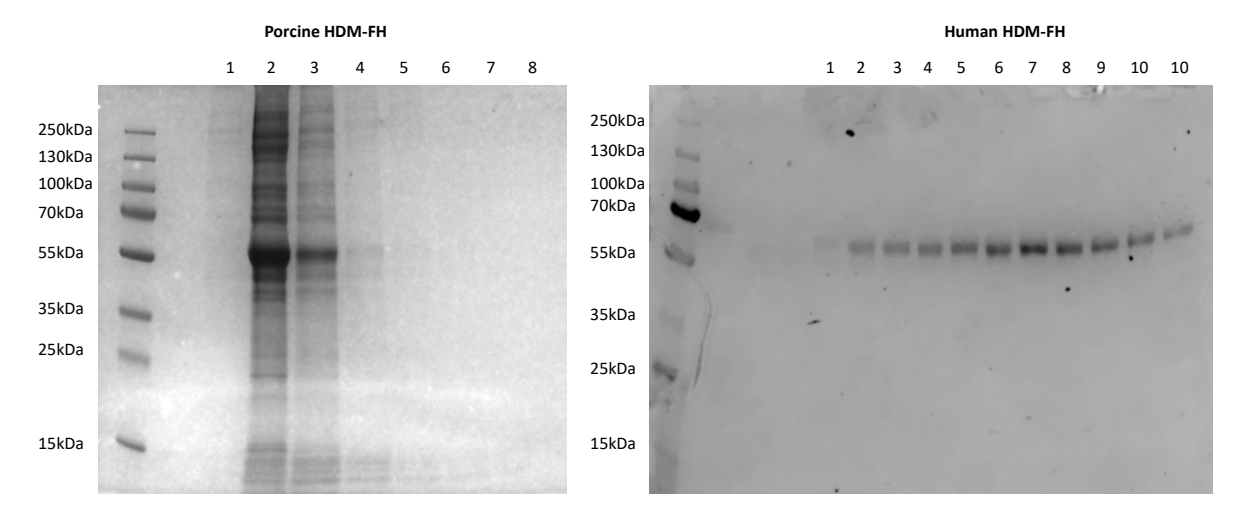


Figure 4.4 Porcine and human FH

Eluted fractions of porcine and human HDM-FH were assessed on SDS-PAGE under reducing conditions. The 10-20% polyacrylamide gel was stained using InstantBlue and imaged using the Odyssey® Fc imaging system. Eluted HDM-FH can be seen at approximately 60 kDa.

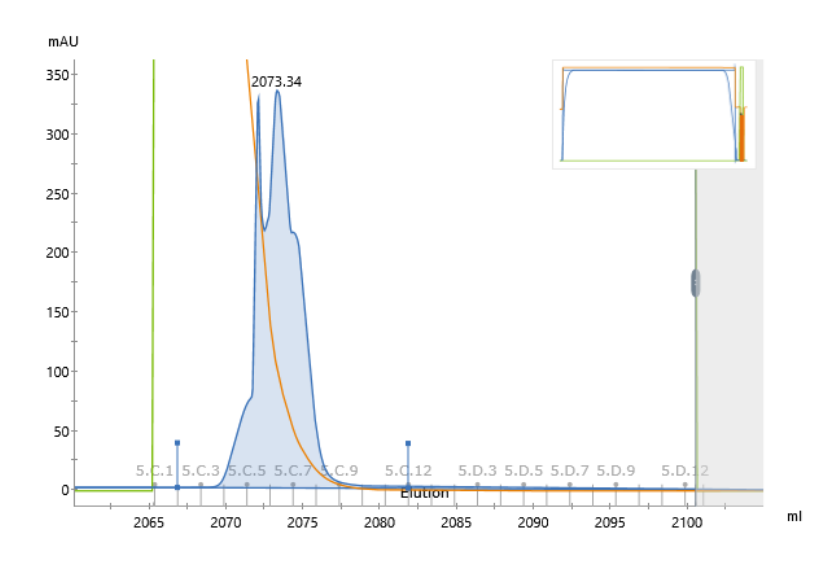


Figure 4.5 Chromatogram of human HDM-FH elution from an OX-24 column.

Chromatogram trace showing affinity chromatography of HDM-FH using a HiTrap NHS-activated HP with bound OX-24. Bound HDM-FH was eluted with 0.1 M glycine-HCl pH 2.7 and collected into 500  $\mu$ L fractions with 80  $\mu$ L 1 M Tris pH 9.0. The UV trace (mAU) is shown in blue.

# 4.3.2 HDM-FH binding to porcine tissue at 4°C

In addition to confirming that HDM-FH is able to bind to porcine tissue, investigations into whether HDM-FH binds at 4°C would widen the clinical application of the drug and indicate whether administering HDM-FH 'cold' prior to EVNP or transplantation would be feasible.

The intravenous volume of kidneys was calculated to ensure the entire kidney vasculature would contain UW with HDM-FH before incubation on ice. Control kidneys were perfused with 10 µg/mL methylene blue in 4°C saline. Perfusion of the two control kidneys with methylene blue was variable, with one kidney showing heterogeneous perfusion (Figure 4.6). The transplant research group at Cambridge University observed that porcine kidneys were uniquely sensitive to adrenaline causing vasospasm, necessitating the use of the vasodilator papaverine hydrochloride in the EVNP circuit. This mechanism of vasospasm may have led to the heterogenous perfusion seen in control kidney A. The volume of flow-through from the renal vein following the start of the methylene blue flush collected before turning blue was approximately 20 mL. However, the methylene blue had not reached the outermost area of kidney parenchyma at this point, so perfusion was continued. Global perfusion was not possible with kidney A. Global perfusion was achieved in kidney B following the perfusion of around 100 mL of methylene blue.

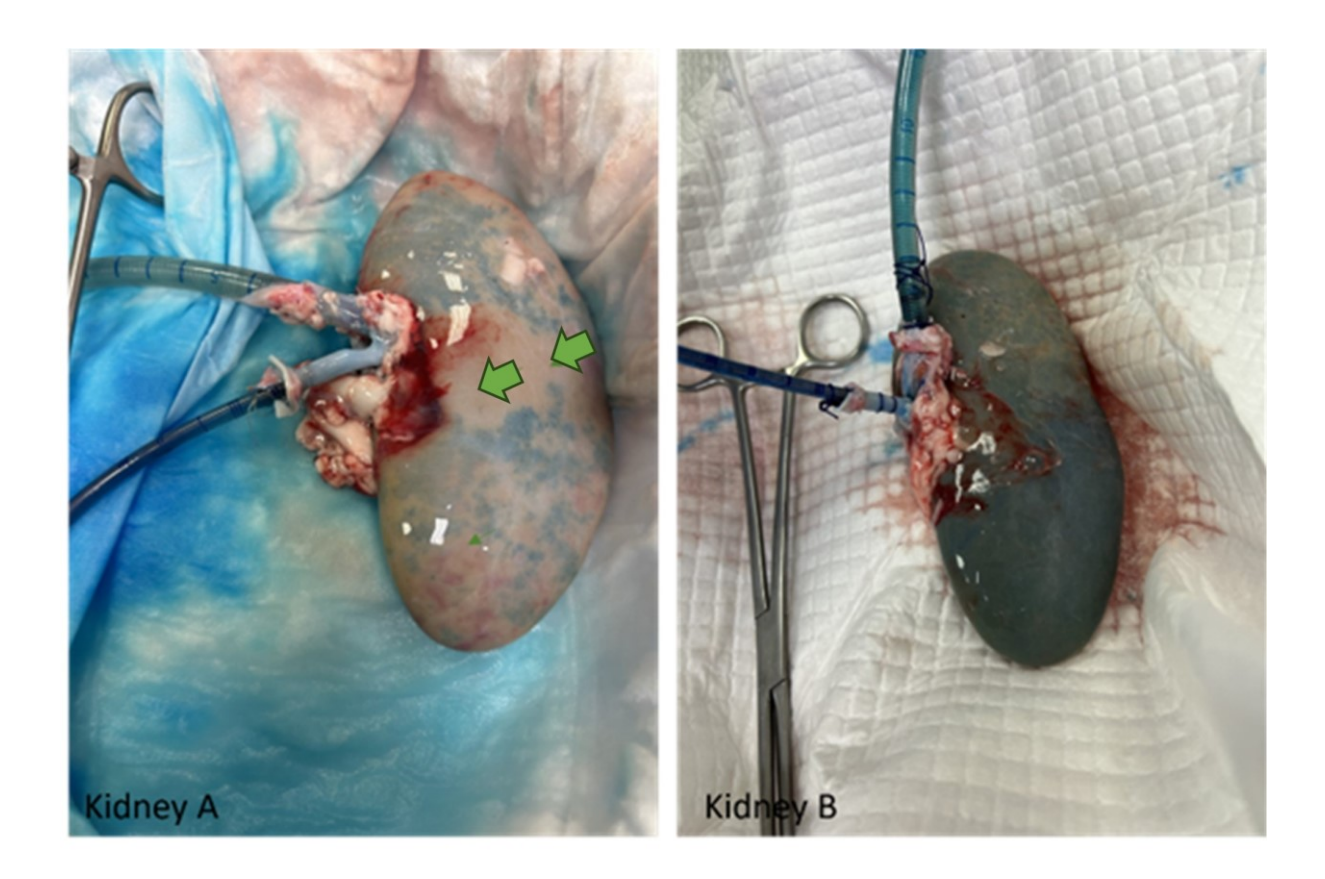


Figure 4.6 Cold perfusion of control kidneys with methylene blue.

Two control kidneys were flushed with 10  $\mu$ g/mL methylene blue in 4°C saline. Kidney A shows heterogenous perfusion with green arrows indicating areas of poor perfusion with methylene blue. Kidney B perfused homogenously with methylene blue.

OX-24 was detected in 50% of glomeruli imaged from snap-frozen biopsies taken from experimental kidney A. It is probable that the UW with HDM-FH was not able to perfuse the whole kidney. It could be assumed that the experimental kidney will have perfused heterogeneously due to the poor perfusion of the control kidney, as work in chapter 4 demonstrates that kidney pairs have similar physiological outcomes. All glomeruli imaged in experimental kidney B had a positive OX-24 signal.

When quantifying OX-24 in only glomeruli with positive signal, glomeruli in experimental kidney A had a 2.5-fold higher mean percentage area with a positive signal compared with glomeruli in kidney B **Figure 4.8**. Immunofluorescent images showing HDM-FH in glomeruli are shown in **Figure 4.7**.

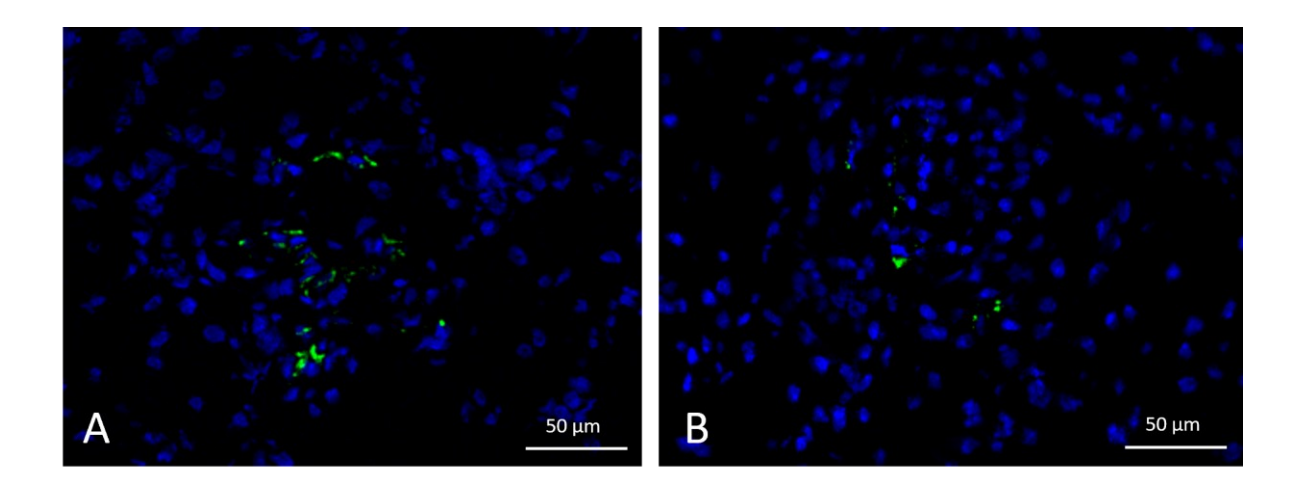


Figure 4.7 Immunofluorescent images showing OX-24 binding within kidney tissue following cold flush with HDM-FH.

Snap-frozen wedge biopsies taken following perfusion and incubation for 1 hour with HDM-FH in 4°C UW solution were stained with the OX-24 antibody which binds to HDM-FH. DAPI was used as a counter stain. Sections were then imaged using the LEICA DM2000 LED microscope and processed using LAS X software OX-24 (green) can be seen bound to glomeruli in kidney A (A) and kidney B (B), DAPI is shown in blue.

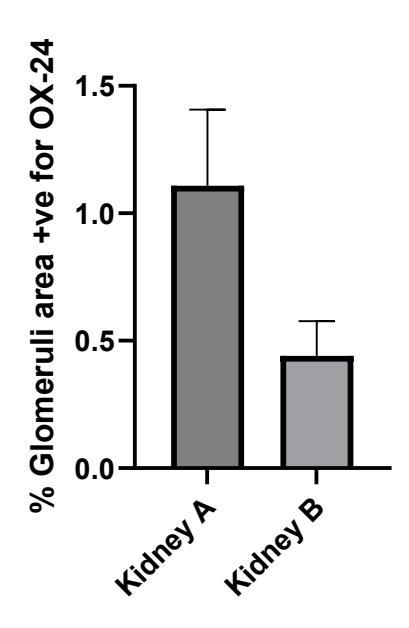


Figure 4.8 Glomerular area positive for OX-24 following cold perfusion with HDM-FH.

Snap-frozen wedge biopsies taken following perfusion and incubation for 1 hour with HDM-FH in 4°C UW solution were stained with the OX-24 antibody which binds to HDM-FH. Sections were imaged using the LEICA DM2000 LED microscope and processed using LAS X software. The percentage area of positive OX-24 signal of 10 glomeruli with positive signal was measured from each biopsy. Two kidneys were perfused with cold HDM-FH. Mean is presented with SEM.

# 4.3.3 Classical Haemolytic assay assessing HDM-FH in human and porcine serum

Porcine or human serum was incubated with sensitised SRBCs and HDM-FH titrated to assess the ability of HDM-FH to control complement activation on the surface of SRBCs in a classical haemolytic assay. HDM-FH controls complement activation more effectively when porcine serum is used than when human serum is used at concentrations below 10  $\mu$ g/mL. With porcine serum, haemolysis begins to plateau at concentrations higher than 10  $\mu$ g/mL.

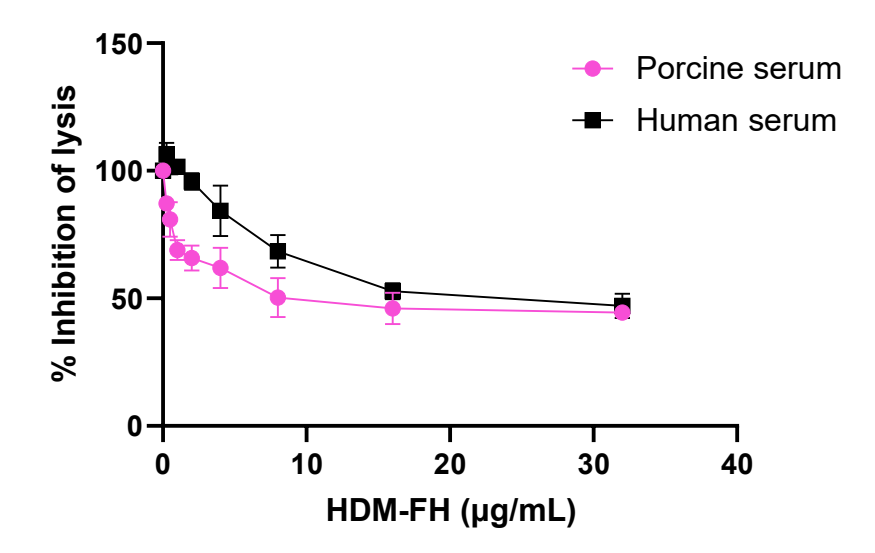


Figure 4.9 Control of complement in porcine and human serum by HDM-FH.

SRBCs coated with anti-sheep antibodies were incubated with porcine or human serum with titrated HDM-FH in a modified classical haemolytic assay as described in chapter 2. 100% lysis was calculated from incubation of sensitised SRBCs, serum and PBS only.

# 4.3.4 Binding profile of HDM-FH to porcine and human C3b

Traditionally when measuring affinity kinetics using SPR, the affinity (K<sub>D</sub>) is calculated by plotting the RU of the serial concentrations of the analyte adjusted for the blank values against the actual concentrations to give an affinity curve. The K<sub>D</sub> value is defined as the analyte concentration required to achieve 50% of the maximum RU value (RUmax). However, traditional kinetic analysis is not possible with HDM-FH due to it having a heterogenous binding profile. Therefore, the binding responses of HDM-FH on porcine and human C3b were compared qualitatively, as was shown by (Yang et al., 2018). The binding response of human FH to C3b was approximately six-fold higher than the binding response to pig FH. The binding response of human HDM-FH to human C3b is approximately 3-fold

higher than that of human FH, and approximately 2.5-fold higher to porcine C3b than that of human FH. The binding affinity of human HDM-FH to human C3b was approximately 4-fold higher than to porcine C3b (**Figure 4.10**).

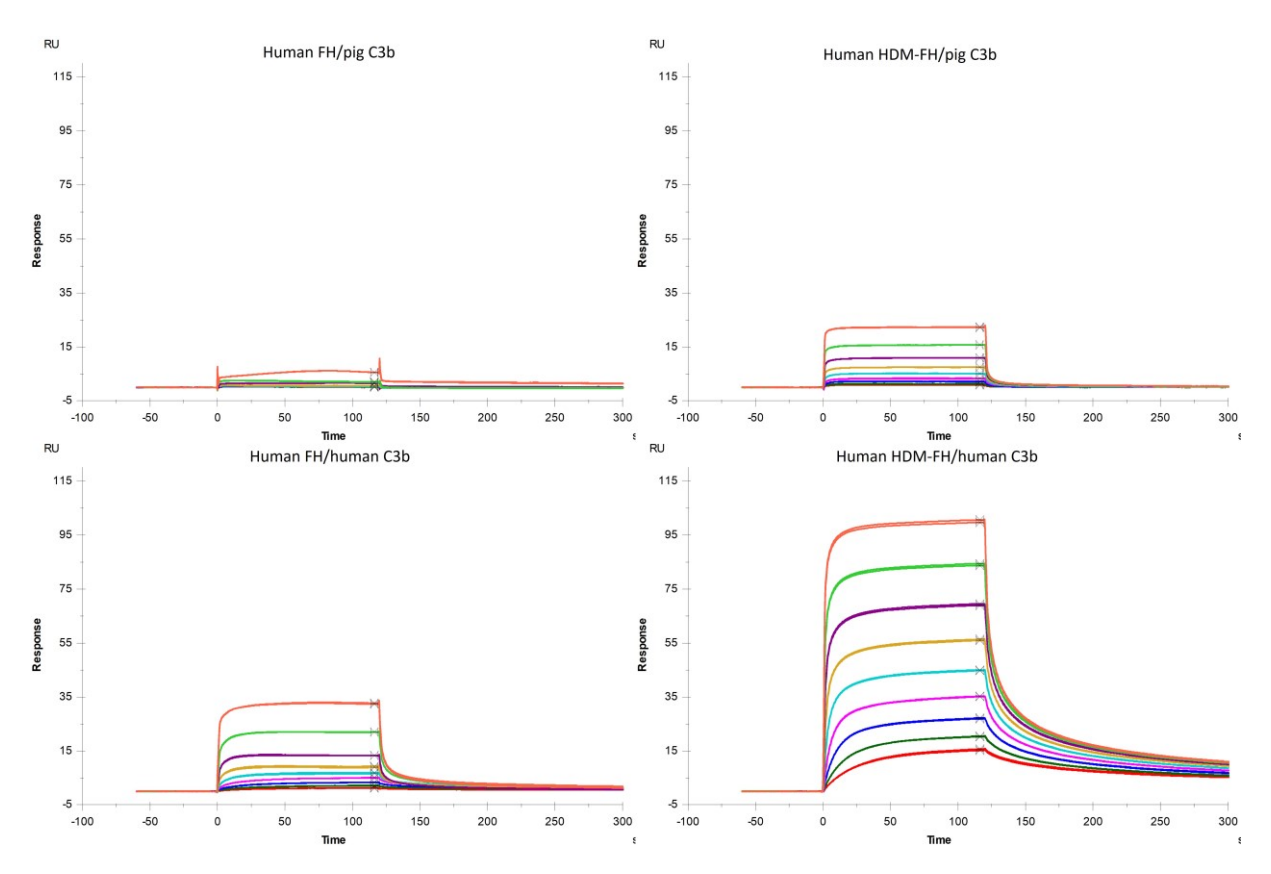


Figure 4.10 Steady state affinity of human FH/HDM-FH to porcine/human C3b on a CM5 chip.

A sensorgram produced by the Biacore S200 showing the steady state binding of human FH and human HDM-FH to porcine and human C3b amine coupled on a CM5 chip with the values from the blank flow cells subtracted. The relative RU is shown against time over the flow period. Decreasing concentrations of analyte (1000-3.9065 nM) in HBST are shown by individual colours, causing a lower response.

# 4.4 DISCUSSION

HDM-FH was initially described by (Yang et al., 2018) who demonstrated that it efficiently controlled deposition of C3 on the GBM of kidneys from *CFH*<sup>-/-</sup> mice which otherwise have uncontrolled complement activation on this surface. Since this work, administration of a mouse specific HDM-FH to *CFH*<sup>-/-</sup> mice has been described by (Kamala et al., 2021). This chapter outlines the process of the transfection, production, and purification of HDM-FH. Initially, it was planned to produce a porcine HDM-DH based on porcine FH and human FHR1. However, the yield and purity were consistently low, despite the addition of a His tag which was added to allow purification using a metal ion affinity chromatography. In the interest of time and resources it was therefore decided to assess the ability of human HDM-FH (which could be produced at a high yield and purity) to control complement activation in porcine serum, to bind porcine C3b *in vitro*, and to bind to porcine tissue.

Work by Yang and colleagues (Yang et al., 2018) demonstrated that HDM-FH has a superior ability to protect the surfaces of SRBCs coated with human C3b compared to full-length FH when incubated with human serum in a modified haemolytic assay. For the work in this chapter, we used a classical haemolytic assay to test the ability of HDM-FH to inhibit the activity of the complement components in porcine serum, compared to normal human serum.

While not perfect, a classical haemolytic assay is able to demonstrate the complement regulatory ability of HDM-FH as the AP and the amplification loop is reportedly responsible for up to 80% of the lytic potential of the CP (Harboe et al., 2004). Furthermore, HDM-FH can accelerate the decay of the C5 convertase, a convertase common to all three complement pathways, and essential for formation of the MAC and red cell lysis. HDM-FH was found to be as effective at preventing lysis of antibody coated SRBCs incubated with human and porcine serum, indicating that it is effective at controlling porcine complement activation on SRBCs.

SPR was used to evaluate the avidity of human HDM-FH to porcine C3b, with human C3b as a control. As C3b binding is key to the function of FH and HDM-FH, we compared the binding of HDM-FH to both human and porcine C3b. The SPR results indicate that binding of HDM-FH to both human C3b and porcine C3b was approximately 4-fold stronger than the binding of human FH. This is consisted with the findings of (Yang et al., 2018), validating the C3b binding function of the HDM-FH produced in this work. The binding of HDM-FH to porcine C3b was however 4-fold weaker than the binding to human C3b. Work by (Hegasy et al., 2003) found

that porcine FH SCRs 1-4 bound human C3b with equal avidity as human FH, while binding of porcine FH SCRs 15-20 was around 4-fold weaker. This suggests that C3b binding of SCRs 1-4 may be more conserved across species than that of SCRs 15-20. Therefore, the reduced binding of HDM-FH to porcine C3b may point to an important role for SCRs 18-20 in HDM-FH/C3b binding interactions.

Despite the SPR findings, classical haemolytic assays demonstrated that HDM-FH was equally effective at controlling complement activation in porcine serum as in human serum. As the complement regulatory domains of FH are at SCRs 1-4, this supports that the reduced binding of HDM-FH to porcine C3b may be due to differences in homology between porcine and human SCRs 18-20. Moving forward, this suggests that while HDM-FH may bind less avidly to complement activated porcine tissue than it would to human tissue, it should still effectively regulate complement activation.

Following confirmation of binding to HDM-FH to porcine C3b, we assessed if HDM-FH bound to the tissue of porcine kidneys. HDM-FH binding is dependant not only on C3b, but the presence of sialic acids and GAGs identifying tissue as 'self'. The kidneys used had extended WIT and CIT as described in chapter 3, which was implemented to induce complement activation and ischaemic injury. The binding of HDM-FH to porcine tissue seen in this chapter therefore further confirms binding of HDM-FH to porcine C3 breakdown products, and binding to porcine polyanions.

This work, and work by (Yang et al., 2018) demonstrated that HDM-FH is able to bind to both porcine and human C3b and polyanions, which is the basis for its complement regulatory ability. This makes HDM-FH a viable candidate as a therapeutic to regulate complement in porcine kidneys, with C3 activation products deposited on tissue surfaces undergoing IRI. The structure and function of the relevant SCRs conferring the complement regulatory ability of HDM-FH that were described by (Yang et al., 2018) and by work in this chapter are discussed below.

C3b is produced following the proteolytic cleavage of native C3 and consists of eight macroglobulin (MG) domains and one linker domain formed by a  $\beta$ -chain and an  $\alpha'$  chain. C3b contains a CUB domain and a thioester-containing domain (TED) which allows it to covalently bind to surfaces, while the C-terminus is contains a C345C domain, which is also common to C3 C4 and C5 (Janssen et al., 2006). FH binds C3b specifically and not native C3 because

following proteolytic cleavage, the MG7, CUB and TED domains undergo significant changes, differentiating C3b from the native C3 structure. The crystal structure of the complex formed following SCRs 1-4/C3b binding were described by (Wu et al., 2009b) (Figure 4.10). FH/C3b bind over four contact regions that span the length of SCRs 1-4, with MG7 and MG8 of C3b being most important for binding. SCRs 1-2 were found to be key for the decay acceleration activity of FH as they displace Bb from the C3 convertase C3bBb, while the negative charge of both Bb and FH encouraged C3Bb destabilisation through electrostatic repulsion. Furthermore, the mechanism behind the cofactor activity of FH was investigated. FI was found to bind to the FH/C3b complex at the region formed by SCRs 1-3 and the C345C and CUB domains of C3b.

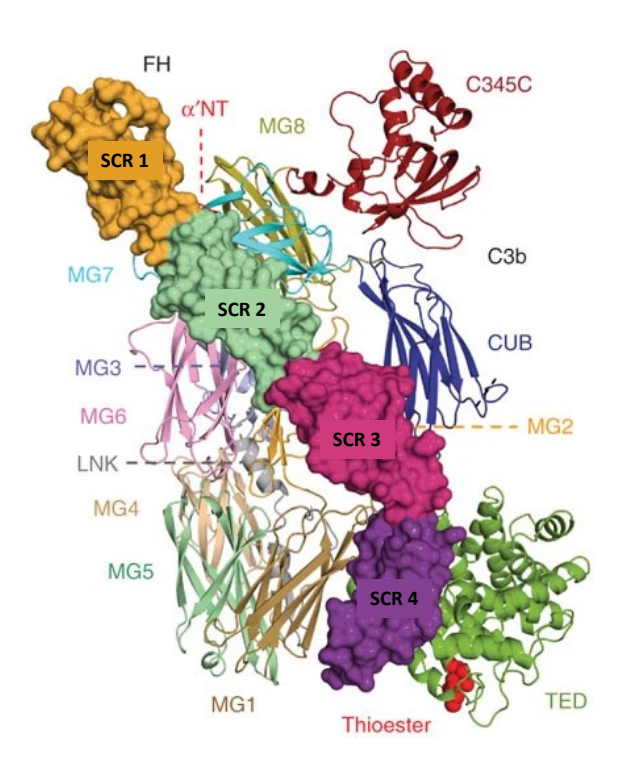


Figure 4.11 The FH SCRs 1-4/C3b complex.

Shown is the crystal structure of the complex formed by the binding of SCRs 1-4 with C3b by (Wu et al., 2009b). SCRs 1-4 bind the eight MGs of C3b, which also possesses a TED, CUB and C345 domain.

Work by (Dopler et al., 2019) demonstrated that while SCRs 1-4 are the minimally required SCRs for the complement regulatory activity of FH, the addition of SCRs 5-7 confers additional activity, with SCR 5 leading to a small increase in C3b binding avidity, and a more marked increase in decay accelerating activity and cofactor activity to Factor I compared to full length

FH. Hence why HDM-FH contains SCRs 1-5, in addition to SCRs providing a binding site for the commercially available OX-24 antibody which would allow straightforward purification of HDM-FH, as demonstrated in this chapter.

Minimal FH constructs containing only SCRs 1-4 linked to SCRs 19-20, which are responsible for GAG and sialic acid binding, exhibit improved complement regulatory functions and C3b binding compared to full-length FH, even in the absence of SCRs 5-7 (Nichols et al., 2015). In full-length FH, SCRs 19-20 are capable of binding C3b. However, their functional contribution to overall C3b binding is relatively modest. This suggests that the binding site for C3b within SCRs 19-20 may be partially obstructed in full-length FH until the N-terminal domains engage C3b, thereby requiring conformational changes for optimal binding (Harder et al., 2016). By omitting the central SCRs, the minimal FH constructs appear to make SCRs 19-20 more accessible for binding, eliminating the need for these conformational adjustments, enhancing C3b binding.

(Morgan et al., 2011) elucidated the structure of the FH 19-20/C3d complex. C3b is a proteolytic fragment of C3b equivalent to the TED domain. They demonstrated that SCRs 19-20 can bind C3d, while SCR 20 can also bind proximal polyanionic ions allowing self it to distinguish self surfaces. As FH can bend back on itself, C-terminus binding can occur while the N-terminus can carry out cofactor and decay accelerating activity while also binding C3b.

HDM-FH additionally contains SCR 18 at the C-terminus in addition to SCRs 19-20. Although SCRs 19-20 bind directly with C3b, GAG and sialic acid binding, missense mutations in SCR 18 have been seen to cause an increased risk of complement mediated diseases (Boon et al., 2008, Saunders et al., 2006, Guigonis et al., 2005). SCRs 19-20 form a rigid rod structure due to their short 3 residue linker, however the 6-residue linker between 18-19 permits a kink leading to a 'J'-shaped conformation with high mobility (**Figure 4.11**). This causes the adoption of a bent-back confirmation allowing residues of the surface of SCR 18 to be close to C3b of the FH/C3b complex. Although the functional consequences of SCR 18 are yet to be elucidated, it could affect FH/C3b binding and will provide flexibility to HDM-FH.

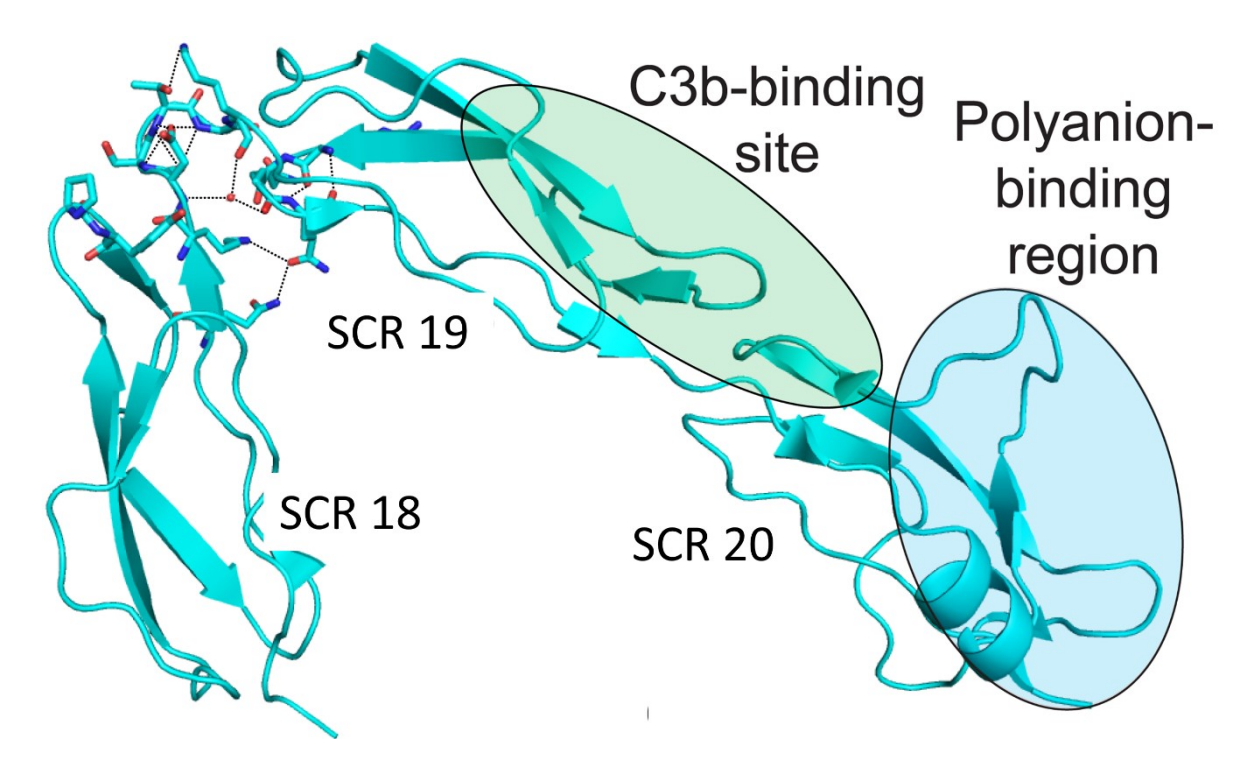


Figure 4.12 The crystal structure of SCRs 18-20.

Shown is the crystal structure of FH SCRs 18-20, in green the binding site of C3b spanning SCRs 19-20 is shown.

To conclude, work in this chapter outlines the methods for the production and purification of HDM-FH in a mammalian cell line. A porcine HDM-FH could not be produced or purified in sufficient quantity or purity, however the human HDM-FH was found to bind porcine C3b, and have good complement regulatory activity in a porcine system *in vitro*. Furthermore, it can bind to porcine tissue. These results mean HDM-FH would be appropriate for use in controlling complement activity in porcine kidneys *ex vivo*.

#### 5.1 Introduction

Multiple therapies including stem cells, nano particles and antisense oligonucleotides, have been successfully tested using EVNP (Pool et al., 2019, Thompson et al., 2021, DiRito et al., 2021, Thompson et al., 2022, Lohmann et al., 2021). Several complement inhibitors including anti-C5 and anti-FB antibodies and siRNAs targeting C5a and C3 have been used to reduce injury in IRI models (Bongoni et al., 2019, Qin et al., 2016, Thurman et al., 2006, Zheng et al., 2008, Zheng et al., 2006). To date, however, no complement inhibiting therapies have been assessed for the treatment of IRI using EVNP. Mirococept, a targeted CR1 modality, has been administered cold to porcine kidneys that were then perfused, however this was part of a dosing and toxicity study with no downstream effects of treatment measured other than physiological parameters, which were unchanged (Kassimatis et al., 2021).

A caveat of some therapies, including antisense oligonucleotides, is that they only bind at normothermic conditions (Thompson et al., 2022). However, work in chapter 4 identified that HDM-FH can bind to porcine tissue at 4°C. The avid binding profile of HDM-FH at multiple sites may make it more successful at binding in different conditions, expanding the clinical applications of the drug as it could be administered at both normothermic and cold temperatures.

Considering the effectiveness of HDM-FH at controlling complement in mouse models, and the important role of the complement system in IRI, administration of HDM-FH during EVNP and subsequent analysis of whether it prevents complement activation and downstream ischaemic injury is warranted.

# This chapter aims to:

- Assess binding of HDM-FH to kidneys when administered during EVNP.
- Assess the effects of HDM-FH on complement activation during EVNP, and whether this influences organ function and downstream ischaemic injury markers.

# 5.2 Specific Methods

#### 5.2.1 Administration of HDM-FH to kidneys

HDM-FH (produced and purified as described in chapter 4) was administered to porcine kidneys both to assess the effects it has on kidneys in a 37°C EVNP circuit, and to assess binding alone in 'cold' conditions. When administered via the EVNP circuit, 5 mg HDM-FH in PBS (LPS free by Triton X-114 phase separation as described in chapter 4) was injected directly into the reservoir of the EVNP circuit attached to the randomly selected experimental kidney immediately upon reperfusion of the kidney with perfusate. The approximate concentration of HDM-FH in the circuit was 8  $\mu$ g/mL. PBS (LPS free by Triton X114 phase separation as described in chapter 4) was administered to the EVNP circuit of the control kidney at the equivalent time point, start times were staggered to allow time between sampling. HDM-FH administration was conducted in a blinded manner. All kidneys analysed in this chapter were perfused following 25 minutes initial WIT and 16 hours CIT, as described in chapter 3.

## 5.2.2 Ultrasound imaging

Contrast enhanced ultrasound (CEUS) was used to assess microvascular perfusion within the kidneys in real time during perfusion. For CEUS imaging, microbubbles of sulphur hexafluoride in a phospholipid shell were administered to organs. These bubbles are around  $2-3~\mu m$  in diameter, allowing them to pass through the microvasculature without impeding flow, while increasing ultrasound signal return allowing the capillaries and main vessels of the organ to be visualised. This technique has previously been successfully used by the transplant research group at Newcastle University to assess microvascular flow of human kidneys undergoing EVNP (Thompson et al., 2021).

#### 5.2.2.1 Contrast enhanced ultrasound imaging of porcine kidneys

For CEUS imaging, 1 mL sulphur hexafluoride contrast agent (SonoVue \*, Bracco) was drawn into a syringe with 4 mL perfusate solution. The contrast agent was then administered via a three way tap to the arterial limb of the kidney as a rapid bolus. The ultrasound probe was positioned to capture cortex and medulla using standard B-mode ultrasound techniques using the eL18-4 probe of the Philips EPIQ7 Ultrasound machine with QLab 8.1 software (Philips). The probe was covered with gel and sheathed in a sterile cover (Advance medical designs).

The probe was placed directly onto the organ and held stationary, capturing a longitudinal view of the kidney (**Figure 5.1**).

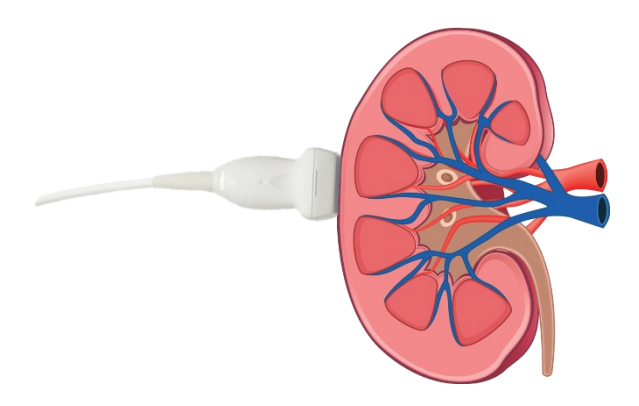


Figure 5.1 Imaging plane for ultrasound imaging.

The linear eL184 ultrasound probe was placed on the lateral edge of the kidney on the EVNP circuit to capture a longitudinal view of the parenchyma.

A Cineloop was captured ensuring a full 1 minute after contrast first appeared in an interlobar/segmental artery. CEUS images were recorded at 2 and 6 hours of perfusion.

# 5.2.2.2 Analysis of CEUS images

Analysis of CEUS data was performed by Mr Sam Tingle. Raw CEUS DICOM files were imported into QLAB Advanced Quantification Software (Release 15.5 Philips) and analysed using the ROI QApp. The region of interest for the cortex was a 5x5mm square. A freeform polygon was used to draw further regions of interest around the medulla and deepest visible artery (representing interlobar or segmental arteries). The medulla was split equally into outer medulla (closest to the kidney surface) or inner medulla (closest to kidney hilum). **Figure 5.2** displays the drawing of the region of interest, as well as a representative CEUS loop.

All loops were cut so that time zero was the first frame that contrast was seen. The software then calculates the mean contrast intensity in the various regions of interest, for each frame of the ultrasound loop. This raw data was then exported for downstream analysis.

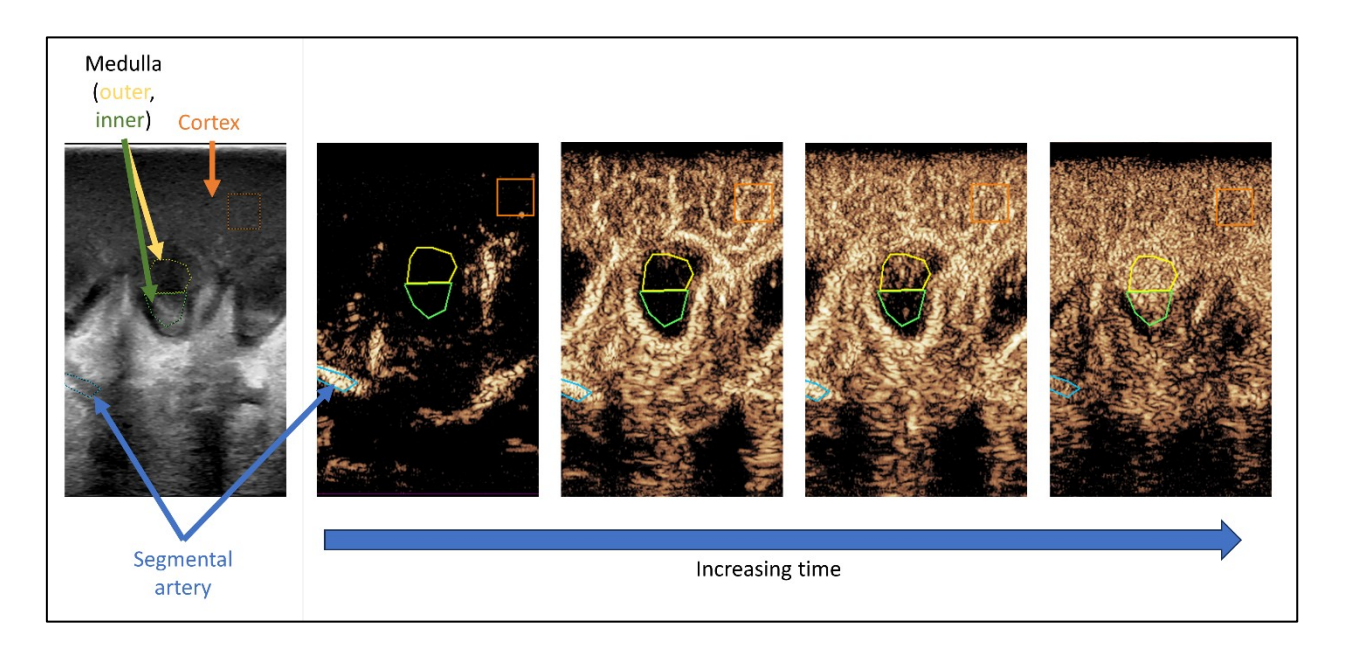


Figure 5.2 Representative contrast enhanced ultrasound loop with regions of interest selected.

Standard B mode ultrasound image (left panel) is used to ensure cortex and medulla are in view. CEUS images following administration of 1 mL of sulphur hexafluoride bubbles to the arterial limb of kidneys is shown in the left panel. As time progresses there is sequential perfusion of segmental artery, cortex, outer medulla and inner medulla.

Analysis of this raw CEUS data was performed in R (R Foundation for Statistical Computing, Vienna, Austria) (Figure 5.3). All clips were cut to 30 seconds from contrast first appearing in the segmental artery. A curve was plotted to the raw data, using a LOESS smoother. This was performed using the loess() base R function with loess.span set to 0.06. Data was extracted from this curve and the following values outputted: peak intensity, time to peak, time to 90% of peak intensity. Area under the intensity-time curve was analysed using the trapezium method for integration on the raw data.

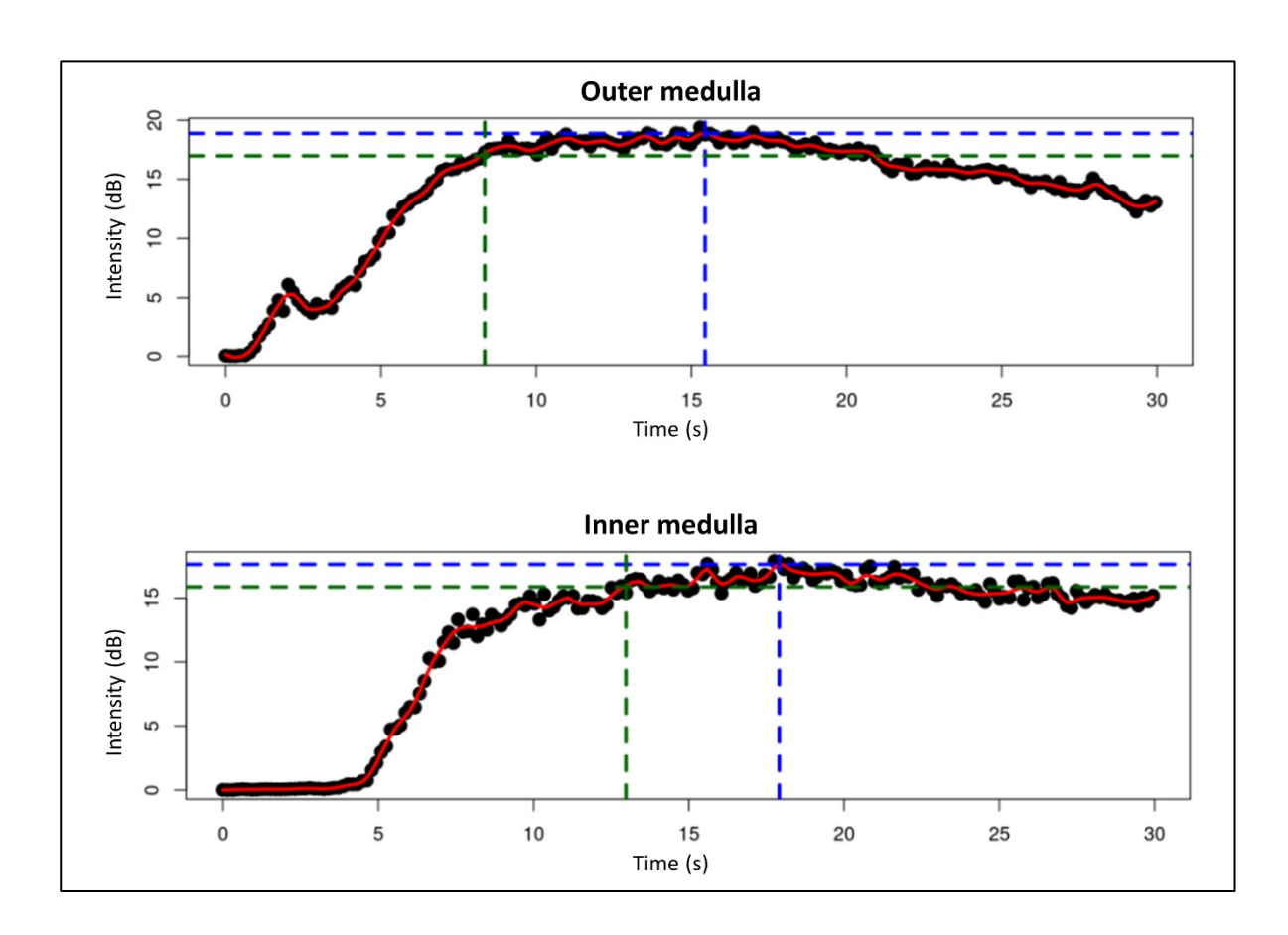


Figure 5.3 Example intensity time plots from CEUS.

Black dots represent raw data (mean contrast intensity in the given region of interest for that frame). The red line is a LOESS smoother through the raw data. Blue dotted line represents the peak intensity, and time to peak intensity, and green dotted line shows 90% of the peak intensity and time until 90% peak intensity. These plots demonstrate the sequential perfusion of outer then inner medulla.

# 5.2.3 Colocalisation of HFM-FH with glomerular structures

Snap-frozen wedge biopsies taken at the end of perfusion were sectioned and stained with antibodies against HDM-FH (anti-FH), endothelium (anti-CD31), podocytes (anti-WT-1), and the basement membrane (anti-laminin), as described in chapter 2, to determine which glomerular structures HDM-FH localised to. Sections were imaged and processed by Dr Rolando Berlinguer-Palmini at the Newcastle University Bioimaging service using the Leica SP8 point scanning confocal microscope with white light super continuum lasers at 40× using a 40×/1.3NA HC PL APO CS2 oil immersion lens at Nyquist rate (voxel size: X, Y 46 nm, Z 165 nm) applying 2× line average and acquiring each channel sequentially. Ten images of glomeruli were captured. Images were deconvoluted using the Huygens Essential (Scientific Volume Imaging [SVI]) deconvolution express (standard) algorithm. All images were acquired and

processed at the Newcastle University Bioimaging Unit. Colocalisation analysis was performed using Manders colocalisation coefficients (MOC) comparing the distribution of fluorescently labelled HDM-FH with fluorescently labelled glomerular structures (Dunn et al., 2011).

#### 5.2.4 Western blot

#### 5.2.4.1 Bicinchoninic Acid Protein Assay

Protein concentration of perfusate samples were measured using a Pierce<sup>TM</sup> Bicinchoninic Acid Protein Assay Kit (Pierce, Thermofisher Scientific). A set of standards of known concentration were made by serially diluting BSA with PBS from 2 mg/mL to 0.125 mg/mL with 0 mg/mL used as a blank. 25 μL of sample, standard and blank was added per well in duplicate to a 96 – well flat-bottomed plate (Greiner). 200 μL of working reagent consisting of working reagents A and working reagent B at a ratio of 50:1 was then added to each well. The plate was sealed and incubated at 37°C for 30 minutes. Following equilibration to room temperature, absorbance was read at 562 nm using a plate reader. Blank values were subtracted from all values, a standard curve of known protein concentration was plotted from standard absorbance values and used to calculate unknown protein concentrations.

#### 5.2.4.2 Sample preparation and separation by SDS-PAGE

10  $\mu$ g sample was diluted with 4x concentrate reducing Laemmli sample buffer and boiled at 95°C for 5 minutes. 10  $\mu$ L sample was loaded to separate wells of a Novex<sup>TM</sup> WedgeWell<sup>TM</sup> 10-20% Tris-Glycine 1.0 mm gel alongside 5  $\mu$ L of PageRuler<sup>TM</sup> Plus Prestained Protein Ladder, 10 to 250 kDa. The gel was run in running buffer (2.5 mM Tris, 19 mM glycine, 0.1% sodium dodecyl sulphate, pH 8.3) at 100 V until the visible dye reached the end of the gel.

#### 5.2.4.3 Protein transfer

Protein and protein ladder were transferred onto a nitrocellulose membrane using a Trans-Blot turbo Mini  $0.2~\mu m$  nitrocellulose transfer pack with the Trans-Blot Turbo Transfer system (Bio-Rad).

# 5.2.4.4 Protein normalisation

Immediately following transfer, the membrane was dried for 10 minutes at 37°C, then rehydrated using PBS for 5 minutes with gentle shaking. The membrane was then briefly rinsed with ultrapure water and stained with 5 mL Revert 700 total Protein Stain (Licor) for 5 minutes with gentle shaking. The stain was decanted, then the membrane rinsed with 5 mL

Revert 700 Wash solution (Licor) twice for 30 seconds with gentle shaking. The membrane was then briefly rinsed with ultrapure water, then imaged using the 700 nm channel using the Odyssey® Fc imaging system. Total protein load was then quantified using Image Studio™ Lite version 5.2 software.

# 5.2.4.5 Immunoblotting and visualisation

The membrane was blocked for 1 hour in blocking solution (5% milk (Sigma) in 0.1% tris buffered saline with 0.05% tween 20 (TBST)). The membrane was then incubated with rabbit anti-pig C3 antibody (ab180640, abcam) diluted 1:500 in blocking solution overnight at 4°C. The membrane was the washed in TBST 3 times for 5 minutes with gentle shaking. The membrane was then incubated with AffiniPure™ Goat Anti-Rabbit IgG secondary antibody (111-035-144, Jackson Immunoresearch) diluted 1:10000 in blocking solution for 1 hour at room temperature. The membrane was then washed in TBST 3 times for 5 minutes. The membrane was incubated with 5 mL PierceTM ECL Western Blotting Solution (ThermoFisher Scientific) for 1 minute. The ECL solution was then decanted, and the membrane imaged using the chemi channel using the Odyssey® Fc imaging system. Densitometry analysis was carried out using Image Studio<sup>TM</sup> Lite version 5.2 software. Band size was normalised to total protein load.

# 5.3 RESULTS

#### 5.3.1 HDM-FH binding

# 5.3.1.1 HDM-FH in kidneys throughout perfusion

The anti-human FH antibody OX-24 which binds SCR 5 of human FH (Sim et al., 1983, Sakari Jokiranta et al., 1996) was used to identify HDM-FH in tissue of treated kidneys (HDM-FH contains two FH SCR 5 regions). HDM-FH demonstrated binding within glomeruli from 30 minutes of perfusion, which increased over the time of perfusion, OX-24 was 1.5-fold higher as assessed by pixel intensity/area at 360 minutes of perfusion compared to 30 minutes of perfusion (**Figure 5.4** and **Figure 5.5**).

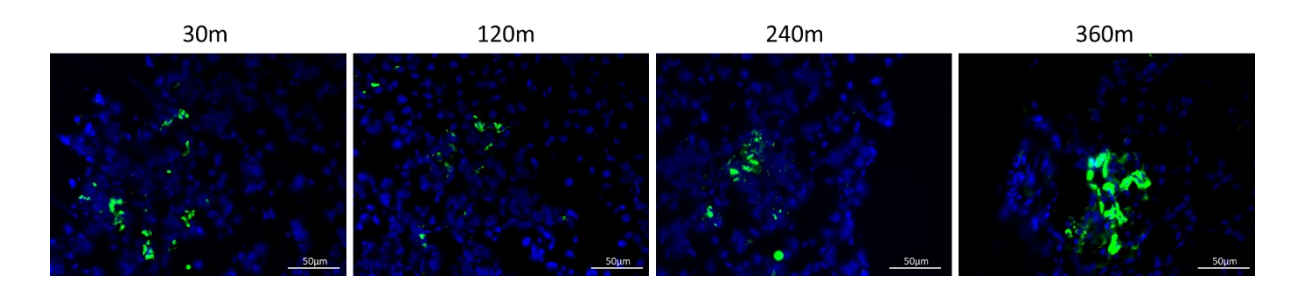


Figure 5.4 Immunofluorescent images showing OX-24 binding within tissue of kidneys treated with HDM-FH from 30 minutes to 360 minutes of perfusion.

Snap-frozen core biopsies taken at 30 minutes, 120 minutes, 240 minutes and 360 minutes of perfusion from treated kidneys were stained using the OX-24 antibody which binds to HDM-FH, DAPI was used as a counter stain. Sections were then imaged using the LEICA DM2000 LED microscope and processed using LAS X software. OX-24 (green) can be seen bound to glomeruli at all perfusion time points, DAPI is shown in blue.

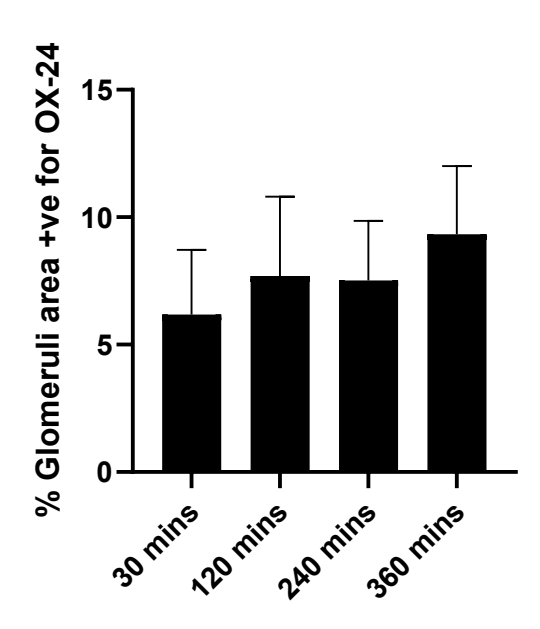


Figure 5.5 Glomerular area positive for OX-24 from 30 minutes to 360 minutes of perfusion within tissue of kidneys treated with HDM-FH.

Snap-frozen wedge biopsies taken at the end of perfusion from treated kidneys were stained using the OX-24 antibody which binds to HDM-FH. Sections were imaged using the LEICA DM2000 LED microscope and processed using LAS X software. The percentage area of positive OX-24 signal of 10 glomeruli was measured from each biopsy, N=8. Mean is presented with SEM.

HDM-FH binds to C3 activation fragments allowing it to home to damaged self-cells (Yang et al., 2018). OX-24 glomerular binding at the end of perfusion was correlated with C3 deposition just prior to perfusion to investigate whether HDM-FH binding was dependant on complement activation in the kidney prior to perfusion of the organ. An antibody that binds exclusively to pig C3 fragments is not available, so a pan-C3 antibody was used which binds fragments and full-length C3. HDM-FH deposition at the end of perfusion significantly correlated with C3 deposition in glomeruli in biopsies of treated kidneys taken prior to perfusion after static cold storage (p=0.0482, r=0.7106) (Figure 5.6).

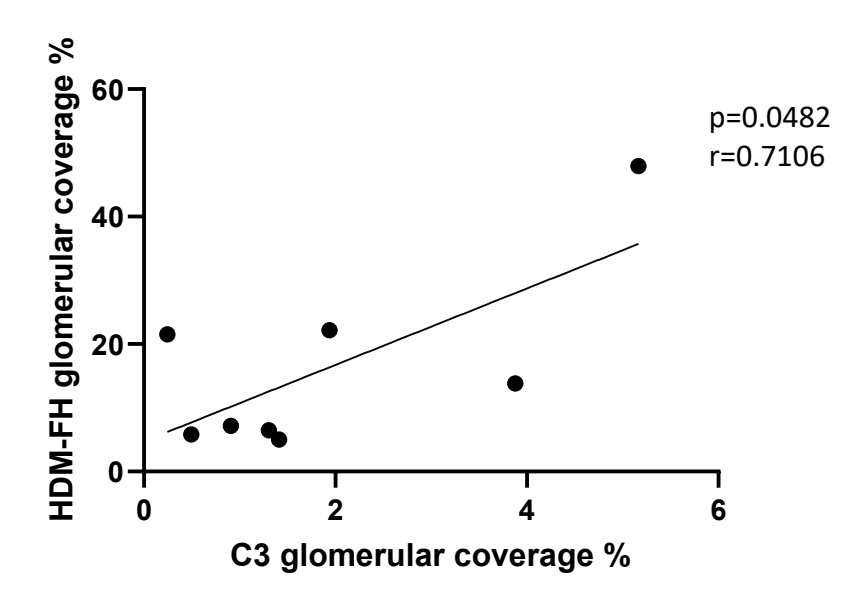


Figure 5.6 OX-24 binding at 360 minutes of perfusion correlated with C3 deposition preperfusion in tissue of kidneys treated with HDM-FH.

FFPE core biopsies taken pre-perfusion after 16 hours SCS from treated kidneys were stained with an anti-C3 antibody. Snap-frozen wedge biopsies taken at the end of perfusion from treated kidneys were stained using the OX-24 antibody which binds to HDM-FH. All sections were imaged using the LEICA DM2000 LED microscope and processed using LAS X software. The percentage area of positive OX-24 and C3 signal of 10 glomeruli was measured from each biopsy. Mean values for percentage positive signal were calculated and correlated using GraphPad Prism 10 (Pearson correlation), N=8. Individual values are presented.

# 5.3.1.2 Colocalisation of HDM-FH with glomerular structures

Manders Overlap Coefficient (MOC) quantitatively measures the proportion of overlapping signal from multiple fluorophores indicating spatial overlap with 1=complete co-occurrence and 0=no co-occurrence. The separate channels and overlayed images from one glomerulus of treated kidneys are displayed in **Figure 5.7**. The mean MOC values from the OX-24 signal with WT-1, laminin and CD31 signals from 10 single glomeruli are plotted in **Figure 5.8**. A MOC of 0.9363 was achieved when comparing the signal overlap of OX-24-stained areas and CD31 stained areas and this indicates a high level of spatial overlap between HDM-FH and the endothelium. An average MOC of 0.702 between OX-24 and laminin also indicates high spatial overlap between HDM-FH and the basement membrane. An average M1 of 0.1498 between OX-24 and WT-1 suggests a lower spatial overlap between HDM-FH and podocytes.

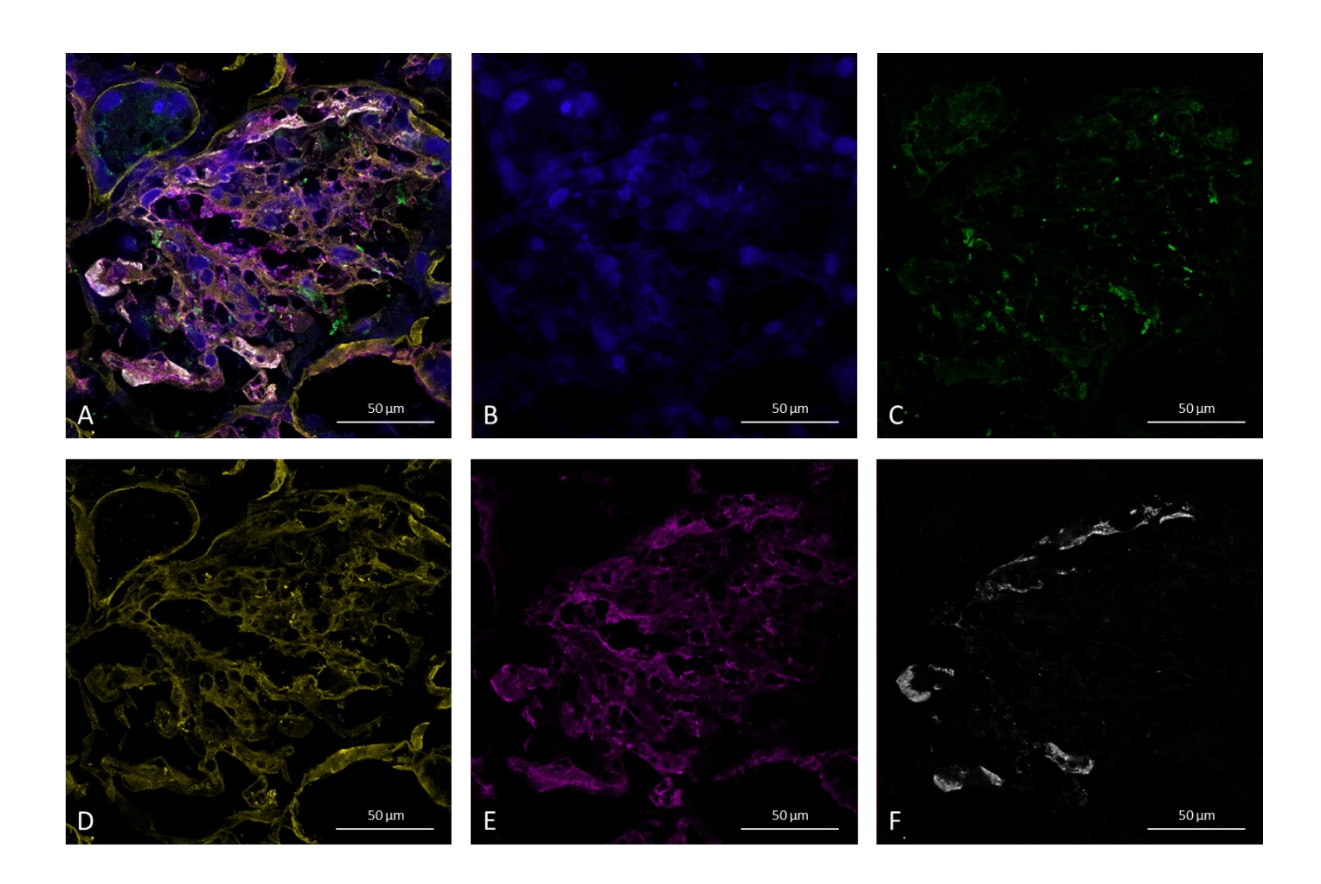


Figure 5.7 Immunofluorescent images depicting HDM-FH colocalisation with glomerular structures within tissue of a kidney treated with HDM-FH at 360 minutes of perfusion.

A snap-frozen wedge biopsy taken at 360 minutes of perfusion from a treated kidney was stained concurrently with OX-24, anti-WT-1, anti-laminin and anti-CD31 antibodies, DAPI was used as a counterstain. Sections were imaged using the Leica SP8 point scanning confocal microscope with white light super continuum lasers at  $40\times$  and processes using LAS X software. A = an overlayed image of all channels. B = Blue indicates DAPI, C = green indicates WT-1 (podocytes), D = yellow indicates laminin (basement membrane), E = magenta indicates CD31 (endothelium), F = white indicates OX-24 (HDM-FH).

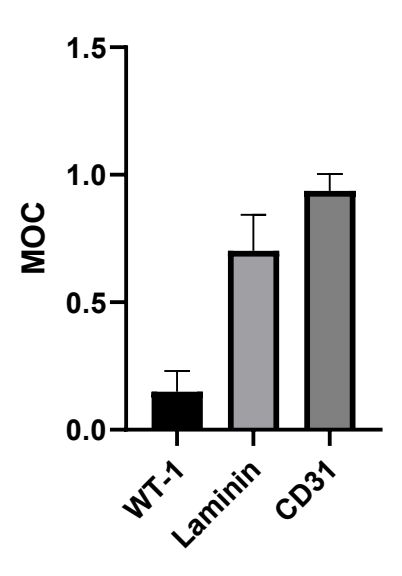


Figure 5.8 Signal overlap of HDM-FH with glomerular structure markers within tissue of a kidney treated with HDM-FH at 360 minutes of perfusion.

A snap-frozen wedge biopsy taken at the end of perfusion from a treated kidney was stained concurrently with OX-24, anti-WT-1, anti-laminin and anti-CD31 antibodies and imaged using the Leica SP8 point scanning confocal microscope with white light super continuum lasers at 40× and processed using LAS X software. 10 glomeruli were imaged and the MOC between signals from OX-24 and each of the other antibodies were calculated using Huygens Essential software. Glomeruli were imaged from 1 kidney. Mean is presented with SEM.

# 5.3.2 Physiological parameters and kidney function

# 5.3.2.1 Renal physiology

Physiological outcomes were measure in real-time throughout EVNP as a basic measure of kidney function. Urine output, RBF and RR are presented at multiple time points from 0 minutes to 360 minutes of perfusion grouped into treated and control kidneys in **Figure 5.9**. The AUC summarises the data over the whole perfusion. There was no difference in urine output, RBF or RR between the treated and control kidneys throughout perfusion.

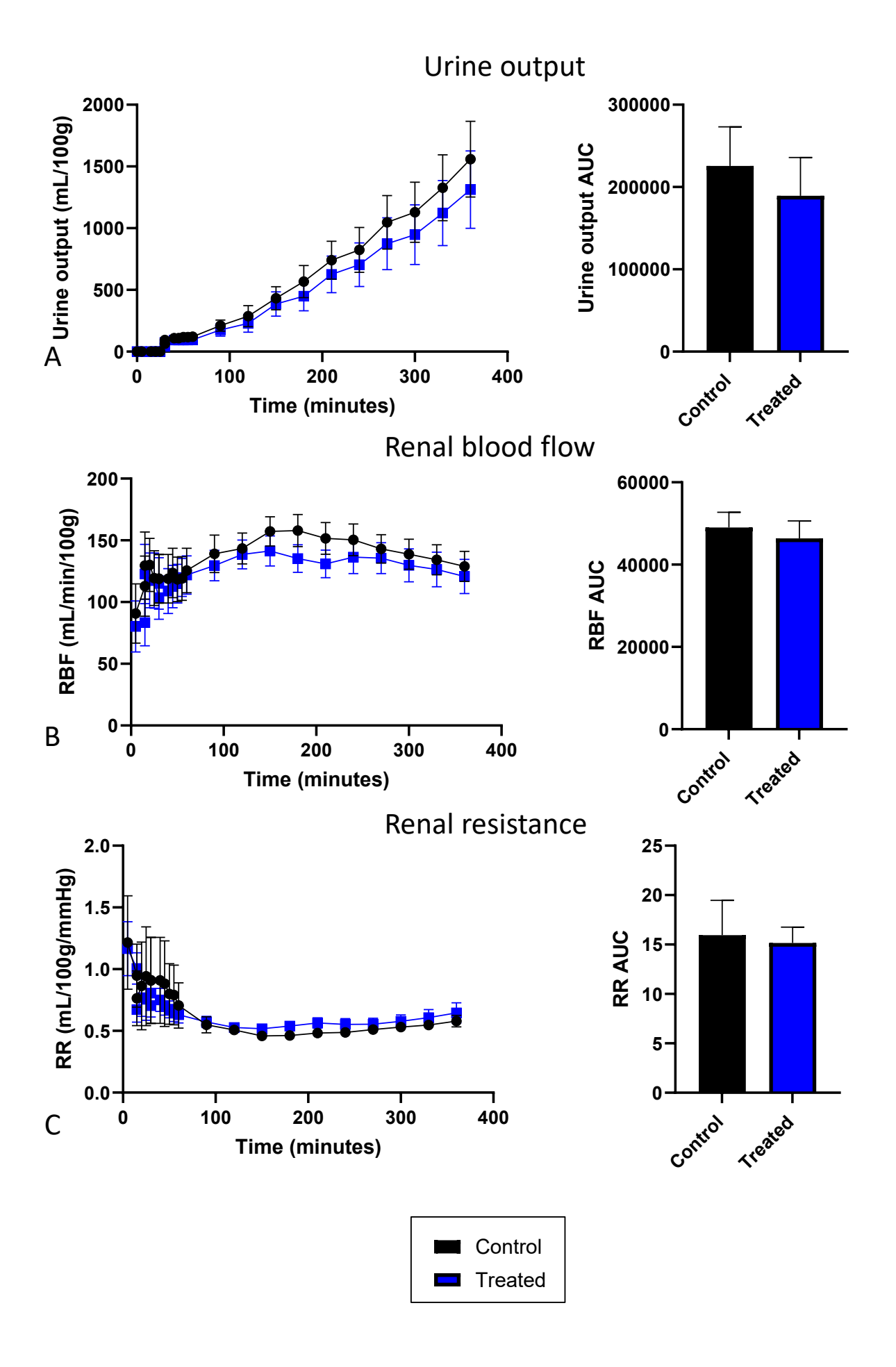


# Figure 5.9 Physiological parameters of kidneys treated with HDM-FH and control kidneys from 5 minutes to 360 minutes of perfusion.

Urine output, RBF and RR were measured from 5 minutes to 360 minutes of perfusion from treated and control kidneys and normalised for kidney weight. Panel A shows urine output over the course of perfusion (left) and AUC values (right), mean values with SEM are presented N=8. Panel B depicts RBF over the course of perfusion (left) and AUC values (right), mean values with SEM are presented, N=8. Panel C depicts RR over the course of perfusion (left) and AUC values, mean values with SEM are presented (right), N=8. Paired t-test was used to calculate statistical significance.

# 5.3.2.2 Electrolyte concentration

Electrolytes were measured throughout perfusion from arterial perfusate. There was no difference in ionised calcium, potassium, sodium or glucose levels throughout perfusion between treated and control kidneys (**Figure 5.13**).

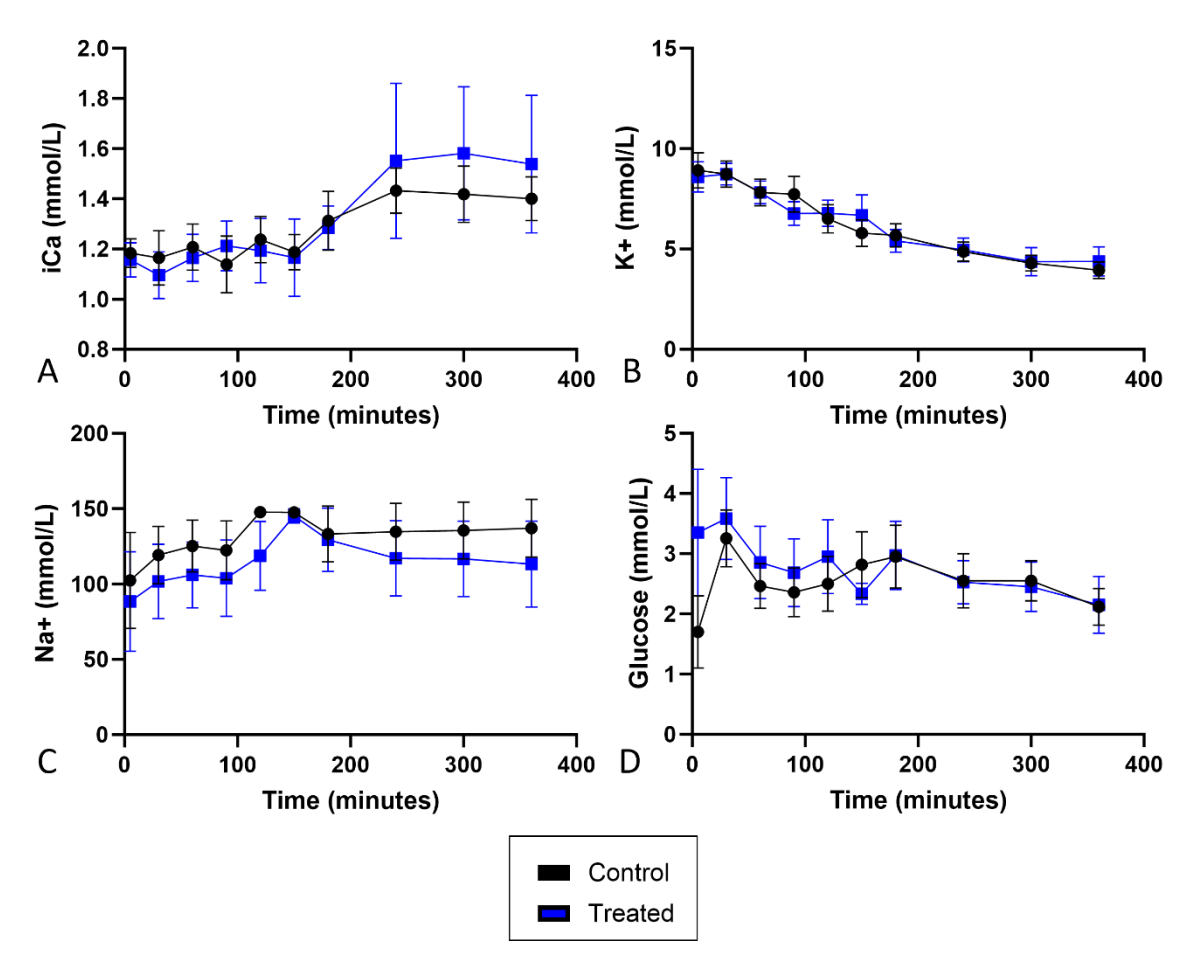


Figure 5.10 Electrolyte concentration in perfusate of kidneys treated with HDM-FH and control kidneys from 5 minutes to 360 minutes of perfusion.

Electrolytes were measured from arterial perfusate samples from treated and control kidneys taken from 5 minutes to 360 minutes of perfusion using the RAPIDpoint 500e Blood Gas System, N=8. Mean is presented with SEM. Two-way ANOVA was used to calculate statistical significance.

# 5.3.2.3 Cellular metabolism

Oxygen consumption and lactate production were measured as indicators of cellular metabolism. Oxygen consumption was calculated from measurements from arterial and venous perfusate as described in chapter 2. Oxygen consumption remained stable throughout perfusion in both treated and control kidneys with no difference seen in overall oxygen consumption. Lactate production increased 2-fold from 5 minutes of perfusion to 30 minutes

of perfusion in treated and control kidneys then remained stable until the end of perfusion, with no difference between treated and control kidneys (Figure 5.14).

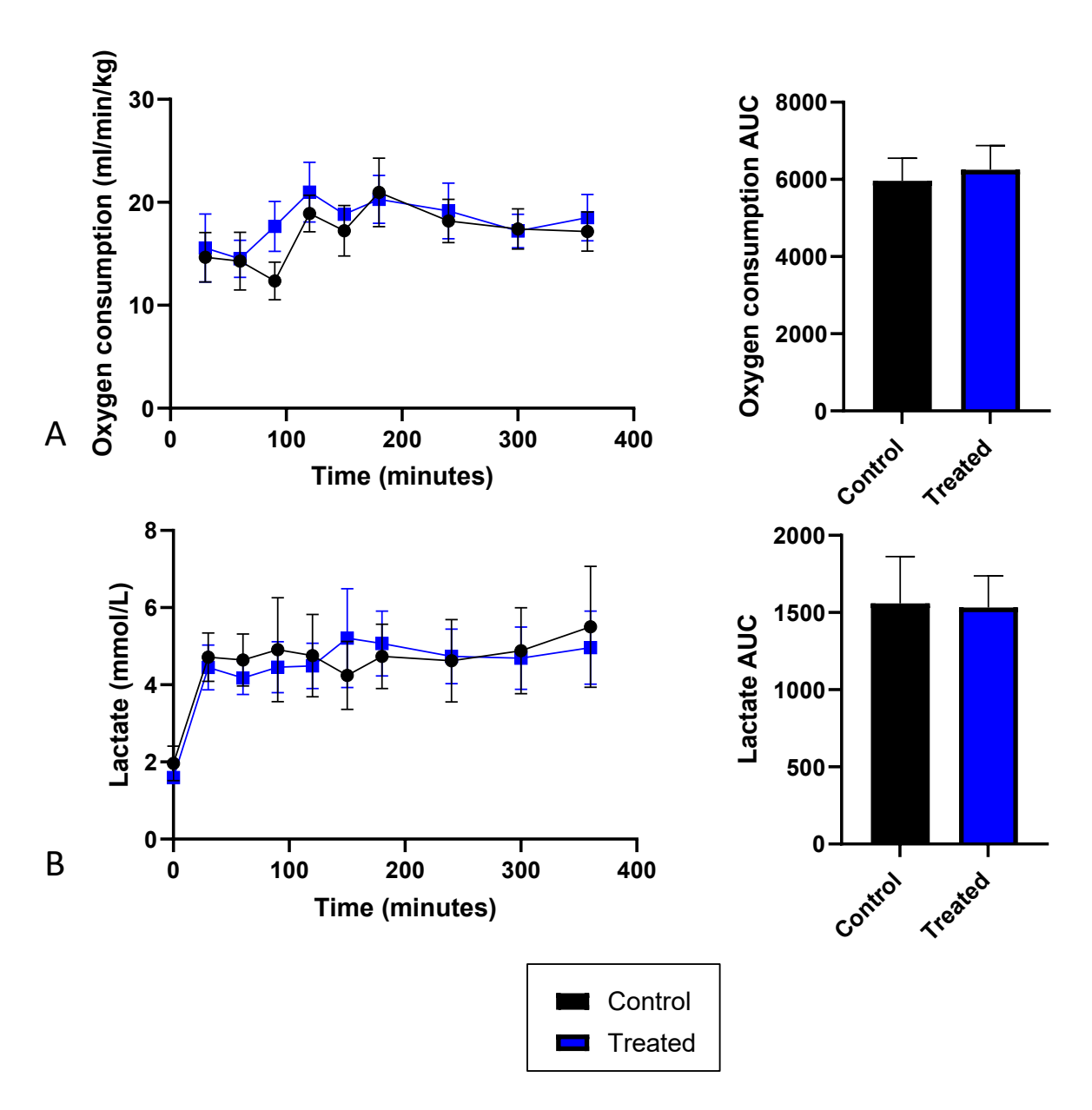


Figure 5.11 Cellular metabolism of kidneys treated with HDM-FH and control kidneys from 5 minutes to 360 minutes of perfusion.

Oxygen consumption was calculated from arterial and venous blood gas samples from treated and control kidneys taken from 5 minutes to 360 minutes of perfusion using the RAPIDpoint 500e Blood Gas System and normalised for weight. Panel A shows oxygen consumption over the course of perfusion (left) and AUC values (right), mean values with SEM are presented N=8. Lactate was measured from arterial perfusate samples from treated and control kidneys taken from 5 minutes to 360 minutes of perfusion using the RAPIDpoint 500e Blood Gas System. Panel B shows lactate levels over the course of perfusion (left) and AUC values (right), mean values with SEM are presented N=8. Paired t-test was used to calculate statistical significance.

# 5.3.2.4 Renal function

Creatinine clearance from perfusate was measured to assess the effect of HDM-FH on GFR. There was no difference in clearance of creatinine between treated and control kidneys (Figure 5.15).

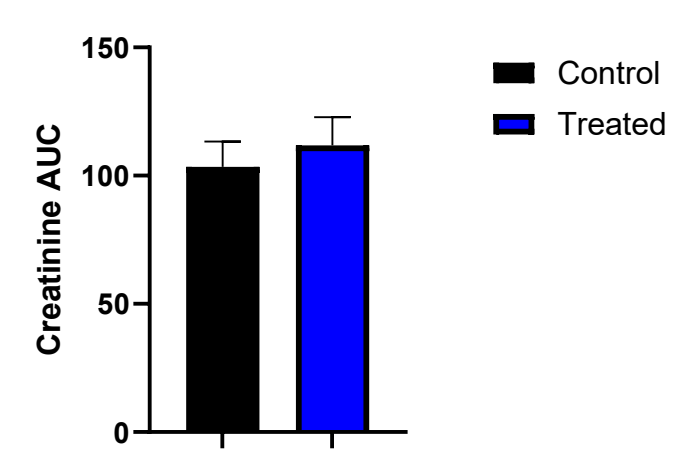
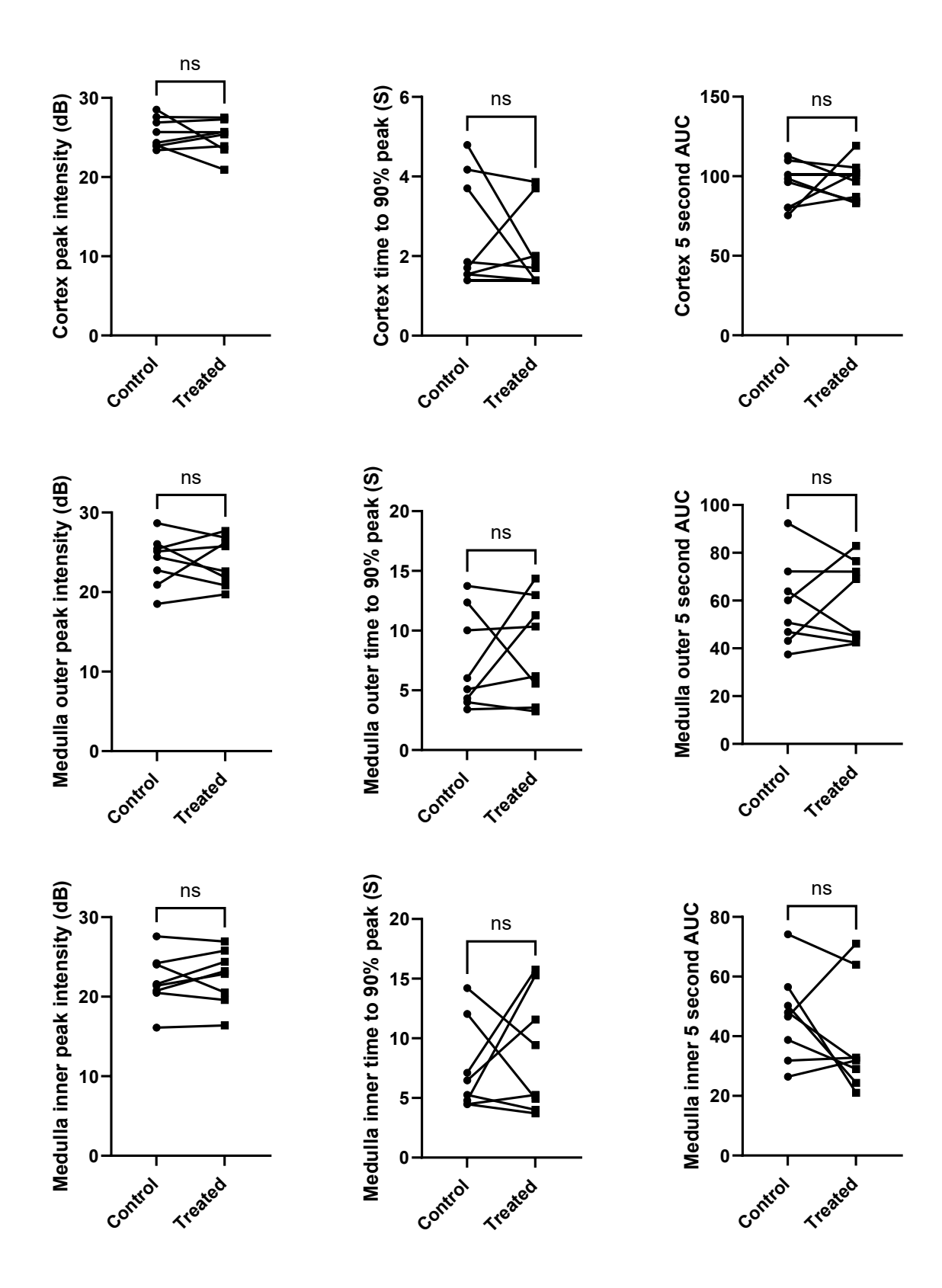


Figure 5.12 Clearance of creatinine from perfusate of kidneys treated with HDM-FH and control kidneys.

Creatinine levels were measured in perfusate from 5 minutes to 180 minutes of perfusion and normalised for kidney weight and 5-minute creatinine values. An AUC value was calculated from individual plots, N=8. Mean from combined AUC values is presented with SEM. Paired t-test was used to calculate statistical significance.

### 5.3.2.5 Contrast enhanced ultrasound

CEUS was performed to assess if HDM-FH affected microvascular perfusion of kidneys. Microbubbles (sulphur hexafluoride in a phospholipid shell) were administered to the renal artery at the end of perfusion. The small size of the microbubbles allows them to infiltrate the capillary bed. This creates an increased ultrasound signal which can be assessed to give a quantifiable measurement of microvasculature perfusion in specific regions of interest. There was no difference in peak intensity, time to 90% peak or the AUC of 5 seconds of perfusion within the cortex or inner or outer medulla at 330 minutes of perfusion (**Figure 5.16**).



# Figure 5.13 Contrast enhanced ultrasound results from treated and control kidneys at 330 minutes of perfusion.

1 mL sulphur hexafluoride contrast agent (SonoVue \*, Bracco) was administered to the renal artery at 330 minutes of EVNP to increase ultrasound signal. Images were taken using the eL18-4 probe of the Philips EPIQ7 Ultrasound machine with QLab 8.1 software. DICOM files were imported into QLAB Advanced Quantification Software and analysed using the ROI QApp. Peak intensity, time to 90% peak and 5 second AUC values were measured for ROIs in the cortex, outer medulla and inner medulla. Individual values are presented, N=8. Paired t-test was used to calculate statistical significance. ns = non-significant.

# 5.3.2.6 Neutrophil gelatinase-associated lipocalin

NGAL was measured in urine throughout perfusion to assess if HDM-FH affected tubular injury. There was no significant difference in urinary NGAL levels between treated and control kidneys (**Figure 5.18**).

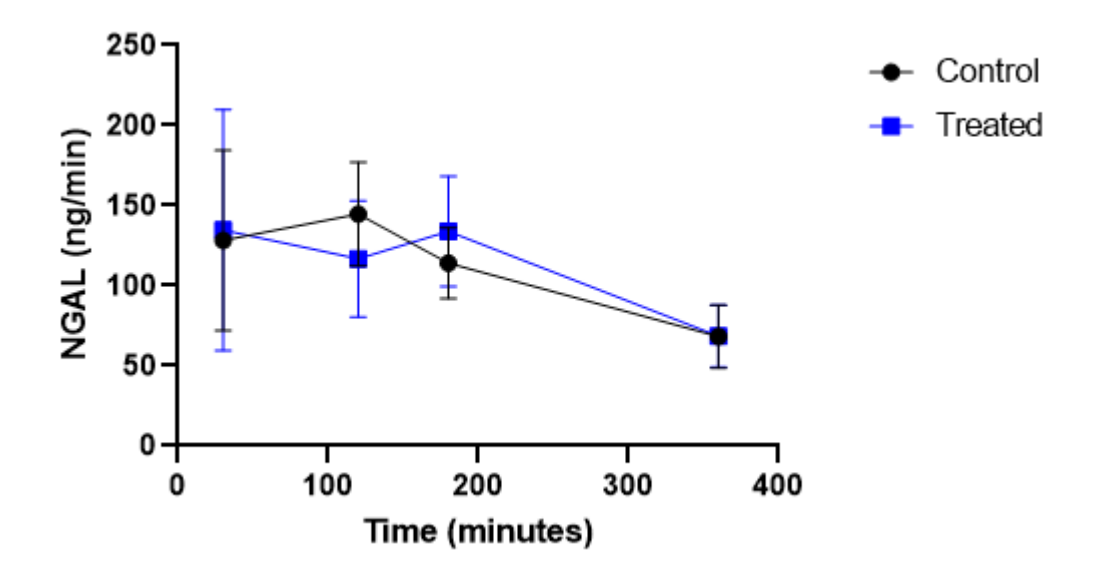


Figure 5.14 Neutrophil gelatinase-associated lipocalin levels in urine of kidneys treated with HDM-FH and control kidneys from 30 minutes to 360 minutes of perfusion.

NGAL concentrations in urine samples taken throughout perfusion were measured via ELISA and normalised for kidney weight and urine output, N=8. Mean is presented with SEM. Twoway ANOVA was used to calculate statistical significance.

# 5.3.3 Complement regulation

FH regulates complement activity by cofactor activity to FI in the inactivation of C3b to iC3b, and through decay accelerating of the C3 and C5 convertase. Less convertase assembly on C3b and decay of formed convertase should lead to a reduction in C3 and C5 cleavage, Bb formation which depends on C3b binding to be cleaved by factor D, and MAC formation. A reduction in general inflammation/damage may also lead to a reduction in the other pathways of complement.

# 5.3.3.1 C3 and C3 activation products

C3 deposition in kidney glomeruli at the end of perfusion was identified using an anti-C3 antibody which binds full length C3 and C3 fragments. There was no significant difference in C3 deposition at the end of perfusion between treated and control kidneys (**Figure 5.19** and **Figure 5.20**).

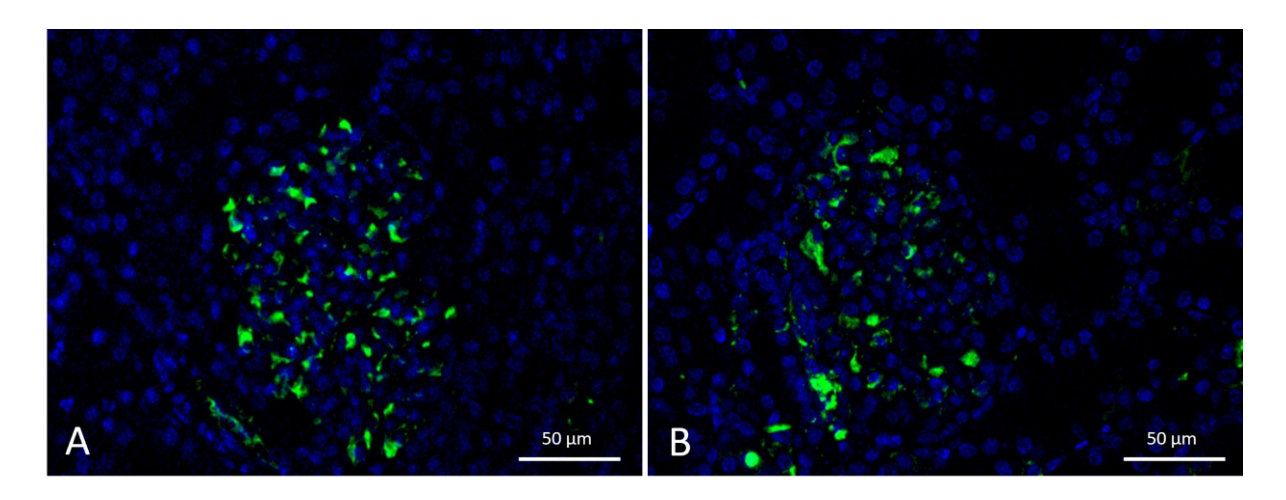


Figure 5.15 Immunofluorescent images of C3 deposition in glomeruli of kidneys treated with HDM-FH and control kidneys at 360 minutes of perfusion.

FFPE wedge biopsies from treated and control and kidneys taken at 360 minutes of perfusion were stained with an anti-C3 antibody, DAPI was used as a counterstain. Sections were then imaged using the LEICA DM2000 LED microscope and processed using LAS X software. C3 is shown in green, DAPI is shown in blue. C3 can be seen within the glomeruli of control (A) and treated (B) kidneys.

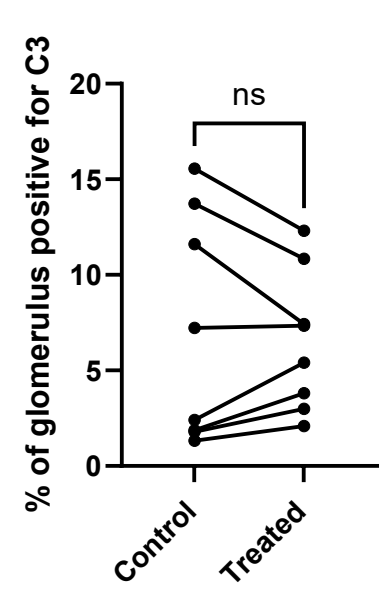


Figure 5.16 C3 deposition in glomeruli of kidneys treated with HDM-FH and control kidneys at 360 minutes of perfusion.

FFPE wedge biopsies taken at from treated and control kidneys at 360 minutes of perfusion were stained with an anti-C3 antibody. Sections were then imaged using the LEICA DM2000 LED microscope and processed using LAS X software. The percentage area of positive C3 signal of 10 glomeruli was measured from each biopsy, N=8. Individual values are presented. Paired t-test was used to calculate statistical significance. ns = non-significant.

Due to the inability to differentiate between full length porcine C3 and C3 fragments using immunofluorescence, a western blot was carried out to investigate the ratio of full-length C3 to C3 breakdown fragments. The same anti-C3 antibody was used as in the immunofluorescence protocol that would bind C3 fragments, however SDS-PAGE separates proteins by size so different size fragments can be identified. A ratio of the amount alpha chain of full-length C3 to the amount of the C3C alpha chain in perfusate samples taken at the end of perfusion was measured (Figure 5.21). This was to identify whether treatment with HDM-FH affected C3 activation leading to a higher ratio of C3 fragments to full-length C3. There was no difference between the amount of full length C3 to C3 activation product C3C in perfusate samples taken at the end of perfusion.

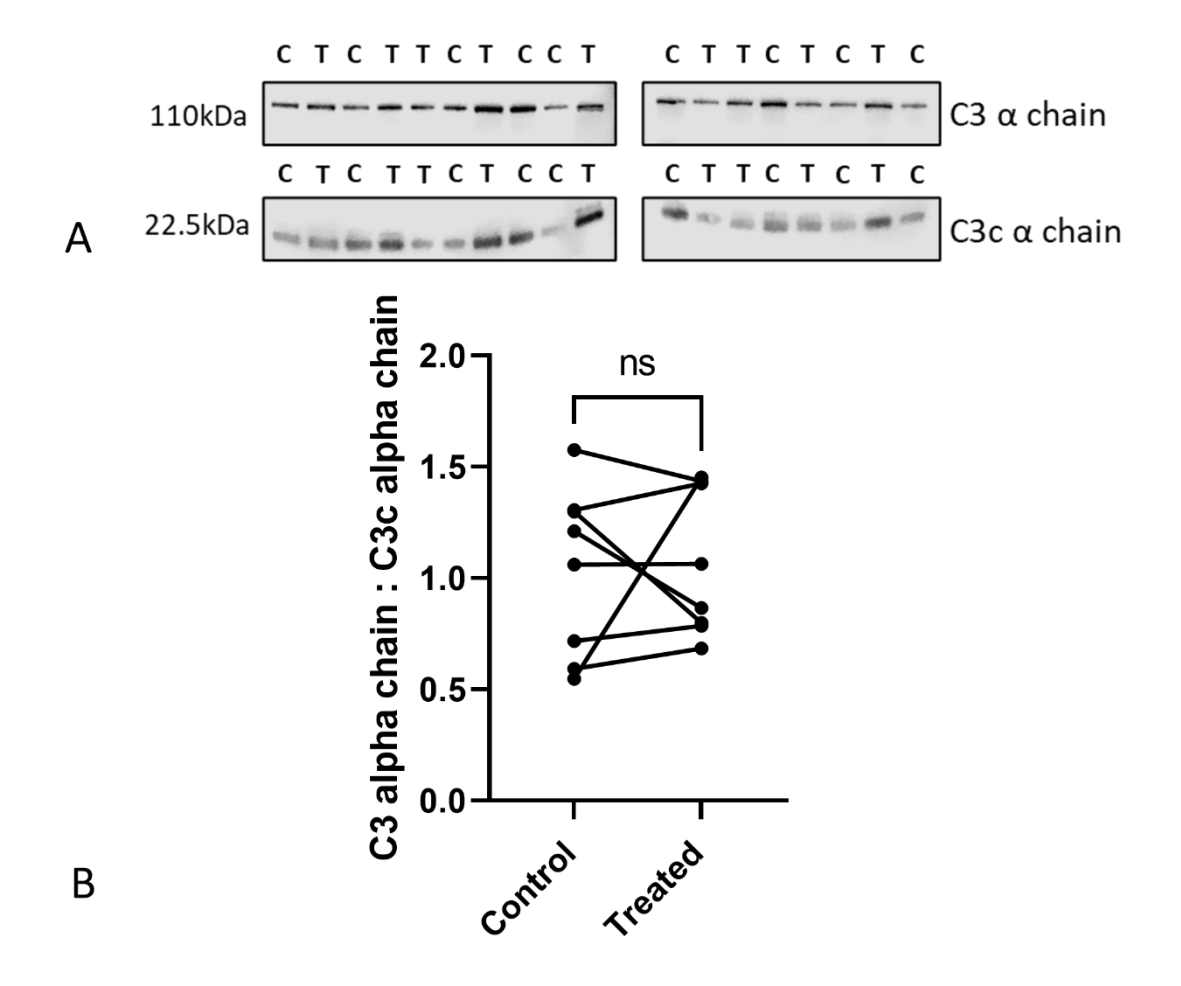


Figure 5.17 Ratio of C3 alpha chain to C3C alpha chain on Western blot in perfusate from kidneys treated with HDM-FH and control kidneys at 360 minutes of perfusion.

Perfusate samples from treated and control kidneys taken at 360 minutes of perfusion were ran on SDS-PAGE for Western blot under reducing conditions (panel A). the SDS-PAGE gel was imaged using the Odyssey® Fc imaging system. Band signal was normalised for total protein load and quantified using Image Studio Lite version 5.2. The ratio of C3 alpha chain to C3C alpha chain for treated and control kidneys is shown in panel B. Paired t-test was used to calculate statistical significance. ns = non-significant.

C3a levels in perfusate and urine were measured to indicate C3 breakdown. There was no significant difference in C3a levels in urine or perfusate between treated and control kidneys throughout perfusion (Figure 5.22).

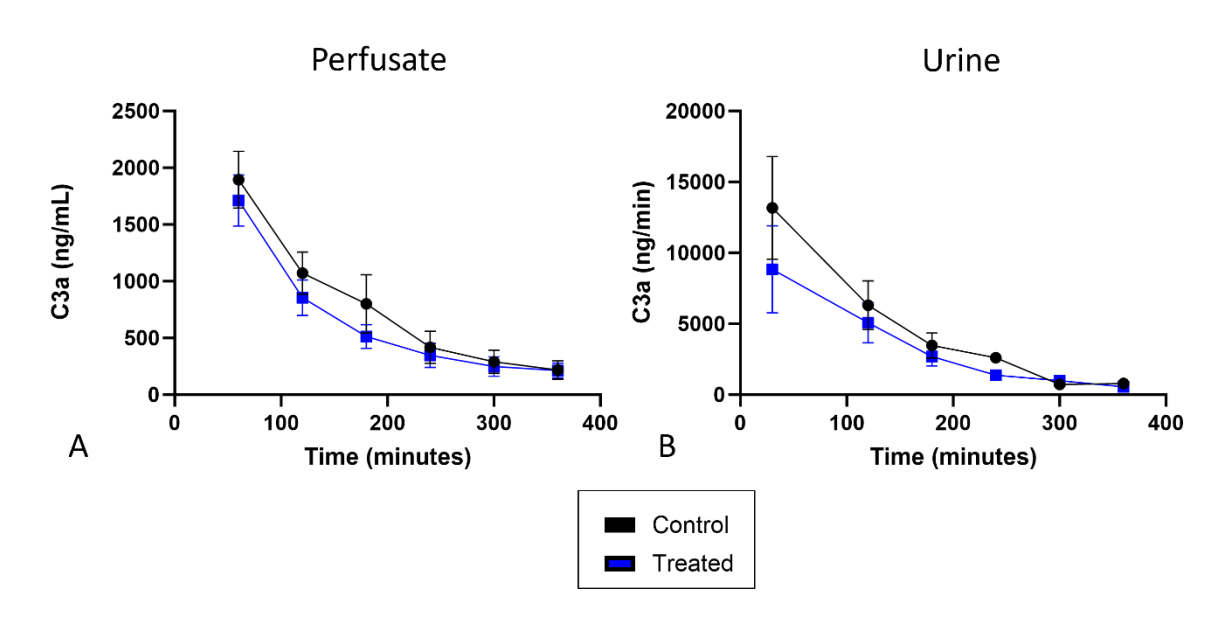


Figure 5.18 C3a levels in perfusate and urine in perfusate from kidneys treated with HDM-FH and control kidneys from 30 minutes to 360 minutes of perfusion.

C3a concentrations in perfusate and urine samples taken from treated and control kidneys from 30 minutes to 360 minutes of perfusion were measured. Perfusate concentrations are shown in A, N=8. total C3a produced per minute in urine is shown in B, N=8. Mean is presented with SEM. Two-way ANOVA was used to calculate statistical significance.

# 5.3.3.2 C5a

C5a levels in urine were measured to investigate if HDM-FH altered C5 breakdown. C5a levels in urine were significantly reduced throughout perfusion (**Figure 5.23**).

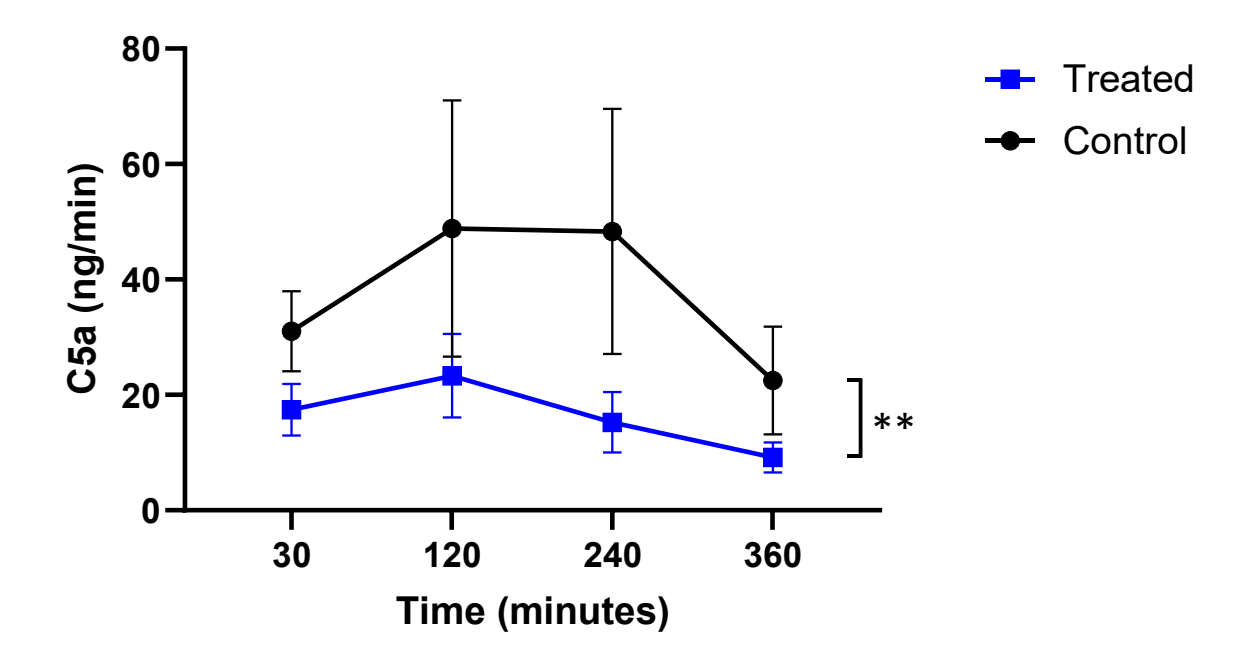


Figure 5.19 C5a levels in urine from kidneys treated with HDM-FH and control kidneys at 30 minutes to 360 minutes of perfusion.

C5a levels in urine samples taken from treated and control kidneys from 30 minutes to 360 minutes of perfusion were measured using ELISA. Total C5a produced per minute is shown. Two-way ANOVA was used to calculate statistical significance. \*\*p<0.01.

# 5.3.3.3 Factor B

The active fragment of FB, Bb was quantified in glomeruli to indicate alternative pathway activation. Glomerular deposition of Bb was significantly reduced in biopsies taken at the end of perfusion in treated kidneys compared with control (**Figure 5.24**). There was no difference in FB levels in perfusate between treated and control kidneys at the end of perfusion (**Figure 5.25**)

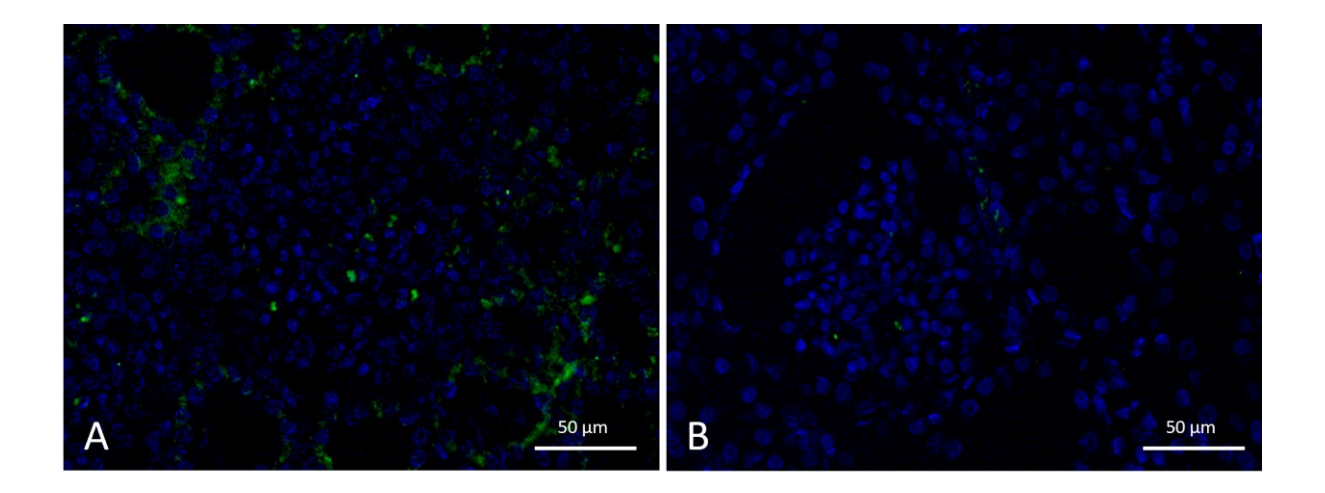


Figure 5.20 Immunofluorescent images of Bb deposition in glomeruli of kidneys treated with HDM-FH and control kidneys at 360 minutes of perfusion.

FFPE wedge biopsies of treated and control kidneys taken at 360 minutes of perfusion were stained with an anti-Bb antibody, DAPI was used as a counterstain. Sections were then imaged using the LEICA DM2000 LED microscope and processes using LAS X software. Bb is shown in green, DAPI is shown in blue. Bb can be seen within the glomeruli of control (A) and treated (B) kidneys.

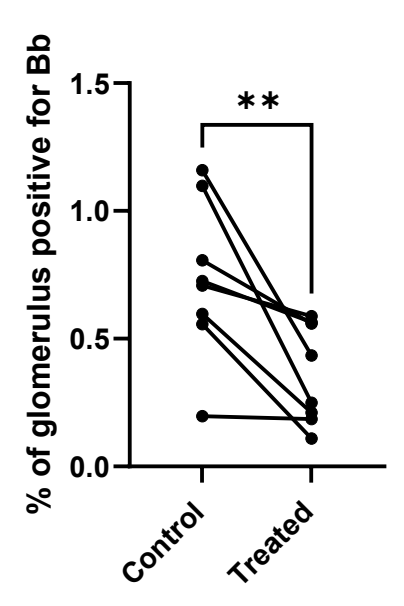


Figure 5.21 Bb deposition in glomeruli of kidneys treated with HDM-FH and control kidneys at 360 minutes of perfusion.

FFPE wedge biopsies of treated and control kidneys taken at 360 minutes of perfusion were stained with an anti-Bb antibody. Sections were then imaged using the LEICA DM2000 LED microscope and processed using LAS X software. The percentage area of positive Bb signal of 10 glomeruli was measured from each biopsy, N=8. Individual values are presented. Paired t-test was used to calculate statistical significance. \*\*p<0.01.

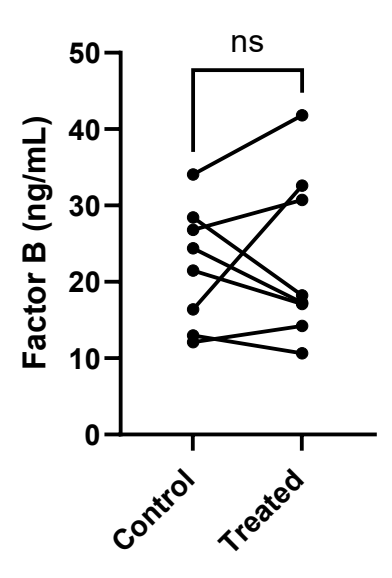


Figure 5.22 FB in perfusate of kidneys treated with HDM-FH and control kidneys from 360 minutes of perfusion.

FB levels in perfusate samples taken from treated and control kidneys taken at 360 minutes of perfusion were measured using ELISA. There was no significant difference between FB levels at the end of perfusion between treated and untreated kidneys, N=8. Individual values are presented. Paired t-test was used to calculate statistical significance. ns = non-significant.

## 5.3.3.4 C1q

C1q deposition in glomeruli was quantified as a measurement of classical pathway activation. Glomerular deposition of C1q was significantly reduced in biopsies taken at the end of perfusion in treated kidneys compared with control (Figure 5.27 and Figure 5.28).

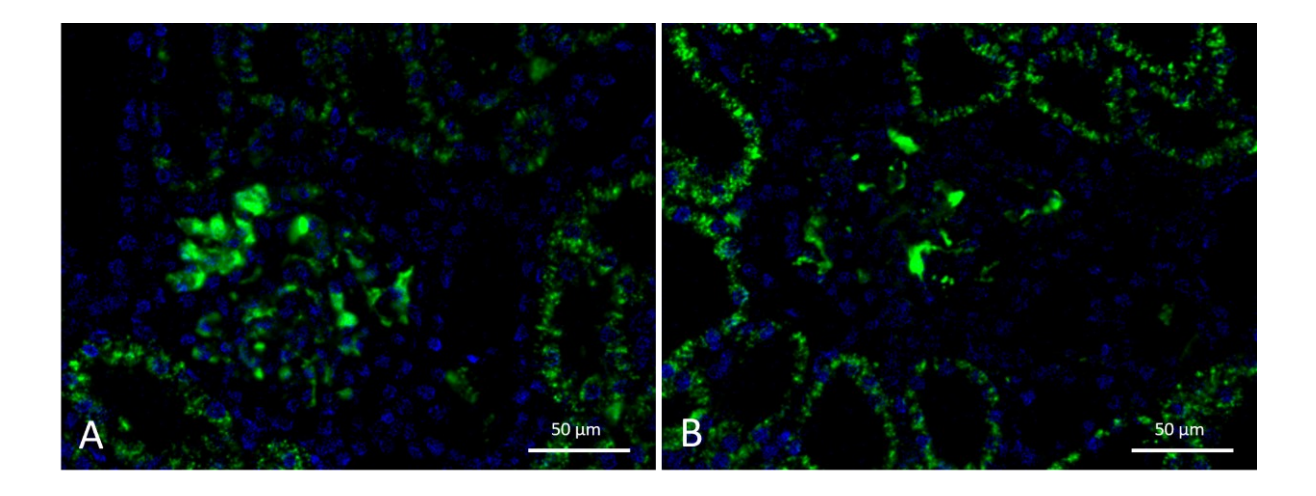


Figure 5.23 Immunofluorescent images of C1q deposition in glomeruli of kidneys treated with HDM-FH and control kidneys at 360 minutes of perfusion.

FFPE wedge biopsies from treated and control kidney taken at 360 minutes of perfusion were stained with an anti-C1q antibody, DAPI was used a counterstain. Sections were then imaged using the LEICA DM2000 LED microscope and processed with LAS X software. C1q is shown in green, DAPI is shown in blue. C1q can be seen within the glomeruli of control (A) and treated (B) kidneys.

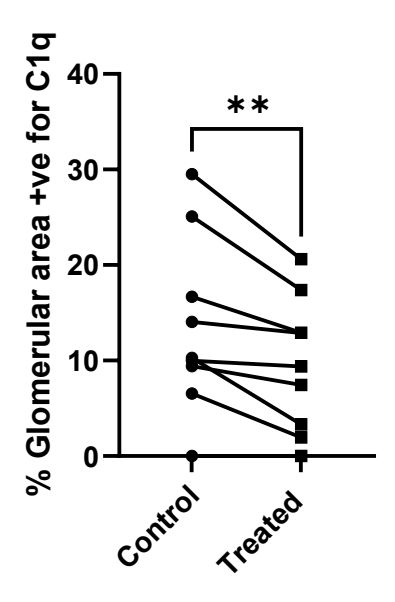


Figure 5.24 C1q deposition in glomeruli of kidneys treated with HDM-FH and control kidneys at 360 minutes of perfusion.

FFPE wedge biopsies from treated and control kidneys taken at the end of perfusion were stained with an anti-C1q antibody. Sections were then imaged using the LEICA DM2000 LED microscope and processed using LAS X software. The percentage area of positive C1q signal of 10 glomeruli was measured from each biopsy, N=8. Individual values are presented. Paired t-test was used to calculate statistical significance. \*\*p<0.01.

# 5.3.3.5 Haemolytic activity of perfusate

The haemolytic activity of perfusate pre-perfusion and at the end of perfusion was measured to indicate complement consumption in the fluid phase. In all kidneys, complement had been consumed at the end of perfusion compared with pre-perfusion. In 5 pairs, there was more complement consumption in untreated kidneys at the end of perfusion, in 3 pairs, there was more complement consumption in treated kidneys at the end of perfusion (**Figure 5.29**).

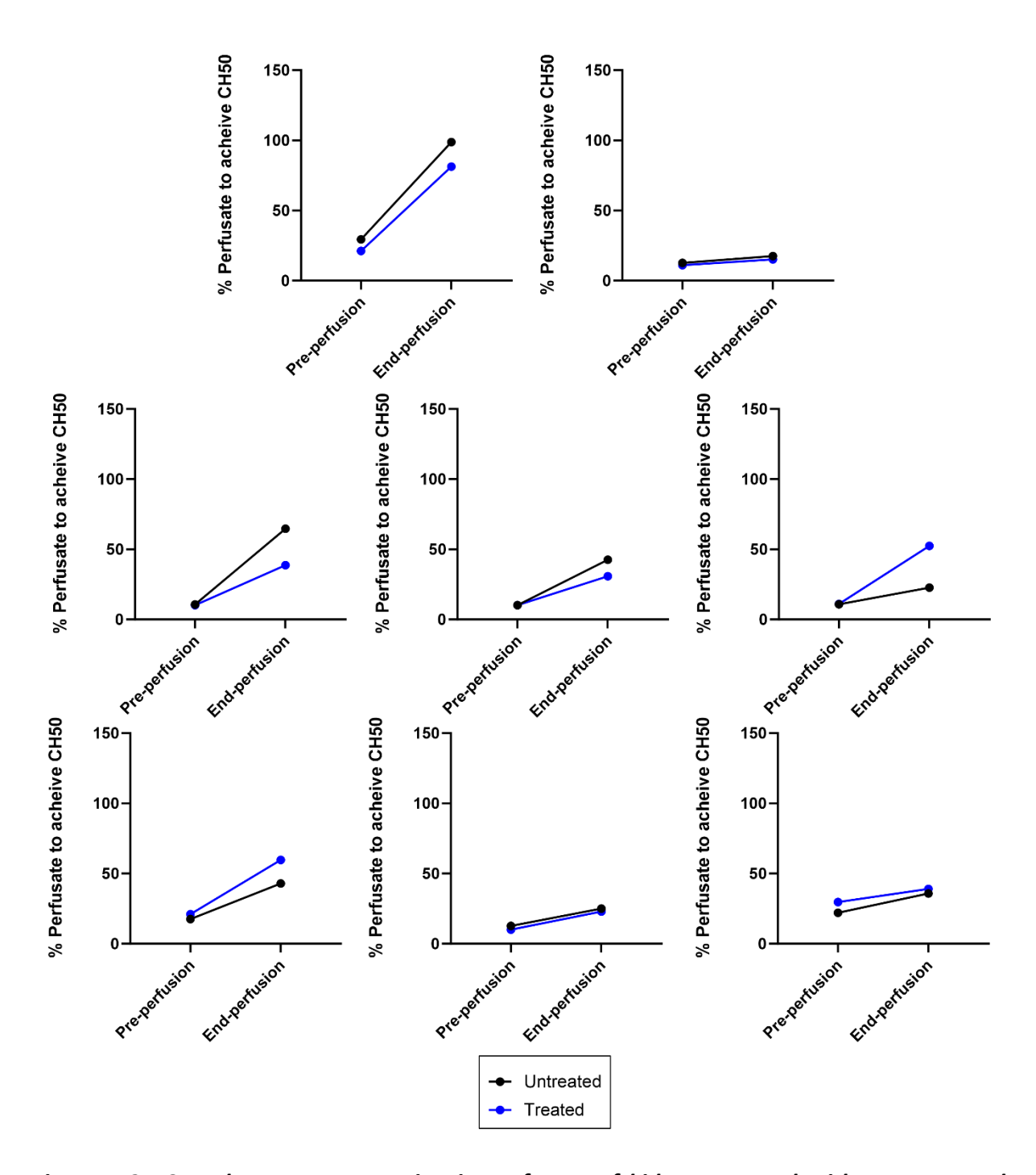


Figure 5.25 Complement consumption in perfusate of kidneys treated with HDM-FH and control kidneys pre-perfusion and at 360 minutes of perfusion.

Perfusate samples from treated and control kidneys taken pre-perfusion and at 360 minutes of perfusion were tested for complement activity using classical haemolytic assays. The percentage of sample required to achieve the  $CH_{50}$  is plotted for each kidney, N=8. Individual values are plotted on separate graphs.

# 5.3.4 Inflammatory cytokines and chemokines

C5a can cause recruitment and activation of macrophages which produce proinflammatory cytokines and chemokines (Markiewski and Lambris, 2007). IL-6 and IL-8 levels were therefore measured in the urine throughout perfusion to see if HDM-FH treatment could reduce inflammation.

There was no significant difference between urine IL-6 or IL-8 levels in treated and control kidneys throughout perfusion (Figure 5.30 and Figure 5.31).

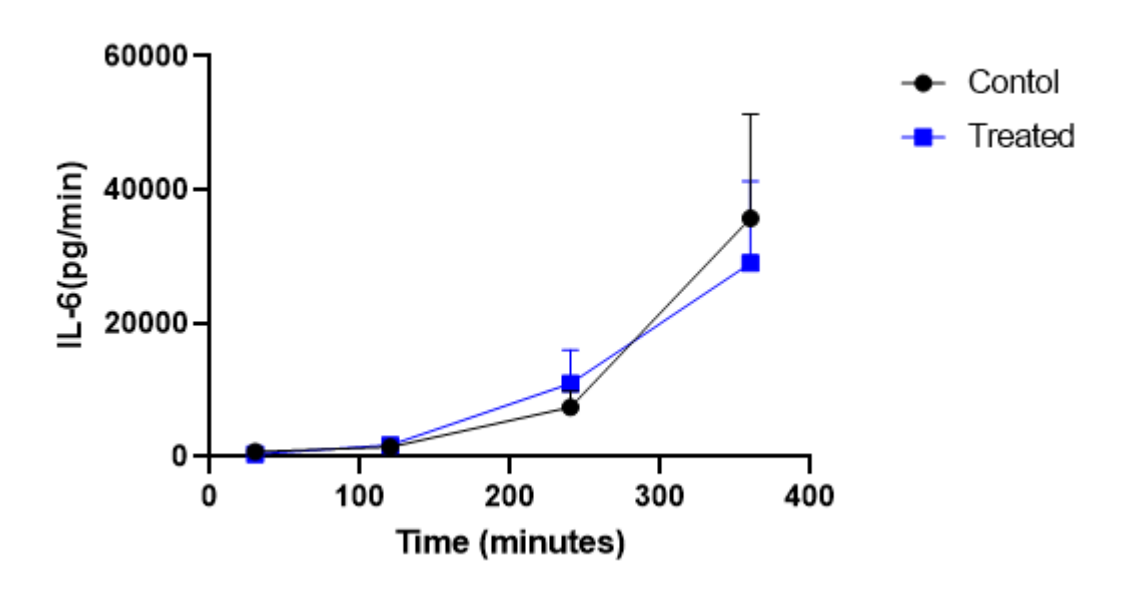


Figure 5.26 IL-6 levels in urine from kidneys treated with HDM-FH and control kidneys from 30 minutes to 360 minutes of perfusion.

IL-6 concentrations in urine samples from treated and control kidneys taken at 30 minutes to 360 minutes of perfusion were measured via ELISA. Total IL-6 produced per minute is shown, N=8. Mean is presented with SEM. Two-way ANOVA was used to calculate statistical significance.

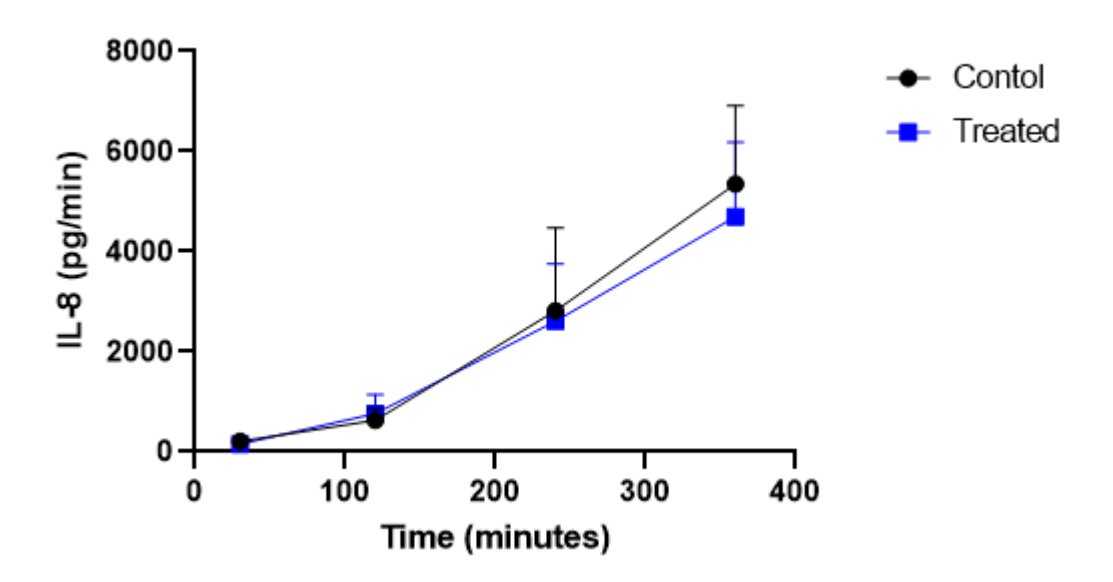


Figure 5.27 IL-8 levels in urine from kidneys treated with HDM-FH and control kidneys from 30 minutes to 360 minutes of perfusion.

IL-8 concentrations in urine samples from treated and control kidneys taken at 30 minutes to 360 minutes of perfusion were measured via ELISA. Total IL-6 produced per minute is shown, N=8. Mean is presented with SEM. Two-way ANOVA was used to calculate statistical significance.

### 5.3.5 Fibrinogen and microthrombi

Complement inhibition can lead to a decrease in fibrosis through C5a dependant TGF-β production and endothelial-to-mesenchymal transition inhibition (Curci et al., 2014, Boor et al., 2007). Microthrombi formation correlated with fibrinogen accumulation during NMP has been previously observed (DiRito et al., 2021), furthermore, uncontrolled complement activation can drive pathophysiology of thrombotic microangiopathies (TMAs), a characteristic feature of which is microvascular thrombosis (George and Nester, 2014). An anti-fibrinogen/fibrin antibody was used to measure fibrinogen in kidneys at the end of perfusion (Figure 5.32 and Figure 5.33). MSB was used to stain erythrocytes in kidney tissue at the end of perfusion to quantify microvascular thrombosis (Figure 5.34 and Figure 5.35).

## 5.3.5.1 Fibrinogen

Fibrinogen deposition was measured in glomeruli of kidneys at the end of perfusion. The antibody used binds fibrinogen and cleaved fibrin. There was no significant difference in the amount of fibrinogen present in glomeruli between treated and untreated kidneys (**Figure 5.31** and **Figure 5.32**).

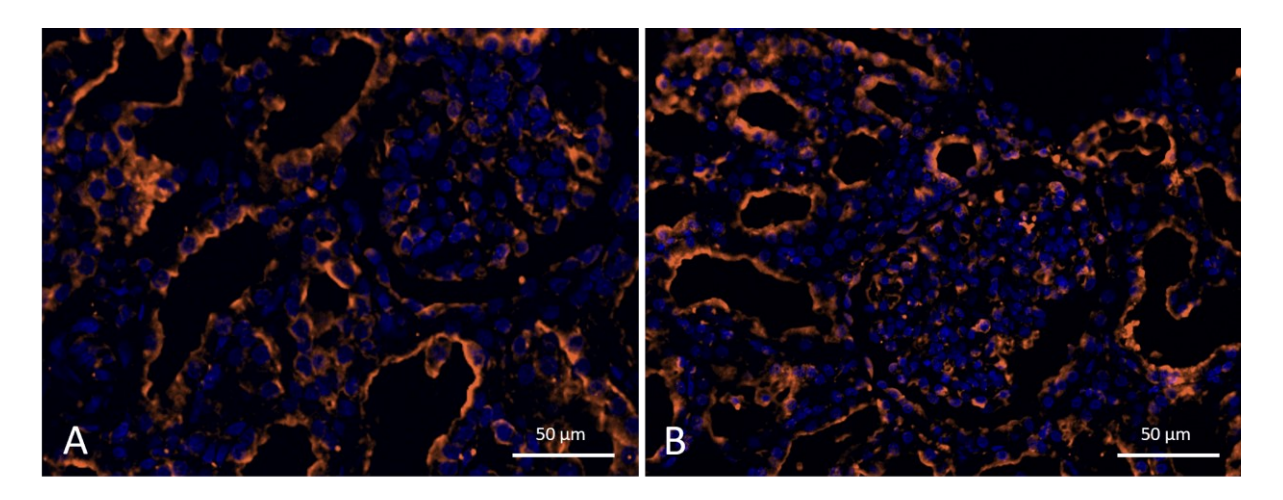


Figure 5.28 Immunofluorescent images of fibrinogen deposition in glomeruli of kidneys treated with HDM-FH and control kidneys at 360 minutes of perfusion.

FFPE wedge biopsies from treated and control kidney taken at 360 minutes of perfusion were stained with an anti-fibrinogen antibody, DAPI was used as a counterstain. Sections were then imaged using the LEICA DM2000 LED microscope and processed using LAS X software. Fibrinogen is shown in orange, DAPI is shown in blue. Fibrinogen can be seen within the glomeruli of control (A) and (B) treated kidneys.

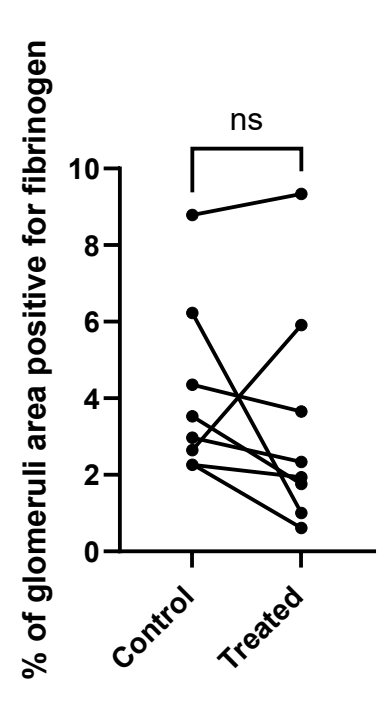


Figure 5.29 Fibrinogen deposition in glomeruli of kidneys treated with HDM-FH and control kidneys at 360 minutes of perfusion.

FFPE wedge biopsies from treated and control kidney taken at 360 minutes of perfusion were stained with an anti-fibrinogen antibody. Sections were then imaged using the LEICA DM2000 LED microscope and processed using LAS X software. The percentage area of positive fibrinogen signal of 10 glomeruli was measured from each biopsy, N=8. Individual values are presented. Paired t-test was used to calculate statistical significance. ns = non-significant.

### 5.3.5.2 Erythrocytes

MSB staining was used to visualise erythrocyte microthrombi. Percentage erythrocyte coverage per 20x field of view and per glomeruli were quantified (**Figure 5.34** and **Figure 5.35**). There was no significant difference in either value between treated or control kidneys, however the percentage erythrocyte coverage per 20x field of view was approximately 3-fold lower in treated kidneys (p=0.063).

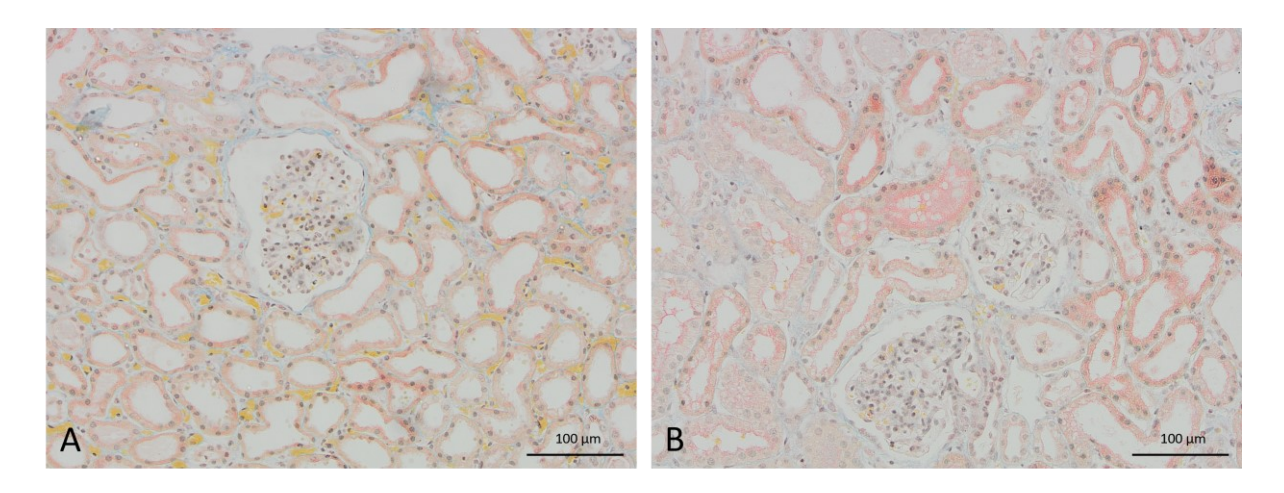


Figure 5.30 MSB stained sections of kidneys treated with HDM-FH and kidneys at 360 minutes of perfusion.

FFPE wedge biopsies of treated and control kidneys taken at 360 minutes of perfusion were stained with MSB. Brightfield images of sections were then taken using the CMOC colour camera SC50 and processes using Cellsens Standard software. A shows a control kidney, B shows a treated kidney.

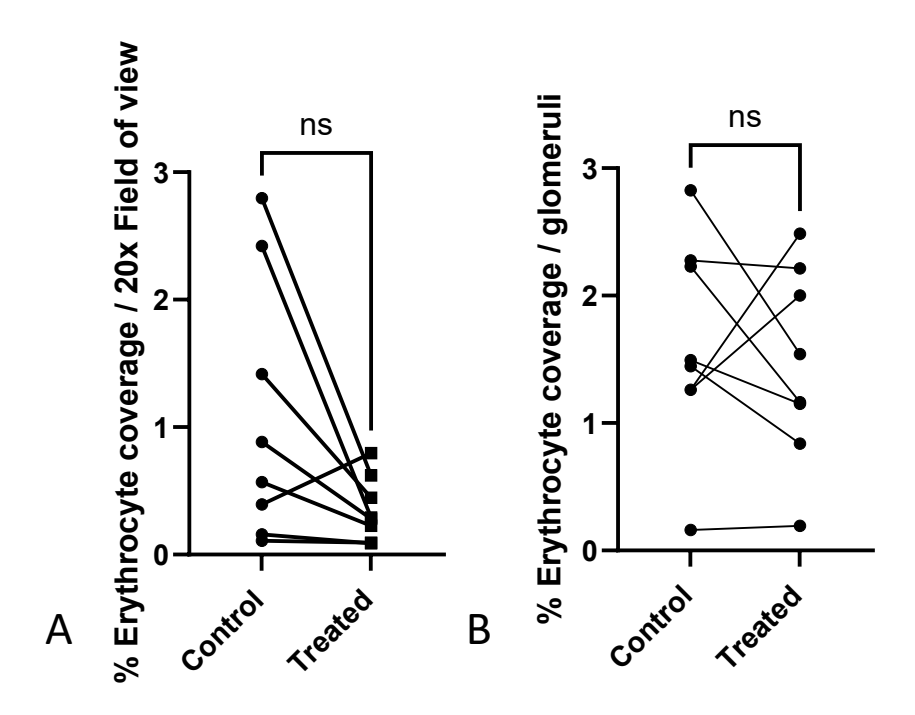


Figure 5.31 Erythrocyte coverage in kidneys treated with HDM-FH and control kidneys at 360 minutes of perfusion.

FFPE wedge biopsies taken at 360 minutes of perfusion were stained with MSB. Brightfield images of sections were then taken using the CMOC colour camera SC50 and processes using Cellsens Standard software. A classifier was trained to segment images identifying erythrocytes using LABKIT plugin on Fiji Image J. Erythrocyte pixels were quantified and percentage pixels per 20x field of view from 10 images (A) or per glomerulus for 10 glomeruli (B) were calculated, N=8. Individual values are presented. Paired t-test was used to calculate statistical significance. ns = non-significant

### 5.3.6 Glycocalyx shedding

Complement mediated endothelial activation following IRI can cause shedding of the surface layer of the endothelium, the glycocalyx (Bongoni et al., 2019). Hyaluronan was therefore measured in plasma to assess whether HDM-FH treatment reduced endothelial activation.

## 5.3.6.1 Hyaluronan

Hyaluronan levels in perfusate throughout perfusion were measures using ELISA. There was no significant difference in perfusate hyaluronan levels between treated and untreated kidneys (**Figure 5.33**).

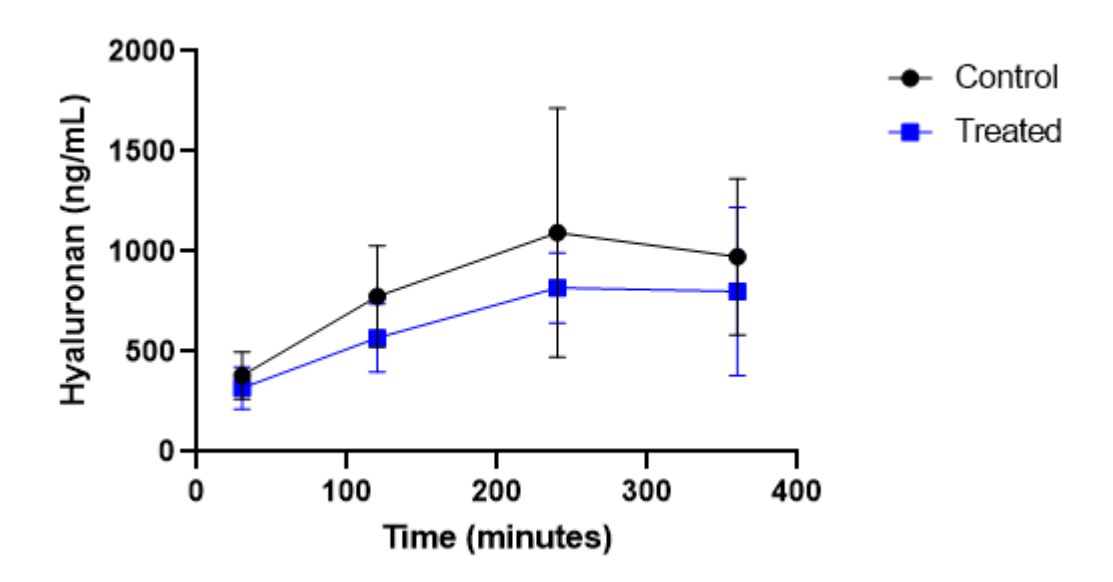


Figure 5.32 Hyaluronan levels in perfusate from kidneys treated with HDM-FH and control kidneys from 30 minutes to 360 minutes of perfusion.

Hyaluronan concentrations in perfusate samples from treated and control kidneys taken from 30 minutes to 360 minutes of perfusion were measured via ELISA, N=8. Mean is presented with SEM. Two-way ANOVA was used to calculate statistical significance.

### 5.3.7 Cell death

Apoptosis is a controlled form of cell death that can be caused by complement activation, a reduction in C5a would suggest reduced MAC formation and therefore cell lysis (Nauta et al., 2002). Moreover, C1q binds apoptotic bodies for clearance (Cai et al., 2015). Tissue apoptosis was therefore measured to assess if reduced C5 cleavage affected apoptosis, or if decreased C1q in treated kidneys could be a consequence of decreased apoptosis.

# 5.3.7.1 Apoptosis

A TUNEL assay was used to detect apoptotic cells in tissue through binding to fragmented nuclear DNA. There were significantly less apoptotic bodies in the tissue of treated kidneys taken at the end of perfusion when compared with control kidneys (**Figure 5.34** and **Figure 5.35**).

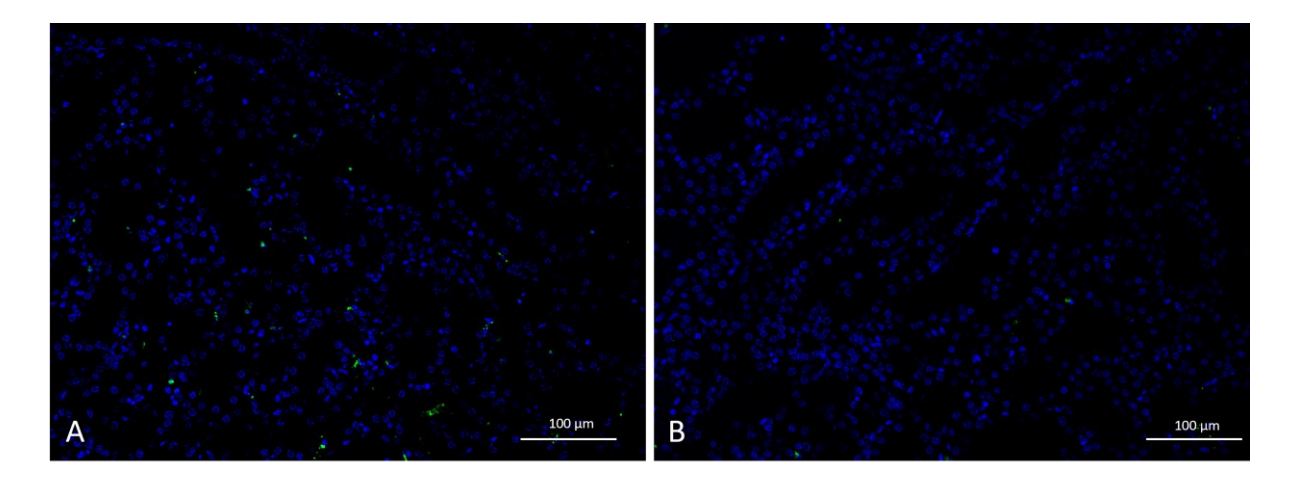


Figure 5.33 Immunofluorescent images of apoptotic bodies in kidneys treated with HDM-FH and control kidneys at 360 minutes of perfusion.

FFPE wedge biopsies from treated and control kidneys taken at 360 minutes of perfusion were stained with a TdT-mediated dUTP Nick-End Labelling assay, DAPI was used as a counterstain. Sections were then imaged using the LEICA DM2000 LED microscope and processed using LAS X software. Apoptotic bodies are shown in green, DAPI is shown in blue. Apoptotic bodies can be seen in control (A) and treated (B) kidneys.

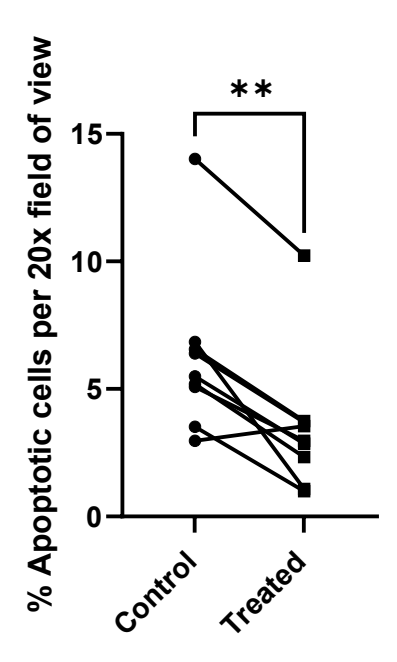


Figure 5.34 Apoptotic bodies in kidneys treated with HDM-FH and control kidneys taken at 360 minutes of perfusion.

FFPE wedge biopsies from treated and control kidneys taken at 360 minutes of perfusion were stained with a TdT-mediated dUTP Nick-End Labelling assay. Sections were then imaged using the LEICA DM2000 LED microscope and processed using LAS X software. Apoptotic bodies and nuclei were counted individually 10 20x magnification images. These values were used to calculate a mean percentage of apoptotic bodies per 20x field of view, N=8. Individual values are presented. Paired t-test was used to calculate statistical significance. \*\*p<0.01.

### 5.3.8 Immune cell infiltration

Immune cell infiltration is a hallmark sign of IRI and is known to be influenced by activation of the complement system (Peng et al., 2012). A unique benefit of a whole blood EVNP model is the presence of immune cells that can be recruited through complement driven mechanisms to the site of injury. Antibodies that bind specific markers of T-cells, macrophages and neutrophils were used to stain, and then quantify immune cell infiltration in treated and untreated kidneys.

#### 5.3.8.1 CD3ε-UNLB

Sections taken at the end of perfusion were stained with an anti-CD3ɛ-UNLB antibody to measure whether HDM-FH administration affects T-cell infiltration. There were significantly less T-cells in tissue taken at the end of perfusion in treated kidneys compared with control kidneys (Figure 5.39 and Figure 5.40).

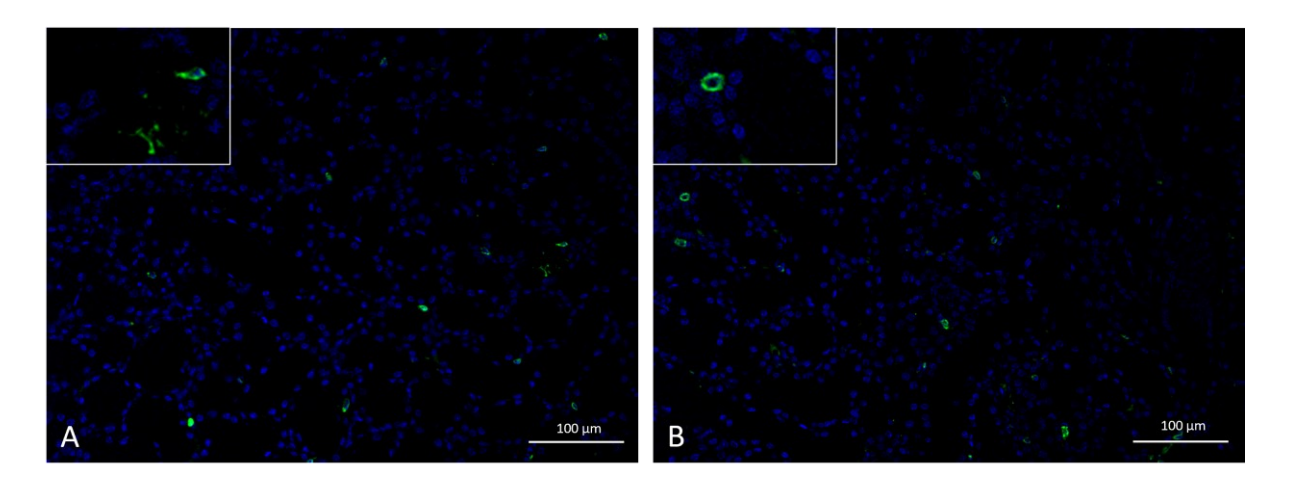


Figure 5.35 Immunofluorescent images of CD3ε-UNLB positive cells in tissue of kidneys treated with HDM-FH and control kidneys at 360 minutes of perfusion.

Snap-frozen wedge biopsies from treated and control kidneys taken at 360 minutes of perfusion were stained with an anti-CD3 $\varepsilon$ -UNLB antibody, DAPI was used as a counterstain. Sections were then imaged using the LEICA DM2000 LED microscope and processed using LAS X software. CD3 $\varepsilon$ -UNLB positive cells are shown in green, DAPI is shown in blue. CD3 $\varepsilon$ -UNLB positive cells can be seen in control (A) and treated (B) kidneys.

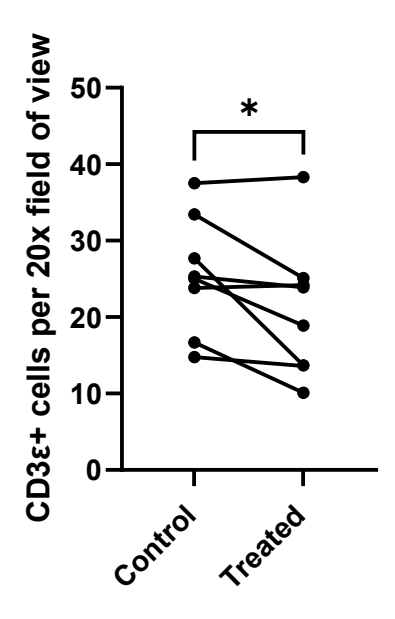


Figure 5.36 CD3 $\epsilon$ -UNLB positive cells in tissue of kidneys treated with HDM-FH and control kidneys at 360 minutes of perfusion.

Snap-frozen wedge biopsies from treated and control kidneys taken at 360 minutes of perfusion were stained with an anti-CD3 $\varepsilon$ -UNLB antibody. Sections were then imaged using the LEICA DM2000 LED microscope and processed using LAS X software. The number of CD3 $\varepsilon$ -UNLB positive cells were counted in 10 20x magnification images, N=8. Individual values are presented. Paired t-test was used to calculate statistical significance. \*p<0.05.

#### 5.3.8.2 CD163

Sections taken at the end of perfusion were stained with an anti-CD163 antibody to measure whether HDM-FH administration affects macrophage infiltration. There were significantly less macrophages in tissue taken at the end of perfusion in treated kidneys compared with control kidneys (Figure 5.41 and Figure 5.42).

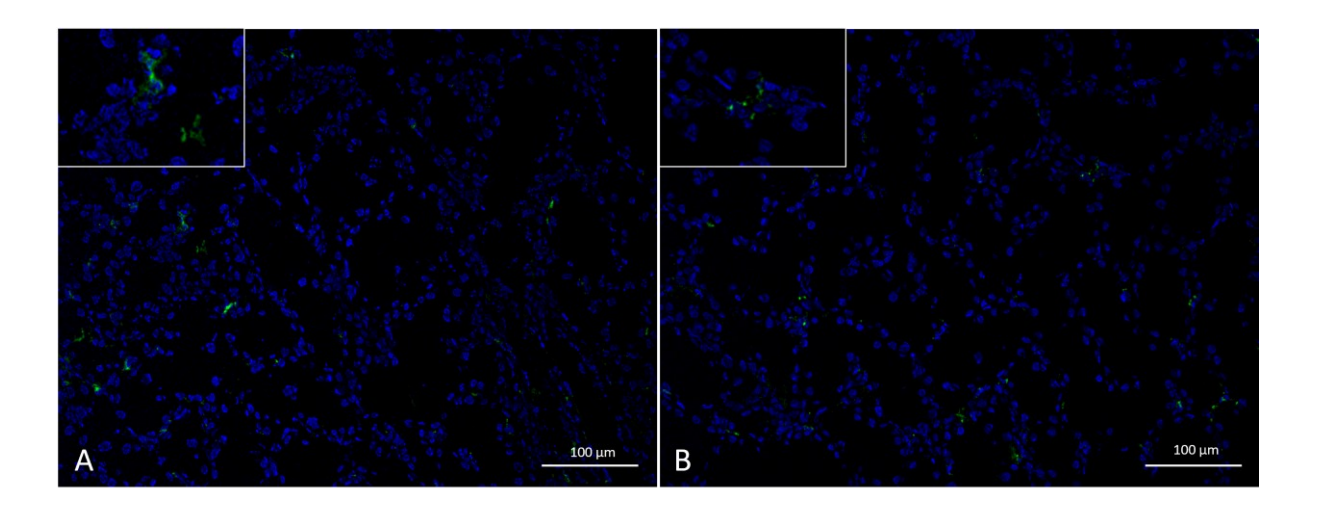


Figure 5.37 Immunofluorescent images of CD163 positive cells in tissue of kidneys treated with HDM-FH and control kidneys at 360 minutes of perfusion.

Snap-frozen wedge biopsies from treated and control kidneys taken at 360 minutes of perfusion were stained with an anti-CD163 antibody, DAPI was used as a counterstain. Sections were then imaged using the LEICA DM2000 LED microscope and processed using LAS X software. CD163 positive cells are shown in green, DAPI is shown in blue. CD163 positive cells can be seen in control (A) and treated (B) kidneys.

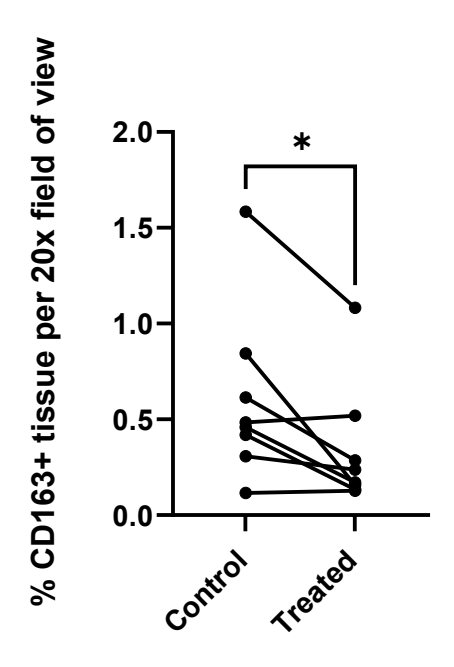


Figure 5.38 CD163 positive cells in tissue of kidneys treated with HDM-FH and control kidneys at 360 minutes of perfusion.

Snap-frozen wedge biopsies from treated and control kidneys taken at the end of perfusion were stained with an anti-CD163 antibody. Sections were then imaged using the LEICA DM2000 LED microscope and processed using LAS X software. The number of CD163 positive cells were counted in 10 20x magnification images, N=8. Individual values are presented. Paired t-test was used to calculate statistical significance. \*p<0.05.

## 5.3.8.3 Neutrophil elastase

Sections taken at the end of perfusion were stained with an anti-neutrophil elastase antibody to measure whether HDM-FH administration affects neutrophil infiltration. There were significantly fewer neutrophils in tissue taken at the end of perfusion in treated kidneys compared with control kidneys (Figure 5.43 and Figure 5.44).

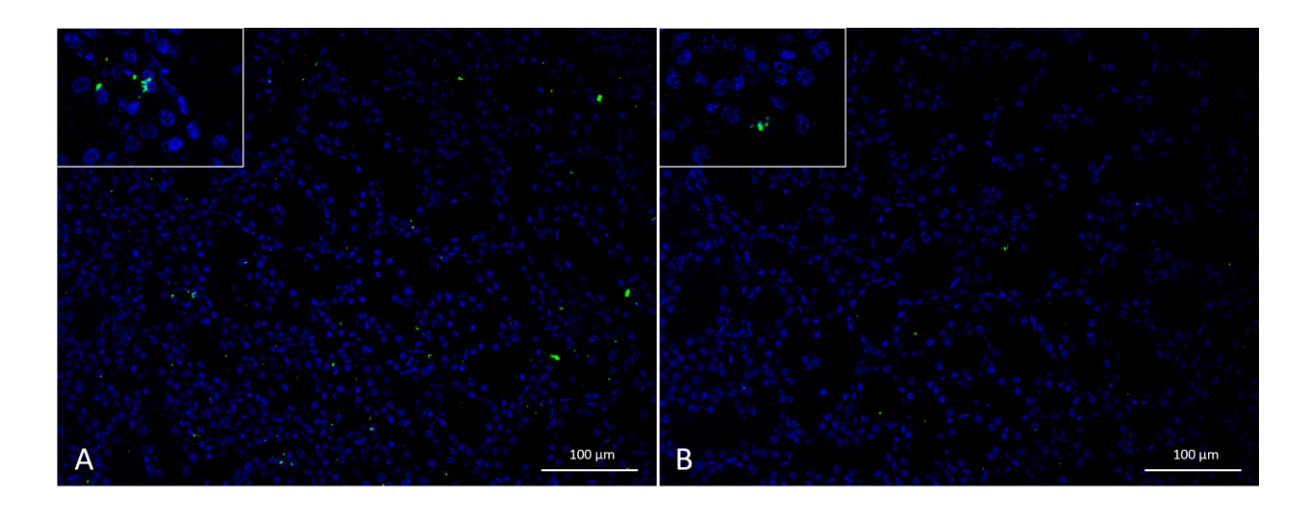


Figure 5.39 Immunofluorescent images of neutrophil elastase in tissue from kidneys treated with HDM-FH and control kidneys at 360 minutes of perfusion.

Snap-frozen wedge biopsies from treated and control kidneys from 360 minutes of perfusion were stained with an anti-neutrophil elastase antibody, DAPI was used as a counterstain. Sections were then imaged using the LEICA DM2000 LED microscope and processed using LAS X software. Neutrophil elastase is shown in green, DAPI is shown in blue. Neutrophil elastase can be seen in control (A) and treated (B) kidneys.

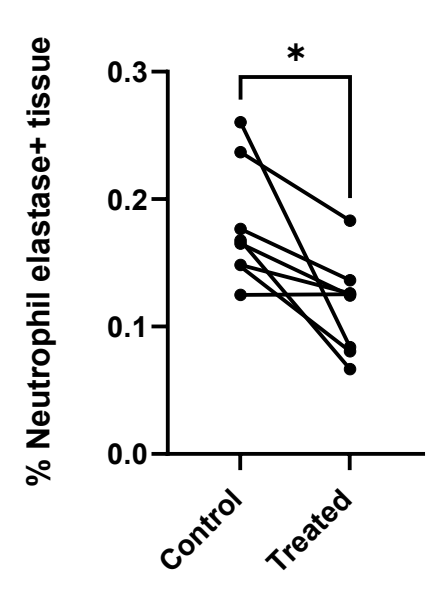


Figure 5.40 Neutrophil elastase positive area in tissue from kidneys treated with HDM-FH and control kidneys at 360 minutes of perfusion.

Snap-frozen wedge biopsies taken at the end of perfusion were stained with an anti-neutrophil elastase antibody, DAPI was used as a counterstain. Sections were then imaged using the LEICA DM2000 LED microscope and processed using LAS X software. The area with positive fluorescent signal was measured using QuPath in 10 20x magnification images, N=8. Individual values are presented. Paired t-test was used to calculate statistical significance. \*p<0.05.

### 5.4 DISCUSSION

FH is the key regulator of the alternative pathway, with HDM-FH displaying avid binding to damaged self-cells to efficiently control complement activation (Yang et al., 2018). In this chapter, the ability of HDM-FH to bind to kidneys during EVNP was assessed, with the downstream effects of this binding on kidney function, complement activation and downstream ischaemic injury during EVNP investigated.

HDM-FH binds C3b very strongly, likely binding to multiple C3b molecules at once with high avidity while also homing to self-cells via sialic acid and GAGs due to multiple binding sites and an 'open' conformation. In this work, HDM-FH bound within glomeruli of kidneys within 30 minutes of perfusion following administration directly to the EVNP circuit and was mainly localised to the endothelium and basement membrane.

Given the affinity of HDM-FH for C3b, it is unsurprising that HDM-FH binding was significantly correlated with C3/C3 breakdown products present in glomeruli prior to perfusion. This data suggests that HDM-FH preferentially binds to kidneys with increased complement activation, which is commonly observed in kidneys from deceased donors and those affected by traumatic injury (Damman et al., 2011, Burk et al., 2012). These kidneys typically exhibit worse function and graft survival compared to those from living donors (Damman et al., 2011, Błogowski et al., 2012). As a result, the potential beneficial effects of HDM-FH are likely to be most pronounced in injured kidneys from deceased donors which are in the greatest need of repair. Furthermore, this suggests that HDM-FH could be utilised as a therapeutic agent in other complement-mediated diseases characterised by complement deposition, such as C3G.

HDM-FH administration did not cause a change in physiological parameters during perfusion indicating that is has no adverse effects on kidney function. Clinically, urine output in the first 24 hours post-transplant is correlated with the occurrence of DGF, but not with 1 year estimated GFR (eGFR) (Seja et al., 2022, Kim et al., 2019). A quality assessment study found kidneys deemed suitable for transplant that would have otherwise been discarded produced significantly more urine during EVNP than those which were not deemed suitable. Urine output was combined with RBF and macroscopic appearance to produce a QAS score. This QAS score was predictive of graft outcomes including DGF (Hosgood et al., 2018). Conversely, the QAS score during EVNP in a clinical trial assessing EVNP as a method to recondition kidneys did not correlate with DGF (Hosgood et al., 2023).

The absence of significant improvements in physiological parameters or kidney function during EVNP following HDM-FH administration is not a major concern. Previous studies investigating therapeutics administered during EVNP have not consistently demonstrated an increase in urine output, despite positive results in other important downstream markers (Pool et al., 2019, Yang et al., 2011, Thompson et al., 2022, Kassimatis et al., 2021, Lohmann et al., 2021, Hameed et al., 2020).

Increased urine output and RBF during EVNP was observed following the administration of MAPCs (Thompson et al., 2021) and combined tPa and plasminogen (DiRito et al., 2021). tPa facilitates blood clot breakdown through conversion of plasminogen to plasmin (Collen and Lijnen, 2009). MAPCs release potent vasodilators Prostaglandin E2 and indoleamine 2,3-dioxygenase, which may also explain why MAPC treatment led to an improvement seen in microvascular perfusion measured via CEUS. These therapies affect immediate physical changes within the microvasculature, improving tissue perfusion and kidney function within a few hours via mechanisms that would not be expected from HDM-FH.

NGAL is a marker of tubular injury, with urinary NGAL correlated with DGF and patient and graft survival (Maier et al., 2018, Hall et al., 2010). Similar levels of NGAL, urine output, RBF, oxygen consumption and creatine clearance between treated and control kidneys suggest that HDM-FH does not cause any adverse effects to kidney function. However, they do, alongside functional data, also suggest that HDM-FH is unable to improve global tissue damage and cellular metabolism in the 6 hours of EVNP.

Complement therapeutics administered in clinical or experimental animal IRI settings have improved kidney function measured via parameters including BUN and creatinine clearance (Zheng et al., 2006, Hu et al., 2018, Zheng et al., 2008, Gueler et al., 2008, Arumugam et al., 2003, de Vries et al., 2003a, Thurman et al., 2006, Castellano et al., 2010, Delpech et al., 2016, Pratt et al., 2003, de Vries et al., 2003b). However, these studies measured function over a longer time period than the 6 hours of perfusion in this work, with data presented from 1 day, to months post reperfusion. Any effect of HDM-FH on kidney function may therefore only be observed following a longer period of time than the 6 hours of EVNP. Only one complement inhibitor has been administered and tested in kidneys using an EVNP model to date. Mirococept, an engineered recombinant CR1 molecule was administered to kidneys in the cold flush preservation solution and incubated for 1 hour prior to EVNP. No perfusion

parameters or kidney function readouts were changed in the three hours of EVNP (Kassimatis et al., 2021).

HDM-FH administration reduced Bb deposition within glomeruli, indicating a reduction in AP activation, although serum FB levels were unaffected. This data aligns with findings from Thurman et al., (2006), demonstrating that an antibody against FB effectively halted AP activation and subsequent injury in a mouse model of IRI, without depleting serum FB levels (Thurman et al., 2006).

Inhibition of the AP appears to have led to a decrease in C5a, likely through a reduction in C5 cleavage due to accelerated decay of the C5 convertase by HDM-FH. A FH based complement inhibitor, CRIg/FH also reduced systemic C5a in a mouse IRI model (Hu et al., 2018). These results are promising given the wealth of evidence implicating C5a as a major contributor to IRI. C5a/C5aR blockade and deficiency leads to improved kidney function, complement regulation, reduced inflammation and immune cell infiltration following IRI. There is also evidence that the C5a/C5aR axis is more important in the pathogenesis of IRI than the C3a/C3aR axis (Lewis et al., 2008, de Vries et al., 2003b, de Vries et al., 2003a, Arumugam et al., 2003, Gueler et al., 2008, Zheng et al., 2008, Peng et al., 2012), while urinary C5a levels have shown correlation with allograft rejection (Müller et al., 1997), with C5 playing a role in thrombotic glomerulonephritis (Kondo et al., 2001) and MGPN (Pickering et al., 2006, Abe et al., 2001).

Evidence for the role of the CP in ischaemia reperfusion injury is conflicting. Mice deficient in C4 or Ig receptor proteins are not protected from renal IRI, suggesting that the CP is not involved in the pathogenesis of IRI (Miwa et al., 2013). However, in a porcine model of IRI, an increase in C1q was observed, while C1INH administration reduced complement activation, tubular damage and immune cell infiltration and improved kidney function. The same results were seen following C1INH administration in a mouse IRI model (Danobeitia et al., 2017).

In this chapter, C1q deposition in kidney tissue was observed, suggesting classical pathway activation plays a role in IRI. Circulating IgM can form complexes with neoantigens on tissue surfaces, which are exposed to oxygen radicals generated during IRI, thus activating C1q (Chan et al., 2003). Treatment with HDM-FH significantly reduced C1q levels in glomeruli, potentially because treated kidneys exhibited fewer apoptotic bodies compared to untreated ones. This reduction in apoptotic cells correlates with the observed decrease in C5a, implying less C5

cleavage and, consequently, reduced MAC formation, which induces apoptosis (Nauta et al., 2002). C1q binds to apoptotic bodies to aid in their clearance, hence the non-canonical role for C1q in in systemic lupus erythematosus pathology (Cai et al., 2015, Botto and Walport, 2002). Additionally, activated neutrophils can induce epithelial cell apoptosis, so the observed reduction in apoptosis in treated kidneys could also be attributed to decreased neutrophil infiltration (Jia et al., 2014).

Treatment with an anti-FB antibody, an anti-C5 antibody and CRIg/FH used in a mouse IRI model led to a reduction in C3 activation (de Vries et al., 2003b, Thurman et al., 2006, Hu et al., 2018). However, there was no reduction in the C3 activation products C3a or C3C in urine or plasma following treatment with HDM-FH. This is surprising as HDM-FH controlled C3 deposition and consumption in a mouse model of uncontrolled complement activation (Yang et al., 2018). Furthermore, a reduction in C3a levels throughout perfusion is in contrast with work by (Jager et al., 2022) who observed an increase in C3a levels over 4 hours of EVNP of porcine kidneys following 30 minutes WIT and 24 hours CIT.

The complement consumption/activation seen in the EVNP system may have been too high for HDM-FH to lead to a reduction in C3 activation. Data in this work shows that while C3a levels are 1.5-fold lower in treated kidneys at 30 minutes of perfusion, levels are equally depleted in both treated and control kidneys at 360 minutes of perfusion, plateauing at around 300 minutes. This aligns with data from haemolytic assays in this chapter and chapter 3 indicating increased complement consumption over the course of EVNP. Furthermore, results in chapter 3 show that the EVNP circuit alone activates complement, even without a kidney present. This is consistent with data showing elevated complement activation is seen during haemodialysis in the fluid phase and in the solid phase on the dialysis membrane (Mares et al., 2010, Hempel et al., 2016).

Contrary to data from other porcine models of IRI (Castellano et al., 2010, Delpech et al., 2016), no C4d was observed in any area of tissue in this study, nor was any MBL, indicating a lack of LP involvement in injury (Castellano et al., 2010). Moreover, the presence of C1q without C4d would suggest that the C1q is primarily an indicator of apoptosis, and not CP activation. Furthermore, it was not possible to detect MAC in tissue, this is in line with work by (de Vries et al., 2003b) who did not observe MAC before 12 hours of perfusion. It is possible

that the injury of porcine kidneys was not sufficient to produce an amount of MAC detectable by immunofluorescence.

A consequence of complement activation is endothelial activation. An anti-C5 antibody used in a mouse IRI model reduced injury, with less endothelial activation and glycocalyx shedding indicated by reduced tissue and plasma hyaluronan (Bongoni et al., 2019). HDM-FH did not significantly reduce glycocalyx shedding within 6 hours of perfusion, despite reducing C5 activation. This indicates that a reduction in C3 activation may be required to reduce endothelial activation, as was seen in the work of (Bongoni et al., 2019), but not following HDM-FH administration.

The EVNP model is clearly a pro-inflammatory environment, with multiple studies observing an increase in pro-inflammatory cytokines (Hameed et al., 2020, Nath et al., 2017, Hosgood et al., 2017, Jager et al., 2022). Activated neutrophils, macrophages and T-cells all release inflammatory cytokines. It may be expected therefore, that there would be lower levels of IL-6 and IL-8 in the urine of treated kidneys due to reduced leucocyte infiltration and C5a. While a number of complement inhibitors used in IRI models did reduce inflammatory cytokine levels (Zheng et al., 2006, Zheng et al., 2008, Castellano et al., 2010, Delpech et al., 2016, de Vries et al., 2003b), this was not seen in the urine of treated kidneys in this work.

LPS can cause a release of inflammatory cytokines IL-6 and IL-8 from tubular epithelial cells following interaction with TLR 2 and 4 (Allam et al., 2012). Furthermore, AKI causes a hypersensitive response to LPS (Naito et al., 2008) . As it was not possible to keep all components of the organ retrieval and perfusion circuit completely sterile, the presence of LPS may have led to an inflammatory response which would bypass or overwhelm any protective effect of HDM-FH in this regard.

(DiRito et al., 2021) suggest that tubular epithelial cells act as a source of extra hepatic fibrinogen, and that this fibrinogen can be scavenged and translocated from urine back to the vasculature. They saw a similar pattern of endothelial fibrinogen following both cold storage and perfusion of kidneys, as was seen in this work. HDM-FH did not lead to a reduction in fibrinogen deposition in treated kidneys, it did however lead to a 3-fold reduction in microthrombi in kidney vasculature. Previous work suggested that microthrombi occur due to RBC aggregates caused by fibrinogen. Activation of the C5a/C5aR axis has been shown to be pro-thrombotic by mediating exocytosis of von Willebrand factor (vWF) and P-selectin from

Weibel-Palade bodies causing platelet adhesion and aggregation on the endothelium due to vWF binding (Aiello et al., 2022). A reduction in C5a in this work may therefore be responsible for the reduction in microthrombi. Unfortunately, it was not possible to detect vWF or P-selectin to validate this assumption due to a lack of porcine specific reagents.

A unique benefit of this porcine model of EVNP is the use of whole blood, which is logistically difficult to source in sufficient quantities/quality for use with human organs. The presence of leukocytes in whole blood allows investigations into whether treatment with HDM-FH affects leukocyte infiltration. Complement inhibition via targeted treatment, or the generation of complement deficient animals often leads to a reduction in leukocyte migration to the site of injury. Previous studies have implicated that this is through complement mediated reduction of cytokines and chemokines (Zheng et al., 2008, Danobeitia et al., 2017, Peng et al., 2012), an established mechanism of action of immune cell recruitment and activation. However, a reduction in IL-6 and IL-8 was not seen in this work, although a reduction in neutrophil, macrophage and T-cell infiltration was seen, suggesting a role for complement in leukocyte recruitment outside of IL-6 and IL-8 signalling.

Results from this work and others suggest a role for endothelial activation in the progression of ischaemic injury (Castellano et al., 2010, Basile, 2007, Peng et al., 2012). The renal endothelium in particular has limited potential for regeneration, due to a low capacity for proliferation and a proclivity for endothelial to mesenchymal transition (Perry and Okusa, 2016). Moreover, complement activation following ischaemic injury can continue over a prolonged period of time, as shown by animal IRI models and clinically following transplantation. Complement inhibitors that have improved responses to IRI, including kidney function, have been assessed over a significantly longer period of time than was possible in this study. Furthermore, HDM-FH caused a reduction in C3 breakdown products at 48 hours through to 96 hour and was still detectable in the glomeruli at 48 hours in a mouse model of complement activation (Yang et al., 2018). Given the reduction in complement activation seen in this short period of time, more downstream effects of HDM-FH may be seen over a longer period, warranting auto transplant studies.

To conclude, HDM-FH shows binding to the endothelium and basement membrane of porcine kidneys in a manor dependant on the presence of C3 breakdown products. HDM-FH caused a significant reduction in alternative pathway activation, reducing C5 cleavage, potentially

leading to a reduction in apoptosis, C1q deposition, and immune cell infiltration. There is potential therefore for HDM-FH to be used as a treatment to protect kidneys from complement mediated damage during transplantation. Studies administering HDM-FH over a longer term may identify further benefits. Investigations into the effect of HDM-FH on complement activation and ischaemic injury following cold administration would provide insight as to whether it would be viable in future to use HDM-FH as a treatment administered during the cold flush of kidneys prior to transplant.

#### 6.1 PROJECT SUMMARY AND DISCUSSION

Kidney transplantation remains the best treatment option for most patients with ESRD. However, an increasing burden of CKD and limited availability of kidneys has necessitated the use of organs from marginal donors who are older and may have a range of comorbidities. These organs are more susceptible to the deleterious effects of IRI, a paradoxical exacerbation of cellular damage and death upon restoration of blood flow following a period of ischaemia, leading to DGF and graft failure (Patel et al., 2023).

The complement system is a key component of the innate immune system, while also contributing to control of the adaptive immune system. It is vital in detecting and eliminating pathogens and aberrant host cells and maintaining homeostasis. Excessive complement activation or insufficient regulation can cause or exacerbate disease, including rare diseases such as PNH and aHUS, but also more common diseases including COVID-19 and IRI (West et al., 2024). A wealth of evidence exists implicating the complement system, in particular the AP in the development and pathogenesis of IRI (Thurman et al., 2003, Thurman et al., 2006, Zhou et al., 2000). AP regulation is primarily exerted by FH and is crucial to prevent uncontrolled complement activation due to the ubiquitous nature of the AP. HDM-FH is a construct consisting of the key complement regulatory and self-recognition domains of FH and has improved complement regulatory activity compared with full length FH (Yang et al., 2018).

While HDM-FH has been shown to be effective in a mouse model of uncontrolled complement activation, prior to this work HDM-FH had not been assessed as a potential therapeutic for IRI. Given the effectiveness of HDM-FH at regulating the AP in kidneys with complement activation, and the clear role for the AP in IRI, we hypothesised that HDM-FH would control complement activation in the setting of IRI.

EVNP is a valuable technique for modelling IRI, providing a unique platform on which to monitor an isolated whole organ, while administering a therapeutic directly via the vasculature. Porcine organs have previously been used to optimise EVNP parameters and to assess therapeutics delivered prior to/during EVNP (Yang et al., 2011, Pool et al., 2020, Pool et al., 2019, Lohmann et al., 2021, Harper et al., 2006). There are several benefits to using porcine organs including predictable availability and the ability to control and standardise the

retrieval and storage conditions. Furthermore, whole autologous blood from pigs can be collected while retrieving the organs for use during EVNP, whereas packed red cells are often used in human kidney EVNP due to difficulties in accessing suitable whole human blood. The use of whole blood has specific benefits within this study as plasma is an important source of complement, and immune cells are both influenced by, and influence complement activation (de Vries et al., 2003b).

A downside to the use of organs from pigs is that they do not mirror most organs clinically available for transplant as pig do not have comorbidities such as hypertension or diabetes which can cause damage to the kidneys. Furthermore, complement activation leading to deposition of C3 activation products on tissue is required for HDM-FH binding. While elevated complement is commonly seen in donor organs (Błogowski et al., 2012, Naesens et al., 2009), optimisation was required to induce complement activation and ischaemic injury to porcine organs. As retrieval times and SCS times can influence transplant outcomes, we hypothesised that extending the ischaemic times of porcine kidneys would induce complement activation and ischaemic injury, facilitating binding of HDM-FH which could regulate the AP when administered during EVNP.

Porcine kidney retrieval and EVNP was first set up and performed at Newcastle University by Ms Emily Thomson in 2019 who used methods developed by Dr Sarah Hosgood at Cambridge University to assess the effect of an antisense oligonucleotide on porcine kidneys (unpublished work). This method used citrated, white cell depleted autologous blood following unstandardised retrieval and cold storage times of approximately 20 minutes and 2 hours respectively. Although these conditions were appropriate for that study as oligonucleotide uptake is cell-type dependant, changes for my work were needed due to the requirement for active complement deposited on tissue for HDM-FH binding and to assess the efficacy of HDM-FH at controlling complement activation. Achieving this was the aim of chapter 3.

Changes to the established porcine EVNP protocol were made in a stepwise manner to confirm that each was tolerated and because a new retrieval/perfusion team was in place. Following confirmation that heparinised blood whole blood could be used during EVNP, retrieval and SCS times were standardised and extended. 25 minutes retrieval time and 16 hours SCS led to worse kidney function and elevated complement activation, providing a more appropriate

model in which to test the efficacy of HDM-FH, and a more active surface to which it could bind.

Work In chapter 5 aimed to administer HDM-FH which was produced and validated *in vitro* in chapter 4 to porcine kidneys, assessing binding and any effect on complement activation and ischaemic injury. HDM-FH bound within glomeruli, dependant on complement activation within kidneys prior to perfusion. As complement activation is often seen in deceased donors and is correlated with worse outcomes (van Werkhoven et al., 2013), HDM-FH binding and positive effect may be greatest in damaged kidneys. The binding of HDM-FH to kidney tissue with complement activation also suggests that HDM-FH could be used as a therapeutic in diseases of uncontrolled complement activation such as C3G and aHUS.

The complement mediated binding of HDM-FH may also prove to be a limitation however, with binding saturation within kidneys limited by the presence of complement breakdown products. This is in contrast with Mirococept, the other complement inhibitor currently under investigation as a therapeutic to treat IRI following administration directly to kidney vasculature that indiscriminately binds cell membranes. This allows a large amount of Mirococept to be administered to the kidneys, although dosing has proved to be an issue previously as the indiscriminate binding means much of the drug may end up bound to regions of the vasculature where it may not be effective (Kassimatis et al., 2021).

The most important outcome following HDM-FH administration was control of complement activation. This was measured at the end of perfusion to assess if administration to complement activated kidneys at the start of perfusion would control complement in the proinflammatory, complement activating environment of EVNP which would mirror the clinical setting of reperfusion of an allograft. A reduction in Bb and C5a indicates that HDM-FH sufficiently regulated the C5 convertase of the AP, leading to a reduction in C5a cleavage. These results are extremely positive giving the wealth of evidence implicating the C5a/C5aR pathway in the pathogenesis of IRI (Lewis et al., 2008, de Vries et al., 2003b, de Vries et al., 2012).

We then measured complement mediated ischaemic injury markers to assess any downstream effects of complement regulation. A reduction in apoptosis suggests that by controlling C5 cleavage, MAC formation was reduced, which may explain why the reduction in C1g was seen in treated kidneys as C1g plays a key role in the clearance of apoptotic bodies

(Botto and Walport, 2002). A reduction in immune cell infiltration in HDM-FH treated kidneys also shows that controlling C5 activation during IR reduces ischaemic injury and is consistent with previous studies demonstrating the efficacy of complement inhibitors in IRI models (Gueler et al., 2008, Delpech et al., 2016, Hu et al., 2018, Pratt et al., 2003, Rodriguez de Cordoba et al., 1985).

Surprisingly given the given the past effectiveness of HDM-FH at controlling C3 activation (Yang et al., 2018), HDM-FH did not affect C3 activation during EVNP in this work. This, alongside a reduction in C5 activation implies that HDM-FH is more effective at dissociating the C5 convertase than the C3 convertase. As a result, HDM-FH may not be sufficient to prevent extravascular haemolysis when administered systemically, although it could still inhibit intravascular haemolysis, making it a potential therapeutic option for complement mediated conditions where the MAC plays a pathological role, such as PNH or aHUS. There is still however potential for increased activity of HDM-FH in a human system, as work in chapter 4 revealed that HDM-FH bound to porcine C3b less strongly than to human C3b, a function key to the activity of FH/HDM-FH.

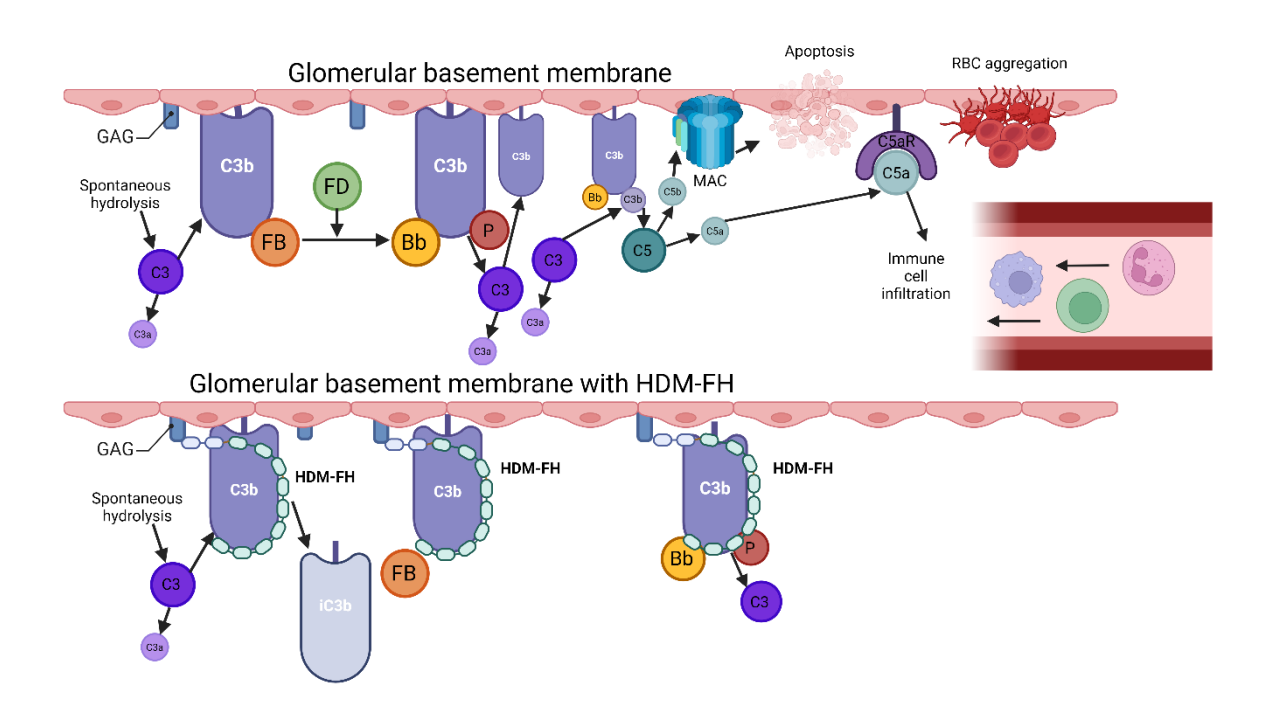


Figure 6.1 Consequences of complement activation and action of HDM-FH

In this study, complement activation on the surface of porcine GBM was achieved through the extension of ischaemic times. HDM-FH produced in house was then administered to kidney during EVNP. This led to a reduction in complement activation, and downstream ischaemic injury including apoptosis, immune cell infiltration and RBC aggregation.

While EVNP is a valuable platform for assessing organ viability and delivering therapeutics to directly to organs, it is not standard clinical practice. A recent multicentre randomised control trial showed no benefit from 1-hour end-ischaemic EVNP (Hosgood et al., 2023). Consequently, it is unlikely that if HDM-FH was to progress to clinical use, that it would be administered during EVNP.

Work in chapter 4 showed that HDM-FH can bind at 4°C, which is highly encouraging for expanding its potential clinical applications. HDM-FH could be administered to kidneys immediately following retrieval during the cold flush with heparinised preservation solution, as described in chapter 5. Moreover, in countries such as Denmark and France, HMP of kidneys prior to transplant is now standard clinical practice as it has been shown to improve graft survival and function when compared with standard SCS (Tingle et al., 2019). It could therefore be possible to administer HDM-FH during HMP of kidneys.

Direct delivery to organs could help mitigate the risk of opportunistic infections associated with systemic complement inhibitor therapies. While the risk is higher in therapeutics that target complement at the level of C3 (West et al., 2024), systemic administration of eculizumab which targets C5, also increases susceptibility to meningococcal infections (Crew et al., 2020). If HDM-FH were to progress to clinical use for IRI or classical complement mediated diseases, infection status of patients would therefore need to be monitored.

Approved complement regulatory therapeutics currently almost exclusively target rare diseases. The complex nature of the complement system including positive and negative feedback loops and interplay with other systems including the coagulation systems and kallikrein–kinin systems has meant development and approval of new therapies has been slow, despite the emergence of the role of complement in a wide range of diseases. The successful treatment of PNH with Eculizumab first confirmed complement as a valuable preclinical target. However, since Eculizumab, only seven complement inhibitors have been approved for use clinically, although several others are currently in clinical trials.

Notably, none of the eight approved complement inhibitors target multiple stages of the complement cascade, a feature that an FH-based therapy like HDM-FH has the potential to offer (West et al., 2024). While this model did not demonstrate C3 inhibition, HDM-FH could provide wider complement regulation by targeting multiple points in the pathway in a

different model of complement activation, or in humans, which distinguishes it from current therapies. There is scope for use therefore of HDM-FH in a range of complement mediated diseases including PNH, aHUS and C3G. Although complement mediated diseases predominantly affect the kidney of all solid organs, in the context of transplantation, the heart, lungs and liver are all affected by complement activation (Grafals and Thurman, 2019). HDM-FH could therefore have potential as a therapeutic in all these organs. However, HDM-FH binds predominantly to the endothelium and basement membrane in a complement-dependant manor which makes it ideally suited to bind within kidneys. Binding of HDM-FH may therefore be less strong/efficient in other organs.

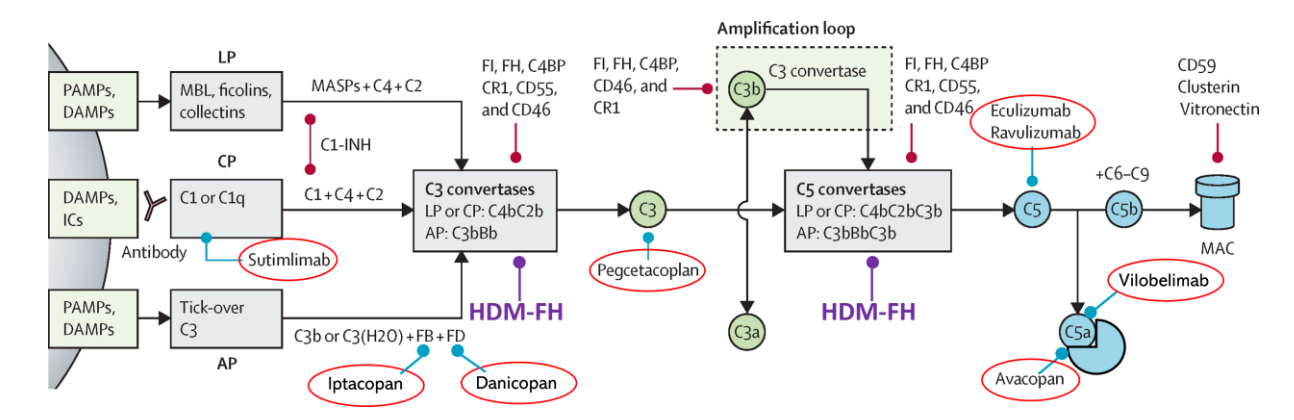


Figure 6.2. Current approved complement inhibitors

Complement inhibitors currently approved for clinical use and which element of the complement pathway they target are outlined in red. HDM-FH is shown in purple. Graph adapted from (West et al., 2024).

### 6.2 Conclusions

To conclude, it is possible to induce complement activation in porcine kidneys, with EVNP causing further complement activation and ischaemic injury. HDM-FH can be successfully produced and purified in house from transfected CHO cells. While HDM-FH is a human construct, it has similar efficacy in a porcine system as a human system in *in vitro* functional assays. When administered to porcine kidneys during EVNP, HDM-FH binds within glomeruli dependant on complement activation prior to perfusion. HDM-FH controls complement activation during EVNP, leading to a reduction in downstream ischaemic injury markers.

This is the first study assessing HDM-FH as a therapeutic for the treatment of IRI, and the first study investigating the efficacy of any complement regulator during kidney EVNP. The ability of HDM-FH to control complement on tissue surfaces suggests that it could be administered to kidneys via a range of techniques with the potential to improve long and short-term outcomes.

#### 6.3 STUDY LIMITATIONS

Due to issues surrounding the production of a porcine specific HDM-FH construct, a human HDM-FH construct was administered. The function and binding of human HDM-FH in a porcine system was confirmed using SPR and classical haemolytic assays prior to perfusion. However, HDM-FH binding to porcine C3b was 4-fold lower than to human C3b. Furthermore, work by (Hegasy et al., 2003) demonstrated that while similarity and cross-functionality exists between porcine and human FH, this is not perfect, with function not completely conserved across species. A porcine construct may therefore have shown improved activity in this system. Work is currently ongoing by Dr Beth Gibson assessing the efficacy of human HDM-FH administered to human kidneys during EVNP. Furthermore, since the start of this project Professor Kevin Marchbank has designed a fully porcine HDM-FH for use in pigs with a synthetic FHR1 (SCRs 1-2) at the C-terminus, with sequence changes predicted to add a dimerisation motif.

Furthermore, while a porcine EVNP model has unique benefits compared to human EVNP in regard to standardisation and availability, reagents that react with porcine proteins are limited, meaning not all desired outcomes could be investigated. I found that this was a particular issue when trying to find biomarkers for endothelial activation, having been unable to measure ICAM-1, P-selectin, E-selectin, VCAM, VE-cadherin or syndecan-1 despite attempts at optimisation.

A major limitation is that the 6 hours of EVNP is a very short period of time compared to the clinical experience of IRI. It is likely that some potential benefits of HDM-FH would only be observed following a greater time duration including pathologies such as the progression of fibrosis, necessitating future auto transplant studies. An auto transplant study would also be more clinically relevant then an isolated EVNP system. Although we took steps to ensure our model mirrored the clinical setting of transplantation including extending the CIT of kidneys and using whole blood, EVNP of course mirrors only a fraction of the whole body.

Investigations into the efficacy of HDM-FH in this work were limited to investigating physiological changes and changes in actual protein levels. Experiments utilising PCR or RNA sequencing may have identified changes in gene expression.

### 6.4 FUTURE DIRECTIONS

Complement is known to influence cytokine production and release, however only IL-6 and IL-8 were present in sufficient quantities to be detected using available ELISAs. A more sensitive multiplex assay could be used in future to identify a wider range of cytokines present in lower levels that may have been affected by administration on HDM-FH.

CEUS imaging as a modality to assess microvascular perfusion during EVNP has only been described once previously (Thompson et al., 2021) and has not been validated as a reliable assessment of kidney function or health in the context of EVNP. Work is ongoing led by Mr Samuel Tingle using data collected in my study and from other human perfusions carried out at Newcastle which will correlate other EVNP functional parameters and injury biomarkers such as NGAL, apoptosis, plasma creatinine and urine output with CEUS results. This work will give more validity to the use of CEUS as a functional outcome measure.

I initiated a collaboration with Professor Tom Eirik Mollnes who has developed a porcine specific soluble MAC ELISA, and a porcine specific anti-MAC antibody, AE11 which recognises the neoepitope formed following the formation of the MAC. Professor Mollnes kindly agreed to send some of the AE11 antibody for use in immunofluorescence, however MAC was not detectable in porcine tissue in this study. Work is currently underway in his lab to measure the soluble MAC in perfusate and urine in kidneys treated with HDM-FH and in control kidneys.

HDM-FH binding to the plastic components of the disposable circuit were not investigated in this study. Excessive binding to plastic could have meant less HDM-FH was available to bind within the kidneys. However as complement activation occurs on the surface of dialysis membranes (Mares et al., 2010), HDM-FH binding to plastics may reduce systemic complement activation. Further experiments detaching any potential HDM-FH from the plastics of the circuit and quantifying the amount of HDM-FH could be conducted in the future.

My current work as a technician has been focusing on the development of assays to detect C3 nephritic factors (NeFs), autoantibodies that stabilise the C3 convertase, leading to increased complement activation. Recently, members of Dr Véronique Frémeaux-Bacchi's lab have visited Newcastle to help establish a magnetic bead based multiplex NeF assay. In this assay C3b is covalently coupled to Luminex magnetic beads. FB is then incubated with FD and the C3bBb convertase is formed on the beads. The convertase is then incubated with isolated patient IgG. If NeFs are present, the convertase will stabilise, while if no NeFs are present, the

convertase will dissociate. Intact convertases are detected using a fluorescently labelled anti-Bb antibody and a semi-quantitively quantified by measuring the MFI of specific bead regions.

While this assay forms an unstable convertase that will dissociate alone over time, properdin could be added to stabilise it. To measure the decay accelerating activity of HDM-FH on porcine C3 convertase, a stable porcine convertase could be formed, then incubated with HDM-FH, and porcine FH separately. The amount of convertase following a set incubation period would indicate how well HDM-FH dissociates the convertase. Furthermore, a C5 convertase could be formed on the beads to validate the circumstantial evidence suggesting that HDM-FH is more effective at dissociating the C5 convertase over the C3 convertase. This could also be assessed using SPR.

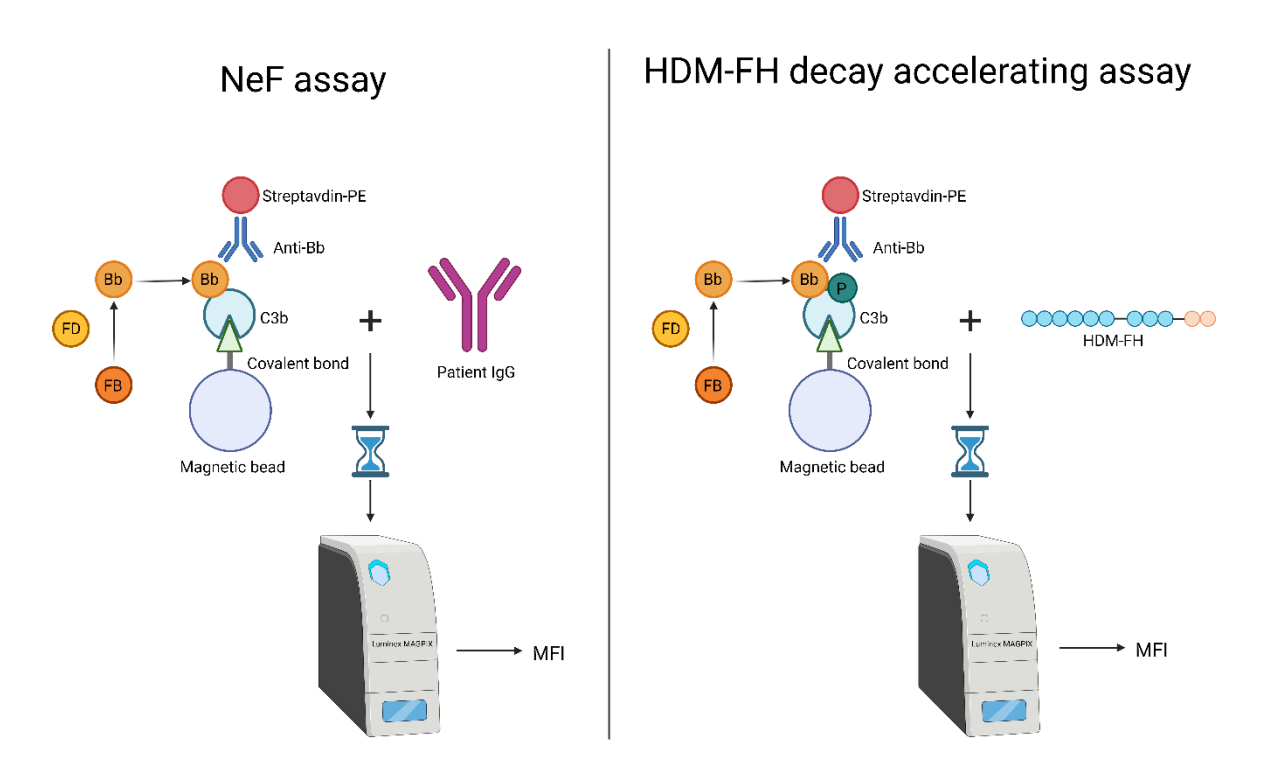


Figure 6.3 Theoretical multiplex assay to assess decay accelerating activity of HDM-FH on the porcine C3 convertase.

The right panel shows the Luminex magnetic beads assay recently set up at Newcastle to detect NeFs in patient samples. Patient IgG is incubated with a C3 convertase formed on a magnetic bead to assess if it stabilises the convertase during a dissociation period. The right panel shows how this assay could be adapted to assess the effect of HDM-FH in dissociating a C3 convertase that has been stabilised by the addition of properdin.

We showed that HDM-FH can bind within kidneys when administered to kidneys via cold UW flush. Ideally, we would then have carried out EVNP on these kidneys to assess efficacy of HDM-FH when administered this way. However, time and financial constraints in addition to the closing of the university pig facility prevented this. Work is currently underway by Professor Carl Atkinson administering HDM-FH via cold flush to porcine kidneys prior to auto transplantation. Auto transplantation studies would provide further information on the safety of HDM-FH, the efficacy of HDM-FH when administered prior to reperfusion via cold flush, and any effects HDM-FH may have over a longer period of time.

Furthermore, previous studies clearly indicate that EVNP is a pro-inflammatory environment that induces complement activation (Jager et al., 2022). The observation of complement activation on dialysis plastics (Mares et al., 2010) could account for some of this due to the plastic components of the EVNP rig. This does reflect the clinical situation as complement has been seen to be elevated in deceased donors, leading to complement activation and worse function in recipients (Damman et al., 2011, Damman et al., 2015). However, the synthetic elements of the EVNP circuit will have some influence on the behaviour of the organs. Moving to *in vivo* animal and human models further down the line would therefore be advantageous.

## 7.1 Publications

- Thompson ER, Connelly C, Ali S, Sheerin NS, Wilson CH. **Cell therapy during machine perfusion**. Transpl Int. 2021 Jan;34(1):49-58. doi: 10.1111/tri.13780. Epub 2020 Nov 24.
- Kamala O, Malik TH, Hallam TM, Cox TE, Yang Y, Vyas F, Luli S, Connelly C, Gibson B, Smith-Jackson K, Denton H, Pappworth IY, Huang L, Kavanagh D, Pickering MC, Marchbank KJ. Homodimeric Minimal Factor H: In Vivo Tracking and Extended Dosing Studies in Factor H Deficient Mice. Front Immunol. 2021 Dec 9;12:752916. doi: 10.3389/fimmu.2021.752916.
- Thompson ER, Sewpaul A, Figuereido R, Bates L, Tingle SJ, Ferdinand JR, Situmorang GR, Ladak SS, Connelly CM, Hosgood SA, Nicholson ML, Clatworthy MR, Ali S, Wilson CH, Sheerin NS. MicroRNA antagonist therapy during normothermic machine perfusion of donor kidneys. Am J Transplant. 2022 Apr;22(4):1088-1100. doi: 10.1111/ajt.16929. Epub 2022 Jan 4.
- Gibson B, Connelly C, Moldakhmetova S, Sheerin NS. Complement activation and kidney transplantation; a complex relationship. Immunobiology. 2023
   Jul;228(4):152396. doi: 10.1016/j.imbio.2023.152396. Epub 2023 Jun 2.
- Kourounis, Georgios, Elmahmudi, Ali Ahmed, Thomson, Brian, Nandi, Robin, Tingle, Samuel J., Glover, Emily K., Thompson, Emily, Mahendran, Balaji, Connelly, Chloe, Gibson, Beth, Bates, Lucy, Sheerin, Neil S., Hunter, James, Ugail, Hassan and Wilson, Colin. Deep learning for automated boundary detection and segmentation in organ donation photography Innovative Surgical Sciences, 2024. doi: 10.1515/iss-2024-0022

## 7.2 CONFERENCES

- International Complement Workshop 2021, Berlin (online) Poster.
- NUTCRI live 2022, Newcastle Talk.
- European Meeting on Complement in Human Diseases 2022, Bern– Poster.
- Complement UK 2023, Cardiff Poster and lightning talk, prize awarded.
- Immunology North East 2023, Durham Talk, prize awarded.
- 16th Aegean Conference on Complement Therapeutics, Crete Talk, travel grant awarded.
- International complement workshop, Newcastle Talk.

## CHAPTER 8. REFERENCES

- DeadEnd™ Fluorometric TUNEL System [Online]. Available:

  <a href="https://www.promega.co.uk/products/cell-health-assays/apoptosis-assays/deadend-fluorometric-tunel-system/?catNum=G3250">https://www.promega.co.uk/products/cell-health-assays/apoptosis-assays/deadend-fluorometric-tunel-system/?catNum=G3250</a> [Accessed 11th January 2024].
- ABE, K., MIYAZAKI, M., KOJI, T., FURUSU, A., NAKAMURA-KURASHIGE, T., NISHINO, T., OZONO, Y., HARADA, T., SAKAI, H. & KOHNO, S. 2001. Enhanced expression of complement C5a receptor mRNA in human diseased kidney assessed by in situ hybridization. *Kidney International*, 60, 137-146.
- AIELLO, S., GASTOLDI, S., GALBUSERA, M., RUGGENENTI, P., PORTALUPI, V., ROTA, S., RUBIS, N., LIGUORI, L., CONTI, S., TIRONI, M., GAMBA, S., SANTARSIERO, D., BENIGNI, A., REMUZZI, G. & NORIS, M. 2022. C5a and C5aR1 are key drivers of microvascular platelet aggregation in clinical entities spanning from aHUS to COVID-19. *Blood Advances*, 6, 866-881.
- AITKEN, E., STEVENSON, R., HANIF, F., RAJ, D., STEVENSON, K. & KINGSMORE, D. 2016. Renal Transplantation: An Update for Anaesthetists. *International Journal of Anesthetics and Anesthesiology*, 3.
- AKCAY, A., NGUYEN, Q. & EDELSTEIN, C. L. 2009. Mediators of inflammation in acute kidney injury. *Mediators Inflamm*, 2009, 137072.
- ALLAM, R., SCHERBAUM, C. R., DARISIPUDI, M. N., MULAY, S. R., HÄGELE, H., LICHTNEKERT, J., HAGEMANN, J. H., RUPANAGUDI, K. V., RYU, M., SCHWARZENBERGER, C., HOHENSTEIN, B., HUGO, C., UHL, B., REICHEL, C. A., KROMBACH, F., MONESTIER, M., LIAPIS, H., MORETH, K., SCHAEFER, L. & ANDERS, H.-J. 2012. Histones from Dying Renal Cells Aggravate Kidney Injury via TLR2 and TLR4. Journal of the American Society of Nephrology, 23, 1375-1388.
- ANDRES-HERNANDO, A., LI, N., CICERCHI, C., INABA, S., CHEN, W., RONCAL-JIMENEZ, C., LE, M. T., WEMPE, M. F., MILAGRES, T., ISHIMOTO, T., FINI, M., NAKAGAWA, T., JOHNSON, R. J. & LANASPA, M. A. 2017. Protective role of fructokinase blockade in the pathogenesis of acute kidney injury in mice. *Nature Communications*, 8, 14181.
- ANNAMALAI, B., PARSONS, N., NICHOLSON, C., JOSEPH, K., COUGHLIN, B., YANG, X., JONES, B. W., TOMLINSON, S. & ROHRER, B. 2021. Natural immunoglobulin M-based delivery of a complement alternative pathway inhibitor in mouse models of retinal degeneration. *Experimental Eye Research*, 207, 108583.
- ARIAS-CABRALES, C. E., RIERA, M., PÉREZ-SÁEZ, M. J., GIMENO, J., BENITO, D., REDONDO, D., BURBALLA, C., CRESPO, M., PASCUAL, J. & RODRÍGUEZ, E. 2021. Activation of final complement components after kidney transplantation as a marker of delayed graft function severity. *Clin Kidney J*, 14, 1190-1196.
- ARUMUGAM, T. V., SHIELS, I. A., STRACHAN, A. J., ABBENANTE, G., FAIRLIE, D. P. & TAYLOR, S. M. 2003. A small molecule C5a receptor antagonist protects kidneys from ischemia/reperfusion injury in rats. *Kidney International*, 63, 134-142.
- ARZT, M., DESCHAMPS, J., SCHMIED, C., PIETZSCH, T., SCHMIDT, D., TOMANCAK, P., HAASE, R. & JUG, F. 2022. LABKIT: Labeling and Segmentation Toolkit for Big Image Data. *Frontiers in Computer Science*, 4.
- ASCON, D. B., LOPEZ-BRIONES, S., LIU, M., ASCON, M., SAVRANSKY, V., COLVIN, R. B., SOLOSKI, M. J. & RABB, H. 2006. Phenotypic and Functional Characterization of Kidney-Infiltrating Lymphocytes in Renal Ischemia Reperfusion Injury1. *The Journal of Immunology,* 177, 3380-3387
- ATKINSON, C., HE, S., MORRIS, K., QIAO, F., CASEY, S., GODDARD, M. & TOMLINSON, S. 2010.

  Targeted Complement Inhibitors Protect against Posttransplant Cardiac Ischemia and
  Reperfusion Injury and Reveal an Important Role for the Alternative Pathway of Complement
  Activation. *The Journal of Immunology*, 185, 7007-7013.
- BAGETTI FILHO, H. J., PEREIRA-SAMPAIO, M. A., FAVORITO, L. A. & SAMPAIO, F. J. 2008. Pig kidney: anatomical relationships between the renal venous arrangement and the kidney collecting system. *J Urol*, 179, 1627-30.

- BAGUL, A., HOSGOOD, S. A., KAUSHIK, M., KAY, M. D., WALLER, H. L. & NICHOLSON, M. L. 2008. Experimental renal preservation by normothermic resuscitation perfusion with autologous blood. *Br J Surg*, 95, 111-8.
- BAO, L., WANG, Y., HAAS, M. & QUIGG, R. J. 2011. Distinct roles for C3a and C5a in complement-induced tubulointerstitial injury. *Kidney International*, 80, 524-534.
- BARNUM, S. R. & SCHEIN, T. N. 2018. The Complement FactsBook (Second Edition), Academic Press.
- BARR, T. A., BROWN, S., RYAN, G., ZHAO, J. & GRAY, D. 2007. TLR-mediated stimulation of APC: Distinct cytokine responses of B cells and dendritic cells. *European Journal of Immunology*, 37, 3040-3053.
- BASILE, D. P. 2007. The endothelial cell in ischemic acute kidney injury: implications for acute and chronic function. *Kidney Int*, 72, 151-6.
- BERA, K. D., TABAK, B. R. & PLOEG, R. J. 2024. No Evidence of Progressive Proinflammatory Cytokine Storm in Brain-dead Organ Donors-A Time-course Analysis Using Clinical Samples. *Transplantation*, 108, 923-929.
- BŁOGOWSKI, W., DOŁĘGOWSKA, B., SAŁATA, D., BUDKOWSKA, M., DOMAŃSKI, L. & STARZYŃSKA, T. 2012. Clinical analysis of perioperative complement activity during ischemia/reperfusion injury following renal transplantation. *Clin J Am Soc Nephrol*, 7, 1843-51.
- BOMBACK, A. S., SMITH, R. J., BARILE, G. R., ZHANG, Y., HEHER, E. C., HERLITZ, L., STOKES, M. B., MARKOWITZ, G. S., D'AGATI, V. D., CANETTA, P. A., RADHAKRISHNAN, J. & APPEL, G. B. 2012. Eculizumab for dense deposit disease and C3 glomerulonephritis. *Clin J Am Soc Nephrol*, 7, 748-56.
- BONGONI, A. K., LU, B., MCRAE, J. L., SALVARIS, E. J., TOONEN, E. J. M., VIKSTROM, I., BAZ MORELLI, A., PEARSE, M. J. & COWAN, P. J. 2019. Complement-mediated Damage to the Glycocalyx Plays a Role in Renal Ischemia-reperfusion Injury in Mice. *Transplantation Direct*, 5, e341.
- BOON, C. J. F., KLEVERING, B. J., HOYNG, C. B., ZONNEVELD-VRIELING, M. N., NABUURS, S. B., BLOKLAND, E., CREMERS, F. P. M. & DEN HOLLANDER, A. I. 2008. Basal Laminar Drusen Caused by Compound Heterozygous Variants in the CFH Gene. *The American Journal of Human Genetics*, 82, 516-523.
- BOOR, P., KONIECZNY, A., VILLA, L., SCHULT, A.-L., BUCHER, E., RONG, S., KUNTER, U., VAN ROEYEN, C. R. C., POLAKOWSKI, T., HAWLISCH, H., HILLEBRANDT, S., LAMMERT, F., EITNER, F., FLOEGE, J. & OSTENDORF, T. 2007. Complement C5 Mediates Experimental Tubulointerstitial Fibrosis. *Journal of the American Society of Nephrology*, 18, 1508-1515.
- BOTTO, M. & WALPORT, M. J. 2002. C1q, Autoimmunity and Apoptosis. *Immunobiology*, 205, 395-406.
- BRITISH TRANSPLANT SOCIETY 2021. UK GUIDELINES ON TRANSPLANTATION FROM DECEASED DONORS AFTER CIRCULATORY DEATH.
- BROCKLEBANK, V., JOHNSON, S., SHEERIN, T. P., MARKS, S. D., GILBERT, R. D., TYERMAN, K., KINOSHITA, M., AWAN, A., KAUR, A., WEBB, N., HEGDE, S., FINLAY, E., FITZPATRICK, M., WALSH, P. R., WONG, E. K. S., BOOTH, C., KERECUK, L., SALAMA, A. D., ALMOND, M., INWARD, C., GOODSHIP, T. H., SHEERIN, N. S., MARCHBANK, K. J. & KAVANAGH, D. 2017. Factor H autoantibody is associated with atypical hemolytic uremic syndrome in children in the United Kingdom and Ireland. *Kidney Int*, 92, 1261-1271.
- BURK, A. M., MARTIN, M., FLIERL, M. A., RITTIRSCH, D., HELM, M., LAMPL, L., BRUCKNER, U., STAHL, G. L., BLOM, A. M., PERL, M., GEBHARD, F. & HUBER-LANG, M. 2012. Early complementopathy after multiple injuries in humans. *Shock*, 37, 348-54.
- BÜTTNER-MAINIK, A., PARSONS, J., JÉRÔME, H., HARTMANN, A., LAMER, S., SCHAAF, A., SCHLOSSER, A., ZIPFEL, P. F., RESKI, R. & DECKER, E. L. 2011. Production of biologically active recombinant human factor H in Physcomitrella. *Plant Biotechnology Journal*, 9, 373-383.
- CAI, Y., TEO, D., YEO, J. & LU, J. 2015. C1q Protein Binds to the Apoptotic Nucleolus and Causes C1 Protease Degradation of Nucleolar Proteins. *The Journal of biological chemistry*, 290.
- CANTSILIERIS, S., NELSON, B. J., HUDDLESTON, J., BAKER, C., HARSHMAN, L., PENEWIT, K., MUNSON, K. M., SORENSEN, M., WELCH, A. E., DANG, V., GRASSMANN, F., RICHARDSON, A. J., GUYMER, R. H., GRAVES-LINDSAY, T. A., WILSON, R. K., WEBER, B. H. F., BAIRD, P. N.,

- ALLIKMETS, R. & EICHLER, E. E. 2018. Recurrent structural variation, clustered sites of selection, and disease risk for the complement factor H (<i>CFH</i>) gene family. *Proceedings of the National Academy of Sciences*, 115, E4433-E4442.
- CARBONE, J. 2007. Adverse reactions and pathogen safety of intravenous immunoglobulin. *Curr Drug Saf*, 2, 9-18.
- CARROLL, MICHAEL C. & ISENMAN, DAVID E. 2012. Regulation of Humoral Immunity by Complement. *Immunity*, 37, 199-207.
- CASTELLANO, G., MELCHIORRE, R., LOVERRE, A., DITONNO, P., MONTINARO, V., ROSSINI, M., DIVELLA, C., BATTAGLIA, M., LUCARELLI, G., ANNUNZIATA, G., PALAZZO, S., SELVAGGI, F. P., STAFFIERI, F., CROVACE, A., DAHA, M. R., MANNESSE, M., VAN WETERING, S., PAOLO SCHENA, F. & GRANDALIANO, G. 2010. Therapeutic Targeting of Classical and Lectin Pathways of Complement Protects from Ischemia-Reperfusion-Induced Renal Damage. *The American Journal of Pathology*, 176, 1648-1659.
- CHAN, R. K., IBRAHIM, S. I., VERNA, N., CARROLL, M., MOORE, F. D., JR & HECHTMAN, H. B. 2003. Ischaemia—reperfusion is an event triggered by immune complexes and complement. *British Journal of Surgery*, 90, 1470-1478.
- CHATAURET, N., COUDROY, R., DELPECH, P. O., VANDEBROUCK, C., HOSNI, S., SCEPI, M. & HAUET, T. 2014. Mechanistic Analysis of Nonoxygenated Hypothermic Machine Perfusion's Protection on Warm Ischemic Kidney Uncovers Greater eNOS Phosphorylation and Vasodilation. *American Journal of Transplantation*, 14, 2500-2514.
- CHEN, J., JOHN, R., RICHARDSON, J. A., SHELTON, J. M., ZHOU, X. J., WANG, Y., WU, Q. Q., HARTONO, J. R., WINTERBERG, P. D. & LU, C. Y. 2011. Toll-like receptor 4 regulates early endothelial activation during ischemic acute kidney injury. *Kidney International*, 79, 288-299.
- CHENG, Z.-Z., HELLWAGE, J., SEEBERGER, H., ZIPFEL, P. F., MERI, S. & JOKIRANTA, T. S. 2006. Comparison of surface recognition and C3b binding properties of mouse and human complement factor H. *Molecular Immunology*, 43, 972-979.
- CHOUCHANI, E. T., PELL, V. R., GAUDE, E., AKSENTIJEVIĆ, D., SUNDIER, S. Y., ROBB, E. L., LOGAN, A., NADTOCHIY, S. M., ORD, E. N. J., SMITH, A. C., EYASSU, F., SHIRLEY, R., HU, C.-H., DARE, A. J., JAMES, A. M., ROGATTI, S., HARTLEY, R. C., EATON, S., COSTA, A. S. H., BROOKES, P. S., DAVIDSON, S. M., DUCHEN, M. R., SAEB-PARSY, K., SHATTOCK, M. J., ROBINSON, A. J., WORK, L. M., FREZZA, C., KRIEG, T. & MURPHY, M. P. 2014. Ischaemic accumulation of succinate controls reperfusion injury through mitochondrial ROS. *Nature*, 515, 431-435.
- CHOWDHURY, D. & LIEBERMAN, J. 2008. Death by a thousand cuts: granzyme pathways of programmed cell death. *Annu Rev Immunol*, 26, 389-420.
- CKD WORK GROUP 2024. KDIGO 2024 Clinical Practice Guideline for the Evaluation and Management of Chronic Kidney Disease. *Kidney Int*, 105, S117-s314.
- COLLARD, C. D., MONTALTO, M. C., REENSTRA, W. R., BURAS, J. A. & STAHL, G. L. 2001. Endothelial Oxidative Stress Activates the Lectin Complement Pathway: Role of Cytokeratin 1. *The American Journal of Pathology,* 159, 1045-1054.
- COLLEN, D. & LIJNEN, H. R. 2009. The Tissue-Type Plasminogen Activator Story. *Arteriosclerosis, Thrombosis, and Vascular Biology,* 29, 1151-1155.
- COLOMBARO, V., DECLÈVES, A.-E., JADOT, I., VOISIN, V., GIORDANO, L., HABSCH, I., NONCLERCQ, D., FLAMION, B. & CARON, N. 2013. Inhibition of hyaluronan is protective against renal ischaemia—reperfusion injury. *Nephrology Dialysis Transplantation*, 28, 2484-2493.
- CORNELL, L. D., SMITH, R. N. & COLVIN, R. B. 2008. Kidney Transplantation: Mechanisms of Rejection and Acceptance. *Annual Review of Pathology: Mechanisms of Disease*, 3, 189-220.
- COWLED, P. & FITRIDGE, R. 2020. Pathophysiology of Reperfusion Injury. *In:* FITRIDGE, R. (ed.) *Mechanisms of Vascular Disease: A Textbook for Vascular Specialists.* Cham: Springer International Publishing.
- CRAVEDI, P., LEVENTHAL, J., LAKHANI, P., WARD, S. C., DONOVAN, M. J. & HEEGER, P. S. 2013. Immune Cell-Derived C3a and C5a Costimulate Human T Cell Alloimmunity. *American Journal of Transplantation*, 13, 2530-2539.

- CREW, P. E., MCNAMARA, L., WALDRON, P. E., MCCULLEY, L., CHRISTOPHER JONES, S. & BERSOFF-MATCHA, S. J. 2020. Antibiotic prophylaxis in vaccinated eculizumab recipients who developed meningococcal disease. *J Infect*, 80, 350-371.
- CRON, D. C., MURAKAMI, N., XIANG, L., MARKMANN, J. F., YEH, H. & ADLER, J. T. 2022. Anastomosis Time and Outcomes after Donation after Circulatory Death Kidney Transplantation. *J Am Coll Surg*, 234, 999-1008.
- CURCI, C., CASTELLANO, G., STASI, A., DIVELLA, C., LOVERRE, A., GIGANTE, M., SIMONE, S., CARIELLO, M., MONTINARO, V., LUCARELLI, G., DITONNO, P., BATTAGLIA, M., CROVACE, A., STAFFIERI, F., OORTWIJN, B., VAN AMERSFOORT, E., GESUALDO, L. & GRANDALIANO, G. 2014. Endothelial-to-mesenchymal transition and renal fibrosis in ischaemia/reperfusion injury are mediated by complement anaphylatoxins and Akt pathway. *Nephrology Dialysis Transplantation*, 29, 799-808.
- DAMMAN, J., BLOKS, V. W., DAHA, M. R., VAN DER MOST, P. J., SANJABI, B., VAN DER VLIES, P., SNIEDER, H., PLOEG, R. J., KRIKKE, C., LEUVENINK, H. G. & SEELEN, M. A. 2015. Hypoxia and Complement-and-Coagulation Pathways in the Deceased Organ Donor as the Major Target for Intervention to Improve Renal Allograft Outcome. *Transplantation*, 99, 1293-300.
- DAMMAN, J., SEELEN, M. A., MOERS, C., DAHA, M. R., RAHMEL, A., LEUVENINK, H. G., PAUL, A., PIRENNE, J. & PLOEG, R. J. 2011. Systemic complement activation in deceased donors is associated with acute rejection after renal transplantation in the recipient. *Transplantation*, 92, 163-9.
- DANOBEITIA, J. S., DJAMALI, A. & FERNANDEZ, L. A. 2014. The role of complement in the pathogenesis of renal ischemia-reperfusion injury and fibrosis. *Fibrogenesis & Tissue Repair*, 7, 16.
- DANOBEITIA, J. S., ZIEMELIS, M., MA, X., ZITUR, L. J., ZENS, T., CHLEBECK, P. J., VAN AMERSFOORT, E. S. & FERNANDEZ, L. A. 2017. Complement inhibition attenuates acute kidney injury after ischemia-reperfusion and limits progression to renal fibrosis in mice. *PLOS ONE*, 12, e0183701.
- DE LATOUR, R. P., SZER, J., WEITZ, I. C., RÖTH, A., HÖCHSMANN, B., PANSE, J., USUKI, K., GRIFFIN, M., KILADJIAN, J. J., DE CASTRO, C. M., NISHIMORI, H., AJAYI, T., AL-ADHAMI, M., DESCHATELETS, P., FRANCOIS, C., GROSSI, F., RISITANO, A. M. & HILLMEN, P. 2022. Pegcetacoplan versus eculizumab in patients with paroxysmal nocturnal haemoglobinuria (PEGASUS): 48-week follow-up of a randomised, open-label, phase 3, active-comparator, controlled trial. *Lancet Haematol*, 9, e648-e659.
- DE VRIES, B., KÖHL, J. R., LECLERCQ, W. K. G., WOLFS, T. G. A. M., VAN BIJNEN, A. A. J. H. M., HEERINGA, P. & BUURMAN, W. A. 2003a. Complement Factor C5a Mediates Renal Ischemia-Reperfusion Injury Independent from Neutrophils1. *The Journal of Immunology,* 170, 3883-3889
- DE VRIES, B., MATTHIJSEN, R. A., WOLFS, T. G. A. M., VAN BIJNEN, A. A. J. H. M., HEERINGA, P. & BUURMAN, W. A. 2003b. Inhibition of complement factor C5 protects against renal ischemia-reperfusion injury: inhibition of late apoptosis and inflammation1. *Transplantation*, 75, 375-382.
- DEBOUT, A., FOUCHER, Y., TRÉBERN-LAUNAY, K., LEGENDRE, C., KREIS, H., MOURAD, G., GARRIGUE, V., MORELON, E., BURON, F., ROSTAING, L., KAMAR, N., KESSLER, M., LADRIÈRE, M., POIGNAS, A., BLIDI, A., SOULILLOU, J.-P., GIRAL, M. & DANTAN, E. 2015. Each additional hour of cold ischemia time significantly increases the risk of graft failure and mortality following renal transplantation. *Kidney International*, 87, 343-349.
- DECLÈVES, A.-E., CARON, N., NONCLERCQ, D., LEGRAND, A., TOUBEAU, G., KRAMP, R. & FLAMION, B. 2006. Dynamics of hyaluronan, CD44, and inflammatory cells in the rat kidney after ischemia/reperfusion injury. *Int J Mol Med,* 18, 83-94.
- DECUYPERE, J.-P., CEULEMANS, L. J., AGOSTINIS, P., MONBALIU, D., NAESENS, M., PIRENNE, J. & JOCHMANS, I. 2015. Autophagy and the Kidney: Implications for Ischemia-Reperfusion Injury and Therapy. *American Journal of Kidney Diseases*, 66, 699-709.

- DEL CONDE, I., CRÚZ, M. A., ZHANG, H., LÓPEZ, J. A. & AFSHAR-KHARGHAN, V. 2005. Platelet activation leads to activation and propagation of the complement system. *J Exp Med*, 201, 871-9.
- DELPECH, P.-O., THUILLIER, R., SAINTYVES, T., DANION, J., LE PAPE, S., VAN AMERSFOORT, E. S., OORTWIJN, B., BLANCHO, G. & HAUET, T. 2016. Inhibition of complement improves graft outcome in a pig model of kidney autotransplantation. *Journal of Translational Medicine*, 14, 277.
- DEMPSEY, L. A. 2013. Interferon-induced necroptosis. Nature Immunology, 14, 892-892.
- DHURIYA, Y. K. & SHARMA, D. 2018. Necroptosis: a regulated inflammatory mode of cell death. Journal of Neuroinflammation, 15, 199.
- DING, H., JIANG, L., XU, J., BAI, F., ZHOU, Y., YUAN, Q., LUO, J., ZEN, K. & YANG, J. 2017. Inhibiting aerobic glycolysis suppresses renal interstitial fibroblast activation and renal fibrosis. *Am J Physiol Renal Physiol*, 313, F561-f575.
- DIRITO, J. R., HOSGOOD, S. A., RESCHKE, M., ALBERT, C., BRACAGLIA, L. G., FERDINAND, J. R., STEWART, B. J., EDWARDS, C. M., VAISH, A. G., THIRU, S., MULLIGAN, D. C., HAAKINSON, D. J., CLATWORTHY, M. R., SALTZMAN, W. M., POBER, J. S., NICHOLSON, M. L. & TIETJEN, G. T. 2021. Lysis of cold-storage-induced microvascular obstructions for ex vivo revitalization of marginal human kidneys. *Am J Transplant*, 21, 161-173.
- DISCIPIO, R. G. 1982. The activation of the alternative pathway C3 convertase by human plasma kallikrein. *Immunology*, 45, 587-95.
- DOPLER, A., GUNTAU, L., HARDER, M. J., PALMER, A., HÖCHSMANN, B., SCHREZENMEIER, H., SIMMET, T., HUBER-LANG, M. & SCHMIDT, C. Q. 2019. Self versus Nonself Discrimination by the Soluble Complement Regulators Factor H and FHL-1. *The Journal of Immunology,* 202, 2082-2094.
- DRAGON-DUREY, M. A., LOIRAT, C., CLOAREC, S., MACHER, M. A., BLOUIN, J., NIVET, H., WEISS, L., FRIDMAN, W. H. & FRÉMEAUX-BACCHI, V. 2005. Anti-Factor H autoantibodies associated with atypical hemolytic uremic syndrome. *J Am Soc Nephrol*, 16, 555-63.
- DUNI, A., LIAKOPOULOS, V., KOUTLAS, V., PAPPAS, C., MITSIS, M. & DOUNOUSI, E. 2021. The Endothelial Glycocalyx as a Target of Ischemia and Reperfusion Injury in Kidney Transplantation-Where Have We Gone So Far? *Int J Mol Sci*, 22.
- DUNKELBERGER, J. R. & SONG, W.-C. 2010. Complement and its role in innate and adaptive immune responses. *Cell Research*, 20, 34-50.
- DUNN, K. W., KAMOCKA, M. M. & MCDONALD, J. H. 2011. A practical guide to evaluating colocalization in biological microscopy. *Am J Physiol Cell Physiol*, 300, C723-42.
- ELGERT, K. D. 1996. *Immunology: understanding the immune system,* USA, Wiley-Liss.
- ELMORE, S. 2007. Apoptosis: A Review of Programmed Cell Death. *Toxicologic Pathology*, 35, 495-516.
- FALLER, D. V. 1999. Endothelial cell responses to hypoxic stress. *Clin Exp Pharmacol Physiol*, 26, 74-84
- FARRAR, C. A., TRAN, D., LI, K., WU, W., PENG, Q., SCHWAEBLE, W., ZHOU, W. & SACKS, S. H. 2016. Collectin-11 detects stress-induced L-fucose pattern to trigger renal epithelial injury. *J Clin Invest*, 126, 1911-25.
- FEARON, D. T. & AUSTEN, K. F. 1975. Properdin: binding to C3b and stabilization of the C3b-dependent C3 convertase. *J Exp Med*, 142, 856-63.
- FORNERIS, F., RICKLIN, D., WU, J., TZEKOU, A., WALLACE, R. S., LAMBRIS, J. D. & GROS, P. 2010. Structures of C3b in complex with factors B and D give insight into complement convertase formation. *Science*, 330, 1816-20.
- FRIDKIS-HARELI, M., STOREK, M., MAZSAROFF, I., RISITANO, A. M., LUNDBERG, A. S., HORVATH, C. J. & HOLERS, V. M. 2011. Design and development of TT30, a novel C3d-targeted C3/C5 convertase inhibitor for treatment of human complement alternative pathway—mediated diseases. *Blood*, 118, 4705-4713.
- FRIEDEWALD, J. J. & RABB, H. 2004. Inflammatory cells in ischemic acute renal failure. *Kidney International*, 66, 486-491.

- GASQUE, P. 2004. Complement: a unique innate immune sensor for danger signals. *Molecular Immunology*, 41, 1089-1098.
- GEORGE, J. N. & NESTER, C. M. 2014. Syndromes of Thrombotic Microangiopathy. *New England Journal of Medicine*, 371, 654-666.
- GERRITSMA, J. S., VAN KOOTEN, C., GERRITSEN, A. F., VAN ES, L. A. & DAHA, M. R. 1998.

  Transforming growth factor-beta 1 regulates chemokine and complement production by human proximal tubular epithelial cells. *Kidney Int*, 53, 609-16.
- GILMORE, A. C., ZHANG, Y., COOK, H. T., LAVIN, D. P., KATTI, S., WANG, Y., JOHNSON, K. K., KIM, S. & PICKERING, M. C. 2021. Complement activity is regulated in C3 glomerulopathy by IgG–factor H fusion proteins with and without properdin targeting domains. *Kidney International*, 99, 396-404.
- GLOVER, E. K., SMITH-JACKSON, K., BROCKLEBANK, V., WILSON, V., WALSH, P. R., MONTGOMERY, E. K., WONG, E. K. S., JOHNSON, S., MALINA, M., KAVANAGH, D. & SHEERIN, N. S. 2023.

  Assessing the Impact of Prophylactic Eculizumab on Renal Graft Survival in Atypical Hemolytic Uremic Syndrome. *Transplantation*, 107, 994-1003.
- GOICOECHEA DE JORGE, E., CAESAR, J. J., MALIK, T. H., PATEL, M., COLLEDGE, M., JOHNSON, S., HAKOBYAN, S., MORGAN, B. P., HARRIS, C. L., PICKERING, M. C. & LEA, S. M. 2013. Dimerization of complement factor H-related proteins modulates complement activation in vivo. *Proc Natl Acad Sci U S A*, 110, 4685-90.
- GOLIGORSKY, M. S., BRODSKY, S. V. & NOIRI, E. 2004. NO bioavailability, endothelial dysfunction, and acute renal failure: new insights into pathophysiology. *Seminars in Nephrology*, 24, 316-323.
- GOODSHIP, T. H. J., COOK, H. T., FAKHOURI, F., FERVENZA, F. C., FRÉMEAUX-BACCHI, V., KAVANAGH, D., NESTER, C. M., NORIS, M., PICKERING, M. C., RODRÍGUEZ DE CÓRDOBA, S., ROUMENINA, L. T., SETHI, S., SMITH, R. J. H., ALPERS, C. E., APPEL, G. B., ARDISSINO, G., ARICETA, G., ARICI, M., BAGGA, A., BAJEMA, I. M., BLASCO, M., BURKE, L., CAIRNS, T. D., CARRATALA, M., D'AGATI, V. D., DAHA, M. R., DE VRIESE, A. S., DRAGON-DUREY, M.-A., FOGO, A. B., GALBUSERA, M., GALE, D. P., HALLER, H., JOHNSON, S., JÓZSI, M., KARPMAN, D., LANNING, L., LE QUINTREC, M., LICHT, C., LOIRAT, C., MONFORT, F., MORGAN, B. P., NOËL, L.-H., O'SHAUGHNESSY, M. M., RABANT, M., RONDEAU, E., RUGGENENTI, P., SHEERIN, N. S., SMITH, J., SPOLETI, F., THURMAN, J. M., VAN DE KAR, N. C. A. J., VIVARELLI, M. & ZIPFEL, P. F. 2017. Atypical hemolytic uremic syndrome and C3 glomerulopathy: conclusions from a "Kidney Disease: Improving Global Outcomes" (KDIGO) Controversies Conference. *Kidney International*, 91, 539-551.
- GORDON, S. 2003. Alternative activation of macrophages. *Nature Reviews Immunology,* 3, 23-35. GRAFALS, M. & THURMAN, J. M. 2019. The Role of Complement in Organ Transplantation. *Front Immunol,* 10, 2380.
- GROENEN, M. A., ARCHIBALD, A. L., UENISHI, H., TUGGLE, C. K., TAKEUCHI, Y., ROTHSCHILD, M. F., ROGEL-GAILLARD, C., PARK, C., MILAN, D., MEGENS, H. J., LI, S., LARKIN, D. M., KIM, H., FRANTZ, L. A., CACCAMO, M., AHN, H., AKEN, B. L., ANSELMO, A., ANTHON, C., AUVIL, L., BADAOUI, B., BEATTIE, C. W., BENDIXEN, C., BERMAN, D., BLECHA, F., BLOMBERG, J., BOLUND, L., BOSSE, M., BOTTI, S., BUJIE, Z., BYSTROM, M., CAPITANU, B., CARVALHO-SILVA, D., CHARDON, P., CHEN, C., CHENG, R., CHOI, S. H., CHOW, W., CLARK, R. C., CLEE, C., CROOIJMANS, R. P., DAWSON, H. D., DEHAIS, P., DE SAPIO, F., DIBBITS, B., DROU, N., DU, Z. Q., EVERSOLE, K., FADISTA, J., FAIRLEY, S., FARAUT, T., FAULKNER, G. J., FOWLER, K. E., FREDHOLM, M., FRITZ, E., GILBERT, J. G., GIUFFRA, E., GORODKIN, J., GRIFFIN, D. K., HARROW, J. L., HAYWARD, A., HOWE, K., HU, Z. L., HUMPHRAY, S. J., HUNT, T., HORNSHØJ, H., JEON, J. T., JERN, P., JONES, M., JURKA, J., KANAMORI, H., KAPETANOVIC, R., KIM, J., KIM, J. H., KIM, K. W., KIM, T. H., LARSON, G., LEE, K., LEE, K. T., LEGGETT, R., LEWIN, H. A., LI, Y., LIU, W., LOVELAND, J. E., LU, Y., LUNNEY, J. K., MA, J., MADSEN, O., MANN, K., MATTHEWS, L., MCLAREN, S., MOROZUMI, T., MURTAUGH, M. P., NARAYAN, J., NGUYEN, D. T., NI, P., OH, S. J., ONTERU, S., PANITZ, F., PARK, E. W., et al. 2012. Analyses of pig genomes provide insight into porcine demography and evolution. Nature, 491, 393-8.

- GROVER, S. P. & MACKMAN, N. 2019. Intrinsic Pathway of Coagulation and Thrombosis. *Arteriosclerosis, Thrombosis, and Vascular Biology*, 39, 331-338.
- GU, H., MICKLER, E. A., CUMMINGS, O. W., SANDUSKY, G. E., WEBER, D. J., GRACON, A., WOODRUFF, T., WILKES, D. S. & VITTAL, R. 2014. Crosstalk between TGF-β1 and complement activation augments epithelial injury in pulmonary fibrosis. *The FASEB Journal*, 28, 4223-4234.
- GUELER, F., RONG, S., GWINNER, W., MENGEL, M., BRÖCKER, V., SCHÖN, S., GRETEN, T. F., HAWLISCH, H., POLAKOWSKI, T., SCHNATBAUM, K., MENNE, J., HALLER, H. & SHUSHAKOVA, N. 2008. Complement 5a Receptor Inhibition Improves Renal Allograft Survival. *Journal of the American Society of Nephrology*, 19, 2302-2312.
- GUIGONIS, V., FRÉMEAUX-BACCHI, V., GIRAUDIER, S., FAVIER, R., BORDERIE, D., MASSY, Z., MOUGENOT, B., ROSENBLATT, D. S. & DESCHÊNES, G. 2005. Late-onset thrombocytic microangiopathy caused by cblC disease: Association with a factor H mutation. *American Journal of Kidney Diseases*, 45, 588-595.
- GUNNING, K., RIGG, KEITH, MURPHY, PAUL, MARTINEAU, ABIGAIL, RUDGE, CHRIS 2010. Organ Donation after Circulatory dDeath: Report of a consensus meeting. British Transplant Society, Intensive Care Society.
- HADLEY, J. S., WANG, J. E., MICHAELS, L. C., DEMPSEY, C. M., FOSTER, S. J., THIEMERMANN, C. & HINDS, C. J. 2007. ALTERATIONS IN INFLAMMATORY CAPACITY AND TLR EXPRESSION ON MONOCYTES AND NEUTROPHILS AFTER CARDIOPULMONARY BYPASS. *Shock*, 27, 466-473.
- HALL, I. E., YARLAGADDA, S. G., COCA, S. G., WANG, Z., DOSHI, M., DEVARAJAN, P., HAN, W. K., MARCUS, R. J. & PARIKH, C. R. 2010. IL-18 and urinary NGAL predict dialysis and graft recovery after kidney transplantation. *J Am Soc Nephrol*, 21, 189-97.
- HAMEED, A. M., LU, D. B., BURNS, H., BYRNE, N., CHEW, Y. V., JULOVI, S., GHIMIRE, K., ZANJANI, N. T., P'NG C, H., MEIJLES, D., DERVISH, S., MATTHEWS, R., MIRAZIZ, R., O'GRADY, G., YUEN, L., PLEASS, H. C., ROGERS, N. M. & HAWTHORNE, W. J. 2020. Pharmacologic targeting of renal ischemia-reperfusion injury using a normothermic machine perfusion platform. *Sci Rep,* 10, 6930.
- HARBOE, M., ULVUND, G., VIEN, L. T., FUNG, M. S. C. & MOLLNES, T. E. 2004. The quantitative role of alternative pathway amplification in classical pathway induced terminal complement activation. *Clinical & Experimental Immunology*, 138.
- HARDER, M. J., ANLIKER, M., HÖCHSMANN, B., SIMMET, T., HUBER-LANG, M., SCHREZENMEIER, H., RICKLIN, D., LAMBRIS, J. D., BARLOW, P. N. & SCHMIDT, C. Q. 2016. Comparative Analysis of Novel Complement-Targeted Inhibitors, MiniFH, and the Natural Regulators Factor H and Factor H–like Protein 1 Reveal Functional Determinants of Complement Regulation. *The Journal of Immunology*, 196, 866-876.
- HARPER, S., HOSGOOD, S., KAY, M. & NICHOLSON, M. 2006. Leucocyte depletion improves renal function during reperfusion using an experimental isolated haemoperfused organ preservation system. *British Journal of Surgery*, 93, 623-629.
- HEBECKER, M., ALBA-DOMÍNGUEZ, M., ROUMENINA, L. T., REUTER, S., HYVÄRINEN, S., DRAGON-DUREY, M.-A., JOKIRANTA, T. S., SÁNCHEZ-CORRAL, P. & JÓZSI, M. 2013. An Engineered Construct Combining Complement Regulatory and Surface-Recognition Domains Represents a Minimal-Size Functional Factor H. *The Journal of Immunology*, 191, 912-921.
- HEBECKER, M. & JÓZSI, M. 2012. Factor H-related Protein 4 Activates Complement by Serving as a Platform for the Assembly of Alternative Pathway C3 Convertase via Its Interaction with C3b Protein. *Journal of Biological Chemistry*, 287, 19528-19536.
- HEGASY, G. A., WILLHOEFT, U., MAJNO, S. A., SEEBERGER, H., ZIPFEL, P. F. & HELLWAGE, J. 2003. Pig complement regulator factor H: molecular cloning and functional characterization. *Immunogenetics*, 55, 462-471.
- HEIER, J. S., LAD, E. M., HOLZ, F. G., ROSENFELD, P. J., GUYMER, R. H., BOYER, D., GROSSI, F.,
  BAUMAL, C. R., KOROBELNIK, J. F., SLAKTER, J. S., WAHEED, N. K., METLAPALLY, R., PEARCE, I.,
  STEINLE, N., FRANCONE, A. A., HU, A., LALLY, D. R., DESCHATELETS, P., FRANCOIS, C., BLISS,
  C., STAURENGHI, G., MONÉS, J., SINGH, R. P., RIBEIRO, R. & WYKOFF, C. C. 2023.
  Pegcetacoplan for the treatment of geographic atrophy secondary to age-related macular

- degeneration (OAKS and DERBY): two multicentre, randomised, double-masked, sham-controlled, phase 3 trials. *Lancet*, 402, 1434-1448.
- HEMPEL, J. C., POPPELAARS, F., GAYA DA COSTA, M., FRANSSEN, C. F. M., DE VLAAM, T. P. G., DAHA, M. R., BERGER, S. P., SEELEN, M. A. J. & GAILLARD, C. A. J. M. 2016. Distinct in vitro Complement Activation by Various Intravenous Iron Preparations. *American Journal of Nephrology*, 45, 49-59.
- HILLMEN, P., HORNEFF, R., YEH, M., KOLEV, M. & DESCHATELETS, P. 2024. Navigating the Complement Pathway to Optimize PNH Treatment with Pegcetacoplan and Other Currently Approved Complement Inhibitors. *Int J Mol Sci*, 25.
- HILLMEN, P., SZER, J., WEITZ, I., RÖTH, A., HÖCHSMANN, B., PANSE, J., USUKI, K., GRIFFIN, M., KILADJIAN, J.-J., CASTRO, C. D., NISHIMORI, H., TAN, L., HAMDANI, M., DESCHATELETS, P., FRANCOIS, C., GROSSI, F., AJAYI, T., RISITANO, A. & LATOUR, R. P. D. 2021. Pegcetacoplan versus Eculizumab in Paroxysmal Nocturnal Hemoglobinuria. *New England Journal of Medicine*, 384, 1028-1037.
- HILLMEN, P., YOUNG, N. S., SCHUBERT, J., BRODSKY, R. A., SOCIÉ, G., MUUS, P., RÖTH, A., SZER, J., ELEBUTE, M. O., NAKAMURA, R., BROWNE, P., RISITANO, A. M., HILL, A., SCHREZENMEIER, H., FU, C.-L., MACIEJEWSKI, J., ROLLINS, S. A., MOJCIK, C. F., ROTHER, R. P. & LUZZATTO, L. 2006. The Complement Inhibitor Eculizumab in Paroxysmal Nocturnal Hemoglobinuria. *New England Journal of Medicine*, 355, 1233-1243.
- HO, K. J., OWENS, C. D., JOHNSON, S. R., KHWAJA, K., CURRY, M. P., PAVLAKIS, M., MANDELBROT, D., POMPOSELLI, J. J., SHAH, S. A., SAIDI, R. F., KO, D. S. C., MALEK, S., BELCHER, J., HULL, D., TULLIUS, S. G., FREEMAN, R. B., POMFRET, E. A., WHITING, J. F., HANTO, D. W. & KARP, S. J. 2008. Donor Postextubation Hypotension and Age Correlate With Outcome After Donation After Cardiac Death Transplantation. *Transplantation*, 85, 1588-1594.
- HOLERS, V. M. 2014. Complement and Its Receptors: New Insights into Human Disease. *Annual Review of Immunology*, 32, 433-459.
- HOSGOOD, S. A., BARLOW, A. D., HUNTER, J. P. & NICHOLSON, M. L. 2015. Ex vivo normothermic perfusion for quality assessment of marginal donor kidney transplants. *British Journal of Surgery*, 102, 1433-1440.
- HOSGOOD, S. A., CALLAGHAN, C. J., WILSON, C. H., SMITH, L., MULLINGS, J., MEHEW, J., ONISCU, G. C., PHILLIPS, B. L., BATES, L. & NICHOLSON, M. L. 2023. Normothermic machine perfusion versus static cold storage in donation after circulatory death kidney transplantation: a randomized controlled trial. *Nat Med*, 29, 1511-1519.
- HOSGOOD, S. A., HOFF, M. & NICHOLSON, M. L. 2021. Treatment of transplant kidneys during machine perfusion. *Transplant International*, n/a.
- HOSGOOD, S. A., MOORE, T., KLEVERLAAN, T., ADAMS, T. & NICHOLSON, M. L. 2017.

  Haemoadsorption reduces the inflammatory response and improves blood flow during ex vivo renal perfusion in an experimental model. *Journal of Translational Medicine*, 15, 216.
- HOSGOOD, S. A. & NICHOLSON, M. L. 2011. First in Man Renal Transplantation After Ex Vivo Normothermic Perfusion. *Transplantation*, 92, 735-738.
- HOSGOOD, S. A., PATEL, M. & NICHOLSON, M. L. 2013. The conditioning effect of ex vivo normothermic perfusion in an experimental kidney model. *Journal of Surgical Research*, 182, 153-160.
- HOSGOOD, S. A., THOMPSON, E., MOORE, T., WILSON, C. H. & NICHOLSON, M. L. 2018.

  Normothermic machine perfusion for the assessment and transplantation of declined human kidneys from donation after circulatory death donors. *Br J Surg*, 105, 388-394.
- HOTCHKISS, R. S., STRASSER, A., MCDUNN, J. E. & SWANSON, P. E. 2009. Cell Death. *New England Journal of Medicine*, 361, 1570-1583.
- HOWARD, J. F., JR., UTSUGISAWA, K., BENATAR, M., MURAI, H., BAROHN, R. J., ILLA, I., JACOB, S., VISSING, J., BURNS, T. M., KISSEL, J. T., MUPPIDI, S., NOWAK, R. J., O'BRIEN, F., WANG, J. J. & MANTEGAZZA, R. 2017. Safety and efficacy of eculizumab in anti-acetylcholine receptor antibody-positive refractory generalised myasthenia gravis (REGAIN): a phase 3, randomised, double-blind, placebo-controlled, multicentre study. *Lancet Neurol*, 16, 976-986.

- HU, C., LI, L., DING, P., LI, L., GE, X., ZHENG, L., WANG, X., WANG, J., ZHANG, W., WANG, N., GU, H., ZHONG, F., XU, M., RONG, R., ZHU, T. & HU, W. 2018. Complement Inhibitor CRIg/FH Ameliorates Renal Ischemia Reperfusion Injury via Activation of PI3K/AKT Signaling. *The Journal of Immunology*, 201, 3717-3730.
- HUANG, S., SANDHOLM, K., JONSSON, N., NILSSON, A., WIESLANDER, A., GRUNDSTRÖM, G., HANCOCK, V. & EKDAHL, K. N. 2015. Low concentrations of citrate reduce complement and granulocyte activation in vitro in human blood. *Clin Kidney J*, **8**, 31-7.
- HUME, D. A. 2006. The mononuclear phagocyte system. Curr Opin Immunol, 18, 49-53.
- JAGER, N. M., VENEMA, L. H., ARYKBAEVA, A. S., METER-ARKEMA, A. H., OTTENS, P. J., VAN KOOTEN, C., MOLLNES, T. E., ALWAYN, I. P. J., LEUVENINK, H. G. D. & PISCHKE, S. E. 2022. Complement Is Activated During Normothermic Machine Perfusion of Porcine and Human Discarded Kidneys. *Front Immunol*, 13, 831371.
- JANSSEN, B. J. C., CHRISTODOULIDOU, A., MCCARTHY, A., LAMBRIS, J. D. & GROS, P. 2006. Structure of C3b reveals conformational changes that underlie complement activity. *Nature*, 444, 213-216.
- JAYNE, D. R. W., MERKEL, P. A., SCHALL, T. J. & BEKKER, P. 2021. Avacopan for the Treatment of ANCA-Associated Vasculitis. *New England Journal of Medicine*, 384, 599-609.
- JHA, V., GARCIA-GARCIA, G., ISEKI, K., LI, Z., NAICKER, S., PLATTNER, B., SARAN, R., WANG, A. Y.-M. & YANG, C.-W. 2013. Chronic kidney disease: global dimension and perspectives. *The Lancet*, 382, 260-272.
- JIA, S. H., PARODO, J., CHARBONNEY, E., TSANG, J. L. Y., JIA, S. Y., ROTSTEIN, O. D., KAPUS, A. & MARSHALL, J. C. 2014. Activated Neutrophils Induce Epithelial Cell Apoptosis Through Oxidant-Dependent Tyrosine Dephosphorylation of Caspase-8. *The American Journal of Pathology*, 184, 1030-1040.
- JORDAN, S. C., CHOI, J., AUBERT, O., HAAS, M., LOUPY, A., HUANG, E., PENG, A., KIM, I., LOUIE, S., AMMERMAN, N., NAJJAR, R., PULIYANDA, D. & VO, A. 2018. A phase I/II, double-blind, placebo-controlled study assessing safety and efficacy of C1 esterase inhibitor for prevention of delayed graft function in deceased donor kidney transplant recipients. *American Journal of Transplantation*, 18, 2955-2964.
- JOZSI, M., TORTAJADA, A., UZONYI, B., GOICOECHEA DE JORGE, E. & RODRIGUEZ DE CORDOBA, S. 2015. Factor H-related proteins determine complement-activating surfaces. *Trends Immunol*, 36, 374-84.
- KAMALA, O., MALIK, T. H., HALLAM, T. M., COX, T. E., YANG, Y., VYAS, F., LULI, S., CONNELLY, C., GIBSON, B., SMITH-JACKSON, K., DENTON, H., PAPPWORTH, I. Y., HUANG, L., KAVANAGH, D., PICKERING, M. C. & MARCHBANK, K. J. 2021. Homodimeric Minimal Factor H: In Vivo Tracking and Extended Dosing Studies in Factor H Deficient Mice. *Frontiers in Immunology*, 12.
- KASSIMATIS, T., GREENLAW, R., HUNTER, J. P., DOUIRI, A., FLACH, C., REBOLLO-MESA, I., NICHOLS, L. L., QASEM, A., DANZI, G., OLSBURGH, J., DRAGE, M., FRIEND, P. J., NERI, F., KAREGLI, J., HORSFIELD, C., SMITH, R. A. & SACKS, S. H. 2021. Ex vivo delivery of Mirococept: A dose-finding study in pig kidney after showing a low dose is insufficient to reduce delayed graft function in human kidney. *American Journal of Transplantation*, 21, 1012-1026.
- KAVANAGH, D., GOODSHIP, T. H. & RICHARDS, A. 2013. Atypical hemolytic uremic syndrome. *Semin Nephrol*, 33, 508-30.
- KIDNEY RESEARCH UK 2023. Kidney disease: A UK public health emergency: The health economics of kidney disease to 2033.
- KIM, J., PYEON, T., CHOI, J. I., KANG, J. H., SONG, S. W., BAE, H.-B. & JEONG, S. 2019. A retrospective study of the relationship between postoperative urine output and one year transplanted kidney function. *BMC Anesthesiology*, 19, 231.
- KIM, J. J., GOODSHIP, T. H. J., TIZARD, J. & INWARD, C. 2011. Plasma therapy for atypical haemolytic uraemic syndrome associated with heterozygous factor H mutations. *Pediatric Nephrology*, 26, 2073-2076.

- KONDO, C., MIZUNO, M., NISHIKAWA, K., YUZAWA, Y., HOTTA, N. & MATSUO, S. 2001. The role of C5a in the development of thrombotic glomerulonephritis in rats. *Clin Exp Immunol*, 124, 323-9.
- KONO, H. & ROCK, K. L. 2008. How dying cells alert the immune system to danger. *Nat Rev Immunol,* 8, 279-89.
- KOZMA, G. T., MÉSZÁROS, T., BAKOS, T., HENNIES, M., BENCZE, D., UZONYI, B., GYŐRFFY, B., CEDRONE, E., DOBROVOLSKAIA, M. A., JÓZSI, M. & SZEBENI, J. 2021. Mini-Factor H Modulates Complement-Dependent IL-6 and IL-10 Release in an Immune Cell Culture (PBMC) Model: Potential Benefits Against Cytokine Storm. Frontiers in Immunology, 12.
- KRARUP, A., WALLIS, R., PRESANIS, J. S., GÁL, P. & SIM, R. B. 2007. Simultaneous Activation of Complement and Coagulation by MBL-Associated Serine Protease 2. *PLOS ONE*, 2, e623.
- KREIMANN, K., JANG, M.-S., RONG, S., GREITE, R., VON VIETINGHOFF, S., SCHMITT, R., BRÄSEN, J. H., SCHIFFER, L., GERSTENBERG, J., VIJAYAN, V., DITTRICH-BREIHOLZ, O., WANG, L., KARSTEN, C. M., GWINNER, W., HALLER, H., IMMENSCHUH, S. & GUELER, F. 2020. Ischemia Reperfusion Injury Triggers CXCL13 Release and B-Cell Recruitment After Allogenic Kidney Transplantation. *Frontiers in Immunology*, 11.
- KROEMER, G., MARIÑO, G. & LEVINE, B. 2010. Autophagy and the Integrated Stress Response. *Molecular Cell*, 40, 280-293.
- KRYSKO, D. V., AGOSTINIS, P., KRYSKO, O., GARG, A. D., BACHERT, C., LAMBRECHT, B. N. & VANDENABEELE, P. 2011. Emerging role of damage-associated molecular patterns derived from mitochondria in inflammation. *Trends in Immunology*, 32, 157-164.
- KULASEKARARAJ, A. G., GRIFFIN, M., LANGEMEIJER, S., USUKI, K., KULAGIN, A., OGAWA, M., YU, J., MUJEEBUDDIN, A., NISHIMURA, J. I., LEE, J. W. & PEFFAULT DE LATOUR, R. 2022. Long-term safety and efficacy of ravulizumab in patients with paroxysmal nocturnal hemoglobinuria: 2-year results from two pivotal phase 3 studies. *Eur J Haematol*, 109, 205-214.
- KUMBALA, D. & ZHANG, R. 2013. Essential concept of transplant immunology for clinical practice. *World J Transplant*, 3, 113-8.
- KWON, O., HONG, S. M. & RAMESH, G. 2009. Diminished NO generation by injured endothelium and loss of macula densa nNOS may contribute to sustained acute kidney injury after ischemia-reperfusion. *Am J Physiol Renal Physiol*, 296, F25-33.
- LAN, R., GENG, H., SINGHA, P. K., SAIKUMAR, P., BOTTINGER, E. P., WEINBERG, J. M. & VENKATACHALAM, M. A. 2016. Mitochondrial Pathology and Glycolytic Shift during Proximal Tubule Atrophy after Ischemic AKI. *J Am Soc Nephrol*, 27, 3356-3367.
- LATOUR, R. P. D., RÖTH, A., KULASEKARARAJ, A. G., HAN, B., SCHEINBERG, P., MACIEJEWSKI, J. P., UEDA, Y., CASTRO, C. M. D., BONA, E. D., FU, R., ZHANG, L., GRIFFIN, M., LANGEMEIJER, S. M. C., PANSE, J., SCHREZENMEIER, H., BARCELLINI, W., MAUAD, V. A. Q., SCHAFHAUSEN, P., TAVITIAN, S., BEGGIATO, E., CHEW, L. P., GAYA, A., HUANG, W.-H., JANG, J. H., KITAWAKI, T., KUTLAR, A., NOTARO, R., PULLARKAT, V., SCHUBERT, J., TERRIOU, L., UCHIYAMA, M., LEE, L. W. L., YAP, E.-S., FONTBRUNE, F. S. D., MARANO, L., ALASHKAR, F., GANDHI, S., TRIKHA, R., YANG, C., LIU, H., KELLY, R. J., HÖCHSMANN, B., KERLOEGUEN, C., BANERJEE, P., LEVITCH, R., KUMAR, R., WANG, Z., THORBURN, C., MAITRA, S., LI, S., VERLES, A., DAHLKE, M. & RISITANO, A. M. 2024. Oral Iptacopan Monotherapy in Paroxysmal Nocturnal Hemoglobinuria. *New England Journal of Medicine*, 390, 994-1008.
- LEE, J. W., GRIFFIN, M., KIM, J. S., LEE LEE, L. W., PIATEK, C., NISHIMURA, J.-I., CARRILLO INFANTE, C., JAIN, D., LIU, P., FILIPPOV, G., SICRE DE FONTBRUNE, F., RISITANO, A., KULASEKARARAJ, A. G., BARCELLINI, W., BARRACO, F., BENEITEZ PASTOR, D., CAPRA, M., CHEW, L. P., CHRYSAVGI, L., DE CASTRO, C., DE LA TOUR, R. P., DE OLIVEIRA, M. M., DI BONA, E., FORCADE, E., FU, C.-L., FURHA, C., GAYA VALLS, A., GIANNOULI, S., GONZALEZ-FERNANDEZ, A., GRIFFIN, M., GURAL, A., GUTIERREZ, E. O., HERNÁNDEZ-RODRÍGUEZ, I., IBRAHIM, I., IORI, A. P., ISHIDA, T., JANG, J. H., KIM, J.-A., KIM, J. S., KITANO, T., KOSUGI, H., KREINIZ, N., KULASEKARARAJ, A., LEE, J. W., LEE LEE, L. W., MAYER, J., MITCHELL, L., MORI, Y., NISHIWAKI, K., NOTARO, R., NUNEZ, R., OBARA, N., OLIVA, E. N., PATRIQUIN, C., PESSOA, V., PIATEK, C., PIEKARSKA, A., RAZA, S., RISITANO, A. M., ROJNUCKARIN, P., SAMUEL, D., SHAMMO, J., TADMOR, T., TAKAMI, A.,

- TAMARI, R., TERRIOU, L., UCHIYAMA, H., VANNUCCHI, A. M. & YAMAGUCHI, H. 2023. Addition of danicopan to ravulizumab or eculizumab in patients with paroxysmal nocturnal haemoglobinuria and clinically significant extravascular haemolysis (ALPHA): a double-blind, randomised, phase 3 trial. *The Lancet Haematology*, 10, e955-e965.
- LEGENDRE, C. M., LICHT, C., MUUS, P., GREENBAUM, L. A., BABU, S., BEDROSIAN, C., BINGHAM, C., COHEN, D. J., DELMAS, Y., DOUGLAS, K., EITNER, F., FELDKAMP, T., FOUQUE, D., FURMAN, R. R., GABER, O., HERTHELIUS, M., HOURMANT, M., KARPMAN, D., LEBRANCHU, Y., MARIAT, C., MENNE, J., MOULIN, B., NÜRNBERGER, J., OGAWA, M., REMUZZI, G., RICHARD, T., SBERROSOUSSAN, R., SEVERINO, B., SHEERIN, N. S., TRIVELLI, A., ZIMMERHACKL, L. B., GOODSHIP, T. & LOIRAT, C. 2013. Terminal Complement Inhibitor Eculizumab in Atypical Hemolytic—Uremic Syndrome. *New England Journal of Medicine*, 368, 2169-2181.
- LEWIS, A. G., KÖHL, G., MA, Q., DEVARAJAN, P. & KÖHL, J. 2008. Pharmacological targeting of C5a receptors during organ preservation improves kidney graft survival. *Clinical and Experimental Immunology*, 153, 117-126.
- LI, L., HUANG, L., SUNG, S.-S. J., VERGIS, A. L., ROSIN, D. L., ROSE, C. E., LOBO, P. I. & OKUSA, M. D. 2008. The chemokine receptors CCR2 and CX3CR1 mediate monocyte/macrophage trafficking in kidney ischemia—reperfusion injury. *Kidney International*, 74, 1526-1537.
- LIBERTI, M. V. & LOCASALE, J. W. 2016. The Warburg Effect: How Does it Benefit Cancer Cells? *Trends Biochem Sci*, 41, 211-218.
- LICHT, C., GREENBAUM, L. A., MUUS, P., BABU, S., BEDROSIAN, C. L., COHEN, D. J., DELMAS, Y., DOUGLAS, K., FURMAN, R. R., GABER, O. A., GOODSHIP, T., HERTHELIUS, M., HOURMANT, M., LEGENDRE, C. M., REMUZZI, G., SHEERIN, N., TRIVELLI, A. & LOIRAT, C. 2015. Efficacy and safety of eculizumab in atypical hemolytic uremic syndrome from 2-year extensions of phase 2 studies. *Kidney Int*, 87, 1061-73.
- LICHT, C., WEYERSBERG, A., HEINEN, S., STAPENHORST, L., DEVENGE, J., BECK, B., WALDHERR, R., KIRSCHFINK, M., ZIPFEL, P. F. & HOPPE, B. 2005. Successful plasma therapy for atypical hemolytic uremic syndrome caused by factor H deficiency owing to a novel mutation in the complement cofactor protein domain 15. *American Journal of Kidney Diseases*, 45, 415-421.
- LIU, H., LI, Y. & XIONG, J. 2022. The Role of Hypoxia-Inducible Factor-1 Alpha in Renal Disease. *Molecules*, 27.
- LIU , J., MIWA , T., HILLIARD , B., CHEN , Y., LAMBRIS , J. D., WELLS , A. D. & SONG , W.-C. 2005. The complement inhibitory protein DAF (CD55) suppresses T cell immunity in vivo. *Journal of Experimental Medicine*, 201, 567-577.
- LO, S., JIANG, L., STACKS, S., LIN, H. & PARAJULI, N. 2021. Aberrant activation of the complement system in renal grafts is mediated by cold storage. *American Journal of Physiology-Renal Physiology*, 320, F1174-F1190.
- LOHMANN, S., POOL, M. B. F., ROZENBERG, K. M., KELLER, A. K., MOERS, C., MØLDRUP, U., MØLLER, B. K., LIGNELL, S. J. M., KRAG, S., SIERRA-PARRAGA, J. M., LO FARO, M. L., HUNTER, J., HOOGDUIJN, M. J., BAAN, C. C., LEUVENINK, H. G. D., PLOEG, R. J., EIJKEN, M. & JESPERSEN, B. 2021. Mesenchymal stromal cell treatment of donor kidneys during ex vivo normothermic machine perfusion: A porcine renal autotransplantation study. *Am J Transplant*, 21, 2348-2359.
- LUM, E. L., HOMKRAILAS, P., ABDALLA, B., DANOVITCH, G. M. & BUNNAPRADIST, S. 2023. Cold Ischemia Time, Kidney Donor Profile Index, and Kidney Transplant Outcomes: A Cohort Study. *Kidney Medicine*, 5.
- LUNNEY, J. K. 2007. Advances in swine biomedical model genomics. Int J Biol Sci, 3, 179-84.
- MAIER, H. T., ASHRAF, M. I., DENECKE, C., WEISS, S., AUGUSTIN, F., MESSNER, F., VALLANT, N., BÖCKLEIN, M., MARGREITER, C., GÖBEL, G., PRATSCHKE, J., ÖFNER-VELANO, D. & AIGNER, F. 2018. Prediction of delayed graft function and long-term graft survival by serum and urinary neutrophil gelatinase-associated lipocalin during the early postoperative phase after kidney transplantation. *PLoS One*, 13, e0189932.
- MAIRBÄURL, H. & WEBER, R. E. 2012. Oxygen Transport by Hemoglobin. Comprehensive Physiology.

- MAKOU, E., HERBERT, A. P. & BARLOW, P. N. 2013. Functional anatomy of complement factor H. *Biochemistry*, 52, 3949-62.
- MARES, J., RICHTROVA, P., HRICINOVA, A., TUMA, Z., MORAVEC, J., LYSAK, D. & MATEJOVIC, M. 2010. Proteomic profiling of blood-dialyzer interactome reveals involvement of lectin complement pathway in hemodialysis-induced inflammatory response. *PROTEOMICS Clinical Applications*, 4, 829-838.
- MARKIEWSKI, M. M. & LAMBRIS, J. D. 2007. The role of complement in inflammatory diseases from behind the scenes into the spotlight. *Am J Pathol*, 171, 715-27.
- MATSUSHITA, M., ENDO, Y. & FUJITA, T. 2013. Structural and Functional Overview of the Lectin Complement Pathway: Its Molecular Basis and Physiological Implication. *Archivum Immunologiae et Therapiae Experimentalis*, 61, 273-283.
- MERION, R. M., GOODRICH, N. P., JOHNSON, R. J., MCDONALD, S. P., RUSS, G. R., GILLESPIE, B. W. & COLLETT, D. 2018. Kidney transplant graft outcomes in 379 257 recipients on 3 continents. *American Journal of Transplantation*, 18, 1914-1923.
- MILLS, E. L., KELLY, B. & O'NEILL, L. A. J. 2017. Mitochondria are the powerhouses of immunity. *Nature Immunology*, 18, 488-498.
- MIRTSCHINK, P., KRISHNAN, J., GRIMM, F., SARRE, A., HÖRL, M., KAYIKCI, M., FANKHAUSER, N., CHRISTINAT, Y., CORTIJO, C., FEEHAN, O., VUKOLIC, A., SOSSALLA, S., STEHR, S. N., ULE, J., ZAMBONI, N., PEDRAZZINI, T. & KREK, W. 2015. HIF-driven SF3B1 induces KHK-C to enforce fructolysis and heart disease. *Nature*, 522, 444-449.
- MIWA, T., SATO, S., GULLIPALLI, D., NANGAKU, M. & SONG, W. C. 2013. Blocking properdin, the alternative pathway, and anaphylatoxin receptors ameliorates renal ischemia-reperfusion injury in decay-accelerating factor and CD59 double-knockout mice. *J Immunol*, 190, 3552-9.
- MIYAZAWA, S., WATANABE, H., MIYAJI, C., HOTTA, O. & ABO, T. 2002. Leukocyte accumulation and changes in extra-renal organs during renal ischemia reperfusion in mice. *Journal of Laboratory and Clinical Medicine*, 139, 269-278.
- MØLLER-KRISTENSEN, M., WANG, W., RUSEVA, M., THIEL, S., NIELSEN, S., TAKAHASHI, K., SHI, L., EZEKOWITZ, A., JENSENIUS, J. C. & GADJEVA, M. 2005. Mannan-Binding Lectin Recognizes Structures on Ischaemic Reperfused Mouse Kidneys and is Implicated in Tissue Injury. *Scandinavian Journal of Immunology*, 61, 426-434.
- MOLLNES, T. E., GARRED, P. & BERGSETH, G. 1988. Effect of time, temperature and anticoagulants on in vitro complement activation: consequences for collection and preservation of samples to be examined for complement activation. *Clin Exp Immunol*, 73, 484-8.
- MORGAN, H. P., SCHMIDT, C. Q., GUARIENTO, M., BLAUM, B. S., GILLESPIE, D., HERBERT, A. P., KAVANAGH, D., MERTENS, H. D., SVERGUN, D. I., JOHANSSON, C. M., UHRÍN, D., BARLOW, P. N. & HANNAN, J. P. 2011. Structural basis for engagement by complement factor H of C3b on a self surface. *Nat Struct Mol Biol*, 18, 463-70.
- MÜLLER, T. F., KRAUS, M., NEUMANN, C. & LANGE, H. 1997. Detection of renal allograft rejection by complement components C5A and TCC in plasma and urine. *J Lab Clin Med*, 129, 62-71.
- NAESENS, M., LI, L., YING, L., SANSANWAL, P., SIGDEL, T. K., HSIEH, S.-C., KAMBHAM, N., LERUT, E., SALVATIERRA, O., BUTTE, A. J. & SARWAL, M. M. 2009. Expression of Complement Components Differs Between Kidney Allografts from Living and Deceased Donors. *Journal of the American Society of Nephrology*, 20.
- NAITO, M., BOMSZTYK, K. & ZAGER, R. A. 2008. Endotoxin Mediates Recruitment of RNA Polymerase II to Target Genes in Acute Renal Failure. *Journal of the American Society of Nephrology,* 19, 1321-1330.
- NARAYANAN, S. 1999. Multifunctional roles of thrombin. Ann Clin Lab Sci, 29, 275-80.
- NATH, J., SMITH, T. B., PATEL, K., EBBS, S. R., HOLLIS, A., TENNANT, D. A., LUDWIG, C. & READY, A. R. 2017. Metabolic differences between cold stored and machine perfused porcine kidneys: A 1H NMR based study. *Cryobiology*, 74, 115-120.
- NAUTA, A. J., DAHA, M. R., TIJSMA, O., VAN DE WATER, B., TEDESCO, F. & ROOS, A. 2002. The membrane attack complex of complement induces caspase activation and apoptosis. *Eur J Immunol*, 32, 783-92.

- NHS BLOOD AND TRANSPLANT 2023. Organ and Tissue Donation and Transplantation: Activity Report 2022/2023.
- NHSBT. 2009. Cost-effectiveness of transplantation, Factsheet 7 [Online]. Available: <a href="https://nhsbtmediaservices.blob.core.windows.net/organ-donation-assets/pdfs/Organ Donation Registry Fact Sheet 7 21337.pdf">https://nhsbtmediaservices.blob.core.windows.net/organ-donation-assets/pdfs/Organ Donation Registry Fact Sheet 7 21337.pdf</a> [Accessed 23/05/2024].
- NHSBT 2023. Organ and Tissue Donation and Transplantation Activity Report 2022/23.
- NICHOLS, E.-M., BARBOUR, T. D., PAPPWORTH, I. Y., WONG, E. K. S., PALMER, J. M., SHEERIN, N. S., PICKERING, M. C. & MARCHBANK, K. J. 2015. An extended mini-complement factor H molecule ameliorates experimental C3 glomerulopathy. *Kidney International*, 88, 1314-1322.
- NICHOLSON, M. L. & HOSGOOD, S. A. 2013. Renal transplantation after ex vivo normothermic perfusion: the first clinical study. *Am J Transplant*, 13, 1246-52.
- NIETO-RÍOS, J. F., OCHOA-GARCÍA, C. L., SERNA-CAMPUZANO, A., BENAVIDES-HERMOSA, B., CALDERÓN-PUENTES, L. L., ARISTIZABAL-ALZATE, A., OCAMPO-KOHN, C., ZULUAGA-VALENCIA, G. & SERNA-HIGUITA, L. M. 2019. Time of Cold Ischemia and Delayed Graft Function in a Cohort of Renal Transplant Patients in a Reference Center. *Indian J Nephrol*, 29, 8-14.
- NIEUWENHUIJS-MOEKE, G. J., PISCHKE, S. E., BERGER, S. P., SANDERS, J. S. F., POL, R. A., STRUYS, M. M. R. F., PLOEG, R. J. & LEUVENINK, H. G. D. 2020. Ischemia and Reperfusion Injury in Kidney Transplantation: Relevant Mechanisms in Injury and Repair. *Journal of Clinical Medicine*, 9, 253.
- NORIS, M. & REMUZZI, G. 2013. Overview of complement activation and regulation. *Semin Nephrol*, 33, 479-92.
- OLAUSSON, M., ANTONY, D., TRAVNIKOVA, G., JOHANSSON, M., NAYAKAWDE, N. B., BANERJEE, D., SØFTELAND, J. M. & PREMARATNE, G. U. 2022. Novel Ex-Vivo Thrombolytic Reconditioning of Kidneys Retrieved 4 to 5 Hours After Circulatory Death. *Transplantation*, 106, 1577-1588.
- OSBAND, A. J., JAMES, N. T. & SEGEV, D. L. 2016. Extraction Time of Kidneys From Deceased Donors and Impact on Outcomes. *Am J Transplant*, 16, 700-3.
- PANGBURN, M. K., SCHREIBER, R. D. & MÜLLER-EBERHARD, H. J. 1981. Formation of the initial C3 convertase of the alternative complement pathway. Acquisition of C3b-like activities by spontaneous hydrolysis of the putative thioester in native C3. *J Exp Med*, 154, 856-67.
- PARENTE, R., CLARK, S. J., INFORZATO, A. & DAY, A. J. 2017. Complement factor H in host defense and immune evasion. *Cellular and Molecular Life Sciences*, 74, 1605-1624.
- PARK, P., HAAS, M., CUNNINGHAM, P. N., BAO, L., ALEXANDER, J. J. & QUIGG, R. J. 2002. Injury in renal ischemia-reperfusion is independent from immunoglobulins and T lymphocytes. *American Journal of Physiology-Renal Physiology*, 282, F352-F357.
- PARK, T. J., REZNICK, J., PETERSON, B. L., BLASS, G., OMERBAŠIĆ, D., BENNETT, N. C., KUICH, P. H. J. L., ZASADA, C., BROWE, B. M., HAMANN, W., APPLEGATE, D. T., RADKE, M. H., KOSTEN, T., LUTERMANN, H., GAVAGHAN, V., EIGENBROD, O., BÉGAY, V., AMOROSO, V. G., GOVIND, V., MINSHALL, R. D., SMITH, E. S. J., LARSON, J., GOTTHARDT, M., KEMPA, S. & LEWIN, G. R. 2017. Fructose-driven glycolysis supports anoxia resistance in the naked mole-rat. *Science*, 356, 307-311.
- PATEL, K., BROTHERTON, A., CHAUDHRY, D., EVISON, F., NIETO, T., DABARE, D. & SHARIF, A. 2023. All Expanded Criteria Donor Kidneys are Equal But are Some More Equal Than Others? A Population-Cohort Analysis of UK Transplant Registry Data. *Transpl Int*, 36, 11421.
- PATEL, K., SMITH, T. B., NEIL, D. A. H., THAKKER, A., TSUCHIYA, Y., HIGGS, E. B., HODGES, N. J., READY, A. R., NATH, J. & LUDWIG, C. 2019. The Effects of Oxygenation on Ex Vivo Kidneys Undergoing Hypothermic Machine Perfusion. *Transplantation*, 103, 314-322.
- PENG, P., DING, Z., HE, Y., ZHANG, J., WANG, X. & YANG, Z. 2019. Hypothermic Machine Perfusion Versus Static Cold Storage in Deceased Donor Kidney Transplantation: A Systematic Review and Meta-Analysis of Randomized Controlled Trials. *Artificial Organs*, 43, 478-489.
- PENG, Q., LI, K., SMYTH, L. A., XING, G., WANG, N., MEADER, L., LU, B., SACKS, S. H. & ZHOU, W. 2012. C3a and C5a Promote Renal Ischemia-Reperfusion Injury. *Journal of the American Society of Nephrology*, 23, 1474-1485.

- PEREIRA-SAMPAIO, M. A., FAVORITO, L. A. & SAMPAIO, F. J. 2004. Pig kidney: anatomical relationships between the intrarenal arteries and the kidney collecting system. Applied study for urological research and surgical training. *J Urol*, 172, 2077-81.
- PERRY, H. M. & OKUSA, M. D. 2016. Endothelial Dysfunction in Renal Interstitial Fibrosis. *Nephron,* 134, 167-171.
- PETERS-SENGERS, H., HOUTZAGER, J. H. E., IDU, M. M., HEEMSKERK, M. B. A., VAN HEURN, E. L. W., HOMAN VAN DER HEIDE, J. J., KERS, J., BERGER, S. P., VAN GULIK, T. M. & BEMELMAN, F. J. 2019. Impact of Cold Ischemia Time on Outcomes of Deceased Donor Kidney Transplantation: An Analysis of a National Registry. *Transplantation Direct*, 5, e448.
- PICKERING, M. C., COOK, H. T., WARREN, J., BYGRAVE, A. E., MOSS, J., WALPORT, M. J. & BOTTO, M. 2002. Uncontrolled C3 activation causes membranoproliferative glomerulonephritis in mice deficient in complement factor H. *Nature Genetics*, 31, 424-428.
- PICKERING, M. C., WARREN, J., ROSE, K. L., CARLUCCI, F., WANG, Y., WALPORT, M. J., COOK, H. T. & BOTTO, M. 2006. Prevention of C5 activation ameliorates spontaneous and experimental glomerulonephritis in factor H-deficient mice. *Proceedings of the National Academy of Sciences*, 103, 9649-9654.
- PITTOCK, S. J., FUJIHARA, K., PALACE, J., BERTHELE, A., KIM, H. J., OREJA-GUEVARA, C., NAKASHIMA, I., LEVY, M., SHANG, S., YOUNTZ, M., MILLER, L., ARMSTRONG, R. & WINGERCHUK, D. M. 2022. Eculizumab monotherapy for NMOSD: Data from PREVENT and its open-label extension. *Mult Scler*, 28, 480-486.
- PONTICELLI, C. 2013. Ischaemia-reperfusion injury: a major protagonist in kidney transplantation. *Nephrology Dialysis Transplantation*, 29, 1134-1140.
- PONTICELLI, C., REGGIANI, F. & MORONI, G. 2022. Delayed Graft Function in Kidney Transplant: Risk Factors, Consequences and Prevention Strategies. *J Pers Med*, 12.
- POOL, M., EERTMAN, T., SIERRA PARRAGA, J., T HART, N., ROEMELING-VAN RHIJN, M., EIJKEN, M., JESPERSEN, B., REINDERS, M., HOOGDUIJN, M., PLOEG, R., LEUVENINK, H. & MOERS, C. 2019. Infusing Mesenchymal Stromal Cells into Porcine Kidneys during Normothermic Machine Perfusion: Intact MSCs Can Be Traced and Localised to Glomeruli. *Int J Mol Sci*, 20.
- POOL, M. B. F., VOS, J., EIJKEN, M., VAN PEL, M., REINDERS, M. E. J., PLOEG, R. J., HOOGDUIJN, M. J., JESPERSEN, B., LEUVENINK, H. G. D. & MOERS, C. 2020. Treating Ischemically Damaged Porcine Kidneys with Human Bone Marrow- and Adipose Tissue-Derived Mesenchymal Stromal Cells During Ex Vivo Normothermic Machine Perfusion. *Stem Cells and Development*, 29, 1320-1330.
- POPPELAARS, F., GOICOECHEA DE JORGE, E., JONGERIUS, I., BAEUMNER, A. J., STEINER, M.-S., JÓZSI, M., TOONEN, E. J. M., PAULY, D. & , T. S. C. 2021. A Family Affair: Addressing the Challenges of Factor H and the Related Proteins. *Frontiers in Immunology*, 12.
- PORT, F. K., BRAGG-GRESHAM, J. L., METZGER, R. A., DYKSTRA, D. M., GILLESPIE, B. W., YOUNG, E. W., DELMONICO, F. L., WYNN, J. J., MERION, R. M., WOLFE, R. A. & HELD, P. J. 2002. Donor characteristics associated with reduced graft survival: an approach to expanding the pool of kidney donors1. *Transplantation*, 74, 1281-1286.
- PRATT, J. R., ABE, K., MIYAZAKI, M., ZHOU, W. & SACKS, S. H. 2000. In Situ Localization of C3 Synthesis in Experimental Acute Renal Allograft Rejection. *The American Journal of Pathology,* 157, 825-831.
- PRATT, J. R., BASHEER, S. A. & SACKS, S. H. 2002. Local synthesis of complement component C3 regulates acute renal transplant rejection. *Nature Medicine*, 8, 582-587.
- PRATT, J. R., JONES, M. E., DONG, J., ZHOU, W., CHOWDHURY, P., SMITH, R. A. & SACKS, S. H. 2003. Nontransgenic hyperexpression of a complement regulator in donor kidney modulates transplant ischemia/reperfusion damage, acute rejection, and chronic nephropathy. *Am J Pathol*, 163, 1457-65.
- QI, J., PAN, T., YOU, T., TANG, Y., CHU, T., CHEN, J., FAN, Y., HU, S., YANG, F., RUAN, C., WU, D. & HAN, Y. 2022. Upregulation of HIF-1α contributes to complement activation in transplantation-associated thrombotic microangiopathy. *Br J Haematol*, 199, 603-615.

- QIAO, Q., TENG, X., WANG, N., LU, R., GUO, L., ZHANG, X., DU, Y., WANG, W., CHEN, S., WU, Q., HE, G., WANG, Y. & HU, W. 2014. A novel CRIg-targeted complement inhibitor protects cells from complement damage. *The FASEB Journal*, 28, 4986-4999.
- QIN, L., LI, G., KIRKILES-SMITH, N., CLARK, P., FANG, C., WANG, Y., YU, Z. X., DEVORE, D., TELLIDES, G., POBER, J. S. & JANE-WIT, D. 2016. Complement C5 Inhibition Reduces T Cell-Mediated Allograft Vasculopathy Caused by Both Alloantibody and Ischemia Reperfusion Injury in Humanized Mice. *Am J Transplant*, 16, 2865-2876.
- RADI, G., FALLANI, G., GERMINARIO, G., BUSUTTI, M., LA MANNA, G. AND RAVAIOLI, M. 2023. HYPOTHERMIC PERFUSION OF THE KIDNEY: FROM RESEARCH TO CLINICAL PRACTICE. European Journal of Transplantation, 1, 79-91.
- RALIB, A., PICKERING, J. W., SHAW, G. M. & ENDRE, Z. H. 2013. The urine output definition of acute kidney injury is too liberal. *Crit Care*, 17, R112.
- REHM, M., BRUEGGER, D., CHRIST, F., CONZEN, P., THIEL, M., JACOB, M., CHAPPELL, D., STOECKELHUBER, M., WELSCH, U., REICHART, B., PETER, K. & BECKER, B. F. 2007. Shedding of the Endothelial Glycocalyx in Patients Undergoing Major Vascular Surgery With Global and Regional Ischemia. *Circulation*, 116, 1896-1906.
- RENNER, B., TONG, H. H., LASKOWSKI, J., JONSCHER, K., GOETZ, L., WOOLAVER, R., HANNAN, J., LI, Y. X., HOURCADE, D., PICKERING, M. C., HOLERS, V. M. & THURMAN, J. M. 2016. Annexin A2 Enhances Complement Activation by Inhibiting Factor H. *Journal of immunology (Baltimore, Md. : 1950),* 196, 1355-1365.
- RISITANO, A. M., NOTARO, R., PASCARIELLO, C., SICA, M., DEL VECCHIO, L., HORVATH, C. J., FRIDKIS-HARELI, M., SELLERI, C., LINDORFER, M. A., TAYLOR, R. P., LUZZATTO, L. & HOLERS, V. M. 2012. The complement receptor 2/factor H fusion protein TT30 protects paroxysmal nocturnal hemoglobinuria erythrocytes from complement-mediated hemolysis and C3 fragment opsonization. *Blood*, 119, 6307-6316.
- RODRIGUEZ DE CORDOBA, S., LUBLIN, D. M., RUBINSTEIN, P. & ATKINSON, J. P. 1985. Human genes for three complement components that regulate the activation of C3 are tightly linked. *Journal of Experimental Medicine*, 161, 1189-1195.
- ROHRER, B. R., LONG, Q., COUGHLIN, B., WILSON, R. B., HUANG, Y., QIAO, F., TANG, P. H., KUNCHITHAPAUTHAM, K., GILKESON, G. S. & TOMLINSON, S. 2009. A Targeted Inhibitor of the Alternative Complement Pathway Reduces Angiogenesis in a Mouse Model of Age-Related Macular Degeneration. *Investigative Ophthalmology & Visual Science*, 50, 3056-3064.
- RÖTH, A., BARCELLINI, W., D'SA, S., MIYAKAWA, Y., BROOME, C. M., MICHEL, M., KUTER, D. J., JILMA, B., TVEDT, T. H. A., FRUEBIS, J., JIANG, X., LIN, S., REUTER, C., MORALES-ARIAS, J., HOBBS, W. & BERENTSEN, S. 2021. Sutimlimab in Cold Agglutinin Disease. *New England Journal of Medicine*, 384, 1323-1334.
- ROUSCHOP, K. M. A., SEWNATH, M. E., CLAESSEN, N., ROELOFS, J. J. T. H., HOEDEMAEKER, I., VAN DER NEUT, R., ATEN, J., PALS, S. T., WEENING, J. J. & FLORQUIN, S. 2004. CD44 Deficiency Increases Tubular Damage But Reduces Renal Fibrosis in Obstructive Nephropathy. *Journal of the American Society of Nephrology*, 15, 674-686.
- RUSEVA, M. M. & HEURICH, M. 2014. Purification and characterization of human and mouse complement C3. *Methods Mol Biol*, 1100, 75-91.
- SAIDI, R. F., ELIAS, N., KAWAI, T., HERTL, M., FARRELL, M. L., GOES, N., WONG, W., HARTONO, C., FISHMAN, J. A., KOTTON, C. N., TOLKOFF-RUBIN, N., DELMONICO, F. L., COSIMI, A. B. & KO, D. S. C. 2007. Outcome of Kidney Transplantation Using Expanded Criteria Donors and Donation After Cardiac Death Kidneys: Realities and Costs. *American Journal of Transplantation*, 7, 2769-2774.
- SAKARI JOKIRANTA, T., ZIPFEL, P. F., HAKULINEN, J., KÜHN, S., PANGBURN, M. K., TAMERIUS, J. D. & MERI, S. 1996. Analysis of the recognition mechanism of the alternative pathway of complement by monoclonal anti-factor H antibodies: evidence for multiple interactions between H and surface bound C3b. *FEBS Letters*, 393, 297-302.

- SANCHEZ-CORRAL, P., PEREZ-CABALLERO, D., HUARTE, O., SIMCKES, A. M., GOICOECHEA, E., LOPEZ-TRASCASA, M. & DE CORDOBA, S. R. 2002. Structural and functional characterization of factor H mutations associated with atypical hemolytic uremic syndrome. *Am J Hum Genet*, 71, 1285-95.
- SANTOS-LÓPEZ, J., DE LA PAZ, K., FERNÁNDEZ, F. J. & VEGA, M. C. 2023. Structural biology of complement receptors. *Frontiers in Immunology*, 14.
- SAUNDERS, R. E., GOODSHIP, T. H. J., ZIPFEL, P. F. & PERKINS, S. J. 2006. An interactive web database of factor H-associated hemolytic uremic syndrome mutations: insights into the structural consequences of disease-associated mutations. *Human Mutation*, 27, 21-30.
- SCHINDELIN, J., ARGANDA-CARRERAS, I., FRISE, E., KAYNIG, V., LONGAIR, M., PIETZSCH, T., PREIBISCH, S., RUEDEN, C., SAALFELD, S., SCHMID, B., TINEVEZ, J.-Y., WHITE, D. J., HARTENSTEIN, V., ELICEIRI, K., TOMANCAK, P. & CARDONA, A. 2012. Fiji: an open-source platform for biological-image analysis. *Nature Methods*, 9, 676-682.
- SCHMIDT, C. Q., BAI, H., LIN, Z., RISITANO, A. M., BARLOW, P. N., RICKLIN, D. & LAMBRIS, J. D. 2013. Rational Engineering of a Minimized Immune Inhibitor with Unique Triple-Targeting Properties. *The Journal of Immunology*, 190, 5712-5721.
- SCHMIDT, C. Q., HARDER, M. J., NICHOLS, E.-M., HEBECKER, M., ANLIKER, M., HÖCHSMANN, B., SIMMET, T., CSINCSI, Á. I., UZONYI, B., PAPPWORTH, I. Y., RICKLIN, D., LAMBRIS, J. D., SCHREZENMEIER, H., JÓZSI, M. & MARCHBANK, K. J. 2016. Selectivity of C3-opsonin targeted complement inhibitors: A distinct advantage in the protection of erythrocytes from paroxysmal nocturnal hemoglobinuria patients. *Immunobiology*, 221, 503-511.
- SCHMIDT, C. Q., SLINGSBY, F. C., RICHARDS, A. & BARLOW, P. N. 2011. Production of biologically active complement factor H in therapeutically useful quantities. *Protein Expr Purif*, 76, 254-63.
- SCHMITZ, R., FITCH, Z. W., SCHRODER, P. M., CHOI, A. Y., JACKSON, A. M., KNECHTLE, S. J. & KWUN, J. 2020. B cells in transplant tolerance and rejection: friends or foes? *Transpl Int*, 33, 30-40.
- SCHRÖPPEL, B., AKALIN, E., BAWEJA, M., BLOOM, R. D., FLORMAN, S., GOLDSTEIN, M., HAYDEL, B., HRICIK, D. E., KULKARNI, S., LEVINE, M., MEHROTRA, A., PATEL, A., POGGIO, E. D., RATNER, L., SHAPIRO, R. & HEEGER, P. S. 2020. Peritransplant eculizumab does not prevent delayed graft function in deceased donor kidney transplant recipients: Results of two randomized controlled pilot trials. *Am J Transplant*, 20, 564-572.
- SCHWAEBLE, W., ZWIRNER, J., SCHULZ, T. F., LINKE, R. P., DIERICH, M. P. & WEISS, E. H. 1987. Human complement factor H: expression of an additional truncated gene product of 43 kDa in human liver. *Eur J Immunol*, 17, 1485-9.
- SEJA, I. A., SANTOSO, B., RASYID, N. & SITUMORANG, G. R. 2022. Association of Postoperative Urinary Output in the First 24 Hours with Delayed Graft Function After Living and Deceased Donor Kidney Transplant: A Systematic Review. *Nephro-Urol Mon*, 14, e119447.
- SHAHBAZ, H. & GUPTA, M. 2021. Creatinine Clearance, StatPearls Publishing, Treasure Island (FL).
- SHARMA, A. K. & PANGBURN, M. K. 1994. Biologically active recombinant human complement factor H: synthesis and secretion by the baculovirus system. *Gene*, 143, 301-2.
- SHEERIN, N. S., RISLEY, P., ABE, K., TANG, Z., WONG, W., LIN, T. & SACKS, S. H. 2008. Synthesis of complement protein C3 in the kidney is an important mediator of local tissue injury. *Faseb j*, 22, 1065-72.
- SHI, Y., YAO, W., SUN, L., LI, G., LIU, H., DING, P., HU, W. & XU, H. 2019. The new complement inhibitor CRIg/FH ameliorates lupus nephritis in lupus-prone MRL/lpr mice. *BMC Nephrology*, 20, 424.
- SHIGEOKA, A. A., HOLSCHER, T. D., KING, A. J., HALL, F. W., KIOSSES, W. B., TOBIAS, P. S., MACKMAN, N. & MCKAY, D. B. 2007. TLR2 Is Constitutively Expressed within the Kidney and Participates in Ischemic Renal Injury through Both MyD88-Dependent and -Independent Pathways1. *The Journal of Immunology,* 178, 6252-6258.
- SILVER, J. H., HART, A. P., WILLIAMS, E. C., COOPER, S. L., CHAREF, S., LABARRE, D. & JOZEFOWICZ, M. 1992. Anticoagulant effects of sulphonated polyurethanes. *Biomaterials*, 13, 339-344.

- SIM, E., PALMER, M. S., PUKLAVEC, M. & SIM, R. B. 1983. Monoclonal antibodies against the complement control protein factor H (beta 1 H). *Biosci Rep*, 3, 1119-31.
- SITUMORANG, G. R. & SHEERIN, N. S. 2019. Ischaemia reperfusion injury: mechanisms of progression to chronic graft dysfunction. *Pediatric Nephrology*, 34, 951-963.
- SOBEK, V., BIRKNER, N., FALK, I., WÜRCH, A., KIRSCHNING, C. J., WAGNER, H., WALLICH, R., LAMERS, M. C. & SIMON, M. M. 2004. Direct Toll-like receptor 2 mediated co-stimulation of T cells in the mouse system as a basis for chronic inflammatory joint disease. *Arthritis Res Ther*, 6, R433.
- SOCIÉ, G., CABY-TOSI, M. P., MARANTZ, J. L., COLE, A., BEDROSIAN, C. L., GASTEYGER, C., MUJEEBUDDIN, A., HILLMEN, P., VANDE WALLE, J. & HALLER, H. 2019. Eculizumab in paroxysmal nocturnal haemoglobinuria and atypical haemolytic uraemic syndrome: 10-year pharmacovigilance analysis. *Br J Haematol*, 185, 297-310.
- STEVENS, P. E., AHMED, S. B., CARRERO, J. J., FOSTER, B., FRANCIS, A., HALL, R. K., HERRINGTON, W. G., HILL, G., INKER, L. A., KAZANCIOĞLU, R., LAMB, E., LIN, P., MADERO, M., MCINTYRE, N., MORROW, K., ROBERTS, G., SABANAYAGAM, D., SCHAEFFNER, E., SHLIPAK, M., SHROFF, R., TANGRI, N., THANACHAYANONT, T., ULASI, I., WONG, G., YANG, C.-W., ZHANG, L. & LEVIN, A. 2024. KDIGO 2024 Clinical Practice Guideline for the Evaluation and Management of Chronic Kidney Disease. *Kidney International*, 105, S117-S314.
- SUMMERS, D. M., JOHNSON, R. J., HUDSON, A., COLLETT, D., WATSON, C. J. & BRADLEY, J. A. 2013. Effect of donor age and cold storage time on outcome in recipients of kidneys donated after circulatory death in the UK: a cohort study. *Lancet*, 381, 727-34.
- SUMMERS, D. M., WATSON, C. J. E., PETTIGREW, G. J., JOHNSON, R. J., COLLETT, D., NEUBERGER, J. M. & BRADLEY, J. A. 2015. Kidney donation after circulatory death (DCD): state of the art. *Kidney International*, 88, 241-249.
- SYED, Y. Y. 2021. Ravulizumab: A Review in Atypical Haemolytic Uraemic Syndrome. *Drugs*, 81, 587-594.
- TAKASUMI, M., OMORI, T., MACHIDA, T., ISHIDA, Y., HAYASHI, M., SUZUKI, T., HOMMA, Y., ENDO, Y., TAKAHASHI, M., OHIRA, H., FUJITA, T. & SEKINE, H. 2020. A novel complement inhibitor sMAP-FH targeting both the lectin and alternative complement pathways. *The FASEB Journal*, 34, 6598-6612.
- THOMAN, M. L., MEUTH, J. L., MORGAN, E. L., WEIGLE, W. O. & HUGLI, T. E. 1984. C3d-K, a kallikrein cleavage fragment of iC3b is a potent inhibitor of cellular proliferation. *J Immunol*, 133, 2629-33.
- THOMPSON, E. R., BATES, L., IBRAHIM, I. K., SEWPAUL, A., STENBERG, B., MCNEILL, A., FIGUEIREDO, R., GIRDLESTONE, T., WILKINS, G. C., WANG, L., TINGLE, S. J., SCOTT III, W. E., DE PAULA LEMOS, H., MELLOR, A. L., ROOBROUCK, V. D., TING, A. E., HOSGOOD, S. A., NICHOLSON, M. L., FISHER, A. J., ALI, S., SHEERIN, N. S. & WILSON, C. H. 2021. Novel delivery of cellular therapy to reduce ischemia reperfusion injury in kidney transplantation. *American Journal of Transplantation*, 21, 1402-1414.
- THOMPSON, E. R., SEWPAUL, A., FIGUEREIDO, R., BATES, L., TINGLE, S. J., FERDINAND, J. R., SITUMORANG, G. R., LADAK, S. S., CONNELLY, C. M., HOSGOOD, S. A., NICHOLSON, M. L., CLATWORTHY, M. R., ALI, S., WILSON, C. H. & SHEERIN, N. S. 2022. MicroRNA antagonist therapy during normothermic machine perfusion of donor kidneys. *American Journal of Transplantation*, 22, 1088-1100.
- THUILLIER, R., ALLAIN, G., CELHAY, O., HEBRARD, W., BARROU, B., BADET, L., LEUVENINK, H. & HAUET, T. 2013. Benefits of active oxygenation during hypothermic machine perfusion of kidneys in a preclinical model of deceased after cardiac death donors. *Journal of Surgical Research*, 184, 1174-1181.
- THURMAN, J. M., LJUBANOVIC, D., EDELSTEIN, C. L., GILKESON, G. S. & HOLERS, V. M. 2003. Lack of a Functional Alternative Complement Pathway Ameliorates Ischemic Acute Renal Failure in Mice 1. *The Journal of Immunology,* 170, 1517-1523.
- THURMAN, J. M., ROYER, P. A., LJUBANOVIC, D., DURSUN, B., LENDERINK, A. M., EDELSTEIN, C. L. & HOLERS, V. M. 2006. Treatment with an Inhibitory Monoclonal Antibody to Mouse Factor B

- Protects Mice from Induction of Apoptosis and Renal Ischemia/Reperfusion Injury. *Journal of the American Society of Nephrology*, 17, 707-715.
- TIETJEN, G. T., HOSGOOD, S. A., DIRITO, J., CUI, J., DEEP, D., SONG, E., KRAEHLING, J. R., PIOTROWSKI-DASPIT, A. S., KIRKILES-SMITH, N. C., AL-LAMKI, R., THIRU, S., BRADLEY, J. A., SAEB-PARSY, K., BRADLEY, J. R., NICHOLSON, M. L., SALTZMAN, W. M. & POBER, J. S. 2017. Nanoparticle targeting to the endothelium during normothermic machine perfusion of human kidneys. *Sci Transl Med*, 9.
- TINGLE, S. J., FIGUEIREDO, R. S., MOIR, J. A. G., GOODFELLOW, M., TALBOT, D. & WILSON, C. H. 2019. Machine perfusion preservation versus static cold storage for deceased donor kidney transplantation. *Cochrane Database of Systematic Reviews*.
- TONELLI, M., WIEBE, N., KNOLL, G., BELLO, A., BROWNE, S., JADHAV, D., KLARENBACH, S. & GILL, J. 2011. Systematic Review: Kidney Transplantation Compared With Dialysis in Clinically Relevant Outcomes. *American Journal of Transplantation*, 11, 2093-2109.
- TORTAJADA, A., YÉBENES, H., ABARRATEGUI-GARRIDO, C., ANTER, J., GARCÍA-FERNÁNDEZ, J. M., MARTÍNEZ-BARRICARTE, R., ALBA-DOMÍNGUEZ, M., MALIK, T. H., BEDOYA, R., PÉREZ, R. C., TRASCASA, M. L., PICKERING, M. C., HARRIS, C. L., SÁNCHEZ-CORRAL, P., LLORCA, O. & RODRÍGUEZ DE CÓRDOBA, S. 2013. C3 glomerulopathy—associated CFHR1 mutation alters FHR oligomerization and complement regulation. *The Journal of Clinical Investigation*, 123, 2434-2446.
- TOZZI, M., FRANCHIN, M., SOLDINI, G., IETTO, G., CHIAPPA, C., MARITAN, E., VILLA, F., CARCANO, G. & DIONIGI, R. 2013. Impact of static cold storage VS hypothermic machine preservation on ischemic kidney graft: inflammatory cytokines and adhesion molecules as markers of ischemia/reperfusion tissue damage. Our preliminary results. *International Journal of Surgery*, 11, S110-S114.
- TROPPMANN, C., GILLINGHAM, K. J., BENEDETTI, E., ALMOND, P. S., GRUESSNER, R. W., NAJARIAN, J. S. & MATAS, A. J. 1995. Delayed graft function, acute rejection, and outcome after cadaver renal transplantation. The multivariate analysis. *Transplantation*, 59, 962-8.
- TZOUMAS, N., HALLAM, D., HARRIS, C. L., LAKO, M., KAVANAGH, D. & STEEL, D. H. W. 2021. Revisiting the role of factor H in age-related macular degeneration: Insights from complement-mediated renal disease and rare genetic variants. *Survey of Ophthalmology*, 66, 378-401.
- VAN DER TOUW, W., CRAVEDI, P., KWAN, W.-H., PAZ-ARTAL, E., MERAD, M. & HEEGER, P. S. 2013. Cutting Edge: Receptors for C3a and C5a Modulate Stability of Alloantigen-Reactive Induced Regulatory T Cells. *The Journal of Immunology*, 190, 5921-5925.
- VAN WERKHOVEN, M. B., DAMMAN, J., VAN DIJK, M., DAHA, M. R., DE JONG, I. J., LELIVELD, A., KRIKKE, C., LEUVENINK, H. G., VAN GOOR, H., VAN SON, W. J., OLINGA, P., HILLEBRANDS, J. L. & SEELEN, M. A. J. 2013. Complement mediated renal inflammation induced by donor brain death: role of renal C5a-C5aR interaction. *Am J Transplant*, 13, 875-882.
- VERNON, M. A., MYLONAS, K. J. & HUGHES, J. 2010. Macrophages and Renal Fibrosis. *Seminars in Nephrology*, 30, 302-317.
- VLAAR, A. P. J., WITZENRATH, M., VAN PAASSEN, P., HEUNKS, L. M. A., MOURVILLIER, B., DE BRUIN, S., LIM, E. H. T., BROUWER, M. C., TUINMAN, P. R., SARAIVA, J. F. K., MARX, G., LOBO, S. M., BOLDO, R., SIMON-CAMPOS, J. A., CORNET, A. D., GREBENYUK, A., ENGELBRECHT, J. M., MUKANSI, M., JORENS, P. G., ZERBIB, R., RÜCKINGER, S., PILZ, K., GUO, R., VAN DE BEEK, D., RIEDEMANN, N. C., VLAAR, A. P. J., WITZENRATH, M., VAN PAASSEN, P., HEUNKS, L. M. A., MOURVILLIER, B., DE BRUIN, S., LIM, E. H. T., BROUWER, M. C., TUINMAN, P. R., SARAIVA, J. F. K., MARX, G., LOBO, S., BOLDO, R., SIMON-CAMPOS, J., CORNET, A. D., GREBENYUK, A., ENGELBRECHT, J., MUKANSI, M., JORENS, P. G., ZERBIB, R., RÜCKINGER, S., PILZ, K., GUO, R., VAN DE BEEK, D., RIEDEMANN, N. C., BULPA, P., TACCONE, F. S., HERMANS, G., DILTOER, M., PIAGNERELLI, M., DE NEVE, N., FREIRE, A. T., PIZZOL, F. D., MARINHO, A. K., SATO, V. H., ARNS DA CUNHA, C., NEUVILLE, M., DELLAMONICA, J., ANNANE, D., ROQUILLY, A., DIEHL, J. L., SCHNEIDER, F., MIRA, J. P., LASCARROU, J. B., DESMEDT, L., DUPUIS, C., SCHWEBEL, C., THIÉRY, G., GRÜNDLING, M., BERGER, M., WELTE, T., BAUER, M., JASCHINSKI, U., MATSCHKE, K., MERCADO-LONGORIA, R., GOMEZ QUINTANA, B., ZAMUDIO-LERMA, J. A., MORENO

- HOYOS ABRIL, J., ALEMAN MARQUEZ, A., PICKKERS, P., OTTERSPOOR, L., HERCILLA VÁSQUEZ, L., SEAS RAMOS, C. R., PEÑA VILLALOBOS, A., GIANELLA MALCA, G., CHÁVEZ, V., FILIMONOV, V., KULABUKHOV, V., ACHARYA, P., TIMMERMANS, S. A. M. E. G., BUSCH, M. H., VAN BAARLE, F. L. F., KONING, R., TER HORST, L., CHEKROUNI, N., et al. 2022. Anti-C5a antibody (vilobelimab) therapy for critically ill, invasively mechanically ventilated patients with COVID-19 (PANAMO): a multicentre, double-blind, randomised, placebo-controlled, phase 3 trial. *The Lancet Respiratory Medicine*, 10, 1137-1146.
- VU, T., WIENDL, H., KATSUNO, M., REDDEL, S. W. & HOWARD, J. F., JR. 2023. Ravulizumab in Myasthenia Gravis: A Review of the Current Evidence. *Neuropsychiatr Dis Treat*, 19, 2639-2655.
- WEST, E. E., WOODRUFF, T., FREMEAUX-BACCHI, V. & KEMPER, C. 2024. Complement in human disease: approved and up-and-coming therapeutics. *The Lancet*, 403, 392-405.
- WIGGINS, R. C., GICLAS, P. C. & HENSON, P. M. 1981. Chemotactic activity generated from the fifth component of complement by plasma kallikrein of the rabbit. *J Exp Med*, 153, 1391-404.
- WONG, E. K. S. & KAVANAGH, D. 2018. Diseases of complement dysregulation—an overview. *Seminars in Immunopathology*, 40, 49-64.
- WOODELL, A., JONES, B. W., WILLIAMSON, T., SCHNABOLK, G., TOMLINSON, S., ATKINSON, C. & ROHRER, B. 2016. A Targeted Inhibitor of the Alternative Complement Pathway Accelerates Recovery From Smoke-Induced Ocular Injury. *Investigative Ophthalmology & Visual Science*, 57, 1728-1737.
- WU, J., WU, Y.-Q., RICKLIN, D., JANSSEN, B. J. C., LAMBRIS, J. D. & GROS, P. 2009a. Structure of complement fragment C3b-factor H and implications for host protection by complement regulators. *Nature immunology*, 10, 728-733.
- WU, J., WU, Y.-Q., RICKLIN, D., JANSSEN, B. J. C., LAMBRIS, J. D. & GROS, P. 2009b. Structure of complement fragment C3b–factor H and implications for host protection by complement regulators. *Nature Immunology*, 10, 728-733.
- XUE, X., WU, J., RICKLIN, D., FORNERIS, F., DI CRESCENZIO, P., SCHMIDT, C. Q., GRANNEMAN, J., SHARP, T. H., LAMBRIS, J. D. & GROS, P. 2017. Regulator-dependent mechanisms of C3b processing by factor I allow differentiation of immune responses. *Nature Structural & Molecular Biology*, 24, 643-651.
- YANG, B., HOSGOOD, S. A. & NICHOLSON, M. L. 2011. Naked Small Interfering RNA of Caspase-3 in Preservation Solution and Autologous Blood Perfusate Protects Isolated Ischemic Porcine Kidneys. *Transplantation*, 91, 501-507.
- YANG, Y., DENTON, H., DAVIES, O. R., SMITH-JACKSON, K., KERR, H., HERBERT, A. P., BARLOW, P. N., PICKERING, M. C. & MARCHBANK, K. J. 2018. An Engineered Complement Factor H Construct for Treatment of C3 Glomerulopathy. *J Am Soc Nephrol*, 29, 1649-1661.
- YARLAGADDA, S. G., COCA, S. G., FORMICA, R. N., JR, POGGIO, E. D. & PARIKH, C. R. 2008. Association between delayed graft function and allograft and patient survival: a systematic review and meta-analysis. *Nephrology Dialysis Transplantation*, 24, 1039-1047.
- YSEBAERT, D. K., DE GREEF, K. E., VERCAUTEREN, S. R., GHIELLI, M., VERPOOTEN, G. A., EYSKENS, E. J. & DE BROE, M. E. 2000. Identification and kinetics of leukocytes after severe ischaemia/reperfusion renal injury. *Nephrology Dialysis Transplantation*, 15, 1562-1574.
- YU, L., WANG, L. & CHEN, S. 2010. Endogenous toll-like receptor ligands and their biological significance. *Journal of Cellular and Molecular Medicine*, 14, 2592-2603.
- YU, M., WANG, H., DING, A., GOLENBOCK, D. T., LATZ, E., CZURA, C. J., FENTON, M. J., TRACEY, K. J. & YANG, H. 2006. HMGB1 SIGNALS THROUGH TOLL-LIKE RECEPTOR (TLR) 4 AND TLR2. *Shock*, 26, 174-179.
- YU, Z. X., QI, S., LASARO, M. A., BOUCHARD, K., DOW, C., MOORE, K., WU, Z., BARAMA, A., XU, J., JOHNSON, K., MAROZSAN, A. J. & WANG, Y. 2016. Targeting Complement Pathways During Cold Ischemia and Reperfusion Prevents Delayed Graft Function. *Am J Transplant*, 16, 2589-97.
- ZENS, T. J., DANOBEITIA, J. S., LEVERSON, G., CHLEBECK, P. J., ZITUR, L. J., REDFIELD, R. R., D'ALESSANDRO, A. M., ODORICO, S., KAUFMAN, D. B. & FERNANDEZ, L. A. 2018. The impact

- of kidney donor profile index on delayed graft function and transplant outcomes: A single-center analysis. *Clin Transplant*, 32, e13190.
- ZHANG, Y., FU, Z., ZHONG, Z., WANG, R., HU, L., XIONG, Y., WANG, Y. & YE, Q. 2016. Hypothermic Machine Perfusion Decreases Renal Cell Apoptosis During Ischemia/Reperfusion Injury via the Ezrin/AKT Pathway. *Artificial Organs*, 40, 129-135.
- ZHANG, Y., MEYER, N. C., WANG, K., NISHIMURA, C., FREES, K., JONES, M., KATZ, L. M., SETHI, S. & SMITH, R. J. 2012. Causes of alternative pathway dysregulation in dense deposit disease. *Clin J Am Soc Nephrol*, **7**, 265-74.
- ZHENG, X., FENG, B., CHEN, G., ZHANG, X., LI, M., SUN, H., LIU, W., VLADAU, C., LIU, R., JEVNIKAR, A. M., GARCIA, B., ZHONG, R. & MIN, W. P. 2006. Preventing renal ischemia-reperfusion injury using small interfering RNA by targeting complement 3 gene. *Am J Transplant*, 6, 2099-108.
- ZHENG, X., ZHANG, X., FENG, B., SUN, H., SUZUKI, M., ICHIM, T., KUBO, N., WONG, A., MIN, L. R., BUDOHN, M. E., GARCIA, B., JEVNIKAR, A. M. & MIN, W.-P. 2008. Gene Silencing of Complement C5a Receptor Using siRNA for Preventing Ischemia/Reperfusion Injury. *The American Journal of Pathology*, 173, 973-980.
- ZHOU, W., FARRAR, C. A., ABE, K., PRATT, J. R., MARSH, J. E., WANG, Y., STAHL, G. L. & SACKS, S. H. 2000. Predominant role for C5b-9 in renal ischemia/reperfusion injury. *The Journal of Clinical Investigation*, 105, 1363-1371.
- ZIPFEL, P. F. & SKERKA, C. 2009. Complement regulators and inhibitory proteins. *Nature Reviews Immunology*, 9, 729-740.